Design and Characterisation of an ‘Open Source’ Pyrolyser for Biochar Production

A thesis presented in partial fulfilment of the requirements for the degree of

Master of Engineering

In

Chemical and Bioprocess Engineering

At Massey University, Palmerston North

New Zealand

Rhonda Bridges

2013

ABSTRACT

An ‘open source’ field-scale batch pyrolyser was designed and constructed to produce biochar, which is the solid residue formed when biomass thermally decomposes in the absence of oxygen. The design approach was focused on simplicity for the intended target user, a hobby farmer. This is achieved in a batch process, where temperature ramp rates, gas flows and the end-point are controlled. Solids handling is only required at either end of the process. LPG is used as the initial heating source and later as the ignition source when pyrolysis gases are recycled.

A mathematical model formulation of the process was developed to predict the proportions of products produced as well as the time taken to achieve complete pyrolysis. Reaction kinetics are complex and not fully understood. In this model, simplifications were taken to provide guidelines for the reactor design as well as the effects of moisture on the process efficiencies.

The quality performance of the ‘open source’ pyrolyser was determined by comparing its biochar to that produced in a lab scale gas fired drum pyrolyser. Parameters varied on the lab drum pyrolyser were highest treatment temperature in the range 300 to 700 °C, sample size, moisture content and grain direction for *Pinus radiata*. The properties that were investigated are elemental composition (C, H, N, S), proximate analysis (moisture, volatile matter and fixed carbon) and char yield (% wt/wt). The ash content was determined by residue on ignition. For the lab scale experiments, it was found with increasing peak temperature that yield, volatile matter and hydrogen to carbon ratio decrease. Yield was unaffected by moisture, size and grain direction.

The design of the pilot reactor followed the principle observed with particle size that, in order to get maximum residence time of the vapour and tar in the reactor, the reactor was designed with a perforated core so that the vapours have a tortuous path of travel. This design also meant that heat and mass transfer occurred in the same direction, from the outer wall to the perforated core. In comparison to the lab scale pyrolyser, the same trends were observed in regards to temperature. High yields of 29.7 wt % and 28.8 wt % were obtained from wood with an initial moisture content of 21.9 wt % and 60.4 wt % respectively, confirming yield is unaffected by moisture.

Mass and energy balances were conducted on both the lab scale and pilot scale pyrolysers. For every kilogram of carbon in LPG used on the lab scale pyrolyser, an average of 0.25 kilograms of carbon is produced at 700 °C. Based on the optimum run for the pilot scale, for every kilogram of carbon in LPG used, 2.6 kilograms of carbon is produced at 700 °C.

ACKNOWLEDGEMENTS

Firstly, I would like to thank my supervisors Jim Jones and Tony Paterson for their time and support throughout this project.

I would also like to thank Llewelyn and Judith Richards who were part benefactors of this project. Sadly, Llewelyn passed away prior to the completion of this project.

This project has been very beneficial to me and allowed me to put engineering theory into practice and has enabled me to have a greater understanding of the heat and mass transport processes and engineering design.

Thanks to the Massey University technical staff that have helped when equipment is broken, cleared space for my wood chips and in general have assisted with my many requests.

TABLE OF CONTENTS

1.0 INTRODUCTION 1

2.0 LITERATURE REVIEW 3

2.1 Importance of Biochar and Applications 3

2.2 Biochar 4

2.2.1 Production by Pyrolysis 4

2.2.2 Composition 4

2.3 Types of Pyrolysis 5

2.3.1 Slow Pyrolysis 5

2.3.2 Fast Pyrolysis 6

2.4 Factors Affecting Pyrolysis Products and Composition 6

2.4.1 Temperature 6

2.4.2 Heating Rate 7

2.4.3 Moisture 8

2.4.4 Vapour Residence Time / Soak Time 8

2.4.5 Pressure 8

2.5 Pyrolysis Reaction Kinetics Models 9

2.5.1 Shafizadeh, 1976 9

2.5.2 Mok et al., 1983 10

2.5.3 Koufopanos et al., 1991 11

2.5.4 Miller and Bellan, 1997 11

2.5.5 Fantozzi et al., 2007 12

2.5.6 Functional-Group, Depolymerisation, Vaporisation and Cross-linking (FG-DVC) Models 13

2.5.7 Neves, 2011 13

2.5.8 Summary 14

2.6 Heat and Mass Transfer 14

2.6.1 Heat Transfer 14

2.6.2 Mass Transfer 16

2.6.3 Single Particle....16
2.6.4 Bed of Particles....17
2.7 Reactors....17
2.8 Heat Source....19
2.9 Wood....19
2.9.1 Properties....19
2.9.2 Water....20
2.10 Materials of Construction....21
2.11 Summary....22
2.12 Aims....22
3.0 PYROLYSER DESIGN CRITERIA....25
3.1 Overview....25
3.2 Batch versus Continuous Pyrolysis....26
3.3 Particle Size and Loading/Unloading....26
3.4 Start-up....27
3.5 Drying....27
3.6 Energy Efficiency....28
3.7 Non-thermal Energy Requirements....28
3.8 Running Costs....28
3.9 Cleaning....29
3.10 Safety....29
4.0 MATHEMATICAL MODELLING OF THE PYROLYSIS REACTION....31
4.1 Introduction....31
4.2 Model Objectives....31
4.3 Conceptual Model Development....32
4.4 Assumptions....33
4.5 Model Formulation....35
4.5.1 Heat Transfer Across the Boundary....35
4.5.2 Heat Transfer within the Wood....36
4.5.3 Heat Transfer at the Centre....38

4.5.4 Pyrolysis Primary Reaction Kinetics 38
4.5.5 Heat Balance for Evaporation of Water 39
4.6 Finite Difference Solution 40
4.6.1 For the surface of the reactor 41
4.6.2 For within the reactor 43
4.6.3 For the centre of the reactor 44
4.7 Numerical Error Checking 44
4.8 Mathematical Solution 44
4.9 Conclusions 47
5.0 PYROLYSER DESIGN SPECIFICATION 49
5.1 Process Description 49
5.2 Functional Description 49
5.2.1 Base Frame 50
5.2.2 Loading and Unloading 50
5.2.3 Internal Chamber 51
5.2.4 External Wall / Outer Chamber 52
5.2.5 Fuel Supply 52
5.2.6 Burner 52
5.2.7 Combustion Chamber 53
5.2.8 Flue 53
5.2.9 Tertiary Air 54
5.2.10 Flare 54
5.2.11 Overflow Vent 55
5.2.12 Tar Collection Plate 56
5.2.13 Insulation 57
5.2.14 Monitoring / Measurement Systems 57
5.3 Design Specifications 57
5.4 Control Description 61
5.5 Control Strategy and Testing Procedure 66
5.6 Process and Instrumentation Diagram 71

5.7 Hazard and operability analysis (HAZOP) 74
6.0 CHARACTERISATION 79
6.1 Objective 79
6.2 Methodology for Lab Scale Pyrolyser 79
6.3 Methodology for Field Scale Pyrolyser 81
7.0 ANALYSIS TECHNIQUES 84
7.1 Biomass Sample Preparation 84
7.2 Biochar Sample Preparation 84
7.3 Char Yield 84
7.4 Biomass Constituent Analysis 84
7.5 Porosity and Density 85
7.6 Proximate Analysis 87
7.7 Residue on Ignition (ROI) 88
7.8 Elemental Analysis 88
7.9 Statistical Analysis 90
8.0 FEEDSTOCK 92
9.0 LAB SCALE PYROLYSER RESULTS 96
9.1 Biochar Composition 96
9.1.1 Biochar Yield 96
9.1.2 Particle Density 98
9.1.3 Proximate Analysis 99
9.1.4 Elemental Analysis 105
9.1.5 Heating Value 111
9.1.6 Carbon Efficiency 113
10.0 PILOT SCALE OPERABILITY AND CHARACTERISATION 115
10.1 Discussion of the Results and Operating Conditions for Run 1 115
10.2 Discussion of the Results and Operating Conditions for Run 2 118
10.3 Discussion of the Results and Operating Conditions for Run 3 123
10.4 Discussion of the Results and Operating Conditions for Run 4 128
10.5 Discussion of the Results and Operating Conditions for Run 5 131

10.6 Discussion of the Results and Operating Conditions for Run 6 135
10.7 Operation Summary.....137
11.0 DISCUSSION OF PILOT RESULTS AND COMPARISON TO LAB RESULTS 139
11.1 Yield 139
11.2 Biochar composition 141
11.3 Carbon Footprint 144
11.4 Energy Efficiency 146
11.5 Residence Time 150
11.6 Heating Rate 150
12.0 CONCLUSION 153
13.0 RECOMMENDATIONS 155
14.0 REFERENCES 159

List of Figures

Figure 2.1: The effects of temperature on charcoal properties (Antal Jr & Grønli, 2003) 7

Figure 2.2: One-component mechanism of primary wood pyrolysis (Shafizadeh & Chin, 1976) 10

Figure 2.3: A detailed mechanism for cellulose pyrolysis (Mok & Antal, 1983) 11

Figure 2.4: Kinetic model for the pyrolysis of lignocellulosic material (Koufopanos, et al., 1991) 11

Figure 2.5: Generalised reaction kinetics for cellulose, hemicellulose and lignin (Miller & Bellan, 1997) 12

Figure 2.6: Simplified biomass pyrolysis scheme (Fantozzi, et al., 2007b) 12

Figure 2.7: Thermal degradation of a solid biomass particle under inert atmosphere: drying, primary pyrolysis and secondary pyrolysis 14

Figure 2.8: Pyrolysis of a biomass particle 17

Figure 4.1: Conceptual diagram showing the heat and mass transfer considered in this model as an expansion from the reactor 33

Figure 4.2: The finite difference grid used for pyrolysis 40

Figure 4.3: Temperature profile for conduction through wood 45

Figure 4.4: Conduction and evaporation in wood heated to 700 °C 46

Figure 4.5: Conduction, evaporation and reaction of wood pyrolysed at 700 °C 47

Figure 5.1: Basic block diagram of the process 49

Figure 5.2: Base frame 50

Figure 5.3: Mechanism for loading and unloading 51

Figure 5.4: Process and instrumentation diagram 71

Figure 6.1: Top view of pyrolyser wood holders 81

Figure 6.2: On the left, a front view of the sampling points, on the right, the sampling points when the reactor is in the horizontal unloading position 83

Figure 9.1: Raw data including the variables size, moisture, grain direction and peak temperature against yield 97

Figure 9.2: Raw data from the preferred model 98

Figure 9.3: The effect of peak temperature on bulk density of pine pyrolysed under various conditions 99

Figure 9.4: Volatile matter as a function of peak temperature and particle size 100

Figure 9.5: Fixed carbon as a function of peak temperature and size 101

Figure 9.6: Fitted general linear model for ash content on peak temperature, size moisture and grain direction. S is small, M is medium, L is large, G is with the grain and AG is against the grain 102

Figure 9.7: The effect of ash content on peak temperature and particle size 103

Figure 9.8: Ash predicted versus ash experimental on a dry basis 104

Figure 9.9: The effect of peak temperature against Nitrogen; the average nitrogen percentage in unpyrolysed *Pinus radiata* is 0.13 106

Figure 9.10: The effect of peak temperature on size and carbon; the average carbon percentage in unpyrolysed *Pinus radiata* is 51.3 % 107

Figure 9.11: The effect of size and peak temperature on hydrogen; the average hydrogen percentage in unpyrolysed *Pinus radiata* is 7.1 108

Figure 9.12: van Krevelen diagram of atomic H/C vs O/C ratios for biochar derived from *Pinus radiata* 109

Figure 9.13: Atomic ratios of H/C vs O/C for carbonised coal (Bituminous and semi-anthracite), cellulose (van Krevelen, 1950), the *Pinus radiata* feedstock used in the experiments and the resulting biochar produced from various operating conditions ... 110

Figure 9.14: The effect of peak temperature on H/C ratios and O/C molar ratios respectively 111

Figure 9.15: The effect of peak temperature and size on the higher heating value 112

Figure 9.16: Conversion of Carbon in Feedstock to Biochar on an Ash-free Dry Basis 113

Figure 9.17: Production Efficiency 114

Figure 10.1: Temperature and LPG profile for Run 1 116

Figure 10.2: Temperature profile for Run 2 119

Figure 10.3: LPG profile as a function of time and temperature for Run 2 121

Figure 10.4: Temperature profile for Run 3..... 124

Figure 10.5: Temperature and LPG profile for Run 3 125

Figure 10.6: Temperature and LPG profile for Run 4 128

Figure 10.7: Temperature profile for Run 4..... 129

Figure 10.8: Temperature profile for Run 5..... 132

Figure 10.9: Temperature and LPG profile for Run 5 133

Figure 10.10: Temperature profile for Run 6..... 136

Figure 11.1: Burner location in relation to the sampling points..... 142

Figure 11.2: Comparison of H/C and O/C ratios between the lab and pilot scale reactors . 143

Figure 11.3: The effect of sample position on the hydrogen content of the char in the pilot scale reactor. *Note:* B = Bottom, T = Top. The number refers to the location in which the sample was collected. Front refers to the front side of the reactor which is on the same side as the burners. 144

List of Tables

Table 5.1: Estimates for design 58

Table 5.2: Control scenarios 64

Table 5.3: Set-point descriptions 67

Table5.4: Time counters 67

Table 5.5: Initial set-points 68

Table 5.6: List 72

Table 6.1: Variables tested during lab scale pyrolysis 80

Table 6.2: Parameters tested on the pilot scale reactor 82

Table 6.3: Soak times 82

Table 7.1: Reference standard for elemental analysis 88

Table 7.2: Coal50 procedure inputs 90

Table 8.1: Constituent analysis of the *Pinus radiata* feedstock used in the lab scale experiments (Dry basis) 92

Table 8.2: Constituent analysis of the Pinus radiata wood chips used in the pilot scale experiments (Dry basis) 93

Table 8.3: Proximate analysis of the *Pinus radiata* feedstock used in the lab scale experiments (Dry basis) 93

Table 8.4: Proximate analysis of the *Pinus radiata* wood chips used in the pilot scale experimental (Dry basis) 94

Table 8.5: Elemental analysis of *pinus radiata* (Total basis) 94

Table 8.6: Residue on ignition analysis for ash determination (Dry basis) 95

Table 10.1: Proximate analysis results for Run 1 on dry basis 117

Table 10.2: Elemental analysis results for Run 1 on dry basis 118

Table 10.3: Proximate analysis results for Run 2 122

Table 10.4: Elemental analysis of the sampling points for Run 2 123

Table 10.5: Proximate analysis results for Run 3 126

Table 10.6: Elemental analysis results for Run 3..... 127

Table 10.7: Proximate analysis for Run 4 130

Table 10.8: Elemental analysis for Run 4 131

Table 10.9: Proximate analysis for Run 5 134

Table 10.10: Elemental analysis for Run 5 135

Table 10.11: Proximate analysis results for Run 6 137

Table 10.12: Elemental analysis results for Run 6 137

Table 11.1: Summary of the biochar yields obtained from the six runs 139

Table 11.2: Summary of the fixed carbon yield results for all runs 141

Table 11.3: Char composition summary for the experiments (Dry basis) 141

Table 11.4: Carbon footprint of the process..... 146

Table 11.5: Summary of input values for energy efficiency determination 147

Table 11.6: Summary of calculated efficiencies..... 149

Table 11.7: Residence time 150

Table 11.8: Heating rate..... 151

Table 14.1 Reactor Volume B-3

Table 14.2: Summary of system inputs for excess air requirements B-4

Table 14.3: The effect of flue temperature on the secondary air flow rate B-14

Table 14.4: Radiation heat losses from the reactor sides..... B-21

Table 14.5: Summary of conduction heat losses from the reactor for a lagging thickness of 0.1m B-29

Table 14.6: Summary of system inputs for explosion vent design B-30

Table 14.7: Oxygen flow rate as a function of temperature for the 6 kW and 23 kW burners B-32

Table 14.8: Pyrolysis Gas Composition B-32

Table 14.9: Tar Composition B-33

Table 14.10: Expansion coefficients for mild steel and stainless steel B-34

Table 14.11: Summary of expansion from different reactor components B-35

Table 14.12: Experimental Results C-2

Table 14.13: Elemental Analysis Results C-4

Table 14.14: Proximate Analysis Results on a Dry Basis C-8

1.0 **INTRODUCTION**

Charcoal has been used in many different applications for thousands of years ranging from cave paintings to its use as fuel for example in the iron and steel industries. Traditionally charcoal has been produced in pit kilns, mound kilns and brick kilns. These kilns are notorious for having inefficient conversion technologies, with high product variability and minimal control of emissions. The increasing awareness of the effect of Greenhouse Gas (GHG) emissions combined with opportunity to sequester carbon in charcoal means that charcoal making needs to become more sustainable and environmentally friendly. This is particularly true when it comes to biochar, which is differentiated from charcoal in that it is applied to soil and is intended for biological applications. To qualify as biochar, the feedstock must be sustainably produced biomass, the process must minimise fugitive emissions, and it must reach a quality standard (International Biochar Initiative, 2012) which relates to its stability in the soil. Biochar has an aromatic structure which is related to the production elemental hydrogen to carbon ratio. When this ratio is low, biochar has the potential for long-term stability in soil (Wang et al., 2013; Waters et al., 2011) and therefore the potential to influence the net global flux of CO_2 into the atmosphere.

Biochar is formed by the thermal degradation of biomass in a process known as pyrolysis which occurs in the absence of oxygen. This process produces a solid porous product high in carbon (60-90 wt%) (Antal Jr & Grønli, 2003), as well as generating syngas and tar. The objective of this project was to design a production unit for biochar that is a safe, simple process with low product quality variability and with a minimum carbon footprint. Furthermore, the design and characterisation of the unit was to be made 'open source', that is, publically available.

There were four main phases to this project: investigation, design, construction and characterisation. The investigation phase studied the importance of biochar, its applications, identified a target user for the production unit and defined its performance criteria, and investigated the reaction kinetics as well as the factors that affect the mass and heat transfer at the engineering scale. While the thinking processes involved are presented in the thesis, the outcome of this stage of the work identified the target user was an unskilled person (unskilled in the art of pyrolysis) within a developed economy with stringent emission standards. An example of a typical user may be a small holder or 'hobby farmer' who only farms at weekends. It was further expected that this person had only a small amount of time and will not attend the machine after start-up. In order to obtain consistent quality from an unattended unit, batch-wise processing was selected.

The second phase was design where, based on the criteria determined in phase 1, the process flow diagrams (PID) and piping and instrumentation diagrams (P&ID) were developed. A detailed hazard and operability (HAZOP) analysis was carried out over the

process to ensure the system is safe to operate and to mitigate poor performance such as incomplete pyrolysis and emissions failures. The design was focused on simplicity, safety, quality and efficiency. Simplicity required the equipment to operate with low or no operator input, with no skill requirement, to be as self-regulating as possible, and mobile. For safety, the pyrolyser must be certified as gas safe, safe for the operator and meet environmental emissions standards. The quality specification refers to consistency of quality to establish a 'best practice' method. Efficiency refers to the conversion efficiency of biomass to biochar, the carbon footprint, and the energy efficiency.

The third phase, construction, was contracted to a local engineering firm, JJ Niven Engineering Limited for mechanical drawings and fabrication and the gas engineering to Morrinsville Gas and Plumbing Limited (MPG).

It is well documented that the properties of biochar are affected by many contributing factors such as operating time, heating rate, feedstock and vapour residence time (Antal Jr & Grønli, 2003; Lehmann & Joseph, 2009). Therefore the final phase of this project was to characterise one feedstock, *Pinus radiata*, which is the most common plantation softwood in New Zealand. Characterisation was firstly conducted on a laboratory scale rotary drum pyrolyser to create curves relating char properties to operating conditions against which the performance of the field scale pyrolyser was calibrated. For the pilot scale trials, there were two areas of focus. Firstly, un-steady state characterisation monitored variables during operation such as internal temperature, gas compositions, flow rates and heat production. The char produced was sampled from the reactor and analysed for biochar yield, the fixed carbon content and the heating value. These were related to the operating conditions to determine the soak time necessary to achieve the endpoint and consistency of char quality.

The overall aim was to provide a 'best practise' method for biochar manufacture, which is correlated to the properties of biochar produced and for one feedstock, is independent of initial moisture content. It will enable further research into the stability indicators for these biochars in soil. Determination of the soil stability of biochar is important if ever biochar is to be accepted as a climate mitigation tool.

2.0 LITERATURE REVIEW

2.1 Importance of Biochar and Applications

There are many applications available for biochar, with evidence of the use of charcoal dating back to over 30,000 years ago in cave painting. Since the halocene, traditional agricultural techniques were developed in Brazil to make *terra preta* soils with a high carbon content (Antal Jr & Grønli, 2003). The regions in which this soil was found was in areas where the soil was dense desert soil where it is believed carbon was added to increase the soil quality and provide the capacity to store nutrients which then enables a sustainable and fertile environment for the agricultural industry (Antal Jr & Grønli, 2003; Glaser et al., 2001).

The addition of biochar influences the physical properties of the soil by altering the structure, porosity, pore size distribution, density and packing which has the potential to improve plant growth. Also, biochar can reduce soil acidity, improve soil cation exchange capacity (CEC), water holding capacity and improve the environment for beneficial microbes (Blackwell et al., 2009), provided biochar is placed at depths that coincide with root structures (Lehmann & Rondon, 2006). However, it is important to note that there is considerable variation in soil productivity which is a function of biochar production methods, feed stocks, and pedoclimatic environments (Lehmann & Rondon, 2006). Meta-analysis shows a great range in yield in biochar studies (-28% to +39% with a mean of about +10%) (Jeffery et al., 2011).

In the most favourable cases, biochar as a soil amendment has the potential to ensure food security and reduce malnutrition in regions that currently have soil of poor quality (Lehmann & Joseph, 2009) as well as promoting and enabling sustainable soil management (Sánchez et al., 2009).

Due to the stable nature of biochar, adding it to soil provides a mode for sequestering carbon. The aim of sequestering carbon is to keep the carbon out of the atmosphere by capturing and storing it. However, the carbon may eventually be released back into the atmosphere which means it is important to also focus on mitigating carbon dioxide production (Keller et al., 2008). Biochar is stable due to its unordered structure which is generated from the conversion of a non-aromatic compound to an aromatic carbon in the pyrolysis process (Waters, et al., 2011) and also because of the amorphous nature of the compound. Biochar decomposes at different rates, which is partly due to variations in feedstock and pyrolysis conditions (Lehmann et al., 2009). Research is needed in this area to relate stability indicators to pyrolysis conditions.

The addition of biochar to the soils enables greater nutrient retention due to the high surface area available for sorption of nutrients to occur and hence reduces nutrient leaching. The

main cause of pollution in waterways is phosphorous which occurs as a result of nutrient leaching and untreated effluent. Nutrient leaching from plants is reported to be as high as 80% of applied nitrogen (Lehmann et al., 2004).

2.2 Biochar

2.2.1 Production by Pyrolysis

Biochar has a high carbon content and is produced via the pyrolysis of organic material (biomass) in the carbonisation process, also known as thermal degradation. This process occurs in the absence of oxygen or low levels and usually below temperatures of 700 °C. A pyrolyser is a device in which thermal degradation occurs and enables the conversion of biomass to charcoal production. Gas and tar are also produced. The resulting gas can be captured for electricity generation or burnt off, thus allowing the negative environmental impacts to be reduced.

The process of pyrolysis begins with heat supplied from an external source which increases the temperature inside the reactor and evaporates any moisture remaining in the biomass. Primary reactions begin at around 280 °C for wood, producing char and releasing volatiles which are compounds with low boiling points. As they flow across the pyrolyser the volatiles transfer heat to the unpyrolysed biomass. At lower temperatures, some volatiles condense (Mohan et al., 2006) and at higher temperatures, secondary reactions of the primary volatiles occur, producing further gas, tar and char (Neves et al., 2011). It is well documented that both the primary and secondary reactions can occur in different areas of the particle, simultaneously. The organic vapours from the primary reactions can interact with the solid char to produce secondary char and gas (Antal Jr & Grønli, 2003; Neves, et al., 2011). Additional thermal decomposition occurs until the reactions are complete at temperatures of less than 700 °C.

2.2.2 Composition

The main constituents generated from pyrolysis of biomass are biochar, condensables and syngas from primary reactions as well as further biochar and syngas from secondary reactions.

The biomass most commonly used for biochar production is wood, which is composed of cellulose, hemicelluloses, lignin, organic material and inorganic minerals. The amount of

each varies in terms of species and more significantly in terms of hardwoods or softwoods. In this project, the softwood *Pinus radiata* is the feedstock of choice.

The first main component of the biomass to be degraded via hydrolysis (Murneek, 1929) involves hemicelluloses and occurs at low temperatures ranging from 200-260 °C. This primarily results in the formation of volatiles with some tar and char production. Hemicellulose is a branched polymer with short chains and has an amorphous structure (Mohan, et al., 2006). It typically makes up 25-35% of biomass and is the most reactive component (Roberts, 1971).

Cellulose is an organic compound, located in the cells walls, and is the main structural component of plant fibres, comprising up to 50% of the structure. The long polymer molecules, connected via a series of networks, provide the plants strength. Cellulose is insoluble and can be degraded into anhydrocellulose and levoglucosan at temperatures between 240-350 °C.

The structure and proportion of lignin varies by 16-33% in mass depending on the type of wood. Lignin is a highly branched material that produces phenols as it undergoes decomposition at temperatures of 280-500 °C (Mohan, et al., 2006). It has been established that higher yields of char can be obtained from biomass with a high lignin content (Mok et al., 1992).

A small amount of inorganic minerals and organic extractives remain after pyrolysis.

2.3 Types of Pyrolysis

Slow and fast pyrolysis are the two conventional methods of thermal degradation. Slow pyrolysis employs heating times that take minutes to hours, whereas fast pyrolysis heats the biomass in less than a few seconds. Each is discussed below, but slow pyrolysis produces higher biochar yields, which was the focus of this study.

2.3.1 Slow Pyrolysis

Slow pyrolysis has longer vapour residence times and slower heating rates in comparison to fast pyrolysis, which leads to higher charcoal production rates. The longer residence times allow reactions to occur between the vapour phase components as the other products (char and condensables) are being formed. Slow pyrolysis results in an even distribution of the three main products with a liquid yield of ~30 %, char ~35 % and gas ~35 %. A typical

heating rate for slow pyrolysis ranges between 0.1 - 1 K/s and can be used with a wider range of particles sizes (Mohan, et al., 2006), for instance between 5 - 50 mm (Demirbaş & Arin, 2002).

2.3.2 Fast Pyrolysis

It is well documented that fast pyrolysis results in a greater proportion of bio-oils. Typically this method can be over in a matter of minutes using a fine feedstock which allows rapid reactions to occur. This method for producing bio-oil is of particular interest as a renewable fuel source. This liquid fuel has the advantage of having a high calorific value and has less aromatic and sulphur compounds than other conventional fuels.

On a dry yield basis, fast pyrolysis can yield 75 % liquid, 12 % char and 13 % gas (Bridgwater, 2003). It is important to have a relatively dry feedstock (~10 % moisture content) to prevent excess water in the bio-oil product. The heating rate for fast pyrolysis varies between 10-200 K/s, however only small particles can be used because of mass and heat transfer limitations (Mohan, et al., 2006).

2.4 Factors Affecting Pyrolysis Products and Composition

2.4.1 Temperature

The most important parameter which will determine the final product composition and control of the process is temperature. In particular, temperature has a significant effect on the aromaticity, cation exchange capacity (CEC) and carbon content of the final product. The optimum range for producing biochar is from ~300-600 °C. Above this value the amount of biochar decreases and the amount of gas increases.

Baldock and Smernik (2002) have reported that increasing temperature increases the aromaticity of the biochar by altering the structure, which is supported by NMR evidence (Brewer et al., 2011). It was found that biochars with higher aromaticity are more stable in the soil (Lehmann, et al., 2009).

Cation exchange capacity (CEC) refers to the amount of cations (ions with a positive charge) that can be stored or bound in soil and is an indicator of soil fertility as well as the capacity of nutrients that can be retained in the soil. A high CEC improves soil fertility as more nutrients are retained (Glaser, et al., 2001). The CEC is higher at lower temperatures (Gaskin et al., 2008) but is also dependent on the pH of the soil (Lee et al., 2010). This is because

increasing temperature results in the loss of the acidic carbonyl (C=O) functional groups, resulting in more cations present (Singh et al., 2010). In addition, the O:C molar ratio is affected by temperature and the higher this ratio, the higher the CEC value (Lee, et al., 2010) and the more stable biochar is (Spokas, 2010).

Figure 2.1 below is reproduced from the experimental work of Berstrom and Wesslen (Antal Jr & Grønli, 2003) and shows that the fixed carbon content increased with increasing temperature, but the charcoal yield decreased. The optimum peak temperature for the process is around 600-700 °C to ensure a high fixed carbon content and a high carbon yield.

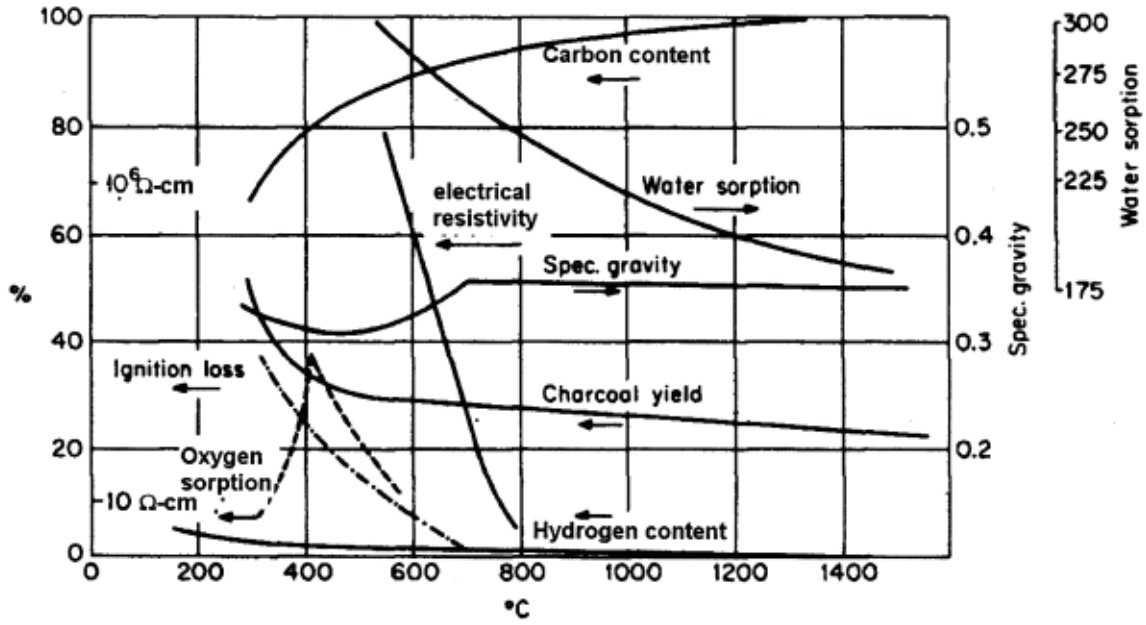

Figure 2.1: The effects of temperature on charcoal properties (Antal Jr & Grønli, 2003)

2.4.2 Heating Rate

The main focus of this project was to produce biochar. As stated earlier, slower heating rates produce a greater proportion of biochar. Another focus is to reduce the effects of emissions and recycle energy where possible to make an efficient, economic process that sequesters as much carbon as possible. Hence, the intention was to heat up enough of the biomass so that the gas coming off can drive the rest of the process.

A slower heating rate ensured a more complete conversion of biomass to biochar as the residence time is greater.

2.4.3 Moisture

The amount of moisture present in the biomass can affect the amount of biochar produced as well as influencing the reaction time. Drying of the feedstock is the most energy consuming process in pyrolysis. If there is a high initial moisture content in the biomass, then more energy (for example from LPG or wood burning) is required to dry the wood before any pyrolysis reactions can take place. In fact, having some moisture present results in slower cellulose degradation (Shimazu & Sterling, 1966) as well as increasing the amount of biochar formed at high temperatures (Mok, et al., 1992). Having the wood completely dry is not economical and it has been reported that a moisture content of 10% is optimum for carrying out pyrolysis.

2.4.4 Vapour Residence Time / Soak Time

The vapour phase residence time is reported to have a significant impact on the yield of biochar. More interactions can occur between the solid material and the vapours when there is a longer vapour residence time as the amount of secondary reactions increase and hence more biochar can be produced (Antal Jr & Grønli, 2003). The following discussion on the effect of pressure is one way to increase the vapour residence time.

2.4.5 Pressure

There have been several studies investigating the effects of elevated pressure on the amount of charcoal produced (Antal Jr et al., 1996; Antal Jr & Grønli, 2003; Antal Jr et al., 2003; Mok, et al., 1992). There is consensus in the literature that increasing the pressure produces greater yields of charcoal. This is because increasing pressure leads to more interactions between the char and the primary vapours, which enhances secondary reactions resulting in greater char yields.

The work by Mok, et al., (1983) involved an inert gas carrier, Argon, and low or high gas flow rates at various pressures. They found that high flow rates and a low pressure lead to a higher heat of reaction and decreased the amount of secondary reactions, hence favouring the formation of tar and volatiles over char. At a higher pressure and lower gas flow rates, the volatile residence time increased enabling further decomposition of the biomass causing higher char yields. Later work by Antal, et al., (2003) confirmed the concentration of the tarry vapour is higher (Elyounssi et al., 2010) and has a smaller specific volume at elevated

pressures which increases the volatile residence time, enabling more decomposition, producing further secondary char.

A two-step pyrolysis process whereby there was an initially low temperature-time profile for hemicellulose and cellulose degradation followed by a temperature increase for lignin degradation was found to maintain the fixed carbon content. These experiments were carried out at atmospheric pressure. Elyounssi et al., (2010) believe that increasing the pressure is not the sole reason for increasing char yields, but more increasing the solid-vapour residence time promotes the secondary char formation.

In summary, to maximise the charcoal yield, a low heating rate is necessary to reduce the formation and escape of the vapours. Also a low temperature for pyrolysis of less than 600 °C favours char formation and produces less tar and gas than other processes such as fast pyrolysis or gasification which employ high temperatures. The longer the vapour phase residence time, the greater the contact between the solid and vapours which increases the secondary reactions and hence more char can be produced. Particle size also has an impact on the yield. As the biomass has a low thermal conductivity, the rate of heat and mass transfer within the particles will be slower with larger particles and will increase char formation. As reported above, having a high process pressure (~1 MPa) increases the vapour concentration and enhances secondary reaction, but a low process pressure in contrast has a negative impact on char yield. High pressure systems become expensive to construct and operate and therefore are not practical.

2.5 Pyrolysis Reaction Kinetics Models

Devolatilization reactions are very complex and so, over time, researchers have offered a series of simplified models to approximate the chemical pathway of decomposition (Neves, et al., 2011). The following sections give a non-exhaustive summary of these.

2.5.1 Shafizadeh, 1976

The model by Shafizadeh & Chin (1976), shown in Figure 2.2, is a very simple model describing a one component mechanism in which wood is pyrolysed and the resulting products of char, tar and gases are formed at different rates. This model is kinetic and does not take into account mass and heat transfer effects important factors such as particle size which changes as a function of time and temperature as the reaction progresses. Also, the mechanism only describes primary pyrolysis of wood and does not include secondary

reactions, i.e., where the primary products interact with themselves to form secondary pyrolysis products.

Figure 2.2: One-component mechanism of primary wood pyrolysis (Shafizadeh & Chin, 1976)

2.5.2 Mok et al., 1983

Cellulose is the main component of biomass, representing up to 50% of the total mass of dry wood (Mohan, et al., 2006) and so, to remove some of the complexity, the next step in understanding devolatilization was to study the decomposition products from cellulose. Mok, et al., (1983) has investigated in detail the reactions that occur in cellulose degradation as well as the effects of pressure and gas flow rate on biomass pyrolysis. Under a high inert gas flow rate, the volatiles are drawn off almost immediately, thus reducing the opportunity for secondary reactions to occur. When they do occur, they are exothermic and hence increase the enthalpy heat of reaction. Increasing the pressure also affects the overall heat of reaction by favouring the exothermic reaction and producing more char. Further experiments were carried out investigating how flow rate and pressure interact on the pyrolysis reactions.

The observations lead to the proposed model in Figure 2.3, which includes two pathways. The anhydrocellulose pathway branches into either an endothermic reaction or an exothermic reaction. In the endothermic reaction, reactive volatiles are formed which then undergo further pyrolysis to produce CO, CO_2, H_2O and other volatiles. The exothermic pathway (4) produces char and gases. The experiments support the theory that char is produced via exothermic reactions. The levoglucosan pathway undergoes two competing reactions, vaporisation or decomposition. The vapours then react to produce tar or gas. In the exothermic reaction, the char the gases decompose further to produce either more or less char.

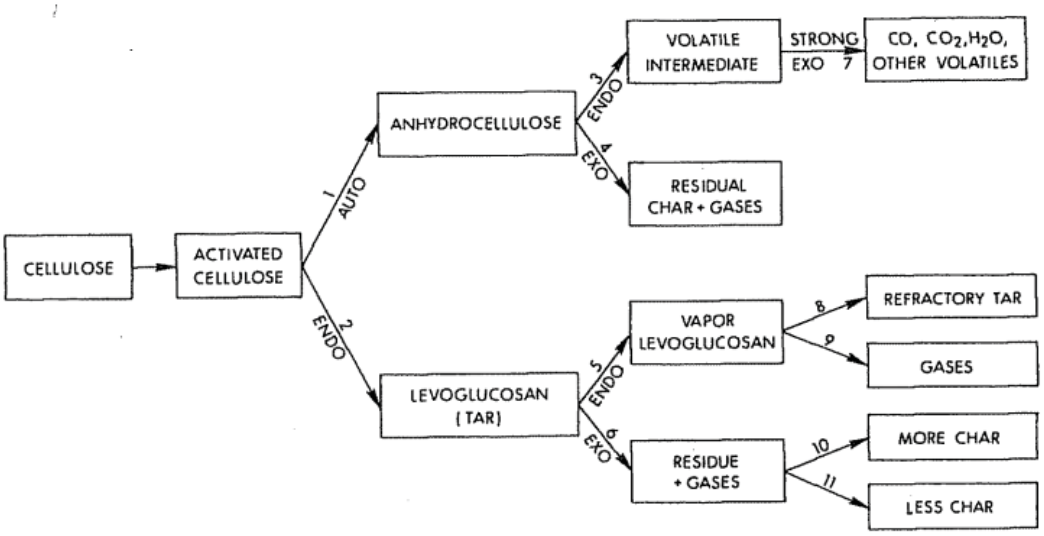

Figure 2.3: A detailed mechanism for cellulose pyrolysis (Mok & Antal, 1983)

2.5.3 Koufopanos et al., 1991

Koufopanois et al. (1991) extended the model of Shafizadeh & Chin (1976) to include secondary reactions. Their proposal was based on the pyrolysis of a single solid particle of biomass.

The representation in Figure 2.4 shows that biomass is converted to volatiles and gases by one reaction and char in another primary reaction. As a result of interactions between the vapours and char, secondary reactions occur producing further volatiles, gases and char (Koufopanos, et al., 1991). Again, this model is kinetic and does not include heat and mass transfer limitation effects.

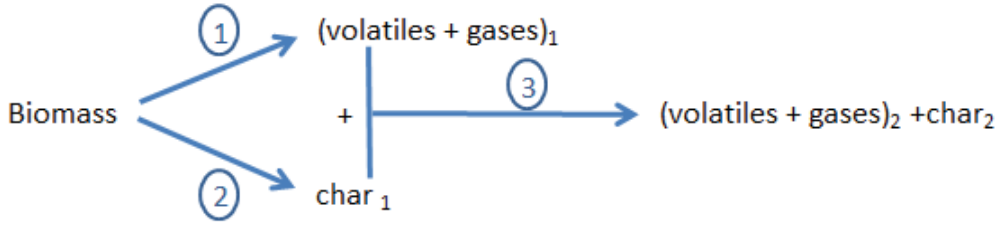

Figure 2.4: Kinetic model for the pyrolysis of lignocellulosic material (Koufopanos, et al., 1991)

2.5.4 Miller and Bellan, 1997

Miller and Bellan (1997) took an alternative view. Instead of basing the devolatilization on the appearance of reaction products, they based it on the composition of the constituents of

wood; namely, cellulose, hemicelluloses and lignin. They proposed a reaction pathway shown in Figure 2.5 for each constituent. This approach has never gained wide support, despite having just as sound a basis for use, probably because it is experimentally easier to measure the appearance of char, tar and gas as decomposition proceeds than to measure the disappearance of the wood constituents.

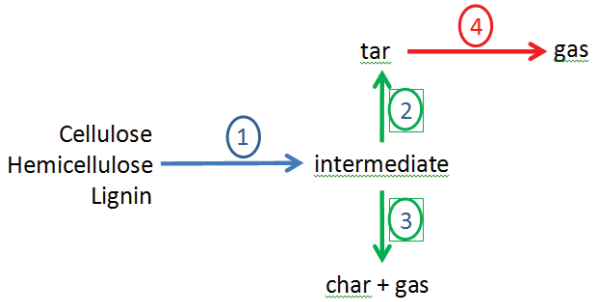

Figure 2.5: Generalised reaction kinetics for cellulose, hemicellulose and lignin (Miller & Bellan, 1997)

2.5.5 Fantozzi et al., 2007

Fantozzi et al. (2007) used a slightly modified devolatisation pathway to that of Koufopanos et al, (1991) to model the operation of a rolling drum continuous pyrolyser. The scheme displayed in Figure 2.6 was derived from the work of Di Blasi, (2008; (as cited in Fantozzi et al., 2007b). This model shows char, tar and gas are produced from biomass degradation in primary endothermic reactions followed by tar degradation to produce secondary gas and char. A series of constants explaining the kinetics of the process were determined from experiments and from the literature. A model was developed showing how the proportions of products change as a result of moisture content, density and rotational speed of the drum.

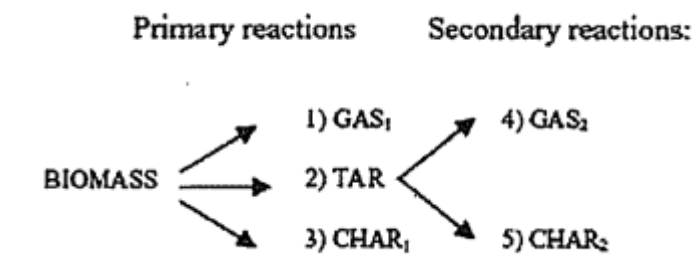

Figure 2.6: Simplified biomass pyrolysis scheme (Fantozzi, et al., 2007b)

2.5.6 Functional-Group, Depolymerisation, Vaporisation and Cross-linking (FG-DVC) Models

FG-DVC models are the most fundamental in terms of the principles of physical chemistry. They have two parts. The first part is a functional group model (FG) describes the gas evolution as well as the elemental and functional group compositions. The second part is the depolymerisation, vaporisation and cross-linking model (DVC) which determines the amount and molecular weight of macromolecular fragments. The lightest of these evolve as tar. The method works by tracking the evolution of the main compounds while determining the precursor species from which they evolved. The kinetic terms are obtained from Thermogravimetric-Fourier Transform Infra-red (TG-FTIR) analysis original proposed by Carangelo et al. (1987).

These models have developed as the understanding of the biochar structure increases (De Jong et al., 2007; De Jong et al., 2003).

2.5.7 Neves, 2011

Neves et al., (2011) considers thermal decomposition as a “black box”, acknowledging that all other models are simplified estimations of a highly complex process using variable biomass feedstocks. Their black box model looks for correlations between feedstock properties, thermal conditions and product composition. Remarkably, they arrive at common trends between inputs and outputs that, they argue, is good enough for system design.

Figure 2.7 provides information about what happens in the primary and secondary phases of pyrolysis. The model is based on the results of others.

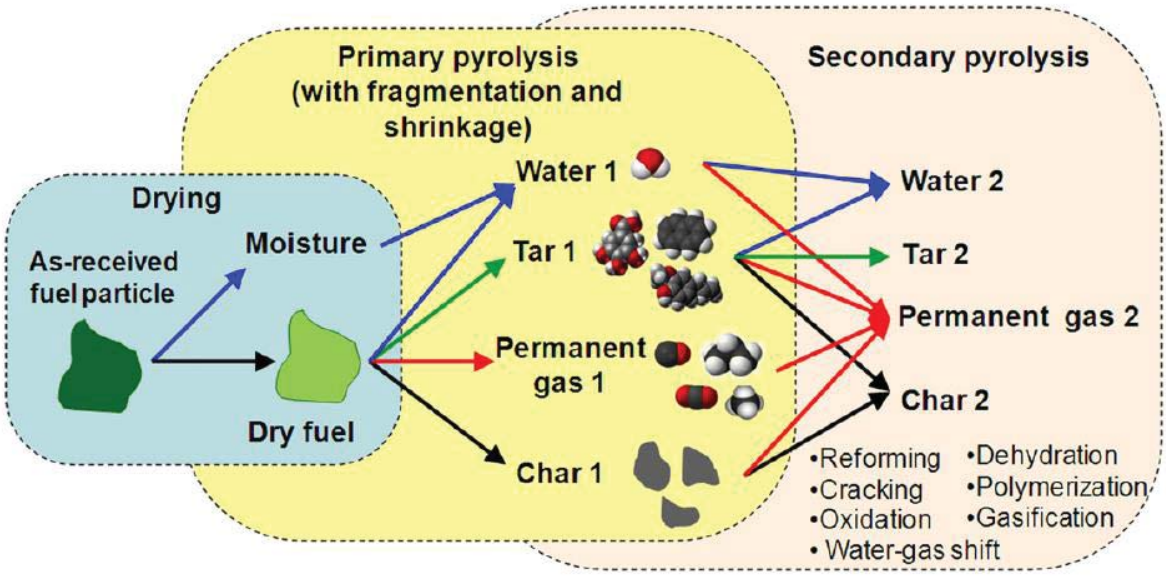

Figure 2.7: Thermal degradation of a solid biomass particle under inert atmosphere: drying, primary pyrolysis and secondary pyrolysis

2.5.8 Summary

All the models are based on approximations; however the model developed by Fantozzi et al. (2007b) was the most practical for our process, because it has been applied to a rotary drum which means the kinetic model includes the heat and mass transfer limitation specific to that operation. Their work has been extensively used. Although Fantozzi has got his parameters from a variety of sources, these were used in the proposed model. The model developed by Neves (2011) shows the inputs and outputs of the process and ignores the complexity that occurs in the middle. As the result they have developed a curve and in their opinion, this is adequate for designing a system. Although the model developed by Neves has merits, the more mechanistic approach of Fantozzi was decided upon.

2.6 Heat and Mass Transfer

2.6.1 Heat Transfer

The kinetic models above generally do not address heat and mass transfer, which can significantly affect the rate and localised conditions at which thermal decomposition occurs. Heat is transferred to the biomass by conduction inside the particle, convection inside the particle pores and radiation from the particle surface. The driving force for heat transfer is

temperature difference. As the pyrolyser is heated, conduction occurs through the metal wall of the reactor to the particles. Above ~200°C decomposition reactions occur.

For even heating and good control it is desirable that there is even contact between the biomass particles and the heat source. A rotating system is one way for achieving homogeneous heating rates during pyrolysis. “This enables mixing to occur, optimising mass and heat transfer, thus accelerating the pyrolysis reactions” (Fantozzi et al., 2007a).

Particle size is also important. It is well known that larger particles have heat and mass transfer limitations due to the outside of the particle being heated first by radiation and convection. Heat then transfer into the particle by these two mechanisms until the temperature reaches the range where thermal decomposition starts. At this point, the gas and volatile decomposition products flow outside towards the particle surface. This transport opposes the inflowing heat and therefore results in large temperature gradients between the centre and surface of particles. Also, larger particles affect the extent of the secondary reactions (Neves, et al., 2011) and hence the proportions of gases, condensables and char formed due to the longer travel path of the gases and volatiles from the centre to the surface. It is important to hold (or “soak”) larger particles for longer time at the set point temperature so that temperatures equilibrate throughout the particles (Kockar et al., 2000).

Longer soak times are also expected to annul the effects of different heating rates, unless they are particularly fast. This can be achieved in the design phase, either by making the system batch operated where soak time becomes a control variable, or using a continuous system dropping into a large long residence time soak bin.

The basic equation describing heat conduction is:

$$\frac{q_x}{A} = -k\frac{dT}{dx} \tag{2.1}$$

Where q_x/A is the heat transfer rate per unit area and is equal to the thermal conductivity, k multiplied be the change in temperature, dT over the change in distance, dx.

The basic equation for radiation is:

$$q_{rad} = h_{rad}A\left(\theta_{rad} - \theta_{surf}\right) \tag{2.2}$$

Where

$$h_{rad} = 5.67 * 10^{-8} * F_{12}\left(T_{rad} + T_{surf}\right)\left(T_{rad} + T_{surf}\right) \quad (2.3)$$

Where θ is temperature in degrees Celsius and T is in Kelvin.

The basic equation for conduction to a surface is:

$$\frac{d\theta}{dt} = \frac{k}{C_p \rho}\left(\frac{d^2\theta}{dx^2}\right) \quad (2.4)$$

Where k is the thermal conductivity has the units W m^{-1} K^{-1}, C_p is the specific heat capacity in J kg^{-1} K^{-1}, t is time in s, density ρ is in kg m^{-3} and x is the distance in m.

2.6.2 Mass Transfer

Heat transfer into a particle drives the devolatilization which generates gases and volatiles, which then move outwards along a concentration gradient toward the particle surface. The initial primary reactions are endothermic which means they absorb heat, but later secondary reactions are exothermic and so generate heat. Because the interaction between kinetics, heat and mass transfer are complex, researchers often regard devolatilization as a receding interface. In this model the interfaces of drying and pyrolysis recede into the particle as the local temperature rises (Babu & Chaurasia, 2004; Fantozzi, et al., 2007b).

Mass transfer by diffusion can be described as the transfer of a substance from a region of high concentration to a region of low concentration. Mass transfer can also occur by fluid flow where the driving force is the pressure gradient between the volatiles in the particle and the atmosphere outside of the particle. In the pyrolysis system, mass transfer occurs as a result of solid biomass being heated and reactions taking place which results in the formation of tar, biochar and gas.

2.6.3 Single Particle

Within a particle, mass, velocity of gases, and energy conservation are important factors when developing a model. In the particle, heating occurs by conduction and convection, as well as convection and radiation between the particle and the hot gas. The gas flow is in the

opposite direction to the heat flow. Figure 2.8 is a schematic diagram showing the heat and mass transfer within a particle (Bezanson, n.d.).

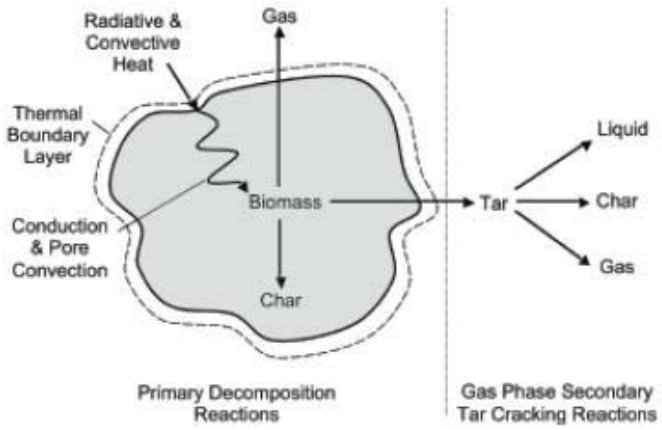

Figure 2.8: Pyrolysis of a biomass particle

2.6.4 Bed of Particles

For a bed of particles, the same principles apply as for a single particle where heat transfer is by conduction, convection and radiation. The relative importance of each of these depends on the amount of gas and volatile evolution. When the temperature is below ~280 °C there is little vapour evolution and therefore conduction is relatively important. Once vapour begins to evolve, its transport carries heat by convection resulting in faster heat transfer.

There is a more gaseous space in a bed as opposed to a single particle. In order to improve the mass transfer, a potential solution is to draw the gases off so that the mass and heat transfer through the bed are in the same direction, both carrying heat from the hot zone to cooler zones.

2.7 Reactors

Charcoal production dates back at least 30,000 years. The stages of pyrolysis were identified by the colour of the smoke emitted with drying producing a white smoke, pyrolysis a yellow smoke and the process concluding when blue smoke is emitted.

Pit kilns have been used in traditional charcoal making, with the sole purpose of producing charcoal. This process works by lighting a small fire which ignites the rest of the wood; this is

then covered to restrict air flow. The disadvantages of this simple process are that charcoal yields are low, requires constant monitoring, has no controls over emissions and produces an inconsistent product in terms of quality. Mound kilns employ the same process; however the wood is pyrolysed above the ground. This is typically because of hard soil or surface saturation.

Developments to the process occurred by constructing kilns with brick providing better heat insulation. Three openings were added, one for allowing air for initiating the fire which was then covered up, and a second for allowing the charcoal to be removed and finally a discharge point for the smoke. Vents were also located around the base of the kiln for air control. A metal kiln was developed which improved control of air into and gas out of the kiln, improved yields and emission reduced through the addition of an afterburner.

The Missouri Kiln has a capacity of almost 200 m^3 of feedstock. This kiln is commonly rectangular in shape and has several chimneys protruding from the roof. The yield and quality of charcoal produced is reported to be higher than other traditional methods, which may be due to better thermal insulation. Larger feedstock material can be used. A downside is there is little control over emissions with this batch process, even though an after burner is employed, as gases are evolving at variable rates in an unsteady state process.

In the hope of producing a more energy efficient process with higher yields a continuous multiple hearth kiln was developed. This system works by the feedstock material entering through the top of the kiln and passing through the various hearths by a rotating shaft where the feedstock is dried, combusted and then cooled to produce the charcoal product. Emissions can be significantly reduced in this process, but it also allows for the recovery of some volatile organic compounds by distillation.

The main problem with the traditional kilns discussed above is pollution caused by the burning of biomass. Also the systems are relatively inefficient with great variation in yields. Now that we are aware of the effects of pollution on the environment it is important to mitigate these effects and produce biochar in a way that is sustainable and renewable (Blackwell, et al., 2009).

Advances have led to newer classifications of the systems that produce biochar, syngas and tar. Kilns are used in traditional charcoal making. Retorts and converters are industrial reactors that are capable of recovering and refining not only the biochar but also products from volatile fraction (liquid condensates and syngases). More specifically, a retort refers to a reactor that has the ability to pyrolyse pile-wood, or wood logs over 30 cm long and over 18 cm in diameter and converters are used to produce biochar by carbonising small particles of biomass such as chipped or pelletised wood (Garcia-Perez et al., 2011).

2.8 Heat Source

Fuels can come in all three states: solid, liquid and gaseous. The most common solid fuel is coal and has been used as a heating source for many centuries, predominantly for cooking. The calorific value varied greatly and is dependent on the combustion process and type of coal. The main disadvantage of coal is that is it not an environmentally friendly fuel as it has high carbon dioxide emissions.

Liquid fuels are the most commonly used form for industrial applications and include fuels such as diesel oil, kerosene and furnace oil. Diesel fuel, for example, is derived from crude oil by fractional distillation. This has a calorific value of 43.1 MJ kg^{-1} which is slightly lower than liquid petroleum gas (LPG).

LPG is the most widely used heating source in New Zealand and is produced by refining natural gas. It is comprised of a combination of propane, butane and other hydrocarbon gases and hence is highly flammable. The calorific value of LPG is 46.3 MJ kg^{-1}(Snow, 2002). LPG produces less greenhouse gases than other fossil fuels as it burns more cleanly. Methane is the other significant gas fuel source found in the environment and is the main constituent of natural gas.

In order for biochar to be accepted for all its potential benefits, it must be produced in a sustainable and economically viable way. Therefore, as LPG is readily available and produces less emissions than other fuel sources, it seems as if it is the most practical option for the fuel source to combust the biomass.

The system can be heated directly, indirectly or via an auto-thermal process in which the biomass is combusted with air so that little or no additional fuel is needed after the initiation stage as enough energy is provided from the initial combustion. This process hence reduces the biochar yield as a portion has been used as the fuel source.

Indirect heating is where an external heating source is used to transfer heat through the pyrolyser walls. The reactor is completely sealed creating an oxygen free environment.

2.9 Wood

2.9.1 Properties

The pyrolyser designed in this work is for biomass residues from farms, crops or orchards. Wood is imperative in today's world not only because of the diverse applications but also as it is a renewable natural resource.

Wood is unique in the sense that no two pieces are alike. Wood has many important factors that are classed into either mechanical (elastic, strength) or physical (density, moisture content) properties that affect how combustion of biomass occurs. Wood is an anisotropic, hygroscopic material comprised of heartwood and sapwood. The moisture content for softwoods is higher in sapwood than heartwood; however there is not a significant difference for hardwoods.

The lower calorific value (LCV) for pine wood is 19 MJ kg^{-1} (Mansilla et al., 1991). That means when 1 kg of wood is combusted, 19 MJ of energy is released. The LCV refers to the water component being in the vapour state at the end of combustion as opposed to the higher calorific value (HCV) which assumes the water is in the liquid state.

The thermal conductivity is based on a temperature gradient. Wood has a low thermal conductivity (0.12 W m^{-1} K^{-1} at 25% moisture content) which means the rate of heat transfer per unit area is slow.

Wood is a complex structure of cells and fibres. It is much stronger in the longitudinal direction and has a greater resistance to loads than across the grain (Arntzen, 1994). The relative (specific) density is the density of a substance relative to the density of water. This parameter provides an indication of the woods strength. Strength is also affected by temperature and decreases with increasing temperature as the wood is degraded and weight is lost.

The density of wood varies greatly between species because of several factors. The cell walls differ in size and type, the moisture content and organic content also vary as well as the environmental conditions. Pine wood has a dry basis density of 450 kg m^{-3} (Di Blasi et al., 2001).

The biomass feedstock typically used in pyrolysis is wood. Wood is an anisotropic material with the grain and growth rings affecting the properties in the radial, axial and longitudinal directions. Wood is stronger in the longitudinal direction, across the grain. This results in the thermal conductivity as well as the fraction of the permeability to gas flow being much higher along the grain as opposed to across the grain (Di Blasi, 2008; Roberts, 1971). As the temperature of the wood increases, fissures or cracks begin to develop. The volatiles then flow into these cracks as they take the path with the least resistance.

2.9.2 Water

Water is an important aspect of drying wood. In wood, water is present in three forms: free water, bound water and water vapour. At the fibre saturation point, there is only bound water in the cell walls and no free water. Water movement in wood occurs via bound water and

water vapour (Kang et al., 2008) and the rate is controlled by pores in the pit membrane (Kang, et al., 2008; Petty & Preston, 1969).

Water is a highly polar substance and the term bound water refers to water chemically bound to cellulose molecules. Bound water is located in the cell walls.

2.10 Materials of Construction

For the pyrolyser construction, a corrosion resistant material is required due to the tarry compounds. Stainless steel is commonly used in the chemical industry and there are wide ranges available. Sinnott (1999) suggests in order for a material to be corrosion resistant it must contain of minimum of 12 % chromium. The higher this value, the more resistant the alloy is to corrosion in oxidising conditions. There are three main categories of stainless steel which are based on their microstructure. They are Ferritic, Austenitic and Martensitic. The type most suited to withstand the effects of pyrolysis is Austenitic which contains high levels of chromium and Nickel, about 20 % and 7 % respectively. Stainless steel is a widely used austenitic material. Stainless steel 316 is more resistant to corrosion and has a greater strength at elevated temperatures due to the addition of molybdenum and makes it a suitable material for the high temperatures of pyrolysis.

2.11 Summary

1. Biochar is produced by the thermal degradation of biomass in the absence of oxygen in a process known as pyrolysis.

2. Biochar is defined by its function as a soil amendment. Biochar has the potential to sequester carbon and improve soil functions.

3. This project employed slow pyrolysis as this enables the greatest char yield. Larger particles were used, which allows longer vapour phase residence times which results in secondary char formation. Slow pyrolysis employs temperatures of up to 700 °C with a heating rate of around 5 °C/min.

4. The properties of biochar are affected by factors including temperature, heating rate, moisture content, vapour residence time and pressure.

5. The reaction kinetics are still not well understood despite numerous models being developed.

6. In order to produce biochar of a consistent quality, the mass and heat transfer limitations need to be understood and the pyrolyser designed in such a way to control these effects.

7. Charcoal production has dated back many years, however there has been little control over the emissions from these processes, and hence it is imperative nowadays to reduce the impact of global warming and produce biochar in a sustainable way.

8. LPG is a commonly used fuel for heating, and has a high calorific value which makes it a suitable heating source for biochar manufacture.

9. Wood is a renewable resource and the biomass residue from the agricultural industry provides a suitable raw material for biochar production.

2.12 Aims

1. To design an ‘open source’ pyrolyser that is as self-sustaining as possible, safe and easy to operate. The pyrolyser will be constructed by an external fabrication company.

2. To produce biochar using various operating conditions and to characterise the resulting samples.

3. To produce a detailed thesis documenting the design, construction and characterisation phases of the project.

3.0 PYROLYSER DESIGN CRITERIA

3.1 Overview

Biochar is charcoal made from sustainably produced biomass which is then put in the soil. It is a stable compound which has the potential to sequester carbon. This stability is due to its highly aromatic nature with unordered graphite layers. However it is known that biochar's properties also depend on many factors including temperature during combustion and feedstock type which results in variation in its stability in the soil (Blackwell, et al., 2009). Once in the soil, biochar is also reputed to improve a range of soil functions including increasing plant productivity, reducing soil acidity and reducing nutrient leaching.

The objectives of this project were to investigate, design and construct an 'open source' pyrolyser for biochar manufacture where open source refers to the design and characterisation details being made publically available. The pyrolyser will utilise locally available materials and employ local engineering fabrication companies.

As the main focus is biochar, the mode of operation will be slow pyrolysis which enables a greater yield of carbon to be obtained compared to fast pyrolysis. The pyrolyser will be designed to operate at temperatures between 300-700 °C.

This pyrolyser was aimed at a lifestyle block owner who generates small amounts of biomass residue. Therefore, the capacity must be between 100-200 kg/day feedstock input, considering a farmer is unlikely to want to spend longer than one hour loading the pyrolyser. However, the size is also a constraint in terms of the budget for this project. As the pyrolyser will be operated in New Zealand, the design is based on situations that occur in New Zealand but it is intended this can also apply to developed countries and rural property owners.

The pyrolyser performance had to comply with performance standards from the International Biochar Initiative (IBI), which are currently under development and also NZ, EU and US standards.

It was intended for this system to be as self-regulated as possible and to recycle energy to reduce the process costs. This design was anticipated to be scalable so it can be suited to an individual's circumstances. The following sections will detail and justify the design specifications for the open source pyrolyser. This was based around heat and mass transfer limitations, rather than the reaction kinetics.

3.2 Batch versus Continuous Pyrolysis

A batch pyrolyser is simply a reactor in which the entire feedstock is placed into and is subsequently pyrolysed by an external or internal heat source. In comparison a continuous pyrolyser requires the feedstock introduced gradually via a mechanical system.

Although there are many advantages and disadvantages to both continuous and batch operations, batch has been selected for the reasons stated below.

a) Pyrolysis is a process that occurs in the absence of oxygen and so it is important that the system is air locked. For a batch process, this is simply a matter of preventing air ingress during the pyrolysis phase of heating. As the loading and unloading operations can be completed before and after pyrolysis, these operations do not have to be sealed against the air. In contrast, continuous processes require effective airlocks at the feed input and char outlet which are more costly to design and must include a range of safety features to monitor their operating effectiveness.

b) Endpoint detection is required in order to determine when pyrolysis has finished. This can be done by monitoring the off-gas quantity and or composition. In a continuous pyrolyser, gases evolve along the whole heating profile meaning gas flow and mixture composition are at constant steady state levels. This means that more sophisticated monitoring composition systems are needed at the temperature soak phase of the process.

c) A disadvantage of batch pyrolysis is that it is more difficult to recycle energy, but this is discussed below in section 3.6.

d) Simplicity of operation is essential for a lifestyle block owner. They are generally busy people with their time divided between many activities. Therefore, a simple operating procedure was developed to minimise the decisions that need to be made, also to ensure it was easy to operate, had clear on-off functions and could be left unattended. These ‘simplicity’ criteria were easier to design around a batch process. A continuous process is more complex, requiring precise measurement and control, and it needs more redundancy. Therefore, for this purpose, a batch system was more appropriate and was designed.

3.3 Particle Size and Loading/Unloading

Even though batch pyrolysers are able to use a larger range of feed stocks, the nature of feedstock supply needs to be considered in the context of the lifestyle block owner. It is expected that a typical lifestyle block will have a range of biomass residue. Typically, large wood will preferentially be used for firewood as this is the principle form of heating in rural

New Zealand. Leaves and vegetative material would make mulch or be left to decay in the natural environment. In terms of pyrolysis, this matter would need to be removed because it inhibits good air and gas flow. The unaccounted material is branches, which would be suitable for charring. Large particles result in mass and heat transfer limitations; hence it is proposed the branches are put through a chipper prior to loading the pyrolyser as a cheap and suitable alternative. To reduce the impacts of mass and heat transfer, agitation of the feedstock is desired. However a chipper is not essential, therefore this system was designed for either branches or chipped wood.

3.4 Start-up

Compared to a continuous pyrolyser, a batch pyrolyser has the disadvantage of requiring more energy during start-up. This is because a larger mass of material needs to be heated before it can become self-sustaining whereas, in a continuous process, material is heated as it passes through the unit meaning that only a small amount is heated at any point in time; thus, heat can be recycled more efficiently. Also, because the heat-up time in a continuous process must be relatively quick, both small particle sizes are required and the dimensions of the heating chamber must be small (e.g. an auger) in order to ensure the distance between heat source and particles is at a minimum.

3.5 Drying

Water drying is an energy cost to the process. Because water removal occurs during the heating phase (mostly between 80-140 °C) the energy cost is incurred before any pyrolysis gases are formed. This fact requires careful design of the pyrolysis process so that some of the biomass is heated quickly to pyrolysis conditions to supply pyrolysis gases that can be used to drive the moisture from the remaining biomass and heat it to pyrolysis temperature (ca. 300 °C). Clearly, the energy balance of the process is more favourable if the biomass is pre-dried. This project considered the benefits of using excess heat from combustion of the pyrolysis gases to pre-dry the next batch of biomass. Doing this optimises the usefulness of the available heat. However, this should not introduce added complexity such as double-handling of biomass.

3.6 Energy Efficiency

Energy efficiency can be measured in a number of ways to relate the thermodynamic energy available and its conversion to the actual obtained. An efficiency measure was devised in this project, but, batch processes will perform worse than continuous systems due to the energy cost of the initial heating and final cooling steps. The performance gap will be less if pre-drying of the next batch is included.

3.7 Non-thermal Energy Requirements

There is less need for external energy sources in a batch operation as there are less motive components. While mains electricity or batteries may be used for the monitoring devices, if agitation or a chipper is used for feedstock preparation then electricity or a petrol/diesel driven drive will be required. A continuous process requires motive components for feed, discharge and passage through the pyrolyser and potentially sophisticated systems to ensure airlocks.

It is possible that the excess pyrolysis gas be used to generate electricity with a conversion efficiency of around 30 %. However, this was not considered here because it greatly increases the complexity and cost of the process. In addition, in order to avoid shortening the operating life of the electrical generator, the pyrolysis gases would need to be upgraded through a gasification and cleaning process. These sorts of improvements can be considered at large industrial scale, but not here.

3.8 Running Costs

The target user is a lifestyle block owner, who has little time available. The user will fill the unit over about 1 hour and then turn it on, leaving it to operate remotely while they attend to other property business. The labour component will be restricted to filling and emptying.

The cost of operating the plant must be at a minimum. Batch operation is simple for all the reasons outlined above, particularly that the pyrolysis is contained in a sealed retort without the possibility of air ingress, and the reactions go to completion of their own accord. After cooling the charcoal can be removed as a stable material, although it does benefit from conditioning in the open air to allow the (exothermic) adsorption of oxygen onto the char surfaces. This conditioning step is important for sawdust charcoals because once stockpiled, the pile becomes a very good insulator. This can be got around by wetting the charcoal.

The principal operating cost of a batch operation will be an external heating source for start-up, and to maintain a flare. LPG is the most readily available fuel in New Zealand, although a diesel burner could also be used. Monitoring equipment will also require an electrical connection or batteries. If the latter, then backup batteries will also be required.

3.9 Cleaning

Tar is a particularly obnoxious substance with a high viscosity. It can cause blockages if allowed to cool in pipelines and can set as hard as bitumen. It is also highly corrosive with a pH of 2-3; therefore all pipework, vessels, and gaskets must be acid resistant (Oasmaa et al., 2005). To avoid tar deposition, the transit path of the tar must also be kept hot to keep it volatile until it is combusted.

A batch operation is less complicated than a continuous operation and therefore should be easier to clean if this is required.

3.10 Safety

As in any operation, safety is always of paramount importance. Specifically for this pyrolyser, it must be safe to be operated in a research environment (by students), in a farm environment (by farmers and for other people on the farm), or forestry users. It must be fire safe, explosion safe, and have environmental carbon monoxide (CO) monitors. More importantly the emissions would need to be controlled, and comply with New Zealand, European and US regulations. Other safety factors include ensuring no sparks, no exposure to excessive heat, and preventing excessive gas build-up.

For the proposed design, a negative system pressure is desired for safety reasons. We do not want flammable gases leaking out. The simplest way is to ensure the stack is sufficiently high to create a natural draft to draw off the combustion gases, thus creating a slightly negative pressure in the pyrolysis chamber, but not too great that the char yield is affected.

4.0 MATHEMATICAL MODELLING OF THE PYROLYSIS REACTION

4.1 Introduction

The main aim of this project was to design a pyrolyser for biochar production and to characterise biochar produced under different operating conditions. Therefore it is important to produce a consistent biochar with consistent properties so that its effects as a soil amendment can be determined. For this to occur, heat and mass transfer limitations need to be minimised. Mathematical modelling has been identified as an effective tool to understand and predict the proportions of products produced and the time taken to achieve complete pyrolysis.

Devolatisation reactions are complex. Several simplified models have been developed to describe the reaction pathway and how different operating conditions can be used to maximise product yields. For this model, a simple approach has also been taken to provide information and guidelines for design purposes.

Charcoal production has been about for centuries; however heat and mass transfer processes are less well understood. In the pyrolysis process, biomass is converted to tar, char and gas. It involves heating biomass using an external source, conduction of heat through the wood, reactions generating heat, convection of the volatiles, condensation of the volatiles and evaporation of water.

To provide additional design information, it was decided to develop a mathematical model describing heat and mass transfer through a cylindrical drum with a hollow core.

4.2 Model Objectives

This model was developed as a simulation tool capable of predicting the temperature profile, moisture content, reactions kinetics and proportions of the products (tar, char and gas) as a function of time and position during the pyrolysis process.

The model is intended to:

- Predict the time-temperature profile across the bed
- Understand how moisture content affects the energy balance of pyrolysis

The outcome is to determine the consistency of the temperature-position-time profile across the pyrolyser because it is believed that the peak temperature reached and the soak temperature (the temperature at which the char is held for a period of time) together determine the char properties.

4.3 Conceptual Model Development

Figure 4.1 shows the model system which is a semi-infinite cylinder of wood chips with a hollow core.

Heat and mass is transferred through a slice of the reactor which is assumed to be a continuous homogeneous porous material, in this case pine wood. At start-up, the heat source is provided by LPG and the heat enters through the sides of the cylindrical reactor. The radiation from the LPG gases transferred heat to the surface of the metal. The metal then radiates heat to the first slice of wood which is absorbed by the wood, hence resulting in the biomass heating up. Heat is also conducted into the slice and subsequently out of the slice, driven by the temperature gradient. The rate at which heat travels through a slice is given by the porous materials thermal conductivity.

Once the temperature of a slice reaches 100 °C evaporation (conversion of water from a liquid to a vapour) begins to occur. In reality, water vapour will evolve at its saturated vapour pressure depending on the temperature of the slice. This is simplified in the model to occur only at 100 °C.

As the wood temperature increases above 200 °C, decomposition reactions occur generating gas, tar and char. The volatiles move through the system by convection (although this is not modelled), transferring mass at a rate established by the rate of production of gas and tar volatiles which are produced by the Arrhenius kinetics developed by Fantozzi (2007). As the gas moves into cooler slices, sensible heat is transferred. Tar also loses some sensible heat plus additional latent heat as some or all volatiles condense.

There is no metal interface depicted in this model due to the assumption below that the heat transfer resistance of the metal is negligible.

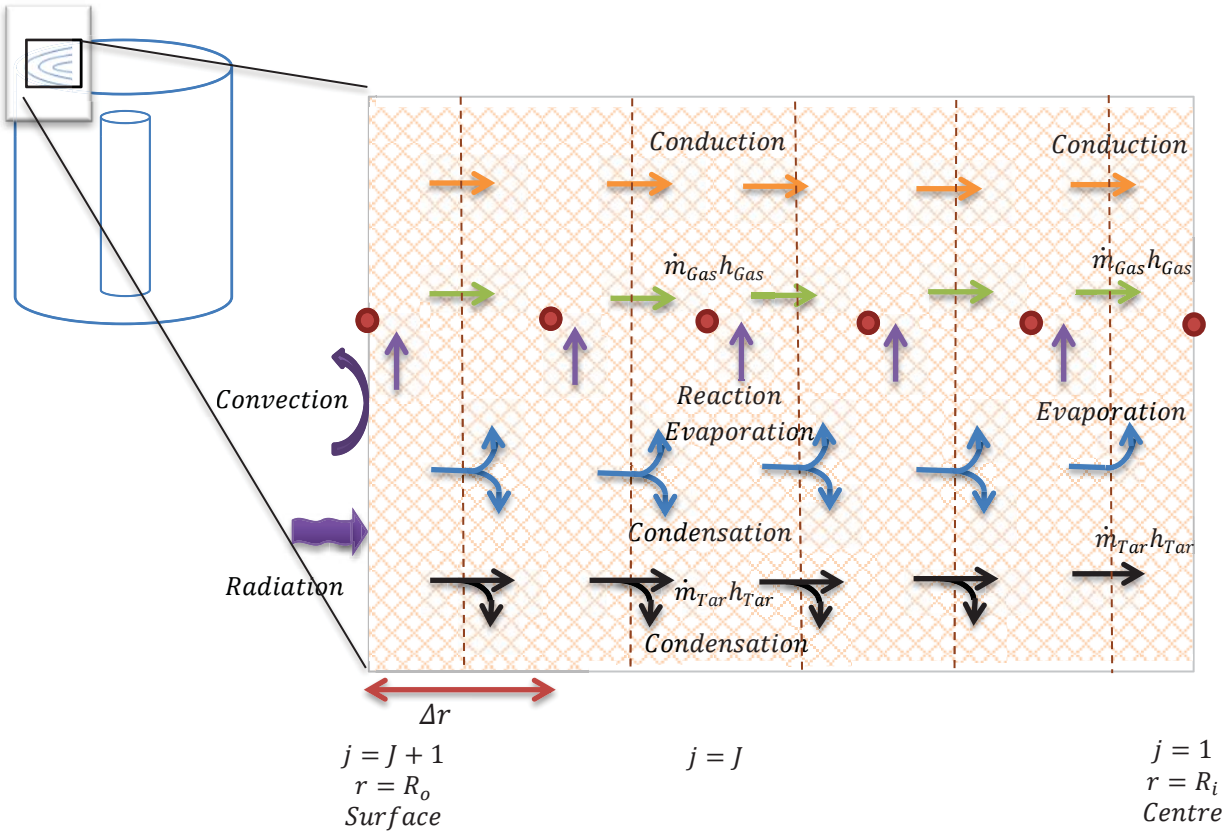

Figure 4.1: Conceptual diagram showing the heat and mass transfer considered in this model as an expansion from the reactor

4.4 Assumptions

The model equations were developed with the following assumptions:

- One-dimensional heat transfer from the sides of a cylindrical reactor. The reactor is assumed to be infinitely long. As a result it can be assumed that heat and mass transfer takes place only in the horizontal direction and hence can be considered as one-dimensional.
- There is axial symmetry which means heating from all sides is equal.
- It is assumed the thermo-physical properties such as heat capacity, thermal conductivity and density change as a function of temperature. Chemical properties refer to a change in the materials properties or structures as a result of a chemical reaction. Examples of chemical properties include heat of combustion and enthalpy of formation.
- This model has radiation to the metal surface of the reactor and convection of the heat source (LPG) gases to the metal. There will be a temperature gradient across the steel wall; however the thermal conductivity of steel is high and the wall is sufficiently thin so the heat transfer resistance of steel was considered negligible. Therefore, the radiation equation used the properties of metal, but the surface node is of the wood and not the metal.

- Reactions are based on the model proposed by Fantozzi (2007). The equilibrium constants of the primary reactions are expressed with an Arrhenius correlation. No secondary reactions occur in this model as the proportion of final products is not significantly impacted by these reactions.
- The rate of evaporation below 100 ° C is low so no evaporation occurs until the temperature reaches 100 ° C. In reality, water vapour will evolve at its saturated vapour pressure depending on the temperature of the slice.
- All vapours that evolve and enter the slice leave the slice at the end of the time step and travel towards the centre. The interstitial space between the particles is assumed at atmospheric pressure. Hence, there is no pressure gradient across the bed. The model assumes no mass transfer resistance.
- Radiative heat transfer occurring at the surface is much higher than the radiative heat transfer occurring within the bed, although radiation in the bed does become significant at higher temperature. For model simplification, radiant heat transfer in the bed is assumed negligible.
- Water is present in three forms in wood: liquid (water from the lumen), bound (water contained within the cell wall) or vapour. The fibre saturation point is reached at around 30% moisture content and at this point all free water is removed and only bound water remains.
  The initial moisture content of the wood depends on how much free water is present in the wood. For simplification of the model, only liquid (free) water is assumed to be present and hence diffusion of water is not modelled in this system and no extra energy is required to remove the bound water.
- Particle shrinkage is not considered. This occurs when bound water leaves the cell walls, altering the woods dimensions and only occurs when the fibre saturation point reaches 30% moisture content. Further shrinkage occurs during thermal decomposition of the wood to char.
- There is no temperature gradient at the core.
- As solids and liquids are denser than gas, we do not consider the accumulation of the gas in the slice, but are interested in the heat that it transfers as it traverses a slice.

4.5 Model Formulation

The model has three independent variables: time, temperature and position. To account for simultaneous changes the heat and mass balances were formulated in the form of partial differential equations (PDEs). The symbols used in this section are defined in the nomenclature which is located in Appendix A.

4.5.1 Heat Transfer Across the Boundary

A word balance was used to describe the heat transfer from the heat source to the wall and into the first slice at the boundary. Conduction into the slice is assumed negligible as the heat from radiation and convection will dominate at the surface.

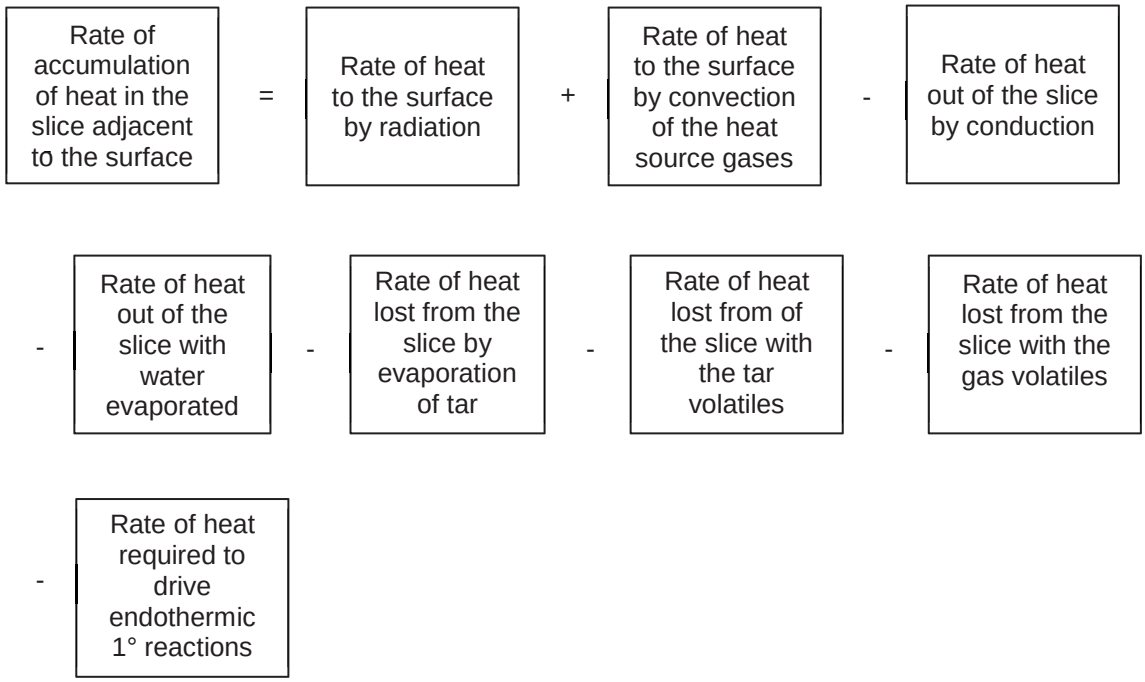

Heat is transferred from the heat source to the surface by radiation and convection. Kirchhoff's law was used to describe the radiative heat transfer and Newton's law was used to describe the convective heat transfer. These laws were used to produce the equations below.

$$\frac{d\left(m_B C_{p\,B} + m_w C_{p\,w} + m_{gas} C_{p\,gas} + m_{tar} C_{p\,tar} + m_{char} C_{p\,char}\right)\theta j}{dt}$$
$$= \sigma A_{LHS}\left(\varepsilon_{wall}(T_a + 273.15)^4 - \alpha_{int}\left(T_j + 273.15\right)^4\right)$$
$$+ h_c A_{LHS}\left(\theta_a - \theta_j\right) - kA_{RHS}\frac{\left(\theta_j - \theta_{j-1}\right)}{\Delta r} - \dot{m}_w(j)h_{fg}$$
$$- \dot{m}_{tar}(j)h_{fg\,tar} - m_B(j)k_{tar}h_{tar} - m_B(j)k_{gas}h_{gas}$$
$$- \left(k_{gas} + k_{tar} + k_{char}\right)m_B(j)h_R \qquad (4.1)$$

for *R=Ro*
t>0

4.5.2 Heat Transfer within the Wood

In all slices away from the outer wall, water vapour, tar and gas both enter and leave the slice. As they enter, water vapour and tar may condense and transfer latent heat to the slice, or cool as they transfer sensible heat.

The equation shows the thermal conductivity is a function of temperature. A word balance was developed to show the modes of heat transfer within a slice of wood.

It should be noted that only endothermic reactions are modelled. This is for the purpose of simplicity, but it should also approximate the actual heat flow below about 300 °C because exothermic reactions begin above this. If, when characterising the reactor performance, the heat flow departs significantly from this model prediction, then it is recommended that a predictive model includes the exothermic component.

Fourier's law was used to define conductive heat transfer for one-dimensional heat transfer through a cylinder.

Rate of accumulation of heat in the slice = Rate of heat into the slice by conduction - Rate of heat out of the slice by conduction - Rate of heat required to drive endothermic 1° reactions - Rate of heat lost from the slice by water vapour leaving the slice + Rate of heat gained in the slice by condensation of water vapour + Rate of heat gained by sensible cooling of water vapour that passes through the slice - Rate of heat lost from the slice by the tar leaving the slice ± Rate of heat gained or lost in the slice by evaporation or condensation of tar + Rate of heat gained by sensible cooling of tar volatiles that pass through the slice + Rate of heat gained by sensible cooling of gases volatiles that pass through the slice - Rate of heat lost from the slice by the gas leaving the slice

Converting to an equation yields

$$\begin{aligned}\frac{d\left(m_B C_{p\,B} + m_w C_{p\,w} + m_{gas} C_{p\,gas} + m_{tar} C_{p\,tar} + m_{char} C_{p\,char}\right)\theta_j}{dt} &= kA_{LHS}\frac{(\theta_{j+1} - \theta_j)}{\Delta r} - kA_{RHS}\frac{(\theta_j - \theta_{j-1})}{\Delta r} \\ &- \left(k_{gas} + k_{tar} + k_{char}\right)m_B(j)h_R \pm \dot{m}_w(j)h_{fg\,w} \\ &- m_w(j)k_w C_{p\,w}(\theta_j - \theta_{j-1}) - k_{tar}m_B(j)\Delta h_{tar} \pm \dot{m}_{tar}(j)h_{fg\,tar} \\ &+ m_B(j)k_{tar}C_{p\,tar}(\theta_j - \theta_{j-1}) + m_B(j)k_{gas}C_{p\,gas}(\theta_j - \theta_{j-1}) \\ &- k_{gas}m_B(j)\Delta h_{gas}\end{aligned} \quad (4.2)$$

for $0<r<R$
$t>0$

4.5.3 Heat Transfer at the Centre

There is no heat accumulation at the perforated core centre. All mass flows and their associated heat flow leaves the slice adjacent to the central core and travels out of the system downwards to the combustion chamber. Therefore, there is no temperature gradient across this boundary and no heat balance is required.

4.5.4 Pyrolysis Primary Reaction Kinetics

The consumption of biomass is equal to the formation of gas, tar and char. The rate constants, k_{gas} k_{tar} and k_{char} are Arrhenius equations, which are dependent on temperature. These constants were obtained Fantozzi, et al., (2007b) and the definitions are located in the nomenclature section (Appendix A).

An overall equation for the consumption of biomass yields

$$\frac{dm_B}{dt} = -k_{gas}m_B(j) - k_{tar}m_B(j) - k_{char}m_B(j) \tag{4.3}$$

This simplifies to

$$\frac{dm_B}{dt} = -\left(k_{gas} + k_{tar} + k_{char}\right)m_B(j) \tag{4.4}$$

The rate of formation of gas is given by

$$\frac{dm_{gas}}{dt} = k_{gas}m_B(j) \tag{4.5}$$

The rate of formation of tar is given by

$$\frac{dm_{tar}}{dt} = k_{gas}m_B(j) \tag{4.6}$$

The rate of formation of char is given by

$$\frac{dm_{char}}{dt} = k_{char} m_B(j) \tag{4.7}$$

4.5.5 Heat Balance for Evaporation of Water

At low temperatures, water is the only species that moves across the reactor. Thus, the overall heat balance from equation 4.5.2 can be reduced to the scenario for temperatures less than 200 °C, below which pyrolysis reactions are insignificant.

Rate of accumulation of heat into the slice	=	Rate of heat into the slice by conduction	-	Rate of heat out of the slice by conduction	-	Rate of heat loss from the slice by water evaporation

+ Rate of heat gain into the slice by water condensation

Converting to an equation yields

$$\frac{d\left(m_B C_{p\,B} + m_w C_{p\,w}\right)\theta_j}{dt} = kA_{LHS}\frac{\left(\theta_{j+1} - \theta_j\right)}{\Delta r} - kA_{RHS}\frac{\left(\theta_j - \theta_{j-1}\right)}{\Delta r} \pm \dot{m}_w(j) h_{fg\,w} \tag{4.8}$$

The associated mass balance is therefore

Rate of accumulation of mass into the slice	=	Rate of mass into the slice by water condensation	-	Rate of mass out of the slice by water evaporation

Assuming the heat leaving the slice is due to conduction only, the mass balance is

$$\frac{d(m_B + m_w)}{dt} = \pm \dot{m}_w(j) \tag{4.9}$$

4.6 Finite Difference Solution

The model formulation described in the previous section contains several algebraic equations and PDE's which make an analytical solution difficult as it involves complex math. Therefore, a numerical method for solving the problem was decided upon.

There are several techniques available to solve a numerical problem which contains partial differential equations. These include finite difference, finite elements and collocation. A finite difference solution was chosen to solve this model because it is a relatively simple and reliable method.

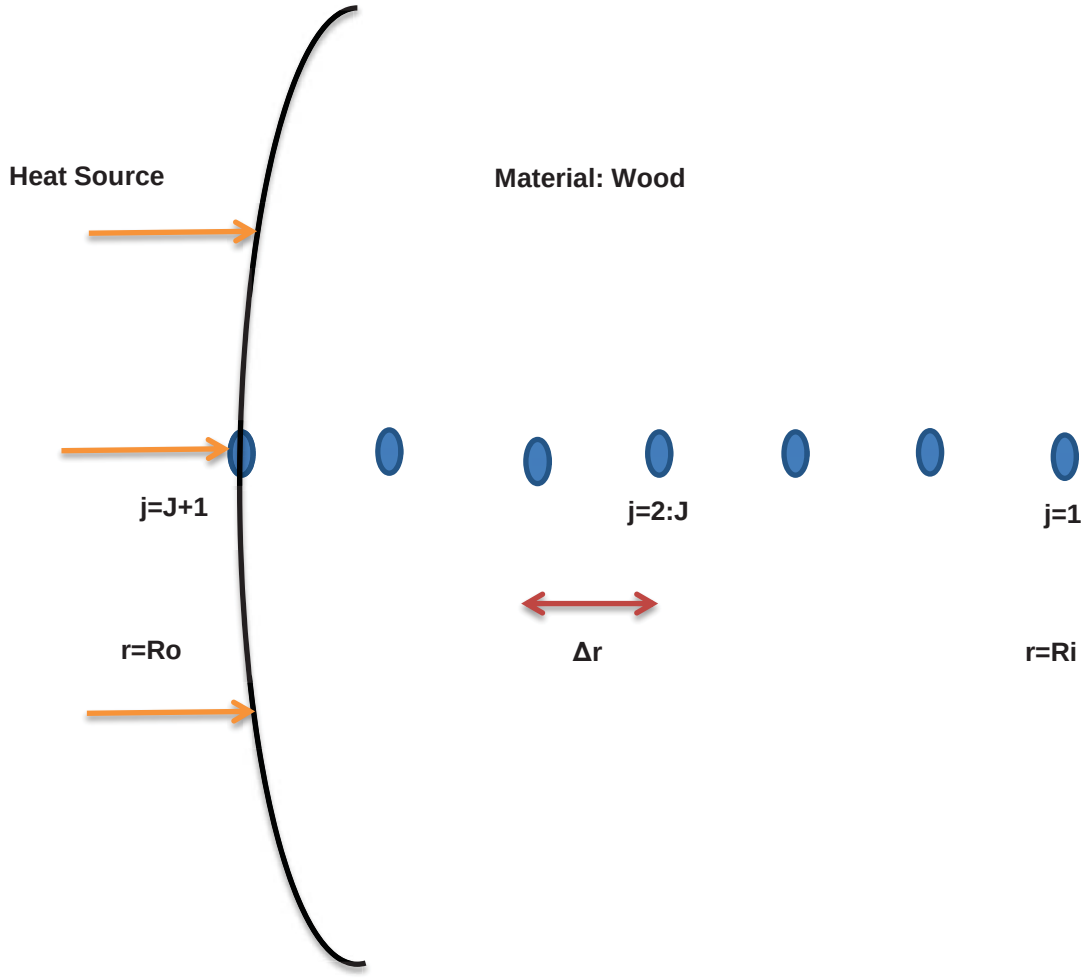

Figure 4.2: The finite difference grid used for pyrolysis

A finite difference grid was developed to describe the heat and mass transfer occurring in the nodes. The nodes are at a constant distance apart defined by delta r which is a function of the number of nodes present.

4.6.1 For the surface of the reactor

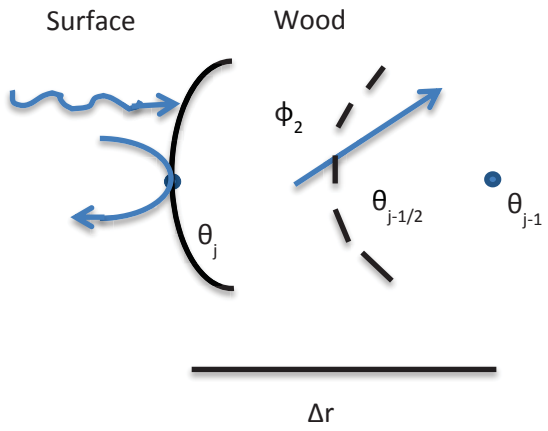

The heat balance for j=J+1 was approximated by

$$\frac{d\left(m_B C_{p\,B} + m_w C_{p\,w} + m_{gas} C_{p\,gas} + m_{tar} C_{p\,tar} + m_{char} C_{p\,char}\right)\theta_j}{dt}$$
$$= \sigma A_{LHS}\left(\varepsilon_{wall}(T_a + 273.15)^4 - \alpha_{int}\left(T_j + 273.15\right)^4\right)$$
$$+ h_c A_{LHS}\left(\theta_a - \theta_j\right) - kA_{RHS}\frac{\left(\theta_j - \theta_{j-1}\right)}{\Delta r} - \dot{m}_w(j) h_{fg}$$
$$- \dot{m}_{tar}(j) h_{fg\,tar} - m_B(j) k_{tar} h_{tar} - m_B(j) k_{gas} h_{gas}$$
$$- \left(k_{gas} + k_{tar} + k_{char}\right) m_B(j) h_R$$

The mass of biomass, gas, tar and char change when the temperature exceeds 200 °C as decomposition reactions begin to occur. As two variables, mass and temperature are changing with respect to time, the product rule needs to be applied to solve the problem. The product rule is

$$\frac{dxy}{dt} = y\frac{dx}{dt} + x\frac{dy}{dt}$$

Applying the product rule to the LHS of the equation gives

$$\frac{d\left(m_B C_{p\,B}\right)\theta_j}{dt} + \frac{d\left(m_W C_{p\,W}\right)\theta_j}{dt} + \frac{d\left(m_{char} C_{p\,char}\right)\theta_j}{dt} = RHS\ of\ equation$$

Expanding gives

$$C_{p\,B}\left(m_B\frac{d\theta}{dt}+\theta\frac{dm_B}{dt}\right)+C_{p\,W}\left(m_w\frac{d\theta}{dt}+\theta\frac{dm_w}{dt}\right)+C_{p\,gas}\left(m_{gas}\frac{d\theta}{dt}+\theta\frac{dm_{gas}}{dt}\right)$$
$$+C_{p\,tar}\left(m_{tar}\frac{d\theta}{dt}+\theta\frac{dm_{tar}}{dt}\right)=+C_{p\,char}\left(m_{char}\frac{d\theta}{dt}+\theta\frac{dm_{char}}{dt}\right)=$$
$$=RHS\ of\ equation$$

Simplifying

$$\left(m_BC_{p\,B}+m_wC_{p\,w}+m_{gas}C_{p\,gas}+m_{tar}C_{p\,tar}+m_{char}C_{p\,char}\right)\frac{d\theta}{dt}$$
$$+\left(C_{p\,B}\frac{dm_B}{dt}+C_{p\,W}\frac{dm_w}{dt}+C_{p\,gas}\frac{dm_{gas}}{dt}+C_{p\,tar}\frac{dm_{tar}}{dt}+C_{p\,char}\frac{dm_{char}}{dt}\right)\theta$$
$$=RHS\ of\ equation$$

Substituting in the highlighted variables gives

$$\left(m_BC_{p\,B}+m_wC_{p\,w}+m_{gas}C_{p\,gas}+m_{tar}C_{p\,tar}+m_{char}C_{p\,char}\right)\frac{d\theta}{dt}$$
$$+\left(C_{p\,B}\left(-\left(k_{gas}+k_{tar}+k_{char}\right)m_B\right)+C_{p\,W}\dot{m}_W+C_{p\,gas}k_{gas}m_B+C_{p\,tar}k_{tar}m_B\right.$$
$$\left.+C_{p\,char}k_{char}m_B\right)\theta=RHS\ of\ equation$$

Adding in the RHS of equation gives

$$\left(m_BC_{p\,B}+m_wC_{p\,w}+m_{gas}C_{p\,gas}+m_{tar}C_{p\,tar}+m_{char}C_{p\,char}\right)\frac{d\theta}{dt}$$
$$+\left(C_{p\,B}\left(-\left(k_{gas}+k_{tar}+k_{char}\right)m_B\right)+C_{p\,W}\dot{m}_W+C_{p\,gas}k_{gas}m_B+C_{p\,tar}k_{tar}m_B\right.$$
$$\left.+C_{p\,char}k_{char}m_B\right)\theta$$
$$=\sigma A_{LHS}\left(\varepsilon_{wall}(T_a+273.15)^4-\alpha_{int}\left(T_j+273.15\right)^4\right)+h_cA_{LHS}\left(\theta_a-\theta_j\right)$$
$$-kA_{RHS}\frac{\left(\theta_j-\theta_{j-1}\right)}{\Delta r}-\dot{m}_w(j)h_{fg}-\dot{m}_{tar}(j)h_{fg\,tar}-m_B(j)k_{tar}h_{tar}$$
$$-m_B(j)k_{gas}h_{gas}-\left(k_{gas}+k_{tar}+k_{char}\right)m_B(j)h_R$$

Subtracting plus dividing through by the LHS of the equation

$$\frac{d\theta}{dt}=\frac{\begin{array}{c}\sigma A_{LHS}\left(\varepsilon_{wall}(T_a+273.15)^4-\alpha_{int}\left(T_j+273.15\right)^4\right)+h_cA_{LHS}\left(\theta_a-\theta_j\right)-kA_{RHS}\frac{\left(\theta_j-\theta_{j-1}\right)}{\Delta r}\\-\dot{m}_w(j)h_{fg}-\dot{m}_{tar}(j)h_{fg\,tar}-m_B(j)k_{tar}h_{tar}-m_B(j)k_{gas}h_{gas}\\-\left(k_{gas}+k_{tar}+k_{char}\right)m_B(j)h_R-\left(C_{p\,B}\left(-\left(k_{gas}+k_{tar}+k_{char}\right)m_B\right)\right.\\\left.+C_{p\,W}\dot{m}_W(j)+C_{p\,gas}k_{gas}m_B(j)+C_{p\,tar}k_{tar}m_B(j)+C_{p\,char}k_{char}m_B(j)\right)\theta\end{array}}{\left(m_BC_{p\,B}+m_wC_{p\,w}+m_{gas}C_{p\,gas}+m_{tar}C_{p\,tar}+m_{char}C_{p\,char}\right)}$$

4.6.2 For within the reactor

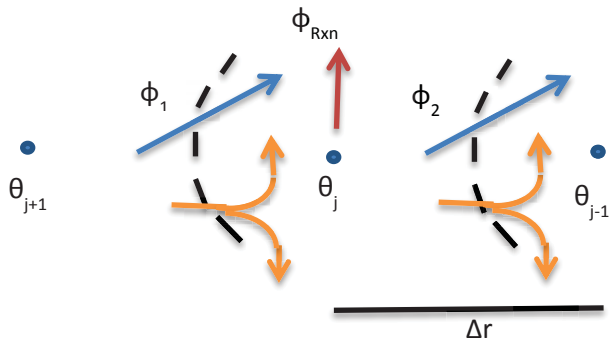

The heat balance for j=2:J was approximated by

$$\frac{d\left(m_B C_{p\,B} + m_w C_{p\,w} + m_{gas} C_{p\,gas} + m_{tar} C_{p\,tar} + m_{char} C_{p\,char}\right)\theta_j}{dt}$$
$$= kA_{LHS}\frac{(\theta_{j+1} - \theta_j)}{\Delta r} - kA_{RHS}\frac{(\theta_j - \theta_{j-1})}{\Delta r} - (k_{gas} + k_{tar} + k_{char})m_B(j)h_R$$
$$\pm \dot{m}_w(j)h_{fg\,w} - m_w(j)k_w C_{p\,w}(\theta_j - \theta_{j-1}) - k_{tar}m_B(j)\Delta h_{tar} \pm \dot{m}_{tar}h_{fg\,tar}$$
$$+ m_B k_{tar} C_{p\,tar}(\theta_j - \theta_{j-1}) + m_B k_{gas} C_{p\,gas}(\theta_j - \theta_{j-1}) - k_{gas}m_B(j)\Delta h_{gas}$$

Applying the product rule to the LHS of the equation, is the same as in section 4.6.1 and gives

$$\left(m_B C_{p\,B} + m_w C_{p\,w} + m_{gas} C_{p\,gas} + m_{tar} C_{p\,tar} + m_{char} C_{p\,char}\right)\frac{d\theta}{dt}$$
$$+ \left(C_{p\,B}\left(-(k_{gas} + k_{tar} + k_{char})m_B\right) + C_{p\,W}\dot{m}_W + C_{p\,gas}k_{gas}m_B + C_{p\,tar}k_{tar}m_B\right.$$
$$\left. + C_{p\,char}k_{char}m_B\right)\theta = RHS\ of\ equation$$

Adding in the RHS of equation gives

$$\left(m_B C_{p\,B} + m_w C_{p\,w} + m_{char} C_{p\,char}\right)\frac{d\theta}{dt}$$
$$+ \left(C_{p\,B}\left(-(k_{gas} + k_{tar} + k_{char})m_B\right) + C_{p\,W}\dot{m}_W + m_{gas}C_{p\,gas} + m_{tar}C_{p\,tar}\right.$$
$$\left. + C_{p\,char}k_{char}m_B\right)\theta$$
$$= kA_{LHS}\frac{(\theta_{j+1} - \theta_j)}{\Delta r} - kA_{RHS}\frac{(\theta_j - \theta_{j-1})}{\Delta r} - (k_{gas} + k_{tar} + k_{char})m_B(j)h_R$$
$$\pm \dot{m}_w(j)h_{fg\,w} - m_w(j)k_w C_{p\,w}(\theta_j - \theta_{j-1}) - k_{tar}m_B(j)\Delta h_{tar} \pm \dot{m}_{tar}h_{fg\,tar}$$
$$+ m_B k_{tar} C_{p\,tar}(\theta_j - \theta_{j-1}) + m_B k_{gas} C_{p\,gas}(\theta_j - \theta_{j-1}) - k_{gas}m_B(j)\Delta h_{gas}$$

Subtracting plus dividing through by the LHS of the equation

$$kA_{LHS}\frac{(\theta_{j+1}-\theta_j)}{\Delta r}-kA_{RHS}\frac{(\theta_j-\theta_{j-1})}{\Delta r}-(k_{gas}+k_{tar}+k_{char})m_B(j)h_R$$
$$\pm\dot{m}_w(j)h_{fg\,w}-m_w(j)k_wC_{p\,w}(\theta_j-\theta_{j-1})-k_{tar}m_B(j)\Delta h_{tar}\pm\dot{m}_{tar}h_{fg\,tar}$$
$$+m_Bk_{tar}C_{p\,tar}(\theta_j-\theta_{j-1})+m_Bk_{gas}C_{p\,gas}(\theta_j-\theta_{j-1})-k_{gas}m_B(j)\Delta h_{gas}$$

$$\frac{d\theta}{dt}=\frac{-\left(C_{p\,B}\left(-(k_{gas}+k_{tar}+k_{char})m_B\right)+C_{p\,w}\dot{m}_w++m_{gas}C_{p\,gas}+m_{tar}C_{p\,tar}+C_{p\,char}k_{char}m_B\right)\theta}{(m_BC_{p\,B}+m_wC_{p\,w}+m_{gas}C_{p\,gas}+m_{tar}C_{p\,tar}+m_{char}C_{p\,char})}$$

4.6.3 For the centre of the reactor

As previously stated, there is no temperature gradient across the core, so no finite difference solution was required.

4.7 Numerical Error Checking

In order to ensure that the right solution to the formulated model is obtained, model checking must be performed. There are two types of errors that may have been made:

1. Numerical solution errors
2. Algebraic or coding errors

In this section, the numerical solution errors were not checked because the model became unstable. The problem lies in the rate of change of variables at the interface of the vapour front and the pyrolysis front which require smaller and smaller time steps. This problem was not able to be overcome within the timeframe of the project. It remains as future work.

4.8 Mathematical Solution

A complete solution was not obtained during the timeframe of this project. The model was developed in stages and these are explained below, which go some way towards the solution. They show the expected trends although these have not been validated.

Heat transfer occurs by conduction through the wood, convection to the reactor surface, convection of gases in the reactor, radiation to the reactor surface and inter-particle radiation. The effect of conduction through wood is shown in Figure 4.3, also including the radiation and convection to the reactor surface. It can be seen that heat transfer by

conduction alone is very inefficient and confirms that radiation and convection within the reactor have a significant effect on the heat transfer.

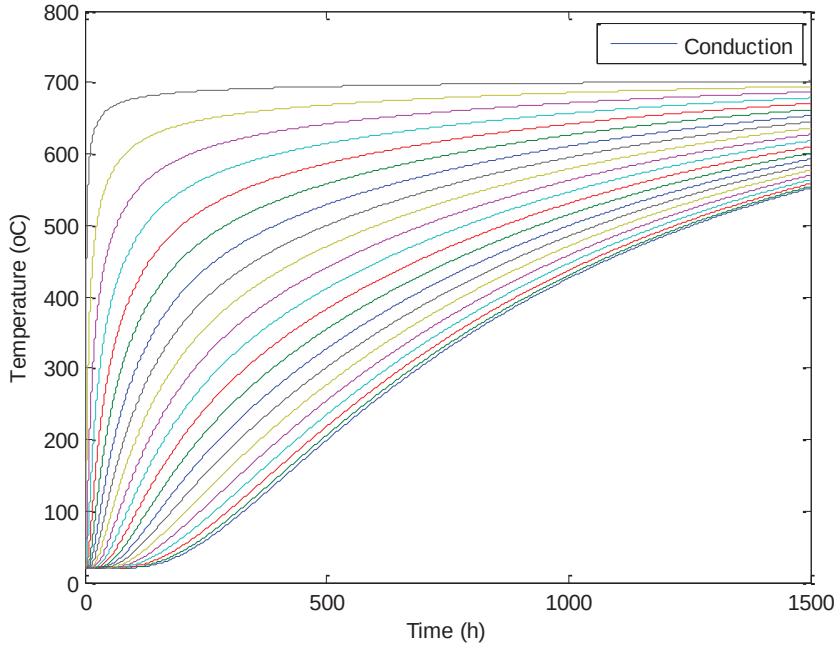

Figure 4.3: Temperature profile for conduction through wood

The next addition to the model was evaporation. As stated earlier in section 5.4, it was assumed that all the evaporation occurred at 100 °C because as although evaporation occurs below 100 °C, it does so at a much slower rate. Figure 4.4 shows conduction and evaporation occurring through a bed of wood over time. The temperature stabilises at 100 °C as the mass of water decreases.

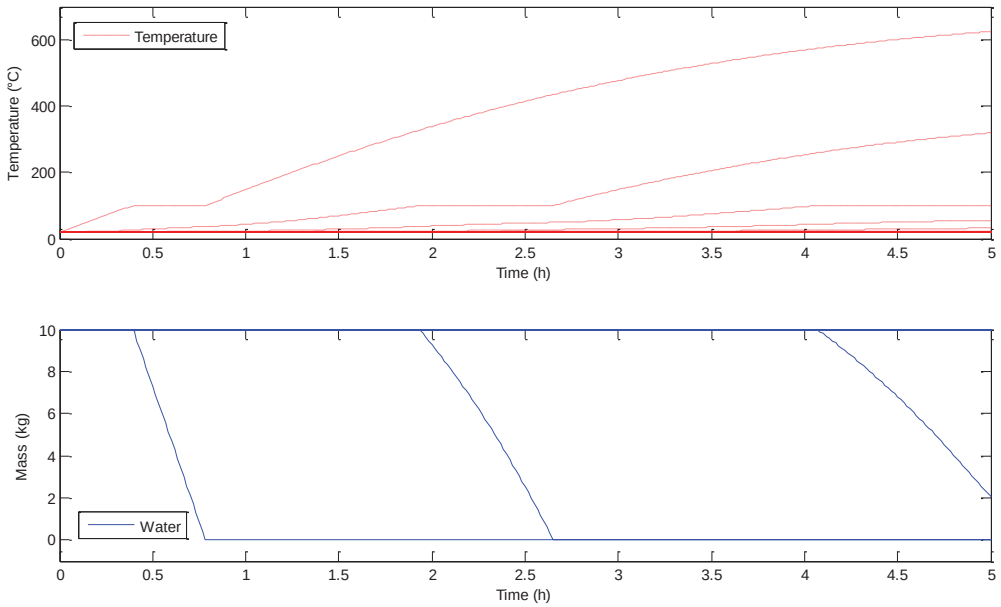

Figure 4.4: Conduction and evaporation in wood heated to 700 °C

When the temperature increases above 200 °C, primary endothermic reactions occur resulting in the formation of gas, tar and char. Figure 6 illustrates 6 subplots showing how the reactor temperature, the mass of biomass, the mass of gas, the mass of tar, the mass of char and the mass of water change as a function of time. It can be seen that the surface node heats up quickly but that the centre temperature remains unchanged after 5 hours. This indicates there are other factors that need to be included in the model.

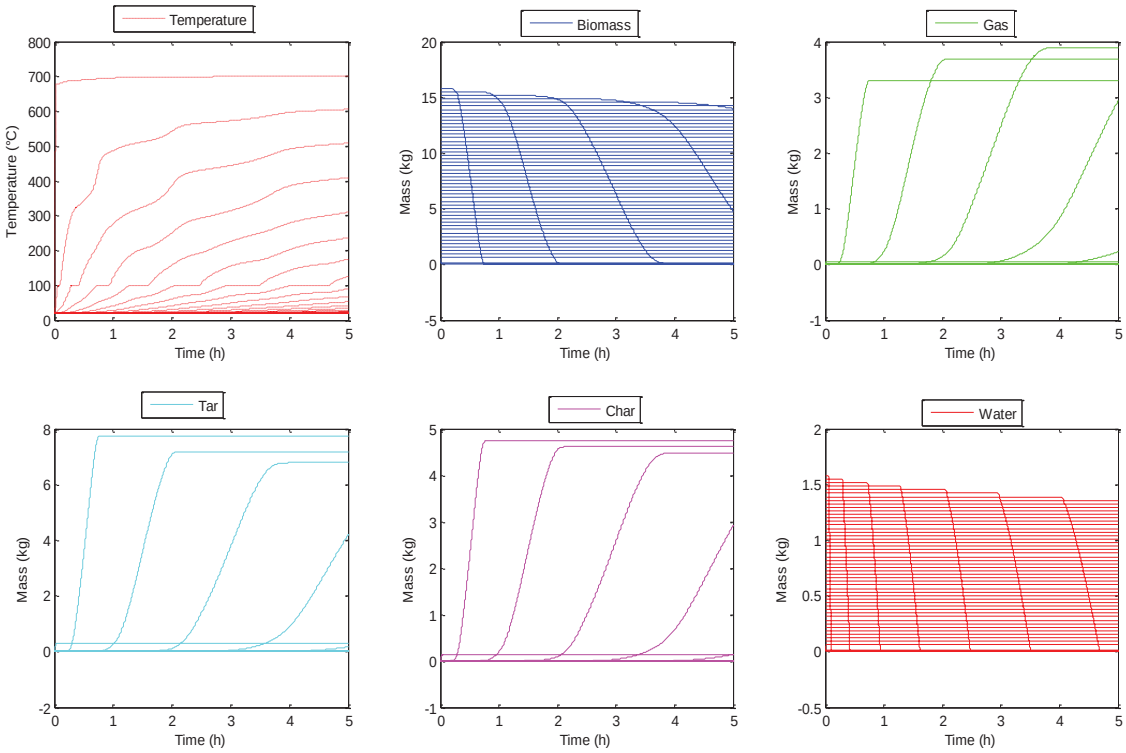

Figure 4.5: Conduction, evaporation and reaction of wood pyrolysed at 700 °C

4.9 Conclusions

The model objectives were stated and a conceptual model was developed describing the modes of heat transfer that occur in the pyrolysis process. The assumptions for this simplified model were stated. Equations were defined for the heat and mass transfer that occurs at the surface of the reactor, the internal nodes and the centre of the reactor.

A finite difference solution was selected for solving this model. Difficulties in the model were encountered due to the inherent instability of the process. This was as a result of the varying rates at which heat and mass transfer occurred.

In future, it is recommended the model is carried out using an alternative program to MATLAB. COMSOL Multiphysics has been identified as a program with more advanced capabilities and is being used by other researchers at Massey University, specifically for cases where the rates of mass and heat transfer vary at interfaces over several orders of magnitude.

5.0 PYROLYSER DESIGN SPECIFICATION

5.1 Process Description

The process of pyrolysis begins with heat supplied from an external source (LPG gas) which heats the outer wall of a vertical cylindrical containing wood chips. Figure 5.1 shows a simplified block diagram of the process. First moisture evaporates and moves inward through a condensation re-evaporation cycle to a central core where the vapour discharges out the bottom of the drum. In this way, the direction of heat and mass flow are both towards the centre. After the water has evaporated away, further heating occurs. Primary wood decomposition reactions begin at around 200 °C for wood, producing char and releasing volatiles which are compounds with low boiling points. As they flow towards the centre of the pyrolyser, the volatiles transfer heat to the unpyrolysed biomass. At lower temperatures, some volatiles condense and at higher temperatures, secondary reactions of the primary volatiles occur, producing further gas, tar and char. Both the primary and secondary reactions can occur in different areas of the particle, simultaneously. Additional thermal decomposition occurs until the reactions are complete for a given heating-side set point temperature which, for the following description, will be set to less than 700 °C.

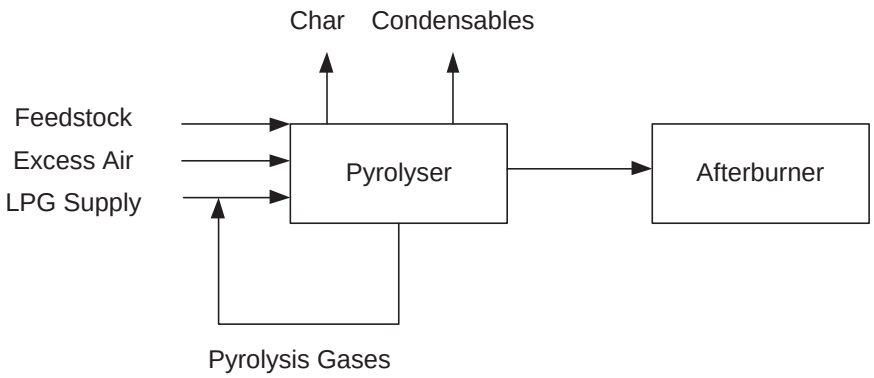

Figure 5.1: Basic block diagram of the process

5.2 Functional Description

A summary of key values referred to in this section can be found in the design specification section (section 5.3).

5.2.1 Base Frame

The base frame consists of an A-frame where the reactor can be pivoted about its centre of gravity. This is designed specifically for the ease of loading and unloading the wood chips which can weigh between approximately 70 kg on a dry basis and 150 kg on a 50 % moisture content.

The reactor can be tilted just beyond a horizontal level so the resulting cooled biochar can be emptied and easily transferred to storage bins. Also, there is a mechanism in place preventing it from tilting further than the desired range. The reactor will be loaded at a 45° angle from vertical so the maximum amount can be loaded at a suitable height for the operator.

However, this base section (defined in the combustion chamber section) must first be slid out before the reactor can be tilted. An advantage of a movable base is that the tar collection plate can be easily cleaned and the reactor can pivot where it is, without having to be lifted above the base section.

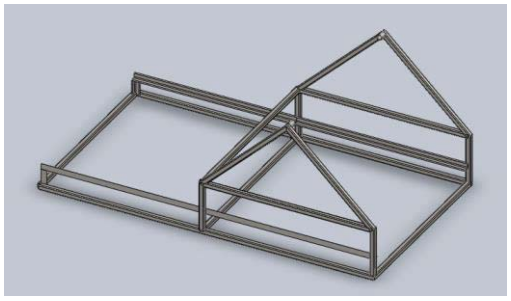

Figure 5.2: Base frame

5.2.2 Loading and Unloading

The pyrolyser will be mounted on an A Frame so the reactor can easily be tilted into a horizontal direction for ease of loading and unloading. The base will contain the tar collection plate, the heat source and will slide out so the tar collection plate can be cleaned as well as enabling the reactor to be tilted.

The flue is on a hinge system so as the reactor tilts forward the flue pivots backwards towards the ground. The reactor is sealed by the use of stainless steel spring loaded latches. The spring loaded latches allow for thermal expansion.

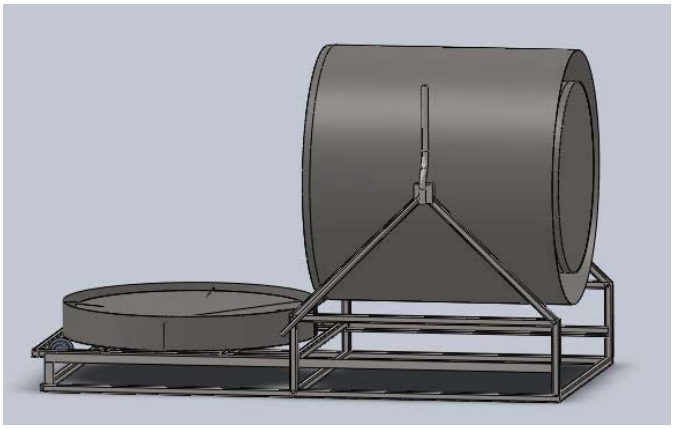

Figure 5.3: Mechanism for loading and unloading

5.2.3 Internal Chamber

The reactor is a vertical cylinder with a total volume of 0.43 m^3. The reactor is designed to minimise mass and heat transfer limitations by allowing conduction and convection to travel in the same direction, towards the centre. The evolved gas is drawn off by natural draft through the hollow core, which is 0.2 m in diameter and 0.9 m in length. The pyrolysis gases exit the base on the cylinder into the combustion chamber where they are ignited to also assist with heating.

There is a lid on the top of the internal chamber which is sealed with a ceramic fibre rope to minimise gas leakage. The seal on this is not critical because any minor about of leakage will be drawn up through the stack to the flare. The lid is secured in place rotating the lid anticlockwise until the three pins have locked in place.

The internal chamber is made of stainless steel 304 to withstand the operating temperature up to a design limit of 1000 °C, although operation is not expected to be above 850 °C. The control strategy here employs set point temperatures ranging from 400 - 700 °C. The stainless steel is able to withstand the acidic tars (pH 2 - 3) that form during parts of the pyrolysis process. The chamber is attached to the external frame so it does not move during loading and unloading, but still allows for expansion and contraction without buckling the system. It is made of 3 mm stainless steel which is strong enough to cope with around 70 kg of dry wood chips or 150 kg wet wood chips based on 50 % moisture content.

Stainless steel 304 has an intermittent service temperature of 870 °C. It has good cold pressing properties, fair machining properties and good welding properties. Although it will continuously be operated at relatively high temperatures, between 550 - 700 °C, a more heat resistant steel is not required for the lifetime of this prototype.

5.2.4 External Wall / Outer Chamber

An external wall surrounds the internal chamber. This allows the pyrolysis gases and heat from the LPG to travel from the combustion chamber to the sides of the reactor and up the flue. The clearance between the inner and outer walls is 20 mm. This outer annular wall is made of stainless steel 304.

5.2.5 Fuel Supply

The heat source is LPG which has a high calorific value of 43.1 MJ kg^{-1}. LPG is a readily available fuel source that is widely used in NZ. It has been chosen as it produces fewer emissions than other sources and also for its simplicity for the intended target user. The LPG is able to be easily disconnected once the pyrolysis process is over to enable unloading and cleaning to occur on the other components.

Two LPG cylinders will be connected in series, however only one will operate at a time. This is to ensure that when the run begins, one LPG bottle is always full. There will be a pressure indicator on the bottles so that when the gas bottle is running low in one, it will then automatically switch to the other full LPG bottle. The LPG line will have three streams, one for the main burner, pilot burner and for the flare.

The mass of LPG required per run to burn 75 kg of wet wood with a dry basis moisture content of 60 wt % is 12 kg. For 62 kg of dry wood with a dry basis moisture content of 22 wt %, the total LPG required is 6.1 kg.

5.2.6 Burner

During pyrolysis, flammable gases evolve and are also combusted to provide heat to drive the process. These are discussed further in the combustion chamber section.

The burner is an independent system with its own air supply and control functions. The burner supplies the heating in the base section of the reactor. The heat then travels up the sides of the reactor to the flue. The rising air causes a natural system draft. Open air holes in the base of the combustion chamber allow secondary air to be drawn upward. This is further discussed in the chamber section below.

The heating capacity of the burner is 6-23 kW and will have four settings: low (6 kW), medium (23 kW), high (both the 6 kW and 23 kW) or OFF. The burner will adjust to one of these settings according to a response from the control system which is based on two

temperature readings, T-004 (located in the flue) and T-002 (located in the central core). The control strategy is discussed later.

5.2.7 Combustion Chamber

The combustion chamber is located underneath the reactor and has a height of 284 mm which was determined by the gas requirements. The burners are mounted on the side of the combustion chamber, with the flame directed across the chamber.

Secondary air inlets are in the form of open holes at the base of the combustion chamber. This creates an environment where the base of the system is open to the atmosphere. The hot gases rising up the flue create a natural draft which draws the gases and air up and away from the combustion chamber. The mixing of pyrolysis gases with the secondary air will create a flammable mixture. This is ignited by either the main burner or pilot burner. The secondary number of secondary air holes required is 9, each an area of 0.0065 m^2 (refer to Appendix B for design calculations). It is important that radiation shields cover the holes to minimise heat loss.

A pilot burner (pilot-001) is located in the combustion chamber near the side of the reactor. Pilot-001 will ensure ignition of the pyrolysis gases and also a further safety mechanism, in the event of the main burner failing. The pilot burners (a second pilot burner is located in the flue) will be either ON/OFF. The combustion chamber is insulated with SHIRACAST 145 which is a cement bonded castable product, similar to firebricks and can withstand temperatures up to 1850 °C. However, this material had to first be fired according to the standard procedure for this particular product. This ensured moisture was evaporated slowly, preventing the material from cracking upon use.

The pressure differential will be monitored between two tubes, one coming out of the base section and one coming out of the flue. Due to the natural draft it is expected that the unit will have a pressure differential of 20 Pa. The tube was positioned 500 mm clear of the cladding to ensure they did not get hot.

5.2.8 Flue

The flue is designed to create a natural draft in the system which draws secondary air in via the holes at the base of the combustion section. Due to heat losses it has been assumed the top of the stack will be 100 °C less that the inlet temperature for calculation purposes. The flue has been designed to be 2.5 m high with a diameter of 0.08 m to create a slightly negative system pressure and to prevent flammable gases leaking out.

Instead the flammable gases are drawn through the combustion chamber where they are either ignited by the burner or the pilot ignition system. The natural draft means additional secondary air is drawn in through the open holes in the base of the combustion chamber.

The draft can be calculated using equation (5.1) (Sinnott, 2005).

$$P_d = 0.35(L_s)(p') \left(\frac{1}{T_a} - \frac{1}{T_{1°+2°}}\right) \quad (5.1)$$

Where L_s is the stack height (m), p' is atmospheric pressure (millibar or N m^{-2}*10^{-2}), T_a is ambient temperature (K), $T_{1°+2°}$ is the average flue gas temperature (K) and P_d is the draft (mm H_2O).

5.2.9 Tertiary Air

Tertiary air is injected through a venturi near the top of the stack supplied by an externally mounted centrifugal fan. This additional air supply may be required for several reasons. These are:

1. During start-up there will be no natural draft initially so in order to draw the gases produced from the LPG supply upward, the tertiary air supply may need to be on. Similarly, during shut down, when all the pyrolysis gases have been produced, the natural draft may not be sufficient to draw the remaining gases out through the stack.
2. To supply cooling air if the system has exceeded its maximum operating set-point temperature
3. To supply additional air to combust the pyrolysis gases

For the reasons discussed above it is important that the tertiary air supply is a key part of the control strategy. Further detail of the use of the tertiary air fan and venturi are discussed in the control strategy.

5.2.10 Flare

The flare's purpose is to burn the remaining products of incomplete combustion. The amount will vary from none to a maximum expected flow of 1.2 L min^{-1} of pyrolysis gases (with a calorific value of 10 MJ kg^{-1}) depending on the operation of the unit (see the control strategy

section). Most of the time there will be very few products of incomplete combustion. The flare is turned on when pyrolysis gases begin to evolve.

Flares operate optimally between 850-1200 °C to ensure complete oxidation of carbon monoxide and to prevent the formation of dioxins, furans and polyaromatic hydrocarbons (PAHs). Not everything can be prevented but to minimise the effects of harmful gases, the temperature must also be less than 1200 °C to prevent the formation of mono-nitrogen oxides, NOx. In order for complete combustion to occur, the residence time must be greater than 0.3 s. To achieve this residence time, a swirl burner addition was required.

The flare will be enclosed flare to meet environmental standards. Open flares are simple and low cost but have no control over the emissions.

There are two types of enclosed flares: diffusion aeration and pre-aerated flares. Diffusion aeration is where the gas is mixed with the air at the burner. For this design, a pre-aeration system will be employed. Pre-aeration was achieved by a venturi where the aeration is proportional to the feedstock flow.

A second pilot burner (pilot-002) is located at the top of the flue. This is to ensure the exhaust gases are completely combusted and this burner is turned on when pyrolysis gases begin to evolve.

In this unit, the flue will not always contain products of incomplete combustion. Instead, it may be a mixture of partially combusted gases with little or no oxygen, or it may be a mixture of both combusted gases, products of incomplete combustion and air. The air to products of incomplete combustion ratio may range from no air to being significantly diluted by air. The control strategy details the various operating modes. Therefore, we regard this flare system, as a backup.

5.2.11 Overflow Vent

During the pyrolysis process, an aerosol and soot cloud may form. The high surface area of such a cloud may absorb all the available oxygen and snuff out combustion resulting in a build-up of fuel.

Even though the natural draft is drawing this cloud upward and away from the combustion zone, if the rate of cloud formation is high, then there will be an accumulation of combustible energy. This is unlikely to occur because a number of ignition sources are present; first, to the burner which operates independently of the temperature and the pressure in the combustion chamber; second, the pilot flame in the combustion chamber; and third, the pilot in the flare at the top of the flue stack. Combustion requires free oxygen which, in this

envisaged scenario has been adsorbed onto the aerosol droplets and soot particles and therefore is unavailable for combustion. However, the natural draw of the system means secondary air continues to be drawn in through the holes in the base of the combustion chamber. In the event that the rate of cloud generation is high and the adsorption rate is high, the gas stream passing around the chamber will be largely products of incomplete combustion. This is regarded as one of the designed operating scenarios for the pyrolyser. When the gas reaches the flare in the flue, where additional air enters and mixes with the gases, they will be ignited by the pilot flame positioned there. This isn't an ideal operating scenario because energy is not returned to further heat the drum containing the wood chips, but is viewed as a safe operating mode. In addition, the tertiary air can be turned on to increase the draw of secondary air at the base of the combustion chamber. Some gases would escape where the air is drawn in through the base of combustion chamber. It is designed so the path of least resistance is taken. If this were to ignite then there would be a large pressure build-up which would need to be vented safely.

It is designed that the overflow vent will be in a vertical direction above eye level for operator safety with a large surface area for release. Some gases would escape where the air is drawn in through the base of the reactor. It is designed so the path of least resistance is taken.

If the pressure does build up, the overflow vent was designed to open by a flap on the top of the vent which is weighted based on gravity. The vent also includes a flare so flammable gases are not getting released into the atmosphere. This overflow vent was for initial commissioning and once the operation was understood, the overflow vent was not used and subsequently removed from the 'open source' design. For commissioning, the overflow vent operated on a separate LPG supply so the carbon balance of the process was not affected. A pilot light was always operating in this area with a continuous spark going to reduce the chance of the pilot light going out.

5.2.12 Tar Collection Plate

This collection plate is conical in shape and situated underneath the pyrolysis gases exit. This is because if any tar is generated this plate would trap it and can be easily removed and cleaned for future runs. Secondly, to distribute the flames around the sides of the reactor and finally so the gases that are drawn off in the middle are not directly being burnt as this would then result an increase in heat in the centre and the system not behaving as intended.

5.2.13 Insulation

Superwool PLUS was used to insulate the reactor. Superwool PLUS is a ceramic wool blanket that is suitable for temperatures up to 1200 °C, has a density of 98 kg m^{-3} and a thermal conductivity of 0.12 W m^{-1} K^{-1} at 600 °C.

This insulation was surrounded by thin sheet metal cladding to hold it in place and reduce the heat losses to the process. It has been estimated that for an insulation thickness of 0.1 m, a wall temperature of 100 °C can be achieved when the annular region inside the reactor is 700 °C. A temperature of 50 - 60 °C was desired, however this meant 0.3 m of insulation was required which would increase the overall reactor size too much.

5.2.14 Monitoring / Measurement Systems

There will be thermocouples indicating the temperature at different points in the reactor, which can be seen on the process and instrumentation diagram in Section 5.6.

All thermocouple readings will be recorded, but T-004 and T-002, the lower flue and reactor core temperatures respectively, will be used for controller inputs. In combination, T-004 and T-002 will determine the stage of pyrolysis and will be used to change the burner setting and the 3° air inlet. This is further explained in the control strategy below.

A gas analyser will be used to monitor in particular the carbon monoxide levels but also has the capability of measuring the CO_2, H_2S, CH_4, SO_2 and C_xH_y levels.

5.3 Design Specifications

Table 5.1: Estimates for design

Inner Reactor		
Height	1	m
Inner diameter	0.75	m
Inner volume	0.43	m^3
Materials of construction: Stainless steel Sheet thickness: 3 mm Maximum operating temperature: 850 °C		
Inner Core		
Height	0.9	m
Diameter	0.2	m
Materials of construction: Stainless steel Sheet thickness: 3 mm Temperature Range: 0-850 °C		
Outer Chamber		
Gap b/t top of inner chamber and lid of outer chamber	0.04	m
Diameter of outer annulus ID	0.796	m
Diameter of outer annulus OD	0.802	m
OD of insulated unit	1.002	m
Materials of construction: Either mild steel of stainless steel Sheet thickness: 3 mm Temperature Range: 0-850 °C Insulation thickness: 0.1 m		
LPG		
Required LPG flow rate	0.03603	$L\ min^{-1}$
Required air flow rate	0.75	$L\ min^{-1}$
LHV propane	46350	$kJ\ kg^{-1}$
HHV propane	50350	$kJ\ kg^{-1}$
Flue		
Length of stack	2.5	m
Diameter	0.08	m
Draft	2.0	mm H_20
Draft	20	Pa
Overflow Vent		
Area of vent	0.1	m^2
Length of the duct	2	m
Material of construction: Stainless steel Gravity flap on the top of the vent		

Flare		
Residence time	>0.3	s
Swirl burner to ensure residence time is reached		
Tar Plate		
Diameter	450	mm
Height of conical plate	100	mm
Height of support legs	200	mm
Material of construction: Mild steel		
Insulation		
Thickness	0.1	m
Material: SuperwoolPLUS Wall temperature: 100°C Insulation is required around the outer reactor as well as on the lid of the reactor		
Estimated Maximum Flow rates (Fantozzi, 2007)		
Pyrolysis gas flow rate	0.02	kg s^{-1}
Tar flow rate	0.053	kg s^{-1}
Minimum Flow Rate of Exhaust Gases		
Carbon dioxide, CO_2	1.09	L min^{-1}
Oxygen, O_2	0.16	L min^{-1}
Water, H_2O	0.69	L min^{-1}
∑ Exhaust Gases	1.94	L min^{-1}
Minimum Flow Rate of Pyrolysis Gases (Greico, 2011)		
Carbon dioxide	0.675	L min^{-1}
Ethylene	0.005	L min^{-1}
Ethane	0.015	L min^{-1}
Propylene	0.005	L min^{-1}
Propane	0.004	L min^{-1}
Hydrogen	0.010	L min^{-1}
Methane	0.134	L min^{-1}
Carbon Monoxide	0.352	L min^{-1}
Flammability Limits (Volume %)		
LPG (Mishra, 2003)	1.81 LFL	8.86 UFL
Carbon monoxide, CO	12 LFL	75 UFL
Methane, CH_4	4.4 LFL	15 UFL
Hydrogen, H_2	4 LFL	75 UFL

Fan Sizing		
Voltage	115	V
Maximum flow rate	227	CFM
Pressure range	0-125	Pa
DAYTON high temperature blower		
Secondary Air Holes		
Hole Diameter	0.05	m
Number of holes	9	-
Holes will be evenly spaced around the reactor A sliding plate will be installed to manually cover the holes if necessary Require radiation shields covering the holes to minimise heat losses		

5.4 Control Description

The system was designed to be inherently safe; that is, to operate at atmospheric pressure with a mild updraft to a flue stack to draw flammable gases through the combustion zone where they are ignited and through a secondary flare mounted in the stack before they are discharged to atmosphere. However, there were also a number of safety issues.

The control objectives of the process were to:

1. Ensure safe operation of the process by combusting all products of incomplete combustion
2. Maintain T-004 at the heating-side set point temperature of 400, 500 or 600 °C
3. Monitor T-002 which will provide process information for implementation of the control strategies (see Section 5.5)

Additional monitoring features include:

3. Ensuring no polycyclic aromatic hydrocarbons (PAH's) form and to limit particulate matter and NOx emissions from the system
4. Ensuring the char meets quality standards (not discussed here)

Points 3 and 4 are not part of the control strategy as the temperature is being controlled to affect these outcomes; however, testing of these will be conducted during the commissioning phase to ensure the standards are met.

The variables that can be manipulated in this process are:

- The tertiary air flow (either ON or OFF) which controls the secondary air and draft in the system, over and above the natural draft to the system
- The LPG flow rate to the base main burner – the burner has four operation modes: OFF, low (6 kW), medium (23 kW) and high (6 kW and 23 kW)
- The LPG flow rate to the pilot burner in the combustion chamber – the pilot burner has two modes of operation: ON or OFF

The flue (being sufficiently high) creates a natural system draft and a slightly negative system pressure. This is also augmented by the tertiary air which enters the flue stack and creates a draw to bring in additional secondary air. It is important that $P_{System} < P_{atm}$ for safety reasons i.e. to prevent egress of flammable gases from the system; all gases are drawn through the base burner then up through the stack flare giving two opportunities for

products of incomplete combustion to be destroyed. This removes the possibility of an explosion occurring. The differential pressure sensor, PI-001, in the base section will monitor the pressure in the system. The design of the secondary air inlets as open holes in the base plate (with an area equal to 2 % of the basal area) provides an environment where the base of the system is essentially open to the atmosphere.

The temperature sensor T-004 will be used to monitor the flue temperature and will be used to control the base burner heat output. The amount of LPG will be adjusted accordingly. If the flue temperature gets too high, then the LPG will be decreased and then the tertiary air flow can be increased. This will increase the secondary air and cool the system. All these potential scenarios can be found in the hazard and control operability in Table 5.2 below.

To ensure pyrolysis gases were completely combusted, a variety of approaches were taken. The expected proportions of gases are given in Table 5.1 above with ranges of minimum and maximum expected proportions. Early on in the heating phase only water vapour will flow out of the reactor as the wood chips dry. Later, beyond 280 °C, pyrolysis gases will evolve. Their exact flow rate depends on the rate at which heat penetrates the particle bed inside the reactor. These gases will be drawn through the base burner and the flue stack flare as explained above. Both the burner and flare pilot flame are independently controlled and are always burning. The flammability limits of the gases are contained in Table 5.1; these refer to each flammable gas concentration in air required to maintain a naked flame. The draw from the stack and the tertiary air entering at the venturi will, at low flow stages of the process, dilute the flammable gas concentrations below the flammability limit; however, this is not a problem as the gases will pass through two independently controlled burners, the base burner and the flare. The flare ensures complete combustion.

The base burner combustion zone will operate at a T>850 °C, which will ensure no PAHs form but less than 1200 °C to prevent NOx formation. The flare system will not exceed this temperature either; the temperature sensor, T-006, will be installed above the flare to monitor this situation and, if exceeded, the tertiary air will be adjusted.

Another safety feature to consider when designing a pyrolyser, is the security of ignition in order to combust all flammable gases, where it is necessary to maintain a pilot light (pilot-001 and pilot-002) and/or a constant spark system. The pyrolysis off gases will contain volatiles as aerosols and soot particles; there is a risk of a soot and aerosol cloud forming which can snuff a flame by adsorbing all available oxygen.

An additional safety component is an overflow vent in the unlikely event of the main burner, the pilot flame and the spark ignition system all failing, while pyrolysis gases are still being generated from the hot reactor and mixing with oxygen and becoming a flammable fuel mixture. If this finds an ignition source, then a gas explosion could occur. The explosion will vent to atmosphere both through the open holes (secondary air holes) in the base of the unit

and to the overflow vent which opens a flap that is gravity weighted. The gases will take the path of least resistance and so the force of the explosion will be vented upwards and away from bystanders.

A spark arrester in the form of wire mesh was placed around the flare at the top of the flue. This will catch for any burning solid char particles that manage to pass through the system and to ensure no sparks leave the system.

Table 5.2: Control scenarios

Scenario	T_{Flue} (°C) T-004	T_{Core} (°C) T-002	3° Air Supply	LPG Supply	
LPG flow rate is too high, no volatiles production	>700	<200	Increase Medium	Decrease Low	Decrea requ Incre
The chamber is too hot as pyrolysis gases are being produced. We will decrease the 3° air to get products of incomplete combustion so the temperature doesn't get too high. They will instead be combusted at the flare.	>700	200<T<SP	Increase Medium	Decrease Low	The L dri produc of t
Volatile production has finished but the soak time has not been meet so turn on the LPG to finish the process	>700	200<T<SP	Increase Medium	Increase High	Increa LPG is
The LPG is on full and pyrolysis gases are being produced increasing both the flue and core temperatures above their set points	>700	>SP	Increase Medium	Decrease High	Increas and re Dec tempe
The burner is on full as the flue temperature is less than 700 °C and the core temperature is less than 100 °C	<700	≤ 100	Decrease Med/High	Increase High	The bu has it

Volatiles are being produced and the LPG supply is on low	<700	200<T<700	Increase Low/Med	Increase or no change	Syng needs reach the L
No volatiles are being produced and the LPG supply in so low	<700	<700	Decrease Low	Increase High	Syng point is sup
The inner core temperature is around the set point temperature	N/A	~SP	No change	No change	Synga i
Carbon monoxide levels after the flare are too high					

5.5 Control Strategy and Testing Procedure

The control strategy was developed and then implemented jointly by Steve McQuarters from Morrinsville Plumbing and Gas Fitting (MPG) and Neil Lummis.

Neil's email: gocservices@xtra.co.nz
Steve's email: steve.mcQuarters@mpg-ltd.co.nz

The items that were actioned by MPG are in yellow boxes. The controls are listed as Level 1, 2 and 3. Note: Level 3 controls only occur if Level 1 and 2 are satisfied.

Safety Features - for characterisation only and not for the OPEN SOURCE design

- Explosion vent flare. This is a precautionary measure. Once the range of operating conditions has been explored without incident, we will remove the flare. Action: MPG to install a flare which is independent from the rest of the system. We will operate this from another gas bottle, so the mass balance of LPG used by the burners is known.
- A sliding plate to close the secondary air holes. This is discussed later.

Additional Mechanical Design

- Swirl burner. The flue stack flare needs to have a swirl design to ensure the right residence time for soot particulate combustion. Soot is likely when no burners are operating in the combustion chamber and the process is going through the peak of pyrolysis gas production.
- Allowance for weigh scales. The LPG bottles will be placed on a weigh scale, so the bottle holding frame needs to allow for the bottles to sit on weigh scales.

Burner Control

The purpose of control is:

a) To avoid the annular heating zone exceeding 1050 °C, which is the maximum safe operating temperature of the Stainless Steel.
b) To heat until the internal pyrolyser T002 target set points are reached (400, 500 and 600 °C), then to maintain at these set points for a period of time (30, 60, 90 minutes).
c) To economise on the use of LPG.
d) To maximise the recycling of combustible heat from the pyrolysis gases to drive the process.

Two thermocouples provide the temperature input:

- T002: This thermocouple is mounted in the perforated core of the pyrolyser. It measures the temperature of the vapours leaving the pyrolyser.

- T004: This thermocouple is mounted in the base of the flue stack. It measures the temperature of the gases after heat has been transferred across the wall of the pyrolyser, but before further heat loss occurs as they go up the stack.

The temperature inputs are used to control:

1. The ON/OFF switching of the flue stack flare burner (6 kW).
2. The ON/OFF switching of the tertiary air fan.
3. The burner level, which may range from (i) both the 6 kW and 23 kW firing, (ii) just the 23 kW firing, (iii) just the 6 kW firing, and (iv) no burners firing.

Control Strategy

The control strategy required the following set-points

Table 5.3: Set-point descriptions

Symbol	Description
$T004_{MAX}$	The maximum operating temperature at the base of the flue. The maximum operating temperature of the stainless steel is 1050 °C. Therefore, $T004_{MAX}$ at the bottom of the flue is indicative of an approached to this, with a margin of safety. It may need changing after actual measurements of temperature are taken in the annular region
$T002_{SET}$	The operating set-point for the core of the reactor. This will be varied between trials from 400-600 °C.
$T002_{LOWER}$	This is the lower boundary of high gas and volatile evolution
$T002_{UPPER}$	This is the upper boundary of high gas and volatile evolution
$T002_{FLAREMIN}$	The temperature in the reactor core below which the flare is OFF
$T002_{FLAREMAX}$	The temperature in the reactor core above which the flare is OFF. Note: the flare will be ON between these values
$HOLD_{SET}$	The hold time once $T002_{SET}$ has been reached. This will be varied between 30-90 minutes. The hold timer starts when T002 reaches $T002_{SET}$ for the first time.
$TIME_{MAX}$	The maximum time of the trial if the $T002_{SET}$ has not been reached. The burners are then turned OFF and the reaction chamber cools

Table5.4: Time counters

Symbol	Variable	Description
t	Time	The timer starts when the trial is turned ON
HOLD	Holding timer	It starts when $T002>T002_{SET}$ for the first time

Table 5.5: Initial set-points

Symbol	Set-point
$T004_{MAX}$	850 °C
$T002_{SET}$	500 °C
$T002_{FLAREMIN}$	200 °C
$T002_{FLAREMAX}$	500 °C
$T002_{LOWER}$	220 °C
$T002_{UPPER}$	450 °C
$HOLD_{SET}$	90 minutes
$TIME_{MAX}$	7 hours

Each of the controls (1-3 above) are discussed below:

1. The ON/OFF switching of the flue stack flare burner (6 kW)

Justification: There is no need for the flue stack flare to be operating when NO products of incomplete combustion are present. This is particularly true when the feedstock is still drying off moisture (i.e., T002 is low) and the annular region temperatures are low (i.e., T004 is low), meaning that the 6 and 23 kW burners will be on in the combustion chamber and should combust any volatile vapours. Also, later, when either the T002 > 500 °C or after the set point has been reached and held for more than 30 min, there are expected to be few volatiles coming through and so there is little point in having the flare operating. However, if the burners are all OFF, then the flare must operate as a safety precaution to ensure combustion of any volatiles.

The INITIAL CONTROL SCENARIO for MPG to test is:

Level 1 control

A. If $T004 > T004_{MAX}$ then the flare is ON (because the burners will be OFF)

Level 2 control

B. If ($t > TIME_{MAX}$) OR ($HOLD > TIME_{SET}$) then the flare is OFF.

Level 3 controls

C. If $T002 < T002_{FLAREMIN}$ then the flare is OFF
D. If $T002_{FLAREMIN} < T002 < T002_{FLAREMAX}$ then the flare is ON
E. If $T002 > T002_{FLAREMAX}$ then the flare is OFF

2. ***The ON/OFF switching of the tertiary air fan.***

Justification: Tertiary air is blown by a fan into a venturi near the top of the flue stack. The effect of doing this is to draw a greater draft of secondary air up through the bottom of the unit, which enhances the combustion of the pyrolysis gases in the combustion chamber. The tertiary air fan need only operate when this combustion is likely, otherwise the unit will needlessly be heating ambient air and so wasting energy. Combustion is only likely when the T002 thermocouple is between a lower and upper limit, estimated to be 250-400 °C. However, should T004 > 850 °C, then the tertiary air fan must be OFF.

The INITIAL CONTROL SCENARIO for MPG to test is:

Level 1 control

A. If T004 > $T004_{MAX}$ then TERTIARY AIR FAN is OFF

Level 2 control

B. If (t > $TIME_{MAX}$) OR ($HOLD$ > $TIME_{SET}$) then the TERTIARY AIR FAN is OFF.

Level 3 controls

C. If T002 < $T002_{LOWER}$ then TERTIARY AIR FAN is OFF
D. If $T002_{LOWER}$ < T002 < $T002_{UPPER}$ then TERTIARY AIR FAN is ON
E. If T002 > $T002_{UPPER}$ then TERTIARY AIR FAN is OFF

3. ***The burner level, which may range from (i) both the 6 kW and 23 kW firing, (ii) just the 23 kW firing, (iii) just the 6 kW firing, and (iv) no burners firing.***

Justification: The 6 and 23 kW burners provide the initial heating that dries the wood chips then heats them until pyrolysis gases being to be generated. These gases are first burnt in the combustion zone and as they pass up the annulus they return heat to the process. While only a finite amount of gas and volatiles can evolve in a batch pyrolysis, the rates at which they evolve are uneven and go through peaks. The natural draft of secondary air has been designed to cope with the early and late stages of pyrolysis where only a limited amount of secondary air is needed. Therefore during peak production of gas and volatiles insufficient air is present. For this reason, the tertiary air fan is used to induce a greater secondary air flow (See §2 above). The consequence of combusting the gases and volatiles in the combustion chamber is that the annular temperature may rise above the working temperature of the stainless steel. If this region increases above 850 °C then the

burners are all switched OFF (and so is the tertiary air fan). If the temperature runaway coincides with the peak production of pyrolysis gases (250-400 °C), without burner operating, the soot carryover into the combustion zone will likely snuff out any flame and so the annular region will begin to cool, which occurs because the pyrolysis volatiles leaving the chamber are at a cooler temperature than the combustion zone. If the soot carryover does not snuff out the flame, the T004 temperature may continue to increase. For this reason, we included a feature which will not be part of the OPEN SOURCE design, that is, a sliding plate to close the secondary air holes. Closing these holes will starve the combustion chamber of air and so the annular region will then cool. It cools because the pyrolysis volatiles will not self-heat beyond about 550 °C, despite their mildly exothermic nature, because by about 550 °C all decomposition reactions have finished. Thus, higher set points have to be achieved using the burners.

The INITIAL CONTROL SCENARIO for MPG to test is:

Level 1 controls

A. If (t > $TIME_{MAX}$) OR ($HOLD$ > $TIME_{SET}$) then the 6 kW burner is OFF and the 23 kW burner is OFF.
B. If T004 > $T004_{MAX}$ then 6 kW burner is OFF and 23 kW burner is OFF
C. If (T002 < $T002_{LOWER}$) then 6 kW and 23 kW burners are ON
D. If (T002 > $T002_{SET}$) then 6 kW burner is OFF and 23 kW burner is OFF.
E. If ($T002_{SET}$ < $T002_{UPPER}$) AND ($T002_{LOWER}$ < T002 < $T002_{SETPOINT}$) then 6 kW burner is ON and 23 kW burner is OFF.
F. If ($T002_{SET}$ > $T002_{UPPER}$) AND ($T002_{LOWER}$ < T002 < $T002_{UPPER}$) then 6 kW burner is ON and 23 kW burner is OFF.
G. If ($T002_{SET}$ > $T002_{UPPER}$) AND ($T002_{UPPER}$ < T002 < ($T002_{SETPOINT}$ – 50 °C)) then 6 kW burner is ON and 23 kW burner is ON.
H. If ($T002_{SET}$ > $T002_{UPPER}$) AND (($T002_{SETPOINT}$ - 50°C)< T002 < $T002_{SETPOINT}$) then 6 kW burner is ON and 23 kW burner is OFF.

5.6 Process and Instrumentation Diagram

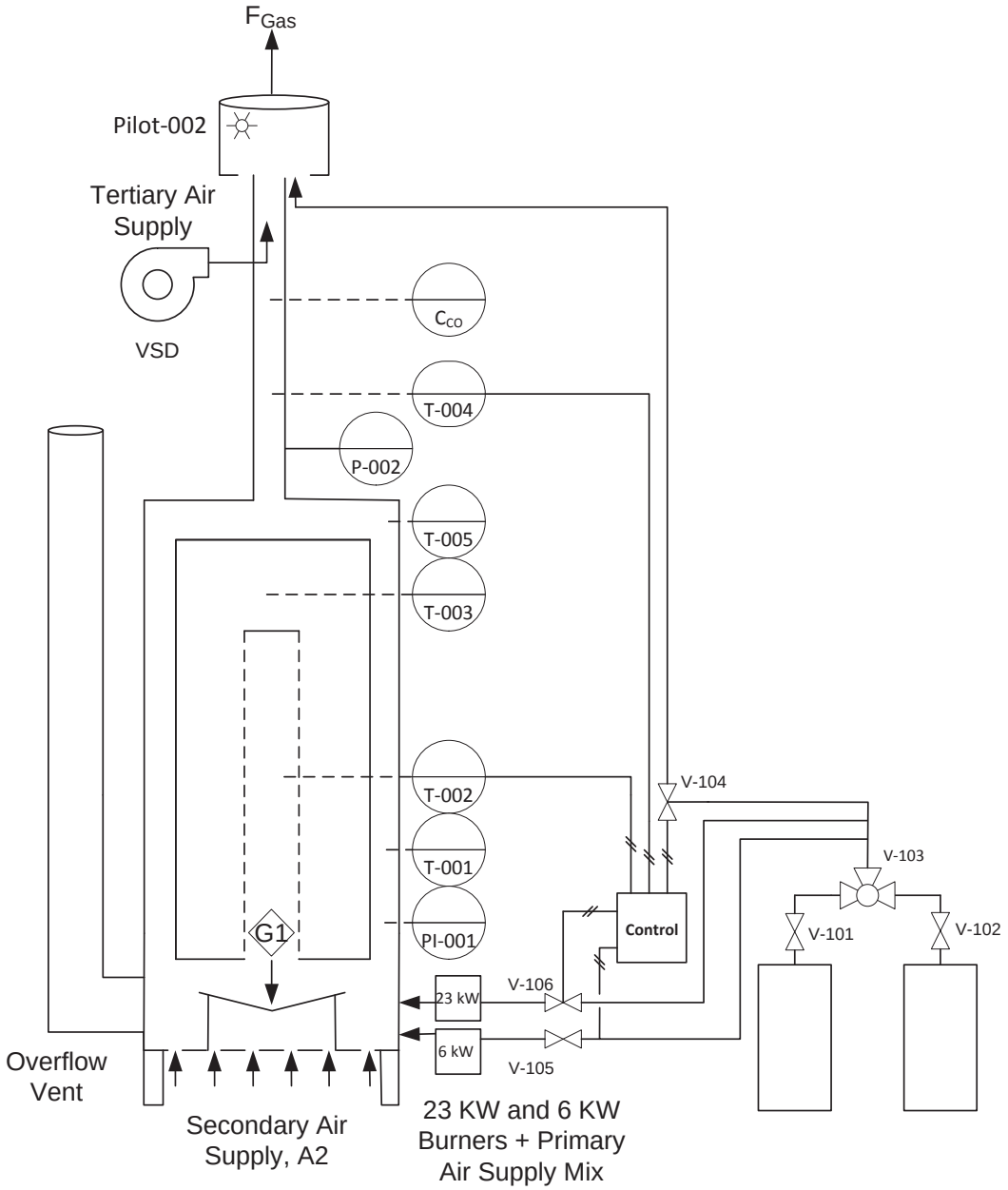

Figure 5.4: Process and instrumentation diagram

Table 5.6: List

Stream List	
Number	Stream Name
L1	LPG
A1	Primary air supply
A2	Secondary air supply
A3	Tertiary air supply
G1	Recycled volatiles
Equipment List	
Number	Description
1	Pyrolyser
2	LPG supply
Control List	
Number	Description
V-101	Gate valve
V-102	Gate valve
V-103	3-way valve
V-104	Solenoid valve
V-105	Solenoid valve
V-105	Solenoid valve
T-001	Temperature indicator
T-002	Temperature indicating controller
T-003	Temperature indicator
T-004	Temperature indicating controller
T-005	Temperature indicator

As discussed in the control description (section 5.4), there will be two thermocouples, one of which is located in the inner core of the reactor (T-002) and the other located in the flue (T-004). These thermocouple inputs are used in the control strategy for the pyrolyser. The thermocouples T-001, T-003 and T-005 will be for reference and will enable monitoring of the temperature at different points in the reactor. Solenoid valves are used to switch between the 6 kW and 23 kW burners.

Pressure sensors P-001 and P-002 will be differential pressure sensors that will enable the pressure to be monitored.

A Testo 350-XL gas analyser will primarily be used to monitor the carbon monoxide levels but has the capability of measuring nitric oxide, nitrogen dioxide, carbon dioxide,

hydrocarbons and hydrogen sulphide. This will be located in the flue, before the gases have been flared.

5.7 Hazard and operability analysis (HAZOP)

No.	Guide-word	Parameter	Deviation	Cause	Effect	Pr S
Stream 1: LPG Supply						
1	None	Flow	No LPG flow and hence no temperature	Faulty valve	No pyrolysis occurs, no temperature	Ins indic
				Empty gas bottle	No LPG supply	Re
				Blockage in line or air holes	No LPG supply reaches the gas ring so no heating	
2	Less	Flow	Lower gas flow rate than the set point	Faulty valve	Longer processing time	Ins indic
				Incorrect air/ LPG ratios	Longer processing time	Ins indic
3		Temperature	Lower flame temperature	Faulty valve	Longer processing time	Ins indic
				Incorrect temperature set point	Longer processing time	
4	More	Pressure	Increased system pressure	Higher gas flow rate due to incorrect set point	Higher heating rate, exothermic reactions happen faster and the pressure builds up in system	Insta re
				Faulty valve	Higher heating rate, exothermic reactions happen faster and the pressure builds	Insta re

					up in system	
5		Flow	More LPG flow than the set point	Faulty valve	Higher heating rate, exothermic reactions happen faster and the pressure builds up in system	Insta indic and fl
				Incorrect LPG set point	Higher heating rate, exothermic reactions happen faster and the pressure builds up in system	Insta indic and fl
6		Temperature	More LPG flow than the set point	Faulty valve	Higher heating rate than required resulting in a higher production of tar	ter indic
				Incorrect LPG set point	Higher heating rate than required resulting in a higher production of tar	ter indic
Stream 2: Recycled Volatiles						
7	None	Flow	No volatiles	Temperature is not high enough so no reactions have occurred	LPG supply will need to remain on	No syste
				Blocked gas outlet preventing gas flow G1	Pressure build up which could lead to a potential explosion	Insta re
8	More	Flow	High volatiles flow rate	Fast reaction rate	Temperature of the reactor increases	Instal
9	Less	Flow	Low volatiles flow rate	Slower reaction rate	Longer processing time	Instal

Stream 3: Air Supply from the Blower and Natural Draft						
10	None	Flow	No air flow	No draft in the system	Pressure build up in the system as LPG is still flowing	Ins indic
				Pipe lines blocked or damaged	Pressure build up in the system as LPG is still flowing	Insta
		Power	No power	Electrical fault	No air is supplied	Ins sole
					No control systems work	Ins sole
11	More	Flow	More air flow	Too much draft in the system	LPG and or pyrolysis gases will not light and produce heat	Install on th abo colle
12	Less	Flow	Less air flow	Not enough draft in the system, faulty valve	Incomplete combustion can occur producing CO, H_2 and unburned hydrocarbons	ter
Stream 4: Pyrolysis Gases Leaving the Reactor through the Flue and Flare						
13	None	Flow	No LPG combustion gases	LPG supply not on or pipes blocked	No pyrolysis occurs	
			No pyrolysis gases	No pyrolysis gases have been produced		
14	Less	Flow	Lower LPG flow rate	Incorrect LPG set point	Longer processing time	Ins indic
				Faulty valve	Longer processing time	Ins indic

15	More	Flow	Higher LPG flow rate	Incorrect LPG set point	Shorter than desired processing time	Ins indic
				Faulty valve	Shorter than desired processing time	Ins indic
			Higher pyrolysis gases flow rate	Exothermic runaway, Gases coming off at a fast rate due to normal pyrolysis rates	Shorter than desired processing time	Insta relie exp
Stream 5: Ignition Source						
16	None	Ignition	No ignition	Faulty sparker	LPG build-up which could lead to a potential explosion	Insta spar
				No available oxygen due to soot cloud or no draft	LPG build-up which could lead to a potential explosion	Ha const

6.0 CHARACTERISATION

6.1 Objective

The International Biochar Initiative (IBI) have developed guidelines for biochar classification for its function in soil (International Biochar Initiative, 2012). Biochar tests are divided into three categories; basic biochar properties, maximum toxic compound levels and advanced biochar properties. For this project, the basic biochar properties (elemental composition, moisture, ash content) were of interest.

The characterisation was comprised of a detailed analysis of the biochar generated under different operating conditions to establish performance measures such as operation efficiency and the global warming commitment of the process. *Pinus radiata* wood was the characterisation material.

There are various tests that can be carried out on the resulting biochar to determine the yield, composition and heating value. Specifically, end-point characterisations are used to determine the mass yield of char, tar and gas. This was carried out by a mass balance over the system. Secondly, the most significant elements (total carbon (C), nitrogen (N), and hydrogen (H)) will be determined by elemental analysis at Massey University. The fixed carbon content, volatile carbon and ash content will be determined by thermogravimetric analysis and the heating value will be determined using the Dulong equation. The total oxygen (O) was determined by the difference between the total mass and the sum of the elemental carbon, nitrogen, hydrogen and ash.

Biochar was first characterised on a small lab scale pyrolyser. These trials were used to create curves relating char properties to operating conditions against which the performance of the field scale pyrolyser was calibrated.

6.2 Methodology for Lab Scale Pyrolyser

A single *Pinus radiata* tree was sent to the mill and cut up into five 1.1 m length blocks; with a square section of 300 mm. From this, the wood was then cut into rectangles of various widths. All experiments used this wood from the same tree for consistency. The wood did not include any bark.

Several variables were tested to determine how the biochar properties were affected. The moisture content was either dry or wet with the purpose to investigate whether moisture content affects yield. Dry samples were prepared and placed into a 105 °C oven for a

minimum of 24 hours or until there was no change in weight. For wood, the convention is to report moisture content on oven-dry basis (see (6.1)) where the gravimetric water content is represented by the symbol, u.

$$u = \frac{m_{wet} - m_{dry}}{m_{dry}} * 100 \quad (6.1)$$

The wet samples were soaked for 1 week or until there was no change in weight.

Particle size was varied to investigate whether size causes heat and mass transfer limitations, which then affect yield. There were three particle size levels, small (15x15 mm), medium (32x32 mm) and large (67x67 mm), all with a length of approximately 175 mm. The last variable of interest was grain direction in which the wood was cut either with the grain or against the grain. The purpose here was partially to investigate the effect of grain direction on heat and mass transfer limitations, but also to investigate the fracture mechanics of charcoal in a separate study. The *Pinus radiata* was weighed prior to pyrolysis and after pyrolysis to determine yields.

Table 6.1: Variables tested during lab scale pyrolysis

Variables			
Temperature	300 °C	500 °C	700 °C
Direction	Grain/A.G	Grain/A.G	Grain/A.G
Moisture Content	Wet/Dry	Wet/Dry	Wet/Dry
Size	S/M/L	S/M/L	S/M/L

For pyrolysis, a lab scale drum pyrolyser was used. The samples were placed in the drum, which rotates while the biomass is pyrolysed to ensure even heating. In order to avoid cracking of the wood samples, which may result from the rolling movement of the drum, three sample holder units were designed as shown in Figure 6.1 (Bashir, 2012).

Figure 6.1: Top view of pyrolyser wood holders

The standard operating procedure was followed to assemble and run the pyrolyser. The gas rate was set to a ramp rate approximately 10 °C min^{-1} until it reached a temperature of either 300 °C, 500 °C or 700 °C and was subsequently held at this temperature for a non-fixed period of time.

The pyrolyser operates using LPG as the heat source. As the temperature inside the reactor increases, reactions occur producing volatiles which are driven off to either a condenser system or an exhaust vent where they were flared. When the set point temperature was reached, the LPG supply was turned off and allowed to cool to room temperature. The LPG was controlled via a mass flow meter and a thermocouple located in the centre of the reactor provided information about the centre temperature. Complete control of the heating rate was not possible and the peak temperatures obtained during the experiments varied.

6.3 Methodology for Field Scale Pyrolyser

The field scale pyrolyser is intended for a hobby farmer, who predominantly feeds branches through a wood chipper. Although the results from the lab scale pyrolyser indicated particle size has an impact on the biochar properties, as the main user will only be using wood chips, we decided not to use particle size as a variable and to kept this parameter constant.

Table 6.2: Parameters tested on the pilot scale reactor

Experiment	Moisture Content	Pyrolysis Temp
1	Air Dried	Temperature 500 °C
2	Air Dried	Temperature 600 °C
3	Air Dried	Temperature 700 °C
4	Wet	Temperature 600 °C

Table 6.2 provides a summary of the experiments studied in this work, which investigate how biochar properties are affected by the moisture content and peak temperature. The lab scale experiments showed grain direction did not alter the yield and so was neglected as a variable of interest.

Trials were conducted using wood chips with a high moisture content. The purpose was to compare the energy efficiency between dry and wet samples.

Soak time / residence time is believed to have an impact on the quality of the biochar. It is important to ensure the batch is evenly pyrolysed. Table 6.3 lists some systematically selected soak times.

Table 6.3: Soak times

Experiment	Holding Time	Pyrolysis Temp
1	30 minutes	Temperature 600 °C
2	60 minutes	Temperature 600 °C
3	90 minutes	Temperature 600 °C

Eight samples were taken from the batch and analysed to determine if the properties are consistent. As the main heat source was from below, and the heating was from the outside, the biochar collection points have been strategically placed to ensure the potential variations were tested for. Samples against the wall were not taken as they may be anomalous; rather samples were drawn 20 cm away from the wall and away from the central perforated core. In Figure 6.2, the burners were located in the combustion chamber on the same side as sampling point 7. This meant the heat was directed across the reactor towards sampling point 5.

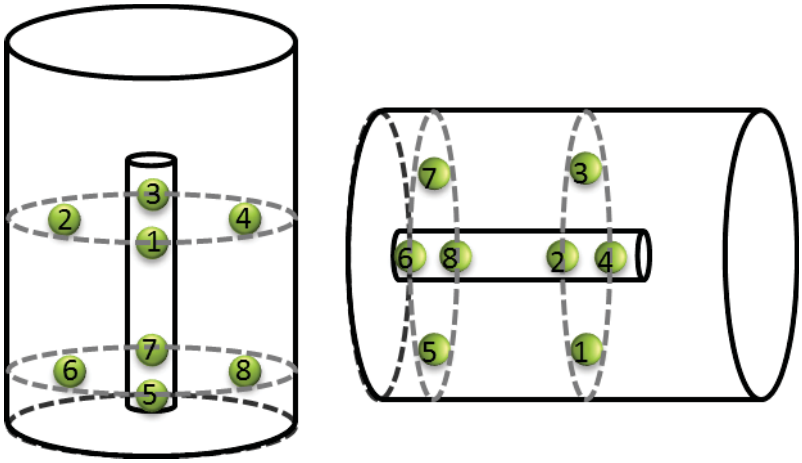

Figure 6.2: On the left, a front view of the sampling points, on the right, the sampling points when the reactor is in the horizontal unloading position

7.0 ANALYSIS TECHNIQUES

This chapter details the laboratory analysis techniques that were used to determine biochar properties formed as a function of pyrolysis temperature and at atmospheric pressure.

7.1 Biomass Sample Preparation

The biomass sample was prepared by taking a full cross section of the wood using an electrical plane. This was then sieved to ensure a particle pore size of <1 mm which was required for testing. The sample was well mixed to ensure homogeneity.

7.2 Biochar Sample Preparation

The pyrolysed samples were placed in a T-bar mill, cleaning between each sample to ensure no contamination, and ground to a fine powder. The samples were well mixed to ensure a homogenous sample.

7.3 Char Yield

Char yield was determined by equation (7.1).

$$Yield\ (wt\ \%) = \frac{Final\ weight - Initial\ weight}{Initial\ weight} * 100 \qquad (7.1)$$

7.4 Biomass Constituent Analysis

Constituent analysis was used to determine the percentage of hemicellulose, cellulose and lignin in the feedstock samples. The biomass samples were prepared as stated above in section 7.1.

Neutral detergent fibre (NDF), acid detergent fibre (ADF) and lignin tests were carried out using the Tecator Fibertec System at Massey Universities Institute of Food, Nutrition and Human Health by the nutrition laboratory manager. The method is based on sequential

treatment with neutral detergent, acid detergent, hydrolysis with H_2SO_4 and ashing (Robertson & Van Soest, 1981). “The neutral detergent step washes out the cellular content and ash; the residual fraction is referred to as neutral detergent fibre (NDF). This residue is further fractionated. With the acid detergent treatment of NDF, cell walls are broken down and the residual fraction is referred to as acid detergent fibre (ADF). Hemicellulose is estimated as the difference between NDF and ADF. With a subsequent H_2SO_4 treatment, cell walls are digested and an acid detergent lignin (ADL) residue is obtained. Cellulose is estimated as the difference between ADF and ADL and ADL is assumed to be mostly lignin” (Calvelo Pereira et al., 2011). Bark remains can contribute to the % ADL; however our *Pinus radiata* sample contained no bark. Duplicates were carried out for reliability.

7.5 Porosity and Density

There are three types of density that can be measured when the sample is porous. They are true density, particle density and bulk density. At Massey University, the particle density could be determined. These experiments were conducting using a GeoPyc 1360. There was not enough sample to measure the bulk density. Although the true density and bulk density could not be determined in this project, the methodology for how they could be determined, if suitable equipment was available is written below.

Two different porosities can be calculated from the densities. These are the interparticle porosity and the bulk interparticle void volume. The bulk interparticle void volume is of interest for transporting biochar. As the lab scale samples were not put through a chipper the bulk density is not of interest, but will be for pilot scale trials.

1. True (Substance, Solid) Density

Place a solid, dry biochar sample in a pycnometer. The equipment measures the solid volume enabling the true density to be determined.

$$True\ density, \rho_s \left(\frac{g}{cm^3}\right) = \frac{Mass\ of\ a\ particle}{Solid\ volume} \tag{7.2}$$

2. Particle Density (Envelope Density, Apparent Density)

Particle density is determined by equation (7.3). An oven dried single particle (approximately 1 cm wide and 2 cm long) was placed into GeoPyc1360. It works by surrounding the irregular sized particle with the powder DryFlo. Only the surface voids are penetrated and the inter-particle voids as well as internal pore volume are included in the volume measurement.

$$Particle\ density, \rho_P \left(\frac{g}{cm^3}\right) = \frac{Mass\ of\ a\ particle}{Solid\ Volume} \tag{7.3}$$

3. Bulk Density

Bulk density is typically recorded as either the "poured" density where the particles settle freely or "tapped" density where the particles have undergone a specified compaction process. Equation (7.4) describes how the bulk density can be calculated.

$$Bulk\ density, \rho_B \left(\frac{g}{cm^3}\right) = \frac{Mass\ of\ particles}{Total\ Volume} \tag{7.4}$$

4. Porosity Calculation

Porosity can be determined using equations (7.5) and (7.6) where ε_P is the interparticle porosity and ε_B is the bulk interparticle void volume.

$$\varepsilon_P = 1 - \frac{\rho_{Particle}}{\rho_{Substance}} * 100\% \tag{7.5}$$

$$\varepsilon_B = 1 - \frac{\rho_{Bulk}}{\rho_{Particle}} * 100\% \tag{7.6}$$

7.6 Proximate Analysis

The fixed carbon content, volatile carbon, moisture and ash content were determined by proximate analysis. These combustion characteristics were evaluated in a SDT Q600 thermogravimetric analyser. This device is capable of simultaneous weight loss (TGA) plus heat flow measurement (DSC).

Thermogravimetric analysis was performed on samples to determine changes in weight in relation to a temperature program in a controlled atmosphere. The primary capability of the TGA includes measurement of a material's thermal stability.

The technique was also useful for determining the percentage of volatiles in the biochar. As the temperature continues to increase, the volatile components in the wood are driven off. The volatile compounds produced from the combustion of wood are principally methane, carbon monoxide, carbon dioxide, hydrogen and water vapour. A range of other hydrocarbons are produced, but in small quantities.

After the volatiles have been driven off, a solid residue remains which is called the fixed carbon content plus the ash, although the fixed carbon content also includes some nitrogen, hydrogen and oxygen.

Ash is the material that cannot be combusted. This is the inorganic content of the biomass and is mostly calcium carbonate ($CaCO_3$).

The biochar samples were prepared as stated in section 7.2. The crucible and lid were sterilised under a flame to ensure no residual material was present. Approximately 25 mg of sample was loaded into an alumina crucible. The sample was run following the procedure as set out by Hayward (2011). The biochar sample was heated at 5 °C/min to 25 °C under a nitrogen atmosphere where it was held for 30 minutes. The sample was then ramped at 5 °C/min to 900 °C. It was then held at this temperature for 100 minutes in an oxidative environment.

Biochar samples were initially tested in a crucible with and without a lid to determine whether there were any variations in the results. The biochar samples showed no difference so the remainder of the experiments were carried out using a lid. This was because some samples were electrostatic and having a lid helped avoid sample loss during processing, which could affect the results.

Wood samples were also compared with and without a lid for thermogravimetric analysis. During the handling of the biochar and wood it was clear that wood was more electrostatic than the biochar. Charged electrostatic particles repel each other which may explain some variability. But also, secondary reactions may generate submicron particles which may be carried away by thermal draft.

7.7 Residue on Ignition (ROI)

ROI is a widely accepted procedure used in the pharmaceutical industry. It determines the inorganic impurities in an organic material by using temperatures as high as 600 °C to pyrolyse the organic matter. Before analysis can be conducted, the crucibles need to be conditioned by heating the crucible in a furnace at 100 °C for 1 hour and then at 600 ± 50 °C for a minimum of 4 hours or until there was no further change in weight and then allowed to cool in a desiccator. This is to prevent any moisture which is easily absorbed and would affect the final weight. ROI is determined by equation (7.7) below

$$\%\, ROI = \frac{Final\ Weight - Initial\ Weight}{OD\ Biomass\ Weight} * 100\% \qquad (7.7)$$

7.8 Elemental Analysis

Elemental analysis was conducted on the biochar samples and the feedstock to determine the percentage of carbon, nitrogen, hydrogen and sulphur in the samples. Oxygen is another important parameter; however, this was determined by the difference between the total mass and the sum of the elemental carbon, nitrogen, hydrogen and ash. The elemental analyses were conducted using an Elementar Vario Macro Cube. The carrier gas used was helium and the combustion gas was oxygen.

The samples were prepared as discussed in section 9.2, dried in a 105 °C oven for a minimum of 24 hours, or until there was no change in weight and then stored in a desiccator until the analysis was carried out. To ensure no contamination of the samples, gloves were worn at all times and the spatula was cleaned each time a new sample was weighed.

Reference standards were prepared at the beginning and end of each run. Table 7.1 summarises the amount of catalyst (Tungsten) and sulphanilamide required. The Elementar automatically adjusts the results according to the curve generated from the standards.

Table 7.1: Reference standard for elemental analysis

Name	Method	Mass of Tungsten (mg)	Mass of Sulfanilamide (mg)
Blank with O2	Blank with O2	0	0
Blank with O2	Blank with O2	0	0
Blank without O2	Blank without O2	0	0
Blank without O2	Blank without O2	0	0
RunIn	Sulf1	50	25
RunIn	Sulf1	50	25
Blank	Coal50	50	-
Blank	Coal50	50	-
Sulfanilamide	Sulf1	50	25
Sulfanilamide	Sulf1	50	25
Sulfanilamide	Sulf1	50	25

Approximately 25 mg of the biochar sample and 50 mg of the catalyst Wolfram Tungsten Oxide were combined for the Biochar25 method. Approximately 50mg of the biochar sample and 100 mg of the catalyst Wolfram Tungsten Oxide were combined for the Coal50 method. The samples were sealed in a tin boat and analysis was performed using either the Biochar25 or Coal50 method. The Biochar25 method used a smaller sample weight and when the nitrogen fell below the detection limits, a larger sample weight was used as in the Coal50 method. All samples were repeated in triplicate to validate the results.

The elemental analysis method used was the CHNS method whereby these elements were determined by combustion analysis. Separate chambers collect the combustion products (Carbon dioxide, water and nitric oxide) and from the area under the curve, the weight percentage of carbon, hydrogen, nitrogen and sulphur was determined. The inputs for determining the elements carbon, hydrogen, nitrogen and sulphur using the coal50 method are detailed in Table 7.2.

Table 7.2: Coal50 procedure inputs

Parameter	Value	Units
O2 dosing time 1	30	S
O2 dosing time 2	200	S
O2 dosing flow 1	50	mL/min
O2 dosing flow 2	100	mL/min
O2 cut of threshold	30	%
Autozero delay N	15	s
Autozero delay S	15	s
Peak anticipation N	70	s
Peak anticipation C	150	s
Peak anticipation H	75	s
Peak anticipation S	80	s
Desorp. CO2	240	°C
Desorp. H2O	150	°C
Desorp. SO2 (1)	100	°C
Desorp. SO2 (1) time	60	s
Desorp. SO2 (2)	230	°C

7.9 Statistical Analysis

Data were analysed using R software version 2.15.1 (R Development Core Team, 2012). For the lab scale pyrolyser, a general linear model was used to analyse the effects of moisture, grain direction and peak temperature on the measurements of nitrogen, carbon, hydrogen, volatile matter, fixed carbon and yield.

From the pilot scale pyrolyser, a general linear model was used to analyse the effects of moisture, peak temperature and residence time on the measurements of nitrogen, carbon, hydrogen, volatile matter, fixed carbon and yield.

Usual model assumptions, including testing for normal distribution of data, were assessed by examining diagnostic residual plots for each model. Outliers were identified using the residuals versus leverage function. The preferred model was obtained after removing terms that were not significant in the general model. Differences were considered highly significant at $p \leq 0.01$, significant at $0.01 < p < 0.05$ and moderately significant at $0.05 < p < 0.1$.

8.0 **FEEDSTOCK**

The feedstock used for both the lab scale and pilot scale experiments was *Pinus radiata*. This is a fast growing wood readily available in New Zealand and is used in several applications including furniture, structural work (both interior and exterior), panels and landscaping. As this wood is heavily processed, there is a large amount of waste material that could be utilised hence why this feedstock was selected for research.

Three tests were carried out on the biomass to determine its composition. The first was constituent analysis to give the main components (lignin, hemicellulose and cellulose) present in wood. The second was proximate analysis for fixed carbon, volatile matter, moisture as well as impurities, and the third was an elemental analysis to determine the elemental composition upon combustion. The results from constituent analysis and proximate analysis are reported on a dry basis and the results from elemental analysis are on a total basis.

For the lab scale analysis, the pine wood used was all from a single tree. This was to minimise tree to tree variation. However, as wood is an anisotropic, hydroscopic material, there will be variation in the wood, so representative samples were taken for analysis. For pilot scale analysis, pine wood chips from various *Pinus radiata* trees were used as this is what will be available to a hobby farmer.

The constituent analysis results for *Pinus radiata* are given in Table 8.1 and Table 8.2 and show the weight percentage of lignin, hemicellulose and cellulose. The remaining minor components are made up of organic (primarily lipid, phenolic and resin acid extractives) and inorganic (ash) material. The reported ranges for constituent analysis of pine wood are lignin (16 - 33 %), hemicellulose (20 - 40 %) and cellulose (40 - 50 %) (McKendry, 2002; Mohan, et al., 2006). The lignin results for both pine feedstock's' fall within the ranges typical for this type of softwood but are lower than that reported for hemicellulose. It can be seen that the percentage of cellulose is higher in the wood chip than the single tree which may be due to the wood chips coming from multiple trees of varying ages.

Table 8.1: Constituent analysis of the *Pinus radiata* feedstock used in the lab scale experiments (Dry basis)

Sample	NDF %	ADF %	Lignin %	Hemicellulose %	Cellulose %
1a	86.5	73.7	24.4	12.8	49.3
1b	86.5	72.5	24.3	14.0	48.2
Average	86.5	73.1	24.4	13.4	48.8

Note: NDF = Neutral detergent fibre, ADF = acid detergent fibre

Table 8.2: Constituent analysis of the Pinus radiata wood chips used in the pilot scale experiments (Dry basis)

Sample	NDF %	ADF %	Lignin %	Hemicellulose %	Cellulose %
2a	94.8	78.5	23.3	16.3	55.1
2b	94.8	80.3	23.3	14.5	56.9
Average	94.8	79.4	23.3	15.4	56.0

Note: NDF = Neutral detergent fibre, ADF = acid detergent fibre

Proximate analysis was conducted in the thermogravimetric analyser (TGA) on the wood to determine the percentage of moisture, volatile matter, fixed carbon and ash in the sample. The results in Table 8.3 were conducted using a closed crucible, to prevent any sub-micron particles being carried away by thermal draft. They show there is not much variation in the fixed carbon content and volatile matter but considerable variation in ash content of the samples which was found by difference from the total mass. This is because the sample weight was small (<20 mg) and the ash is present in low levels (< 1 %), resulting in high error levels. The percentage of fixed carbon and volatile matter are similar to that reported in literature for *Pinus radiata* (Cetin et al., 2004). Table 8.6 provides a summary of ash results obtained from a subsequent test, residue on ignition.

Table 8.3: Proximate analysis of the *Pinus radiata* feedstock used in the lab scale experiments (Dry basis)

Sample	Moisture (wt %)	Fixed Carbon (wt %)	Volatile Matter (wt %)	Ash (wt %)
1a	10.1	78.8	20.0	1.2
1b	9.6	76.8	18.9	4.3
1c	10.5	79.8	19.3	0.9
1d	9.3	80.7	19.3	0.0
1e	9.7	80.3	19.7	0.0
Average	9.9	79.3	19.4	1.3
σ	0.5	1.6	0.4	1.8
CV	0.05	0.02	0.02	1.39

Note: σ = Standard deviation, CV = Coefficient of variation

Table 8.4: Proximate analysis of the *Pinus radiata* wood chips used in the pilot scale experimental (Dry basis)

Sample	Moisture (wt %)	Fixed Carbon (wt %)	Volatile Matter (wt %)	Ash (wt %)
2a	1.449	78.422	21.194	4.154
2b	1.946	79.162	20.445	5.891
2c	3.217	78.160	21.490	-7.135
Average	2.204	78.581	21.043	0.970
σ	0.912	0.519	0.538	7.073
CV	0.414	0.007	0.026	7.292

Note: σ = Standard deviation, CV = Coefficient of variation

Elemental analysis on combustion determined the percentage of nitrogen, carbon, hydrogen and sulphur. The results in Table 8.5 show good reproducibility. The wood is comprised of on average 0.13 % nitrogen, 51.5 % carbon, 7.22 % hydrogen and trace amounts of sulphur (<0.01 %). The remaining components in wood are ash, which was determined by residue on ignition and oxygen, which was determined by difference.

Table 8.5: Elemental analysis of *pinus radiata* (Total basis)

Sample	N %	C %	H %	S %	O %
1a	0.13	51.47	7.18	0.01	40.91
1b	0.14	51.52	7.26	0.01	40.77
1c	0.14	51.48	7.39	0.01	40.68
Average	0.14	51.49	7.28	0.01	40.77
σ	0.01	0.02	0.11	0.00	0.12

Note: σ = Standard deviation

Residue on ignition was conducted after the results from proximate analysis were inconclusive. Residue on ignition used a much larger sample mass (1-2 g) compared with proximate analysis (20 mg). Table 8.6 shows the average ash content of a homogenous ground *Pinus radiata* tree sample is 0.30 % whereas the ash content from the wood chips is slightly higher at 0.39 %. This method shows good reproducibility.

Table 8.6: Residue on ignition analysis for ash determination (Dry basis)

Sample	% Ash [1]	%Ash [2]
1a	0.318	0.384
1b	0.280	0.393
1c	0.309	0.350
Average	0.302	0.376
σ in %	±0.019	0.023

[1] wood used for lab scale experiments, [2] wood chips used for pilot scale experiments.

9.0 LAB SCALE PYROLYSER RESULTS

9.1 Biochar Composition

Chars were made using the lab-scale pyrolyser as summarised earlier in chapter 6.2, at nominal soak temperatures of 300 °C, 500 °C and 700 °C. For each experiment the mass yield was measured and the particle density was determined. Samples were then subjected to proximate analysis, elemental analysis and a residue on ignition test. Each of these methods was described in chapter 7.0. Here the results of these tests are presented.

9.1.1 Biochar Yield

The fitted general linear model of yield on a dry basis versus peak temperature, size, moisture and grain direction shows that yield is highly dependent on peak temperature ($p<0.001$), moisture ($p<0.001$) and grain direction ($p<0.01$). A high correlation coefficient confirms that peak temperature, size and moisture adequately explains biochar yield (R^2=70 %). The dry sample weights were not recorded for the soaked samples, so a dry weight was estimated to enable analysis of the variables that impacted on the yield. Figure 9.1 shows the raw data for all the oven dry samples plotted against the yield. As temperature increases, the yield decreases. Plant biomass is composed of up to 50 % cellulose. The higher yield of carbonised material at 300 - 400 °C may be due to limited thermal decomposition of cellulose in wood at temperatures between 240 - 350 °C (Mohan, et al., 2006). Lignin, which makes up 25 – 30 % of the chemical composition of wood, is thermally stable below 270 °C, but it degrades between 280 - 500 °C as the volatiles are driven off and the yield decreases.

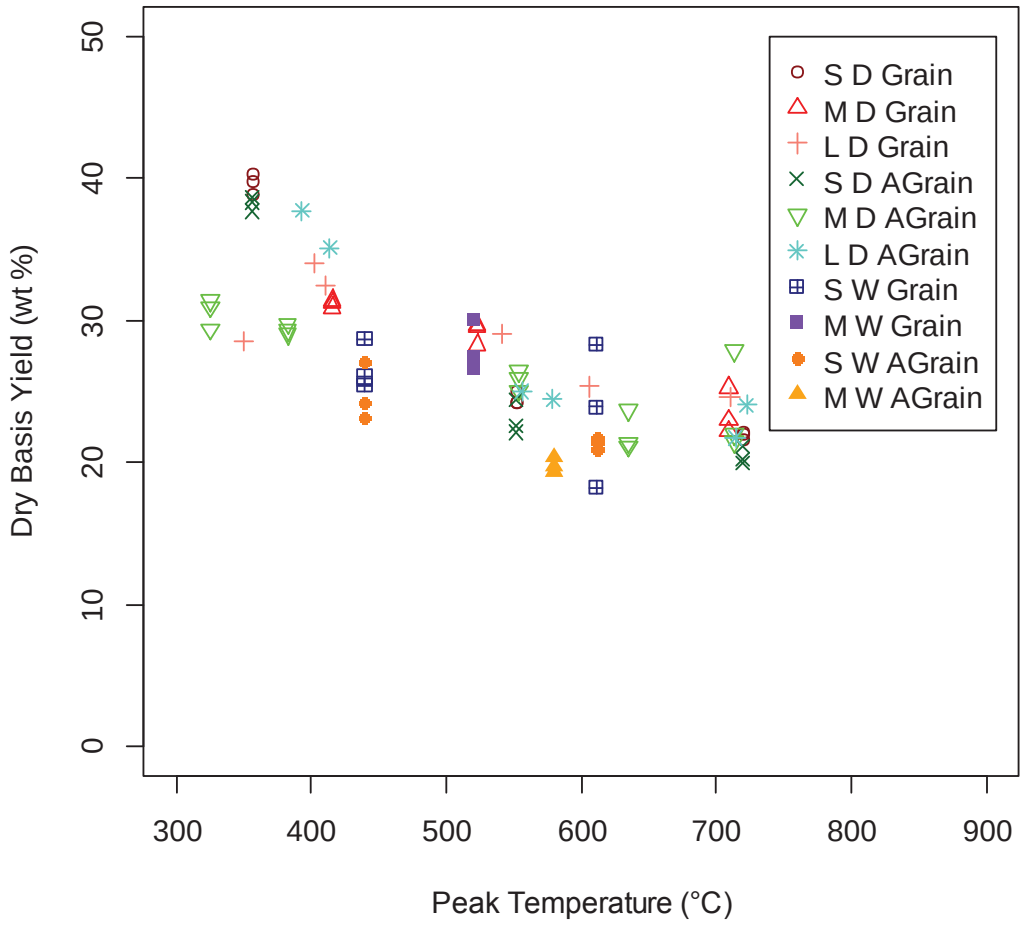

Figure 9.1: Raw data including the variables size, moisture, grain direction and peak temperature against yield; S = small, M = medium, L = large, D = dry wood, W = wet wood, Grain = with the grain, AGrain = against the grain

The preferred model was Yield (wt %) =44.42-3.33x10^{-2} PeakTemp+1.99Grain-3.75Wet. Figure 9.2 shows a plot of the raw data of the preferred model.

The difference between the yields of dry and wet samples can be attributed to wet wood having a higher level of stress due to the steam generated in the wood. This produces the pathway for which the gases have to travel out. This pathway will be shorter than that for the dry wood which means less secondary reactions occur resulting in less char produced and hence a lower yield than the dry samples.

The wood was cut either with the grain or against the grain. The gases have further to travel in wood with the grain which means more contact time for the gases and more secondary reactions. This explains why the yield is higher for wood cut in the grain direction. For wood cut against the grain, the gases can come out each side and have less contact time with other char.

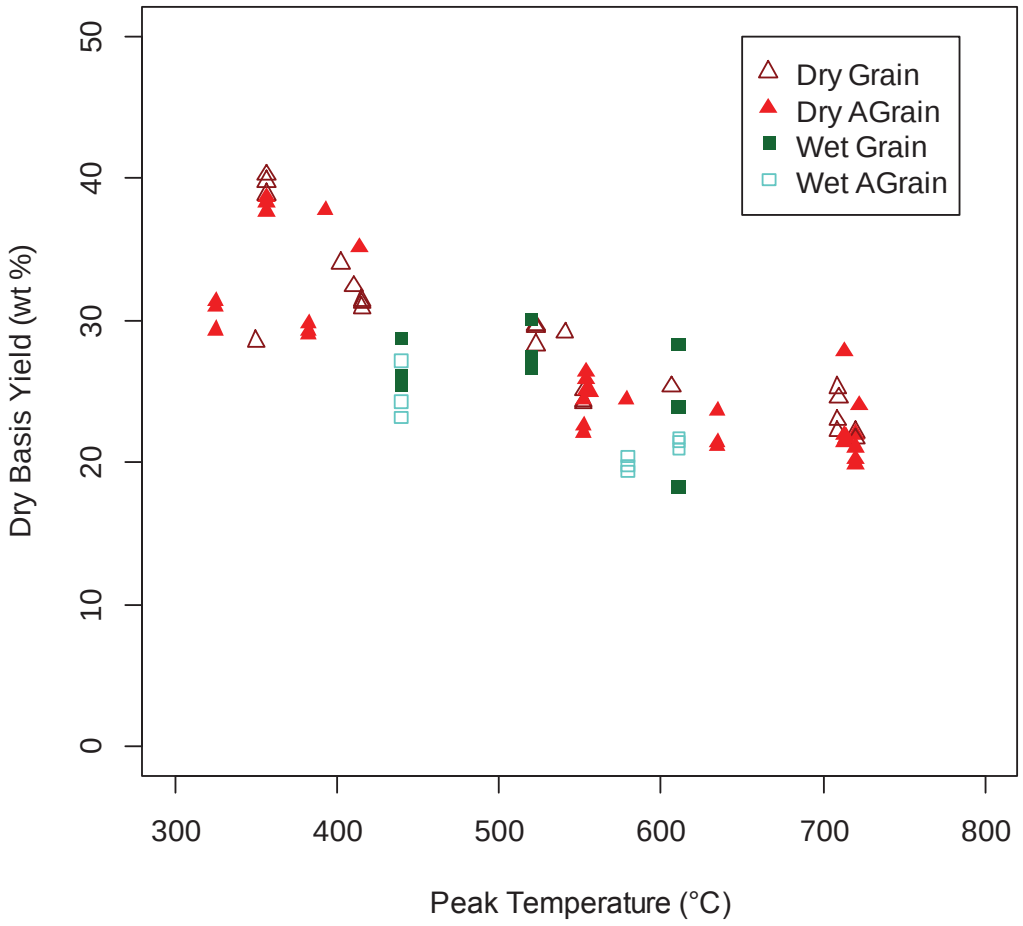

Figure 9.2: Raw data from the preferred model

9.1.2 Particle Density

Figure 9.3 shows the char particle density plotted against peak temperature with the legend showing the other variables. When these are taken into account, a general linear model shows that peak temperature is the only variable that has a significant effect on the particle density ($p<0.01$) with an adjusted R^2 of 23 %. The adjusted R^2 adjusts for the number of explanatory variables in the model, and provides an indication of how well the data fits the regression line. This means the peak temperature only has a weak effect on density; therefore, other factors must be responsible and further investigation of what these might be is recommended.

Nevertheless, the general trend that increasing temperature decreases the particle density is expected as the biochar loses more volatile matter and so becomes more porous with elevated temperatures. This general trend is consistent with the results obtained from Guo &

Lua (1998) who pyrolysed palm oil stones. Their particle density decreased from 1.44 g/cm^3 at 400 °C to 1.27 g/cm^3 at 800 °C whereas our results are much lower.

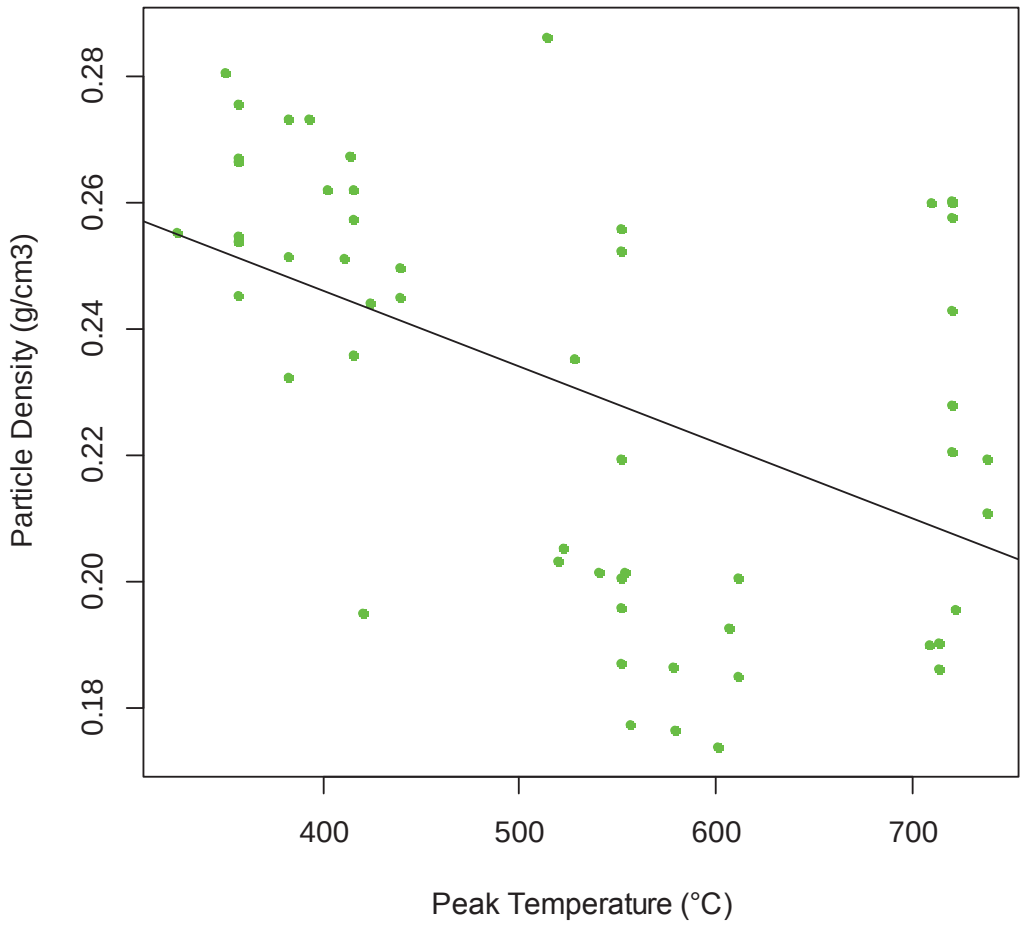

Figure 9.3: The effect of peak temperature on bulk density of pine pyrolysed under various conditions

9.1.3 Proximate Analysis

All samples were analysed in a thermogravimetric analyser to quantify the percentage of volatile matter, fixed carbon and ash content. The moisture was determined at 110 °C where complete dehydration occurred. The sample was decomposed to determine the volatile matter. Oxygen was then introduced which reacted with the fixed carbon. The subsequent weight change determined the fixed carbon content in the sample and the residual matter was the ash.

Thermogravimetric analysis is an important technique for providing an indication of the quality of the biochar.

9.1.3.1 Volatile Matter and Fixed Carbon

Figure 9.4 shows volatile matter decreases with increasing temperature. These results are consistent with research carried out by Fuwape (1996) and Iman & Capareda (2012). As the pyrolysis temperature increases, devolatilisation reactions occur resulting in the loss of volatile organic compounds.

This coincides with the percentage of fixed carbon increases with increasing peak temperature. This is due to the volatile matter being driven off during the pyrolysis process, resulting in the formation of the more stable carbon known as fixed carbon.

The equation describing the preferred model where peak temperature and size are the only variables of significance is Volatile matter (wt %) = $-7.52*10^{-2}$PeakTemp+63.48Small-4.55Medium-5.14Large. The percentage of volatile matter is higher in the smaller particle size in comparison to the larger sizes. This is expected because the distance for the volatiles to travel is less in the smaller size.

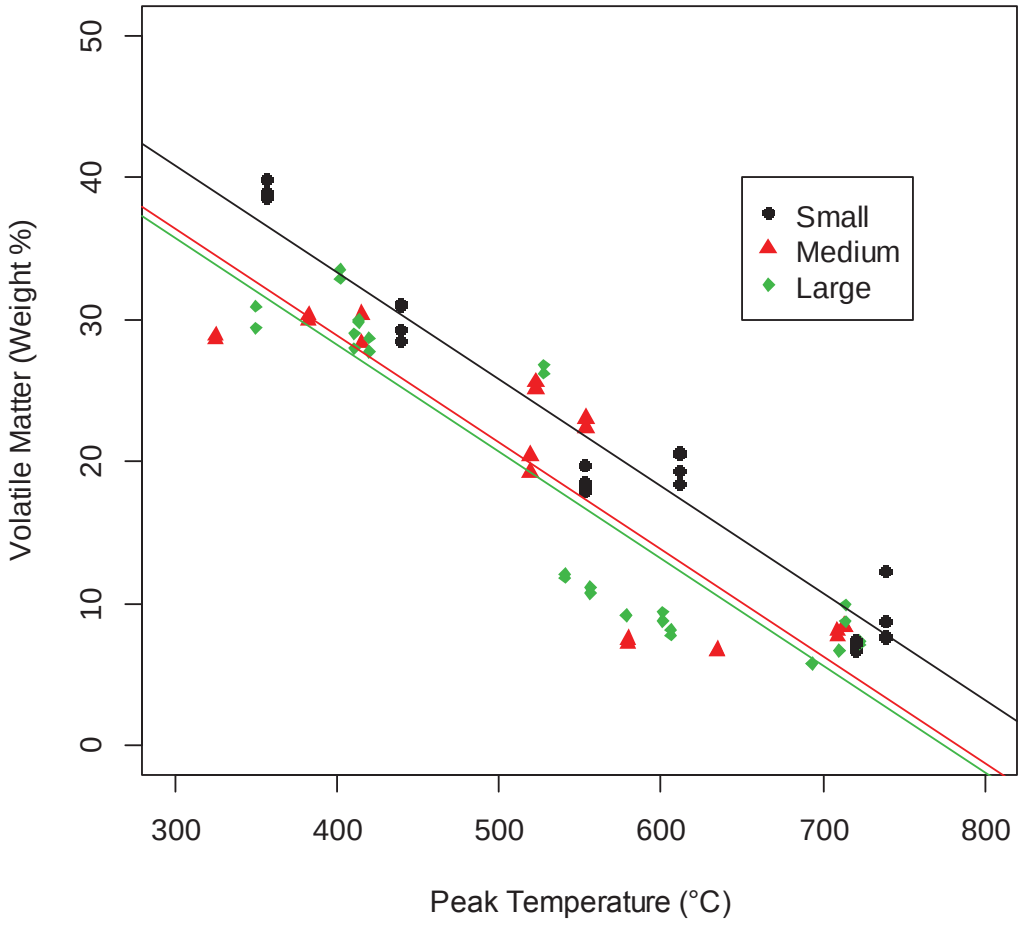

Figure 9.4: Volatile matter as a function of peak temperature and particle size

Statistical analysis for the percentage of fixed carbon showed also that peak temperature and size were the only variables of significance and gave the reduced linear model of Fixed carbon (wt %) = $7.31*10^{-2}$PeakTemp+35.89Small+4.16Medium+5.56Large. The percentage of volatile matter is lower in the larger sample size in comparison to the small sample size. Therefore it is expected that the large sample has a higher percentage of fixed carbon as the volatiles have more contact with the primary char.

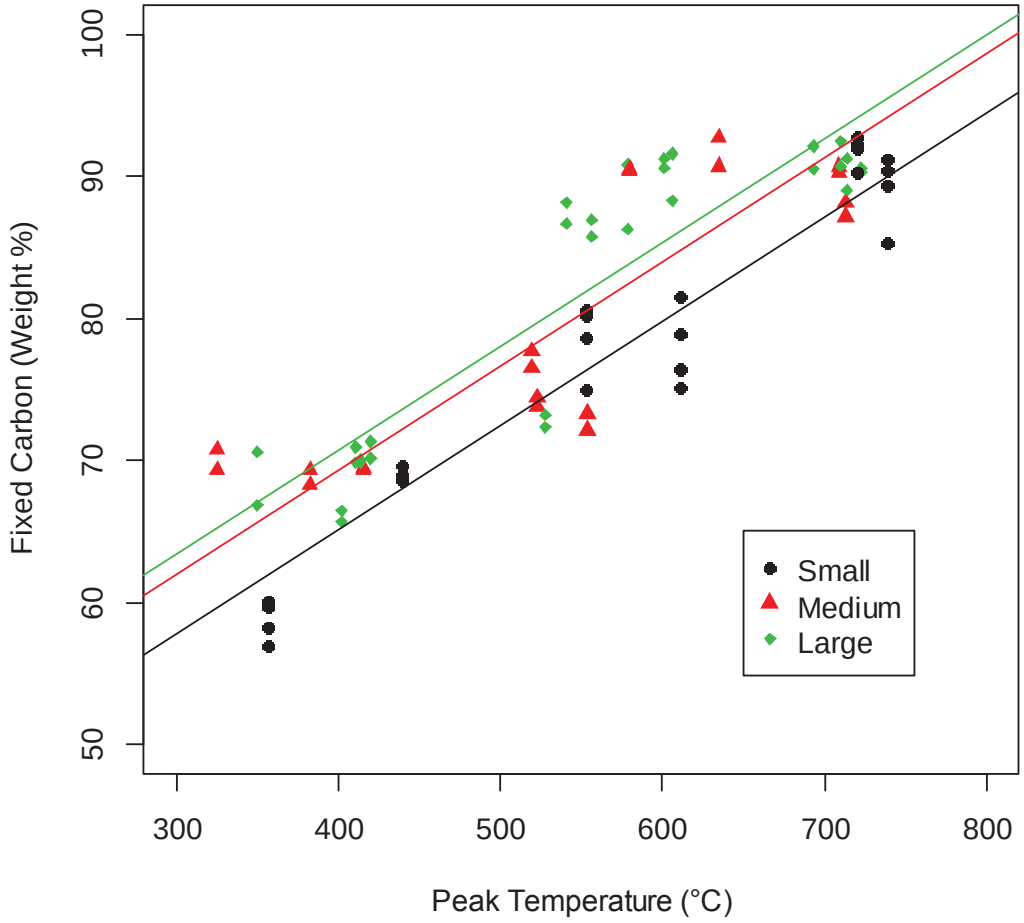

Figure 9.5: Fixed carbon as a function of peak temperature and particle size

9.1.3.2 Ash

Calcium is the most abundant mineral present in wood ash (Ragland et al., 1991) followed by potassium and traces of other minerals such as magnesium, sodium and phosphorous. Most of the basic ions are oxidised during the combustion process resulting in the formation of salt oxides as well as the formation of hydroxides and carbonates (Laird et al., 2011). High mineral contents can reduce the soil acidity and improve microbiological activity.

It is well documented that different feed stocks will have different ash contents and the majority of ash present in the feed stock is retained in the final product. Biomass with higher ash contents, particularly containing calcium and potassium (Dall'Ora et al., 2008) have been found to cause higher char yields (Hoekstra et al., 2012) and subsequently higher heating values.

As wood ash is typically present at low levels (<1 %), it is not generally regarded as a source of nutrients (Major, 2010). The thermogravimetric analysis of the biochar showed significant variation (0 - 5 %) in ash content. This was the same for the wood and is most likely due to the small sample size (~20 mg), the natural low ash content in wood and equipment sensitivity. Therefore, another method, residue on ignition, was conducted to get more accurate measurements.

Residue on ignition tests involved a much greater sample mass, between 1 - 2 g of ground biochar. A general linear model was fitted to the data in Figure 9.6 using moisture, grain direction, particle size and peak temperature as variables on ash content on a total basis.

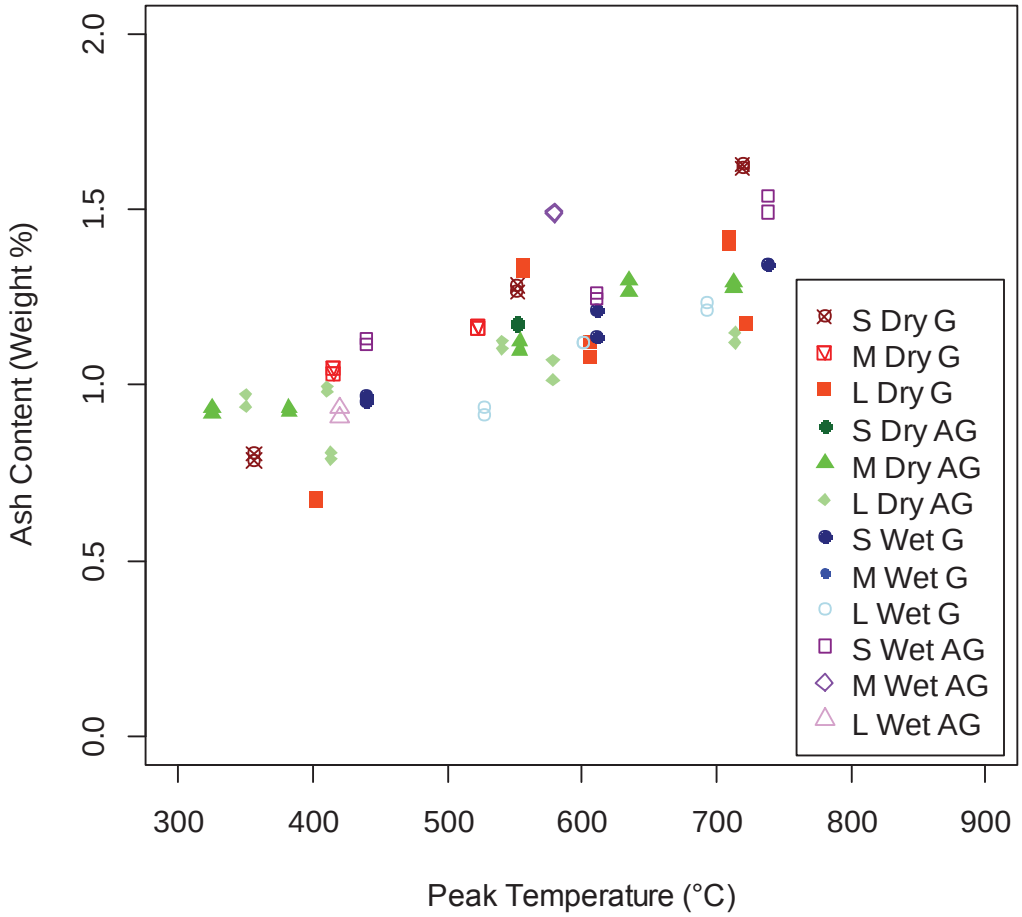

Figure 9.6: The effect of peak temperature, size moisture and grain direction on ash content. S = small, M = medium, L = large, G = with the grain and AG = against the grain

Statistical analysis gave the reduced linear model for ash content on a dry basis of $y=1.32x10^{-3}PeakTemp+4.64x10^{-1}Small-8.94x10^{-3}Medium-1.28x10^{-1}Large$ showing that peak temperature and size had a highly significant effect on the amount of ash produced ($p<0.001$). This relation was also confirmed by the high R^2 value of 70 %. The data for the preferred model is plotted in Figure 9.7 and shows there is a clear trend between the ash content in the sample and the peak temperature, which is consistent with literature (Novak, 2009; Singh, et al., 2010). As the temperature increases, more volatiles are driven off, resulting in a decrease in mass but the mineral components are retained in the solid fraction and therefore the percentage of ash increases. The organic matter undergoes thermal decomposition, resulting in weight loss in the carbon containing fraction. A further interesting result was that size also impacts on the ash content with the large particle size exhibiting lower ash contents in comparison to the small and medium particle sizes. This may be due to the heat and mass transfer limitations in the larger particle size. From section 8.2.3.1, it was shown that the larger the particle size, the higher the fixed carbon yield. Therefore, the same mass was combusted, it is expected that the small particle size exhibits a greater percentage of ash as more volatiles have been driven off.

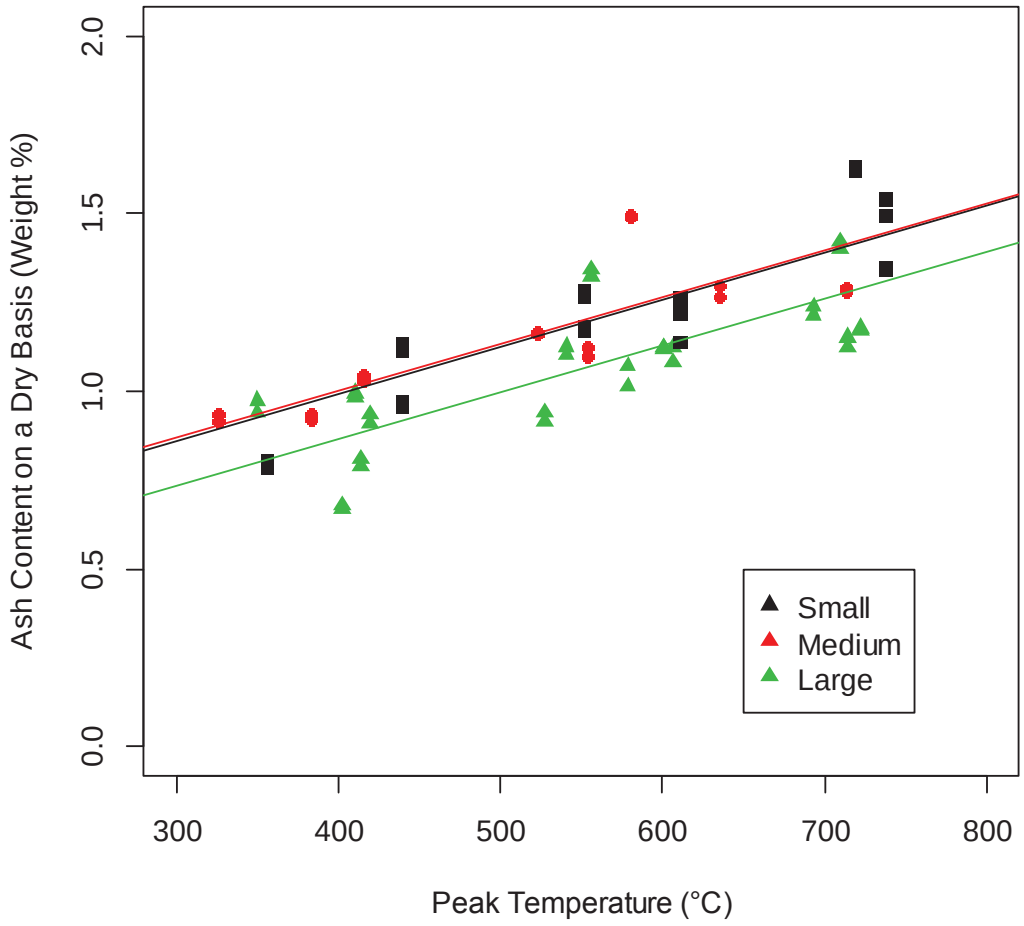

Figure 9.7: The effect of peak temperature on ash content and particle size

Some ash values could not be obtained due to the limited biochar available, therefore, ash predicted values versus ash experimental values (on a dry basis) were plotted to provide an estimate of the ash content of biochar formed under the same conditions. An estimate was required to enable the total oxygen calculation by difference and subsequently the higher heating value could be determined. The preferred model of peak temperature and particle size shows that 70 % of the variation is explained by peak temperature and size.

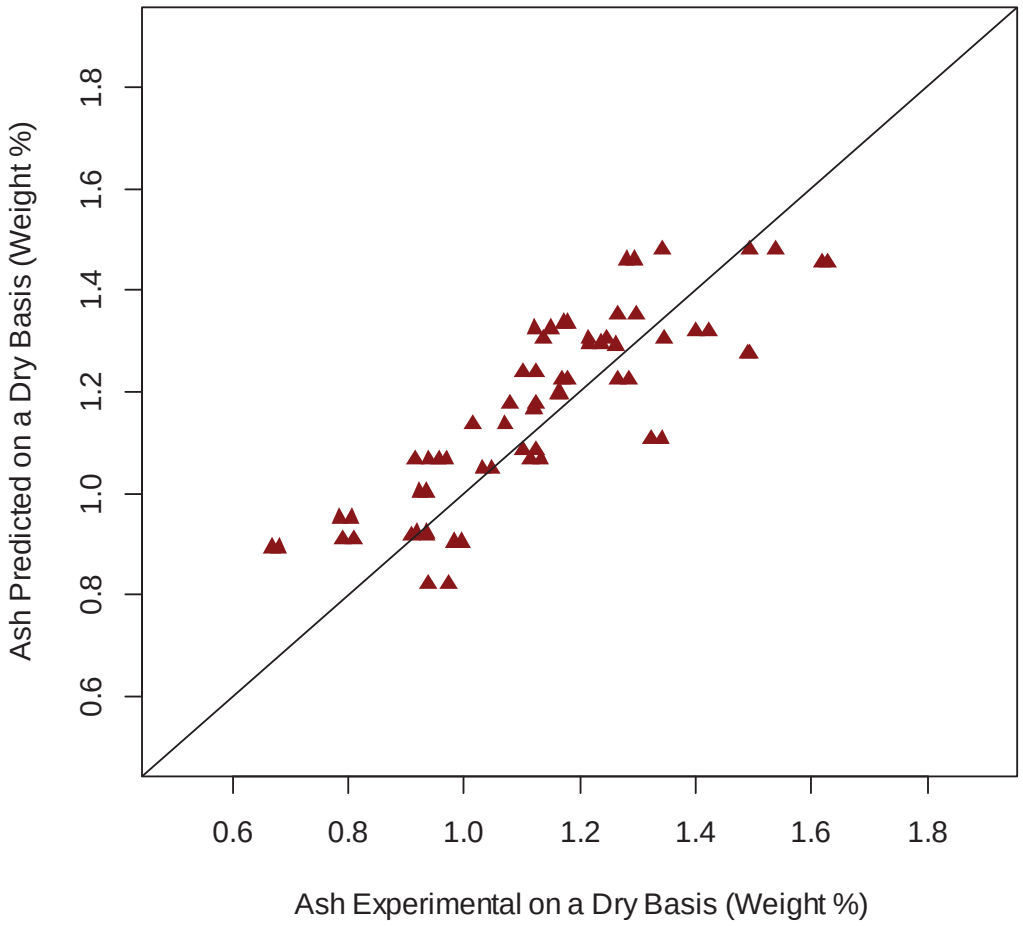

Figure 9.8: Ash predicted versus ash experimental on a dry basis

9.1.4 Elemental Analysis

9.1.4.1 Nitrogen

A general linear model was fitted to analyse the effect of peak temperature, moisture, grain direction and size on the nitrogen content in biochar on a total basis. The results show that peak temperature and moisture were the only variables that had a significant effect on nitrogen ($p<0.01$). The preferred model, which includes only the variables of significance and gave the reduced linear model of Nitrogen (wt %)=$4.67x10^{-4}$PeakTemp +$8.01x10^{-3}$Dry-$3.89x10^{-2}$Wet and shows that only 45 % of the variation in nitrogen was related to peak temperature and moisture. Nitrogen is present in very low levels in biochar (<0.5 %), which is thought to contribute to the low R^2 value and the large spread of data. This high variation is further confirmed by the large range for the coefficient of variation (3.3 % - 49.2 %). The minimum sample range for nitrogen is 0.03 mg, so for 50 mg samples there must be at least 0.06 % nitrogen in the sample to provide a good signal to noise ratio and good repeatability.

A plot of the percentage nitrogen versus peak temperature (Figure 9.9) shows the percentage of nitrogen increases with increasing temperature. This trend can be explained because as the temperature increases, volatiles are driven off resulting in an overall decrease in mass, however, the nitrogen does not have anything to react with which results in the accumulation of nitrogen residues. These results are comparable to other published literature (Baldock & Smernik, 2002; Dan & Robert, 2001).

Wet samples may have affected the nitrogen content because the steam generated may have caused an increase in pressure which meant the wood may have fractured more than the dry samples. This fracturing may have provided a path for the gases to escape, reducing the contact time which may have caused the wet samples having a lower percentage of nitrogen present. Moisture was not shown to have an effect on any other parameter tested. As the nitrogen levels are less than 0.5 %, and the coefficient of variation at times was very high, the difference could possibly be attributed to experimental error.

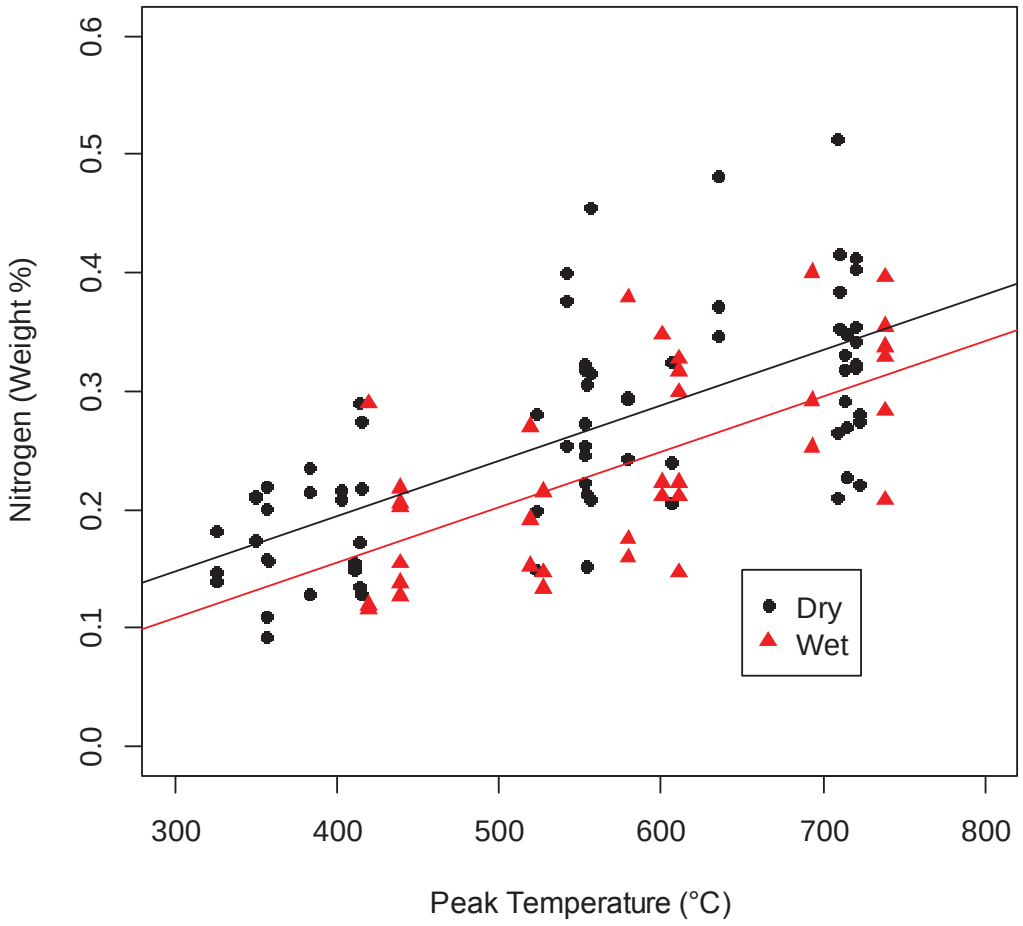

Figure 9.9: The effect of peak temperature against Nitrogen; the average nitrogen percentage in unpyrolysed *Pinus radiata* is 0.13

9.1.4.2 Carbon

The fitted general linear model including the effect of peak temperature, moisture, direction and size on the carbon content in biochar shows that peak temperature and size were variables of significance ($p<0.01$). The preferred model of peak temperature and size against carbon shows that 86% of the variation was explained by peak temperature and particle size is represented by the following equation Carbon (wt %)=$4.95x10^{-2}$PeakTemp+ 54.80Small+2.59Medium+3.55Large. The coefficient of variation ranged from 0 % to 1.1 % which indicated good sample repeatability.

Figure 9.10 illustrates that the percentage of carbon increases with increasing peak temperature. As the volatile matter content decreases as the temperature increases, structural changes occur which result in a more stable carbon, characterised by increasing aromacity. This is further explored when the H/C ratios are discussed later in section 9.1.4.4.

The large particle size had the highest percentage of carbon present in the sample followed by the medium and then small sizes. This relation could be a result of how the particles fracture. Smaller particles fracture less than larger particles. These large particles fracture releasing volatiles which can then interact with the char producing secondary char, which could explain the higher carbon levels.

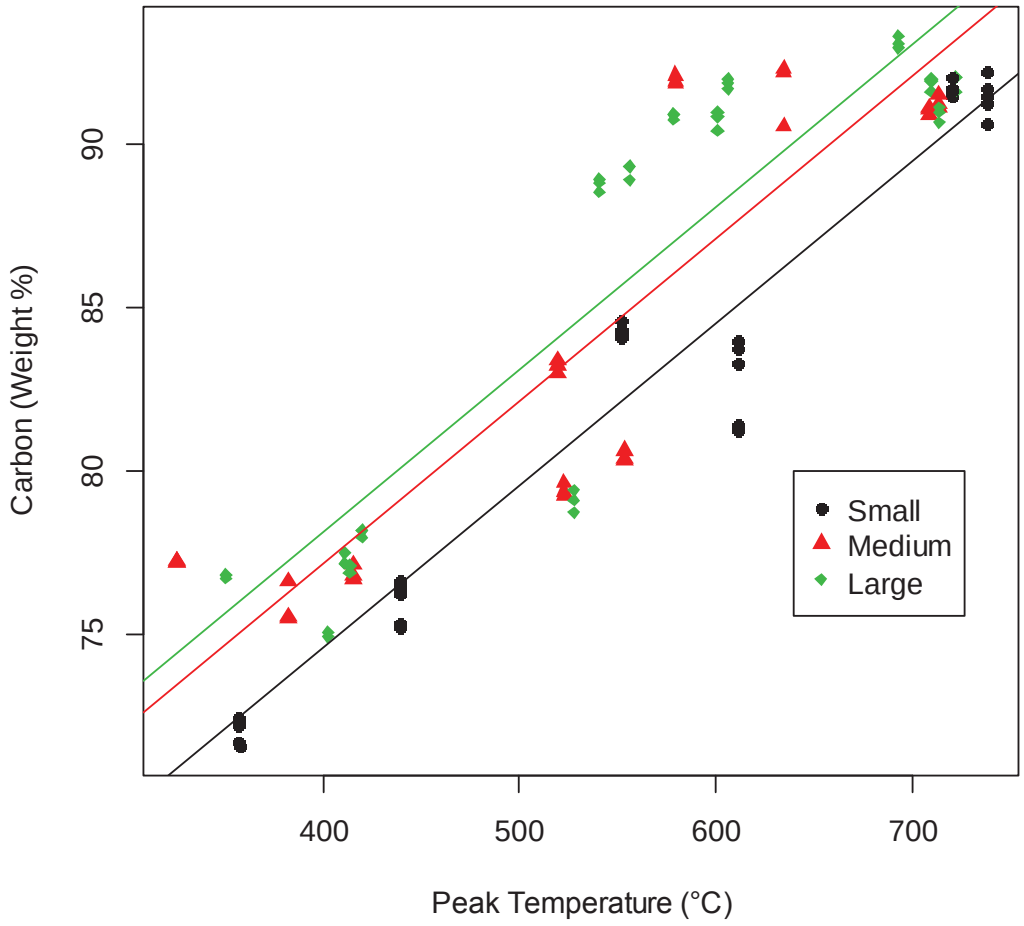

Figure 9.10: The effect of peak temperature on particle size and carbon; the average carbon percentage in unpyrolysed *Pinus radiata* is 51.3 %.

9.1.4.3 Hydrogen

The fitted general linear model of the effect of peak temperature, moisture, direction and size on the hydrogen content in biochar shows that peak temperature and particle size were variables of significance ($p<0.001$). The preferred model of peak temperature and size against hydrogen accounted for 83 % of the variation and was given by the equation Hydrogen (wt %) = -5.83×10^{-2}PeakTemp+6.41Small-3.49×10^{-1}Medium-2.68×10^{-1}Large. The coefficient of variation ranged from a minimum of 1.8 % to a maximum of 10 % which show good reproducibility.

Figure 9.11 shows that the percentage of hydrogen decreases with increasing peak temperature. As the temperature increases, reactions occur which change the structure of carbon and the number of active sites decreases which results in a loss of reactivity. This loss in reactivity is due to weaker bonds breaking and results in the decrease of hydrogen (Cai et al., 1996; Jamil & Li, 2006; Onay, 2007).

The relation between particle size on peak temperature and hydrogen levels may be due to a lower average temperature in the medium and large samples due to thermal lag during the heating phase. There is a not much variation between the medium and large samples. This may be due to thermal cracking.

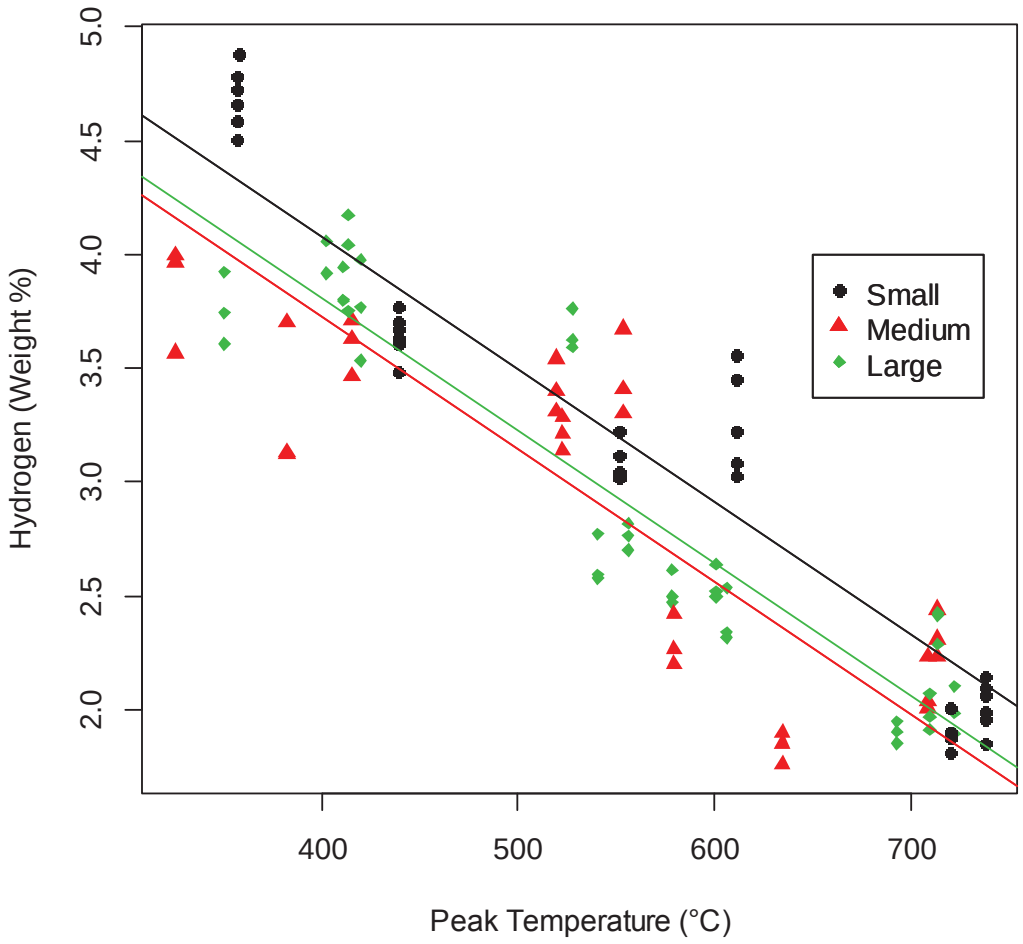

Figure 9.11: The effect of particle size and peak temperature on hydrogen; the average hydrogen percentage in unpyrolysed *Pinus radiata* is 7.1

9.1.4.4 Hydrogen to Carbon and Oxygen to Carbon Ratios

The ratios of H/C and O/C can provide important information on the functional groups present, the extent of carbonisation, as well as the preferred ratio levels and properties which determine how beneficial the biochar will be as a soil amendment.

Figure 9.12 shows H/C plotted against O/C on a mole percent basis. It can be seen that there is a strong positive correlation between H/C and O/C (R^2 = 92 %). The atomic H/C and O/C ratios are low, ranging between 0.2 - 0.82 and 0.04 - 0.26 respectively. Low ratios suggest there is a higher presence of stable carbon compounds and less functional groups (Yonebayashi & Hattori, 1988). Schimmelpfennig & Glaser (2012) have concluded from their work that the molar ratios of H/C and O/C are most beneficial for soil applications when they are less than 0.6 and 0.4 respectively. Figure 9.13 shows the higher temperature chars (greater than 500 °C) are within these ranges and are consistent with other carbonised coals (van Krevelen, 1950).

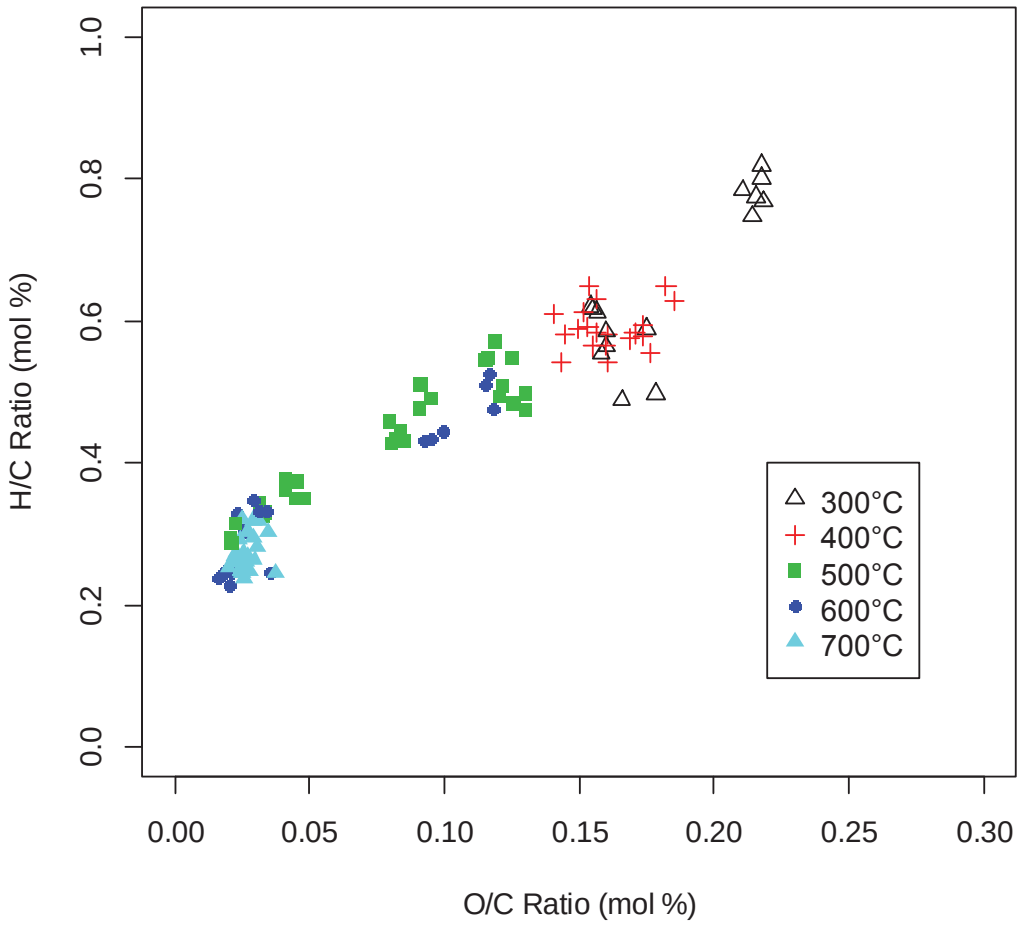

Figure 9.12: van Krevelen diagram of atomic H/C vs O/C ratios for biochar derived from *Pinus radiata*

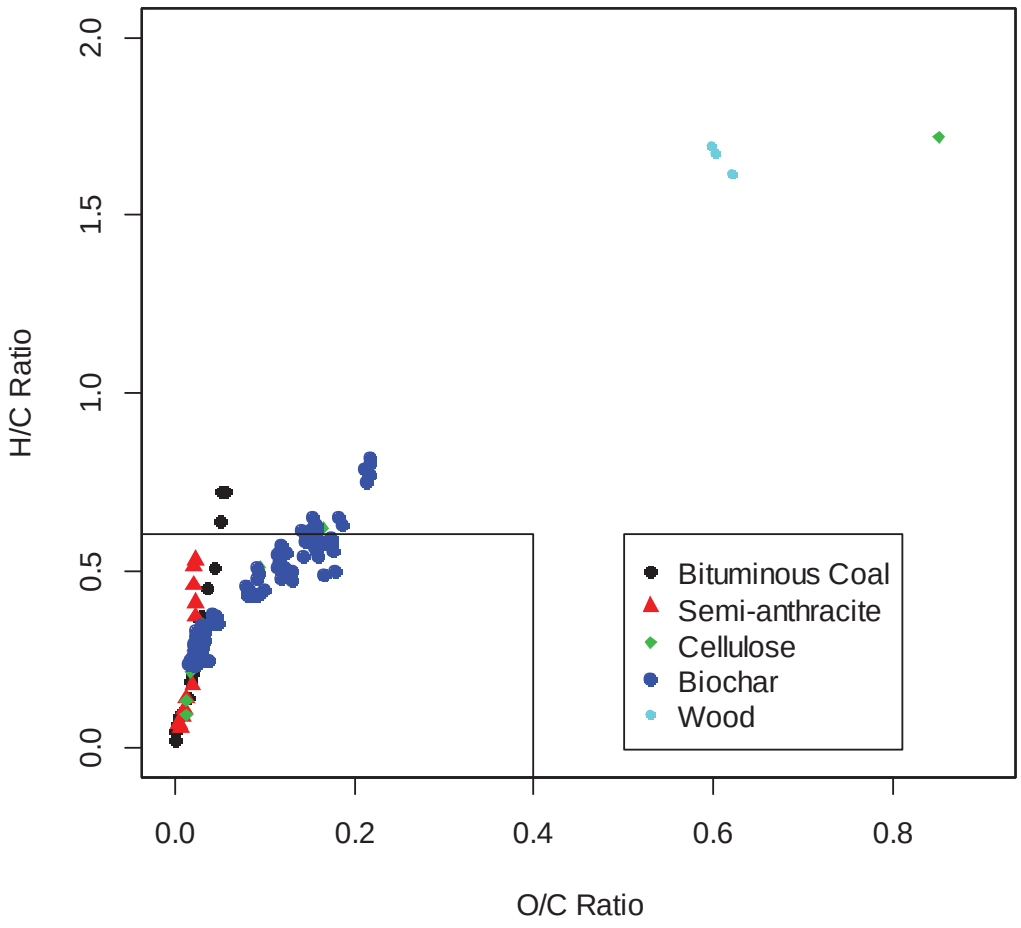

Figure 9.13: Atomic ratios of H/C vs O/C for carbonised coal (Bituminous and semi-anthracite), cellulose (van Krevelen, 1950), the *Pinus radiata* feedstock used in the experiments and the resulting biochar produced from various operating conditions

Figure 9.14 shows that the H/C and O/C ratios decrease with increasing temperature. This is consistent with the results obtained from experiments carried out by Baldock and Smernik (2002) and Chun et al., (2004). It is thought that the decrease in H/C with increasing peak temperatures is a result of structural changes leading to the increase in aromatic compounds and hence an increase in soil stability (Krull et al., 2009). Also, lower soil degradation rates were reported (Glaser et al., 2005) as well as “chemical stability against microbial degradation” (Preston & Schmidt, 2006). The O/C ratio provides information on the polarity of the functional groups. This is useful for determining the surface properties and its ability to absorb water. Chun et al., (2004) observed that chars with low O/C ratios (<0.1) had a lower affinity for water in comparison to char with a higher O/C ratio (~0.3).

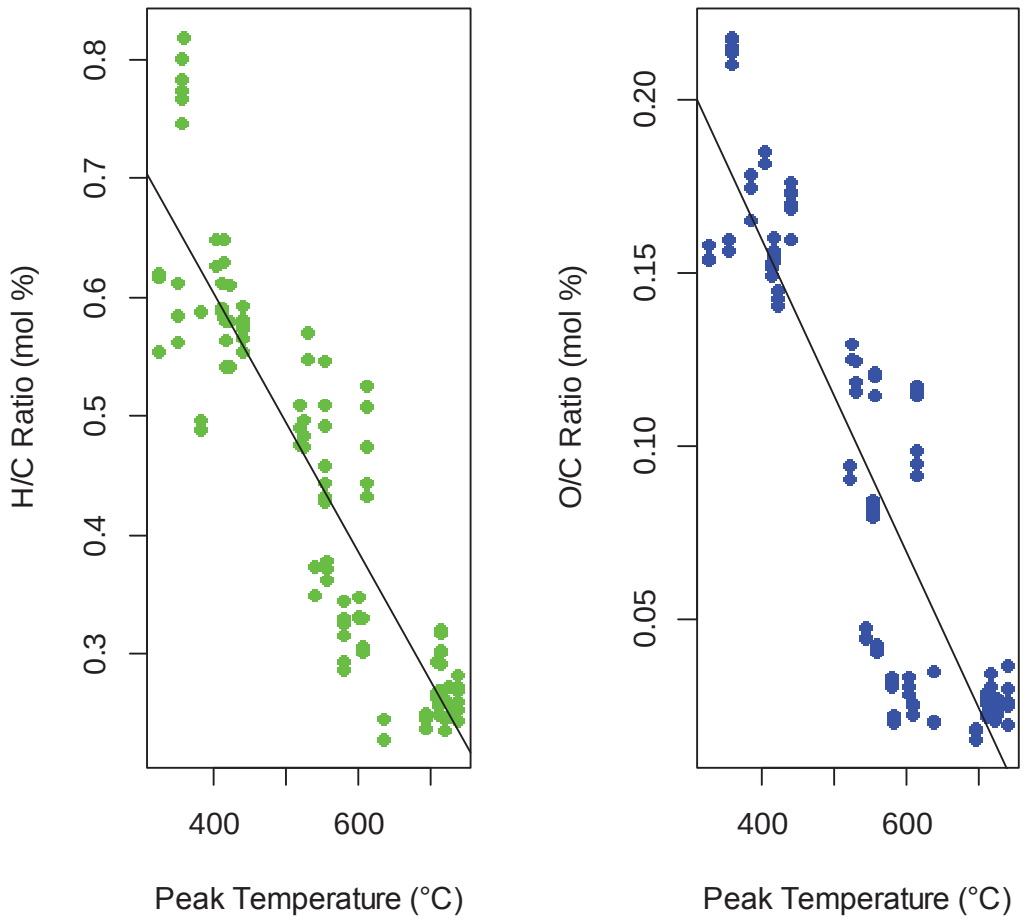

Figure 9.14: The effect of peak temperature on H/C ratios and O/C molar ratios respectively

9.1.5 Heating Value

The higher heating value (HHV) was determined using the Dulong equation, equation (9.1) (Mason & Gandhi, 1980). The sulfur content obtained from elemental analysis was negligible (Appendix B) as the majority of results showed sulphur content was <0.01 % mass and was therefore not included in the HHV calculation. Hydrogen, nitrogen and carbon were obtained from elemental analysis. The oxygen content was calculated by difference, per equation (9.2) where the percentages are on a mass basis. The units of BTU/lb returned by Dulong can be converted to kJ/kg by multiplying it by 2.236.

$$HHV = 145.44\,C + 620.28\left(H - \frac{1}{8}O\right)[=]\frac{BTU}{lb} \tag{9.1}$$

$$Total\ oxygen = 100 - (\%Ash - \%C - \%N - \%H) \quad (9.2)$$

Statistical analysis showed peak temperature and size were the variables of significance and gave the reduced linear model of HHV (wt %) = 16.34PeakTemp+21203.08 Small+824.03Medium+1413.36Large.

Figure 9.15 shows that the higher heating value increases with increasing peak temperature. The heat of combustion of carbon is higher than that of volatile matter, so the higher the proportion of fixed carbon in the sample, the higher the expected heating value. However, as ash content increases with increasing temperature, it has been reported that the gross heat of combustion can be limited because the carbon fraction has a higher heat of combustion compared to the ash (Fuwape, 1996). The ash content in the *Pinus radiata* is less than 2 % so mineralisation processes do not impact the higher heating value over the selected temperature range. The experimental results show a good correlation between heating value, peak temperature and particle size (R^2 = 0.82).

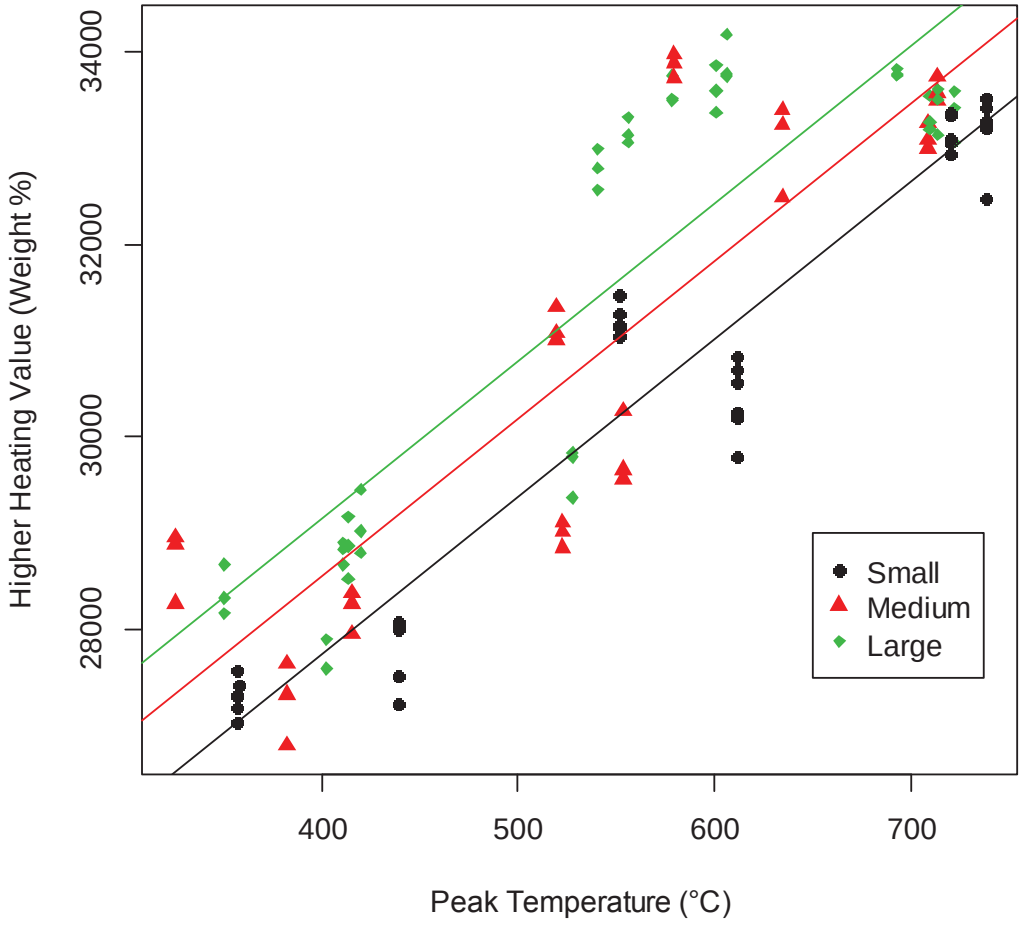

Figure 9.15: The effect of peak temperature and size on the higher heating value

9.1.6 Carbon Efficiency

Equation (9.3) below was used to calculate the fixed carbon yield.

$$Fixed\ Carbon\ Yield = \frac{m_{char} * \%\ FC_{char}}{m_{biomass}(1 - \%\ ash_{biomass})} \quad (9.3)$$

From Figure 9.16, it can be seen that peak temperature does not affect the fixed carbon yield. At lower peak temperatures the mass of char is greater, and at higher peak temperatures the mass of biochar is lower. This results in a level fixed carbon yield and indicates that biochar can be produced at any peak temperature as the fixed carbon yield is not affected.

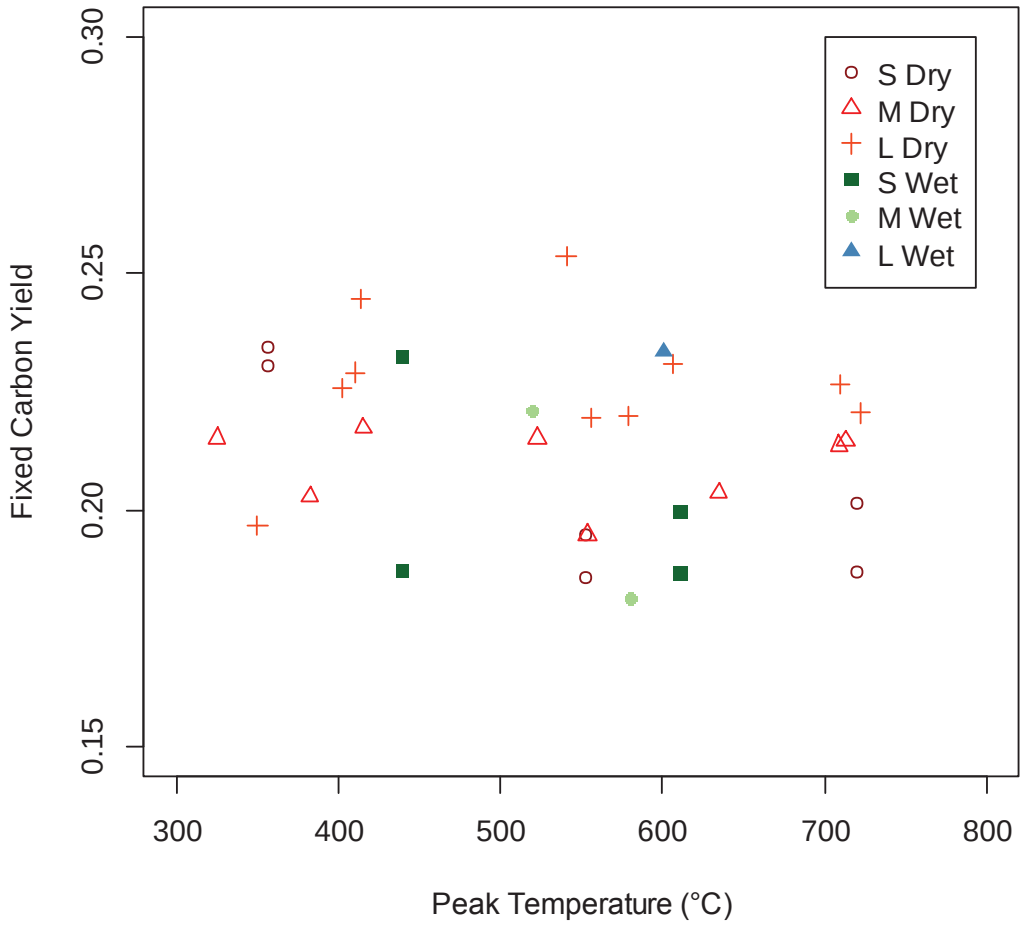

Figure 9.16: Conversion of Carbon in Feedstock to Biochar on an Ash-free Dry Basis

The carbon production efficiency is defined as the output (carbon in biochar) over the input (carbon in LPG).

$$Efficiency\ of\ production = \frac{mass\ of\ C\ in\ Biochar}{mass\ of\ C\ in\ LPG} \tag{9.4}$$

In Figure 9.17, the production efficiency decreases with increasing peak temperature. This is expected because more fuel, LPG, is required as the peak temperature increases. This figure also shows that the efficiency is very low. For every kilogram of carbon in LPG used, between approximately 0.9 - 0.1 kilograms of carbon is produced, with the amount decreasing as the temperature increases. This biochar produced from the small scale pyrolyser was not intended for manufacturing purposes, but for characterisation purposes. It is evident that the current design does not produce biochar in an environmentally friendly and sustainable way.

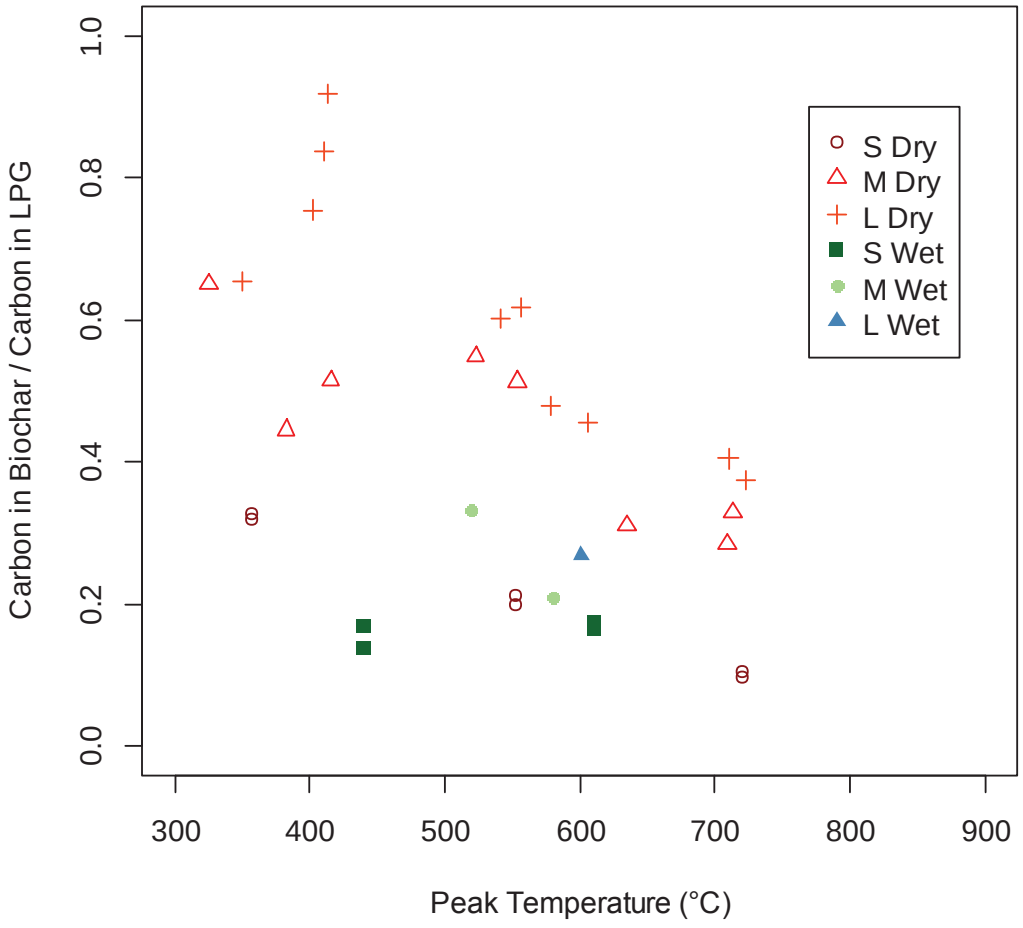

Figure 9.17: Production Efficiency

10.0 PILOT SCALE OPERABILITY AND CHARACTERISATION

In this section, the temperature profiles, LPG use and the char properties for each of the pilot scale experimental runs will be presented. Comparisons of yield, proximate analyses, carbon footprint and energy efficiency between runs will be discussed in the subsequent section. Figure 6.2, shown previously, illustrates the locations of the 8 sampling points that were used to determine the homogeneity of the charcoal and to determine whether the residence time was sufficient. A total of six trials were completed and each is discussed below.

10.1 Discussion of the Results and Operating Conditions for Run 1

Run 1 was a trial run containing 34.6 kg of woodchips (approximately 50 % full) which had an initial dry basis moisture content of 24.04 %. The operating procedure for the trials is presented in Appendix E. The aim of this run was to identify the lowest set point possible whilst still ensuring complete pyrolysis. It was decided to have a set point of 400 °C, after which point both the 23 kW and 6 kW burners will turn off automatically by the control system.

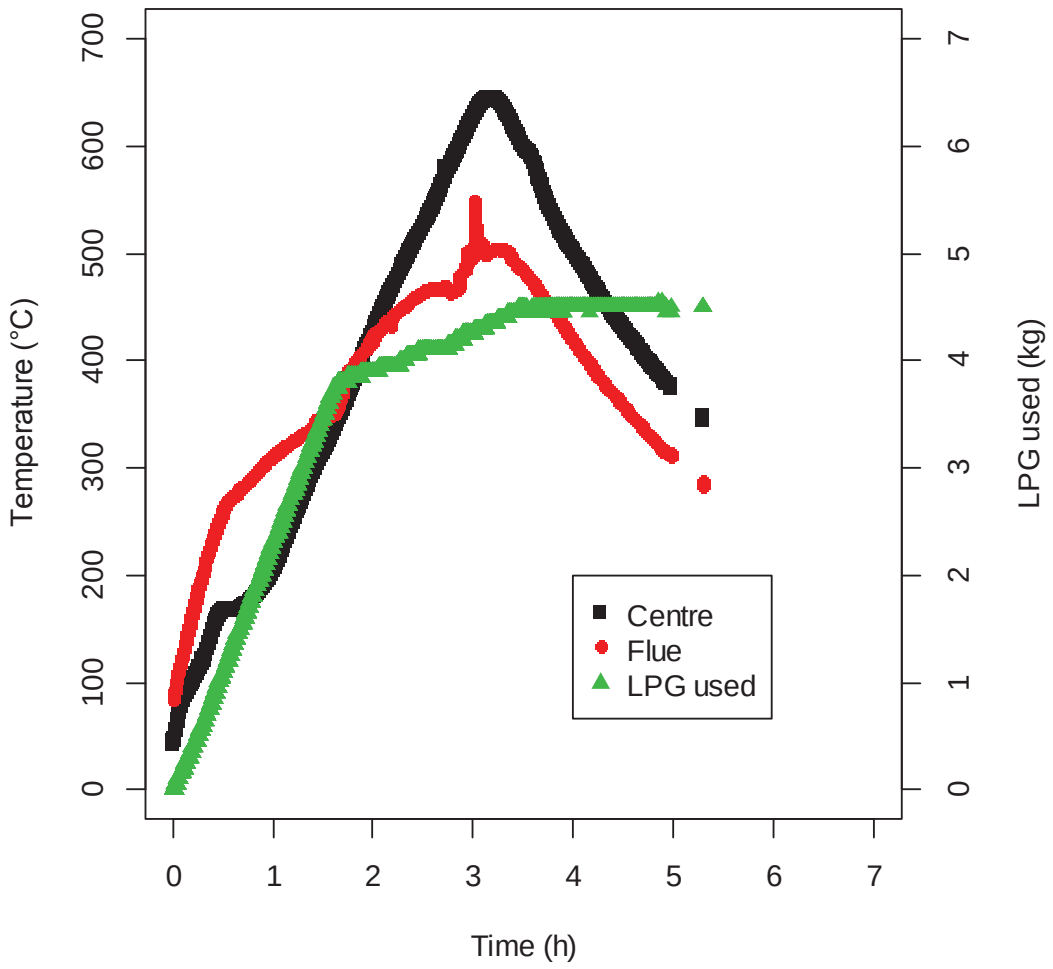

Figure 10.1: Temperature and LPG profile for Run 1

Figure 10.1 shows how the reactor centre temperature, flue temperature and the amount of LPG used change as a function of time. The centre temperature increased until approximately 170 °C, where it stabilised for a short period. This is where the majority of the water has evaporated. As this has not occurred at 100 °C where you would expect the majority of evaporation to occur, it indicates that the thermocouple is receiving additional heating. The reactor core thermocouple well is located directly above the combustion chamber; therefore, it is likely that radiation is responsible for the elevated temperature. The reactor heated up at a constant rate of 3.94 °C/min between 240 - 340 °C. When the centre temperature reached the set point of 340 °C the 23 kW burner turned off and at 400 °C the 6 kW burner turned off. The purpose of keeping the 6 kW burner going was to ensure combustion of the flammable gases so that the process becomes self-heating. The 6 kW burner was then turned off close to the desired operating point after which it is expected that the soot carryover in the gases snuffed out the flame. The products of incomplete combustion were then flared at the top of the flue stack. However, after 400°C, the reactor was producing its own heat through exothermic reactions and reached a final temperature of

646 °C before the centre temperature began dropping. The LPG consumption continued after both the burners were OFF as LPG was the fuel source for the flare. Unfortunately the data logger stopped working after almost 6 hours, but was reset after 25 hours to find the centre temperature was 135 °C.

It was established that the system was not sufficiently air-locked which was evidenced by the high centre temperature after 25 hours as well as the large amount of ash visible along with some embers. A contributing factor was that the combustion chamber had not been slid back into place between 25 and 72 hours. This oxygen ingress meant combustion occurred which resulted in the high ash levels and a low charcoal yield of 6.5 wt % on a dry basis. The inner reactor lid was identified as a potential source for the gases to be escaping out of as it may have warped with the high temperatures, which meant a draft was created enabling oxygen to enter through the secondary air holes and direct air into the base of the hollow core in the inner reactor.

Table 10.1 and Table 10.2 show the results of proximate analysis and elemental analysis respectively. As the yield was low (6.5 wt %), individual sampling locations were not tested. A representative sample of char was collected from the reactor and ground into a homogeneous sample for analysis. The results indicate the char quality is good as the fixed carbon content is high. The replicates for proximate analysis and elemental analysis show good agreement.

Table 10.1: Proximate analysis results for Run 1 on dry basis

Sample	Moisture (wt %)	Volatile Matter (wt %)	Fixed Carbon (wt %)
Run 1.001	2.08	7.12	92.52
Run1.002	2.14	7.19	92.45
Average	2.11	7.15	92.48
Σ	0.04	0.05	0.05
CV	2.00	0.70	0.05

Note: σ = Standard deviation, CV = Coefficient of variation

Table 10.2: Elemental analysis results for Run 1 on dry basis

Sample	Nitrogen (wt %)	Carbon (wt %)	Hydrogen (wt %)	Sulphur (wt %)	Oxygen (wt %)	H/C (mol %)
Run 1.001	0.35	91.57	1.26	0.00	6.46	0.16
Run1.002	0.39	91.70	1.26	0.00	6.28	0.16
Average	0.37	91.64	1.26	0.00	6.37	0.16
σ	0.03	0.09	0.00	0.00	0.12	0.00
CV	8.21	0.10	0.11	0.00	1.00	0.01

Note: σ = Standard deviation, CV = Coefficient of variation

10.2 Discussion of the Results and Operating Conditions for Run 2

The results from Run 1 indicated the set points were suitable as enough heat was provided to heat the biomass and enable the exothermic reactions to continue the heating process. It also indicated that control for lower set point temperatures was not possible because, once pyrolysis was underway, exothermic reactions generated heat and the temperature of the system rose of its own accord. This is a self-limiting heating process eventually all the available fuel is consumed. For this run, a ceramic fibre rope was placed around the inner lid in an attempt to minimise the short circuiting of the pyrolysis gases and hopefully reduce the oxygen ingress. Two additional thermocouples were placed on the same side as the burner, which was directed to the opposite side of the reactor. One thermocouple was placed in the lower annulus and one in the upper annulus approximately 0.20 m from the top and bottom of the inner reactor. This was to provide more information on the heating profile of the process.

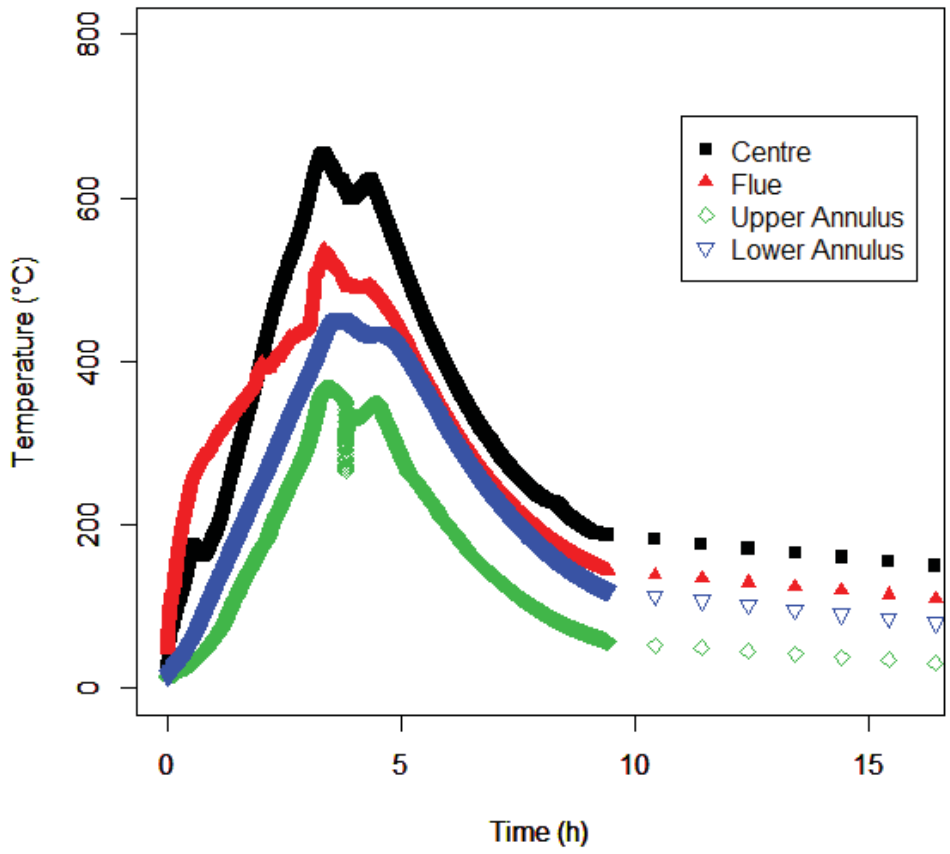

Figure 10.2: Temperature profile for Run 2

37.3 kg of air dried wood chips with an average moisture content of 21.15 % on a dry basis were used in this experiment. Initially both the 23 kW and 6 kW burners were used to heat the reactor and the air entering through the secondary air holes. It can be seen from Figure 10.2 that the centre temperature increases to 175 °C and then it decreases to stabilise at 170 °C while water evaporated (in the same manner as Run 1) before increasing again at a rate of 3.70 °C min^{-1} from between 240 - 340 °C. When the centre temperature reached 350 °C the main (23 kW) burner was turned off, at which the heating rate slowed slightly. Once the centre temperature reached the second set point of 400 °C the pilot (6 kW) burner automatically turned off. The purpose of maintaining the 6 kW going after the 23 kW is turned off is to ignite the flammable pyrolysis gases. The upper and lower annulus temperatures follow a similar profile to each other. As the reactor is heated from the bottom, it is expected that the lower annulus thermocouple temperature will be higher. These thermocouples provided information on the temperature difference between the top and bottom of the reactor. The drop in the upper annulus temperature at 4 hours was due to the tertiary air being turned on temporarily.

Once the set point of 400 °C was reached, the air to the main burner was turned off which corresponded to the flare going out directly after. The air was turned back on which

immediately reduced the smoke coming out of the flue which indicated there was not enough oxygen present when the air was off. Due to the exothermic nature of the reaction, the process carried on heating with no additional heating source until a peak temperature of 654 °C was reached and then the process began to cool down. The main burner set point was changed to 615 °C. The main burner had a 10 °C hysteresis so the main burner came on when the centre temperature reached 605 °C. The temperature increased until 615 °C and then the burner was turned off and the process was allowed to cool down. Smoke came out the flue at the peak production due to the fact the flare had stopped working. This problem recurred in other runs and is related to an improvisation required in order to operate the burner controls. The problem is explained as follows: the burners are forced draft which means that draft air is injected into the combustion chamber whether or not the burners are ON. However, a critical safety limit is to ensure excessive heating does not occur in the combustion chamber. Therefore, it is important that combustion is partially starved when the burners are OFF. Secondary air is already drawn by updraft through the open holes in the base of the combustion chamber. Earlier design calculations established that this air is only enough for partial combustion during the maximum flammable gas evolution phase of pyrolysis. Under these circumstances, when the burners are supposed to be OFF, additional air is undesirable and so the burner draft air must diverted or dumped. However, the blower must remain on because it simultaneously feeds air to the flare (which must remain ON) as well as the 23 kW, the 6 kW burners. As the exact operation of these burners was not clear until they were installed, the dumping was done manually by unscrewing the hose clamps and removing the air line. However, in doing this, it provided a path of least resistance for air from the blower out through the open lines, which had the effect of reducing air flow to the flare. This is why the flare had a habit of going out when the two combustion chamber burners had been switched off and the draft air lines disconnected. Dump valves were purchased but were received after these six trials had been completed. They will dump air while ensuring the dump resistance matches the injection resistance and so avoid affecting the flare. For the remainder of these trials, the flare habitually went out. While it does impact on the carbon footprint, it does not affect the conversion of wood chips into biochar.

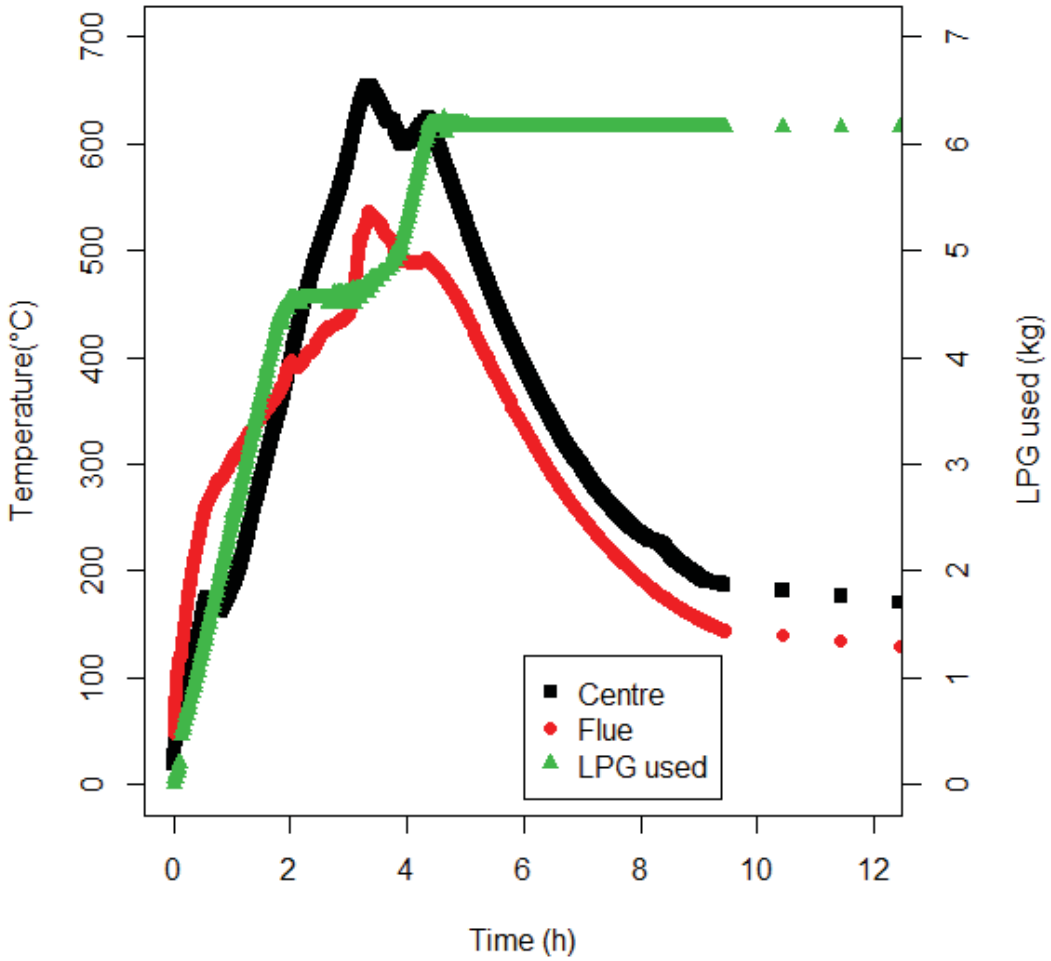

Figure 10.3: LPG profile as a function of time and temperature for Run 2

It was found that the cool down period, as seen in Figure 10.3, was taking longer than expected. This may have been due to inner lid warping allowing the volatiles to escape out of the inner lid instead of out through the hollow perforated core. This meant a draft was created through the reactor bed, allowing oxygen to enter and hence combustion to occur. This was evidenced by a few visible embers at the base near the perforated core. It is also believed the rope moved during the closing of the lid.

After the run, the sliding plate was placed over the secondary air holes. When the reactor was unloaded, it was evidenced that the sliding plate had warped due to the heat resulting in a draw of oxygen upwards. The embers were slowly combusting the charcoal whilst not allowing the reactor to cool down. The charcoal was weighed and there was an improvement in the yield to 16.2 % on a dry basis indicating there was less oxygen ingress than the previous run.

Thermal expansion calculations can be found in Appendix B. It was calculated the lid may expand up to 7.8 mm in the horizontal direction and 10.4 mm in the vertical direction.

Due to the moderate yield only four sampling points (1-4), as shown Figure 6.2 were taken from the reactor in roughly the middle layer of the charcoal. Table 10.3 shows the proximate analysis results. The charcoal had a high fixed carbon content with an average of 94.43 ± 1.41 wt % which corresponded to most of the volatiles being driven off and hence a low volatile matter of 5.19 ± 1.41 wt %. The average total carbon determined by elemental analysis was 90.42 ± 0.71 % by mass. Oxygen was the other significant element composing on average 7.68 ± 0.63 % by mass. The remaining minor constituents are shown in Table 10.4. Each sample point had duplicate elemental analyses which gave very similar results. Between samples points, there was minimal variation in the char properties and the fixed carbon content was high indicating the char was well pyrolysed and of a good quality, where quality is defined by the low H/C_{org} ratio (ranging between 0.4 - 0.7 mol %) which indicates good 100 year stability of biochar in soil (Wang, et al., 2013). Biochar is only biochar if the H/C ratio is lower than 0.7. The C_{org} is used instead of the total carbon, as the inorganic carbonates contained in the ash, do not form aromatic groups and therefore do not contribute to the stability of the char (International Biochar Initiative, 2012). This use of C_{org} particularly important for high ash feed stocks, however *Pinus radiata* is a low ash feedstock. The inorganic component of the *Pinus radiata* wood chips was calculated to be 0.08 % so therefore was considered negligible and was not subtracted from the total carbon in this research. The molar H/C ratios from Run 2 vary from between 0.08 - 0.21 mol %. This is lower than the optimum H/C range for the proposed 100 year stability.

Table 10.3: Proximate analysis results for Run 2

Sample	Moisture (wt %)	Volatile Matter (wt %)	Fixed Carbon (wt %)
Run2-1	2.27	6.27	93.37
Run2-2	2.11	6.21	93.43
Run2-3	1.81	3.26	96.37
Run2-4	2.43	5.03	94.61
Average	2.15	5.19	94.44
σ	0.26	1.41	1.41
CV	12.27	27.08	1.49

Note: σ = Standard deviation, CV = Coefficient of variation

Table 10.4: Elemental analysis of the sampling points for Run 2

Sample	Nitrogen (wt %)	Carbon (wt %)	Hydrogen (wt %)	Sulphur (wt %)	Oxygen (wt %)	H/C (mol%)
Run2-1	0.34	89.83	1.35	0.00	8.12	0.18
Run2-1	0.37	89.95	1.27	0.00	8.05	0.17
Run2-2	0.30	89.97	1.57	0.00	7.80	0.21
Run2-2	0.41	89.74	1.52	0.00	7.97	0.20
Run2-3	0.53	91.30	0.95	0.00	6.86	0.12
Run2-3	0.52	91.65	0.95	0.00	6.52	0.12
Run2-4	0.45	90.59	0.59	0.00	8.00	0.08
Run2-4	0.44	90.34	0.69	0.00	8.16	0.09
Average	0.42	90.42	1.11	0.00	7.68	0.15
σ	0.08	0.71	0.37	0.00	0.63	0.05
CV	19.47	0.79	33.19	0.00	1.00	33.68

Note: σ = Standard deviation, CV = Coefficient of variation

10.3 Discussion of the Results and Operating Conditions for Run 3

For Run 3, the ceramic fibre rope was positioned more carefully and the secondary air holes in the base of the combustion chamber were plugged once the surface temperature of the combustion section had dropped below 200 °C as indicated by an infrared temperature sensor. The aim of this run was to minimise oxygen ingress, improve the yield and to use a full load of air-dried wood chips.

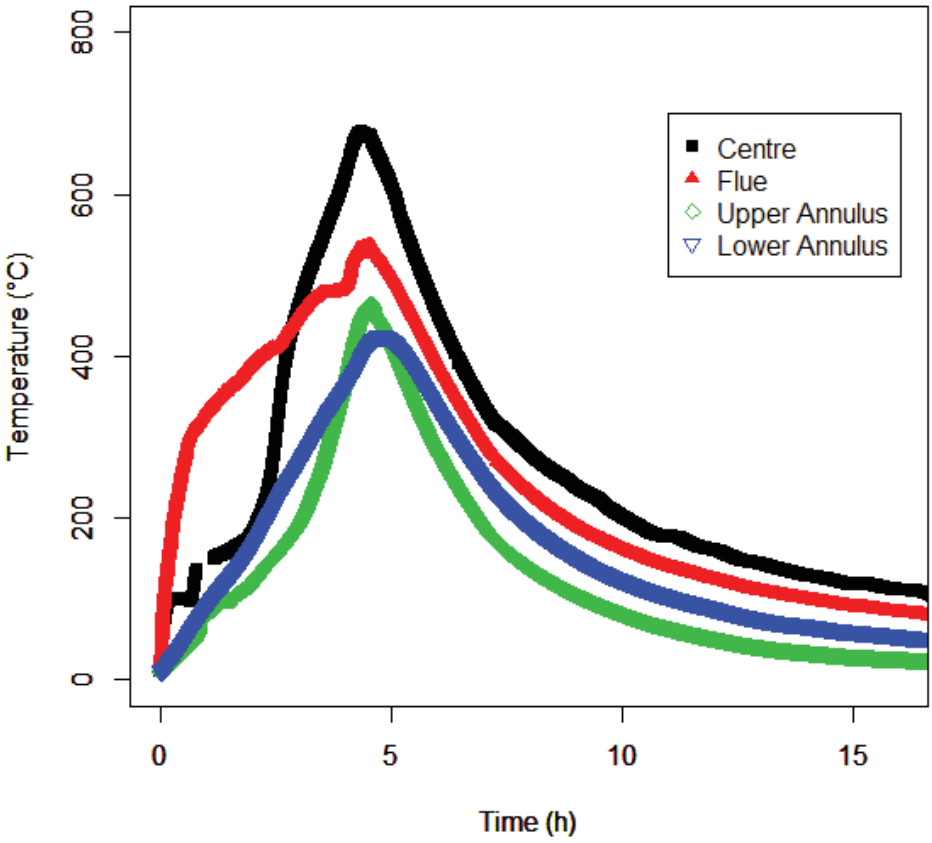

Figure 10.4: Temperature profile for Run 3

Run 3 followed a similar profile to Run 2 however there was no holding time. This was to see whether the natural cycle was sufficient to ensure the batch was evenly pyrolysed. The main difference was the centre temperature flat-lined at 100 °C. This is when the majority of the water evaporated. A potential reason for this difference was that there may have been a better seal on the inner lid due to the addition of a ceramic fibre rope to prevent the gases escaping directly up the flue. The mass of wood chips used in the run was 62 kg on a dry basis, with initial moisture content of 21.94 % on a dry basis.

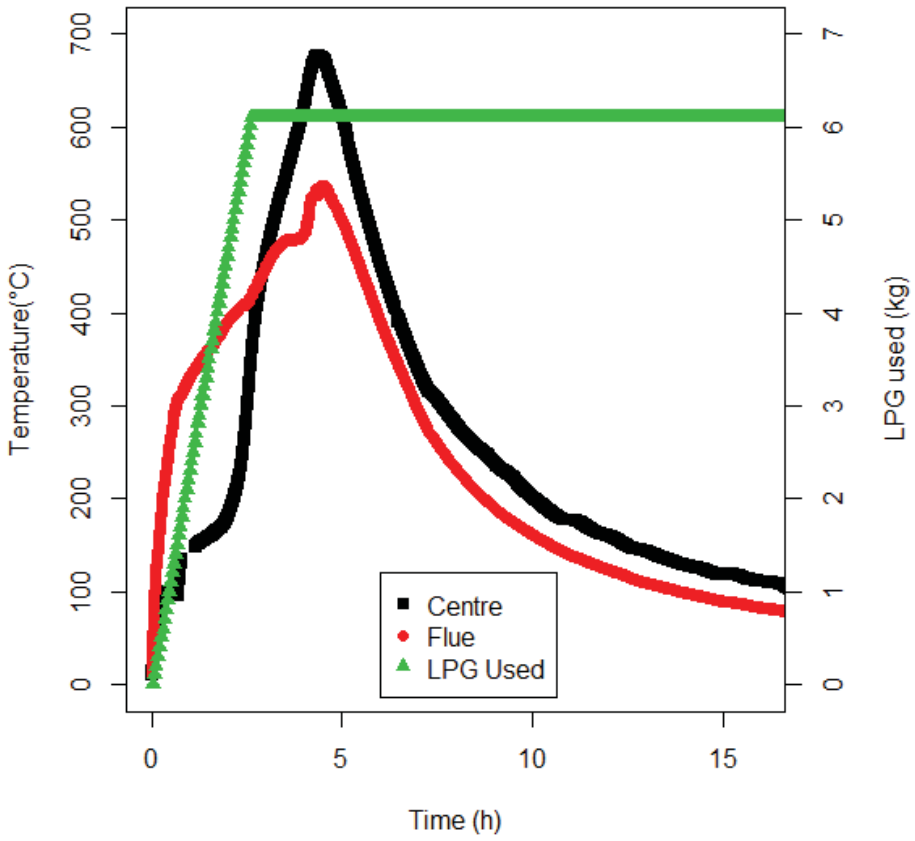

Figure 10.5: Temperature and LPG profile for Run 3

The main burner was set to turn off when the set point of 340 °C was reached at which point the slope of the centre temperature decreased and when the set point for the pilot burner of 400 °C was reached the heating rate decreased further. This can be seen in Figure 10.5. As stated earlier, the exothermic reactions continued to increase the centre temperature until it reached 678 °C after which point the process began to cool. After 16 hours the centre temperature reached 111 °C which meant the charcoal was believed to be at a safe temperature to unload. The exact temperature where charcoal is not at risk of reignition is not known, but it needs to be cool enough so that any temperature increase that occurs due to chemisorption of oxygen and moisture on exposure to air does not result in the charcoal becoming hot enough to ignite.

Proximate analysis showed little variation in the batch for the volatile matter and fixed carbon content of the biochar. The average fixed carbon content was 94.98 ± 1.32 wt % and the average volatile matter was 4.65 ± 1.33 wt %. These results indicated the batch was evenly pyrolysed and the char was of good quality as evidenced by the high fixed carbon content.

While fixed carbon is indicative of stability, Wang et al (2013) have shown it is the H/C that relates to aromaticity . The H/C ratios is Run 3 have an average of 0.19 ± 0.04 mol % indicating the char is highly aromatic.

Table 10.5: Proximate analysis results for Run 3

	Moisture (wt %)	Volatile Matter (wt %)	Fixed Carbon (wt %)
RUN3-01	2.32	6.10	93.53
RUN3-02	1.74	4.78	94.85
RUN3-03	1.84	5.75	93.88
RUN3-04	1.99	4.99	94.65
RUN3-05	2.25	5.41	94.22
RUN3-06	1.77	2.84	96.79
RUN3-07	2.23	4.86	94.77
RUN3-08	2.08	2.42	97.22
Average	2.03	4.65	94.99
σ	0.23	1.33	1.33
CV	11.27	28.56	1.40

Note: σ = Standard deviation, CV = Coefficient of variation

Table 10.6: Elemental analysis results for Run 3

Sample	N wt %	C wt %	H wt %	S wt %	Total O	H/C (mol %)
Run3-1	0.33	89.88	1.39	0.00	8.035	0.19
Run3-1	0.29	89.97	1.41	0.00	7.962	0.19
Run3-2	0.32	89.90	1.66	0.00	7.755	0.22
Run3-2	0.27	90.02	1.73	0.00	7.615	0.23
Run3-3	0.37	89.70	1.79	0.00	7.781	0.24
Run3-3	0.31	89.94	1.77	0.00	7.615	0.24
Run3-4	0.30	90.39	1.44	0.00	7.502	0.19
Run3-4	0.40	90.42	1.54	0.00	7.272	0.20
Run3-5	0.24	89.96	1.58	0.00	7.853	0.21
Run3-5	0.42	89.74	1.55	0.00	7.930	0.21
Run3-6	0.39	90.76	1.09	0.00	7.395	0.14
Run3-6	0.43	91.21	1.05	0.00	6.949	0.14
Run3-7	0.35	90.32	1.42	0.00	7.546	0.19
Run3-7	0.38	90.36	1.36	0.00	7.537	0.18
Run3-8	0.54	91.67	0.76	0.00	6.667	0.10
Run3-8	0.56	91.91	0.76	0.00	6.402	0.10
Average	0.37	90.38	1.39	0.00	7.49	0.19
σ	0.09	0.68	0.32	0.00	0.47	0.04
CV	24.13	0.75	23.26	0.00	1.00	23.76

Note: σ = Standard deviation, CV = Coefficient of variation

10.4 Discussion of the Results and Operating Conditions for Run 4

The purpose of Run 4 was to observe how a high moisture content affects the temperature profile and energy efficiency of the process. The same set points were chosen but it was decided to hold the temperature to ensure the batch was evenly pyrolysed. The temperature profile is shown in Figure 10.6.

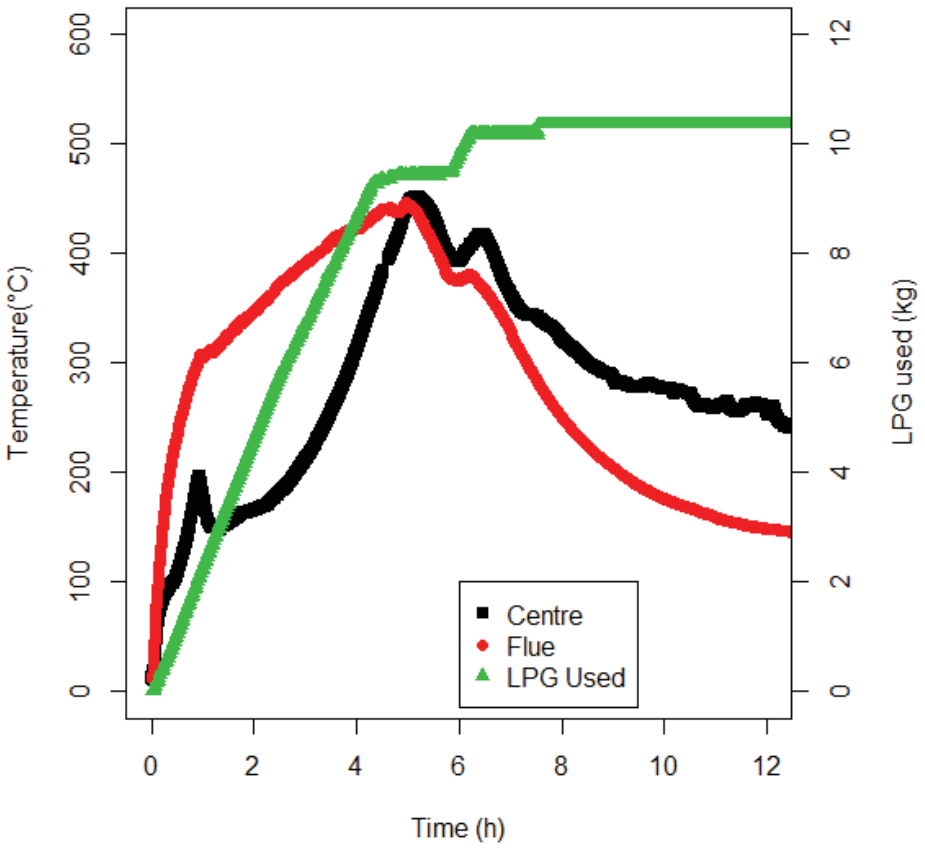

Figure 10.6: Temperature and LPG profile for Run 4

46.77 kg of dry wood with average moisture content of 94.71 wt % on a dry basis was used in this run. The same set points were used as per the air dried wood runs but the temperature only reached a maximum of 452 °C. The temperature was held for a duration of 1.59 hours above 400 °C of which the average temperature during this time was 419 °C. The centre temperature then decreased, but at a much slower rate in comparison to the other runs. The batch carried on pyrolysing for a 24 hour period before the reaction was stopped by cooling the biochar and reactor by opening it up and pouring in water. This profile shown

in Figure 10.7 indicated the set point temperatures were not high enough. There was not enough energy provided to enable the exothermic reactions to continue heating the process.

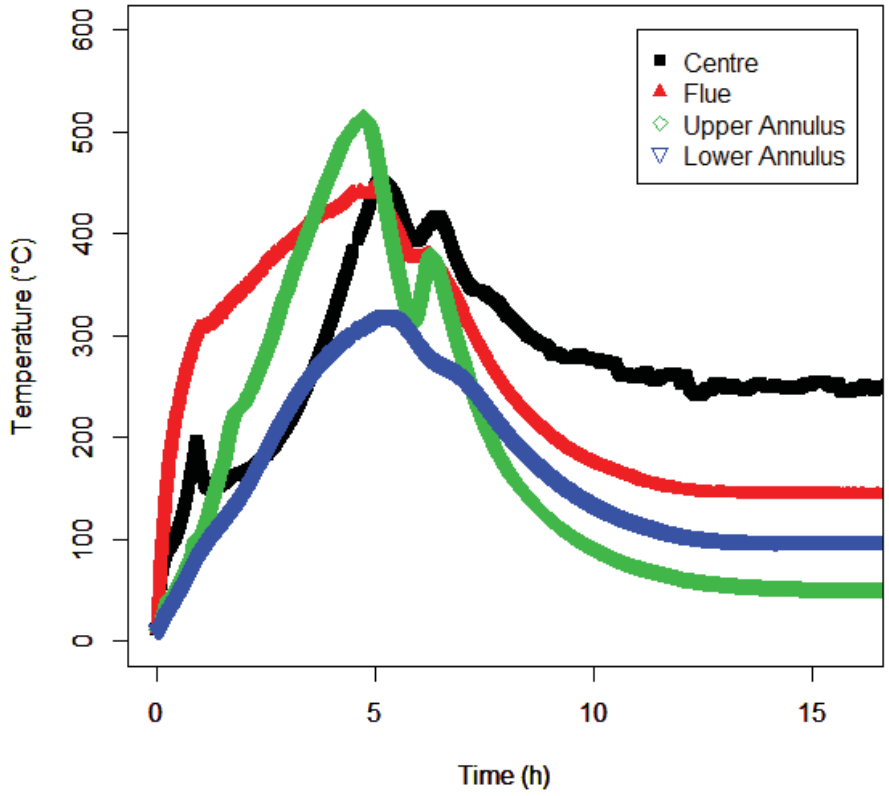

Figure 10.7: Temperature profile for Run 4

The fixed carbon content was significantly lower than the previous runs using air dried wood and corresponded to the lower peak temperature of 452 °C. The volatile matter was higher with an average 32.34 ± 5.25.

The H/C ratio of 0.43 ± 0.05 mol % for Run 4 indicates that good quality, stable char can be obtained at the lower peak pyrolysis temperature of 452 °C. The H/C ratio is approximately 0.20 mol % higher than the other runs which had a peak temperature of approximately 700 °C.

Table 10.7: Proximate analysis for Run 4

Sample	Moisture (wt %)	Volatile Matter (wt %)	Fixed Carbon (wt %)
RUN4-01	2.58	18.31	81.32
RUN4-02	2.34	22.05	77.59
RUN4-03	2.80	37.69	61.94
RUN4-04	3.14	33.67	65.96
RUN4-05	2.87	31.58	68.06
RUN4-06	2.91	29.99	69.65
RUN4-06	3.72	30.55	69.08
RUN4-07	3.59	39.15	60.49
RUN4-08	3.09	33.30	66.33
Average	3.06	32.25	67.39
σ	0.44	5.25	5.25
CV	14.45	16.28	7.79

Note: σ = Standard deviation, CV = Coefficient of variation

Table 10.8: Elemental analysis for Run 4

Sample	Nitrogen (wt %)	Carbon (wt %)	Hydrogen (wt %)	Ave. Ash (wt %)	Sulphur (wt %)	Oxygen (wt %)	H/C (mol %)
Run4-1	0.28	82.21	2.40	0.36	0.00	14.746	0.35
Run4-1	0.36	82.31	2.33	0.36	0.00	14.639	0.34
Run4-2	0.26	79.52	2.85	0.36	0.00	17.005	0.43
Run4-2	0.29	79.54	2.79	0.36	0.00	17.021	0.42
Run4-3	0.32	75.49	2.78	0.36	0.00	21.044	0.44
Run4-3	0.33	75.38	2.77	0.36	0.00	21.159	0.44
Run4-4	0.33	72.46	2.60	0.36	0.00	24.244	0.43
Run4-4	0.35	71.58	2.60	0.36	0.00	25.103	0.44
Run4-5	0.36	73.73	2.53	0.36	0.00	23.019	0.41
Run4-5	0.36	73.76	2.51	0.36	0.00	23.010	0.41
Run4-6	0.37	80.04	2.67	0.36	0.00	16.552	0.40
Run4-6	0.30	79.90	2.74	0.36	0.00	16.694	0.41
Run4-7	0.24	73.45	3.35	0.36	0.00	22.592	0.55
Run4-7	0.28	73.60	3.35	0.36	0.00	22.407	0.55
Run4-8	0.38	77.41	2.72	0.36	0.00	19.129	0.42
Run4-8	0.41	78.21	2.68	0.36	0.00	18.333	0.41
Average	0.33	76.79	2.73	0.36	0.00	19.79	0.43
σ	0.05	3.53	0.28	0.00	0.00	3.44	0.05
CV	14.59	4.60	10.34	0.00	0.00	1.00	12.76

Note: σ = Standard deviation, CV = Coefficient of variation

10.5 Discussion of the Results and Operating Conditions for Run 5

The purpose of Run 5 was to repeat the wet run and select higher set points to ensure the batch is properly pyrolysed.

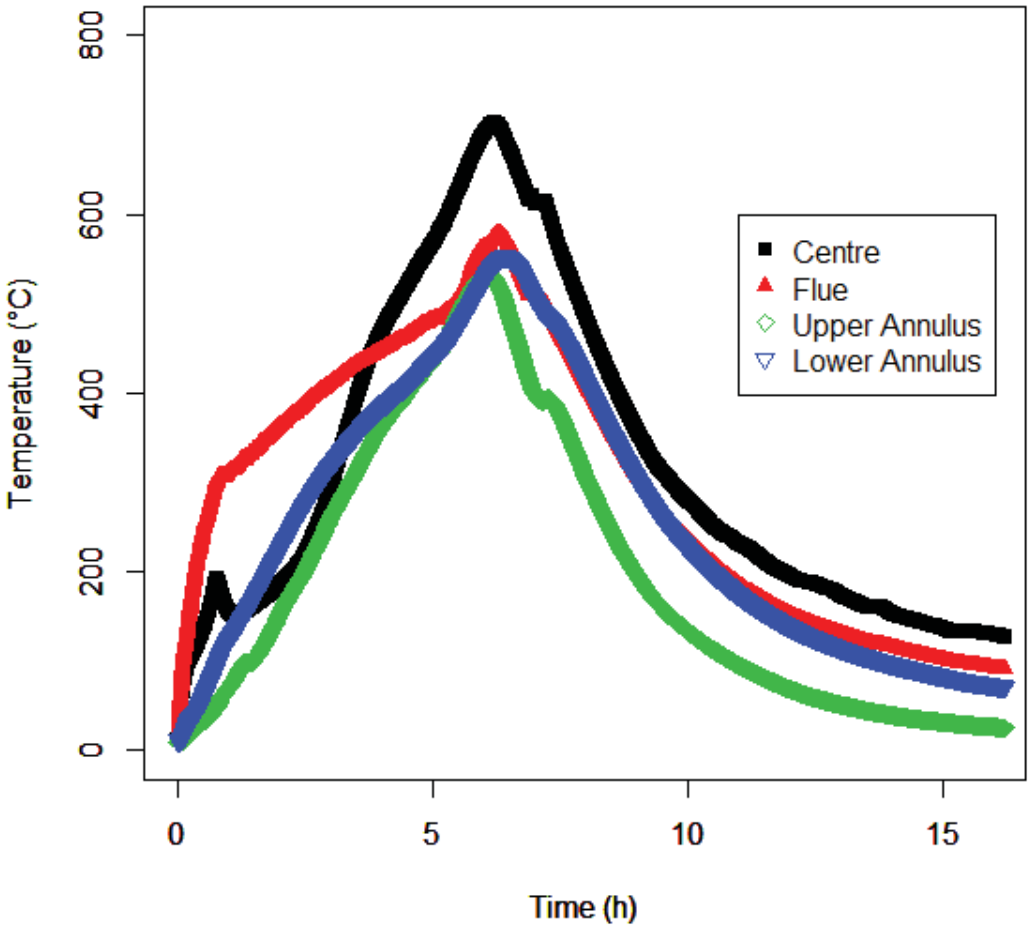

Figure 10.8: Temperature profile for Run 5

The temperature profile against time is shown in Figure 10.8. This profile is similar to that of Run 3. The temperature was held for a very short period before the reactor cooled.

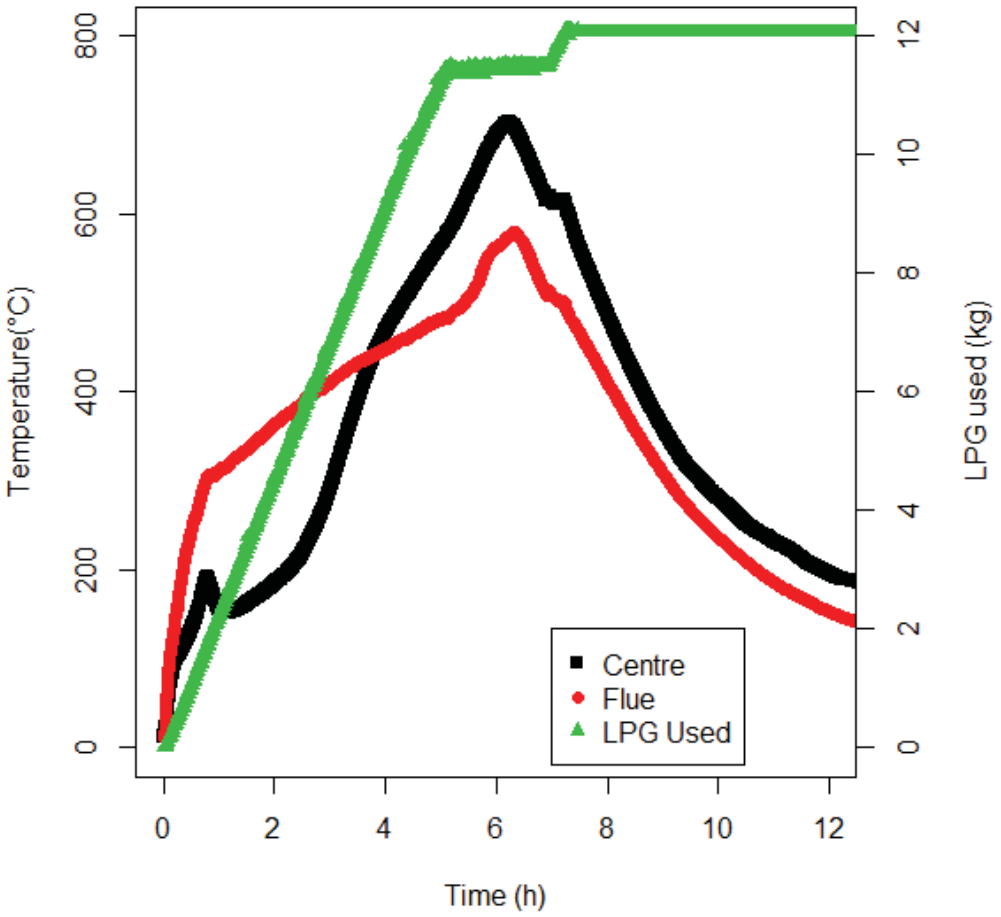

Figure 10.9: Temperature and LPG profile for Run 5

Run 5 used wet wood which had an average moisture content 60.38 % on a dry basis. Due to uneven heating profile the centre temperature increased to 180 °C before it drops to 150 °C and carries on increasing. This may be because of the evaporation / condensation cycle occurring in the reactor.

The pilot burner was turned off when the higher set point temperature of 500 °C was reached and the main burner was turned off when the centre temperature reached 580 °C. A peak temperature of 703 °C was reached before the system began cooling.

The fixed carbon content was consistently high throughout the batch with an average of 95.25 ± 1.21 % by mass. As stated previously, high fixed carbon contents indicates stable fraction char, but the H/C ratios shown in have been shown to directly relate to char stability in soil (Wang, et al., 2013). The H/C ratios shown in Table 10.10 confirm good quality char is obtained at this temperature range.

The elemental analysis results are shown in Table 10.10. There is a large variation between the sampling points with respect to the carbon content which ranges from 89 – 98 wt %. This

variation has also occurred in the other run using wet wood, Run 4. This indicates moisture is affecting the consistency of the batch.

Table 10.9: Proximate analysis for Run 5

Sample	Moisture (wt %)	Volatile Matter (wt %)	Fixed Carbon (wt %)
RUN5-01	1.36	5.77	93.86
RUN5-02	2.44	4.59	95.04
RUN5-03	2.35	4.42	95.21
RUN5-04	1.23	3.53	96.11
RUN5-05	1.52	6.44	93.20
RUN5-06	1.08	3.56	96.07
RUN5-07	1.46	3.72	95.91
RUN5-08	2.51	2.91	96.72
Average	1.74	4.37	95.27
σ	0.59	1.21	1.21
CV	33.87	27.62	1.27

Note: σ = Standard deviation, CV = Coefficient of variation

Table 10.10: Elemental analysis for Run 5

Sample	Nitrogen (wt %)	Carbon (wt %)	Hydrogen (wt %)	Sulphur (wt %)	Oxygen (wt %)	H/C (mol %)
Run5-1	0.40	97.12	1.62	0.00	0.493	0.20
Run5-1	0.50	97.14	1.57	0.00	0.426	0.19
Run5-2	0.46	97.39	1.43	0.00	0.354	0.18
Run5-2	0.49	97.41	1.47	0.00	0.265	0.18
Run5-3	0.57	97.47	1.34	0.00	0.253	0.17
Run5-3	0.51	97.33	1.38	0.00	0.416	0.17
Run5-4	0.50	96.66	1.15	0.00	1.322	0.14
Run5-4	0.63	97.03	1.20	0.00	0.781	0.15
Run5-5	0.36	89.37	1.47	0.00	8.438	0.20
Run5-5	0.51	89.39	1.43	0.00	8.309	0.19
Run5-6	0.47	91.69	1.13	0.00	6.344	0.15
Run5-6	0.56	91.71	1.11	0.00	6.252	0.15
Run5-7	0.39	97.45	1.24	0.00	0.553	0.15
Run5-7	0.42	91.12	1.04	0.00	7.056	0.14
Run5-8	0.70	98.00	0.87	0.00	0.062	0.11
Run5-8	0.59	98.21	0.92	0.00	-0.088	0.11
Average	0.50	95.28	1.27	0.00	2.58	0.16
σ	0.09	3.30	0.22	0.00	3.33	0.03
CV	18.06	3.46	17.60	0.00	1.00	17.88

Note: σ = Standard deviation, CV = Coefficient of variation

10.6 Discussion of the Results and Operating Conditions for Run 6

Run 6 was a full load repeat of Run 3. On a dry basis, 57.11 kg of air-dried wood chips with an initial moisture content of 20.13 wt % was loaded into the reactor.

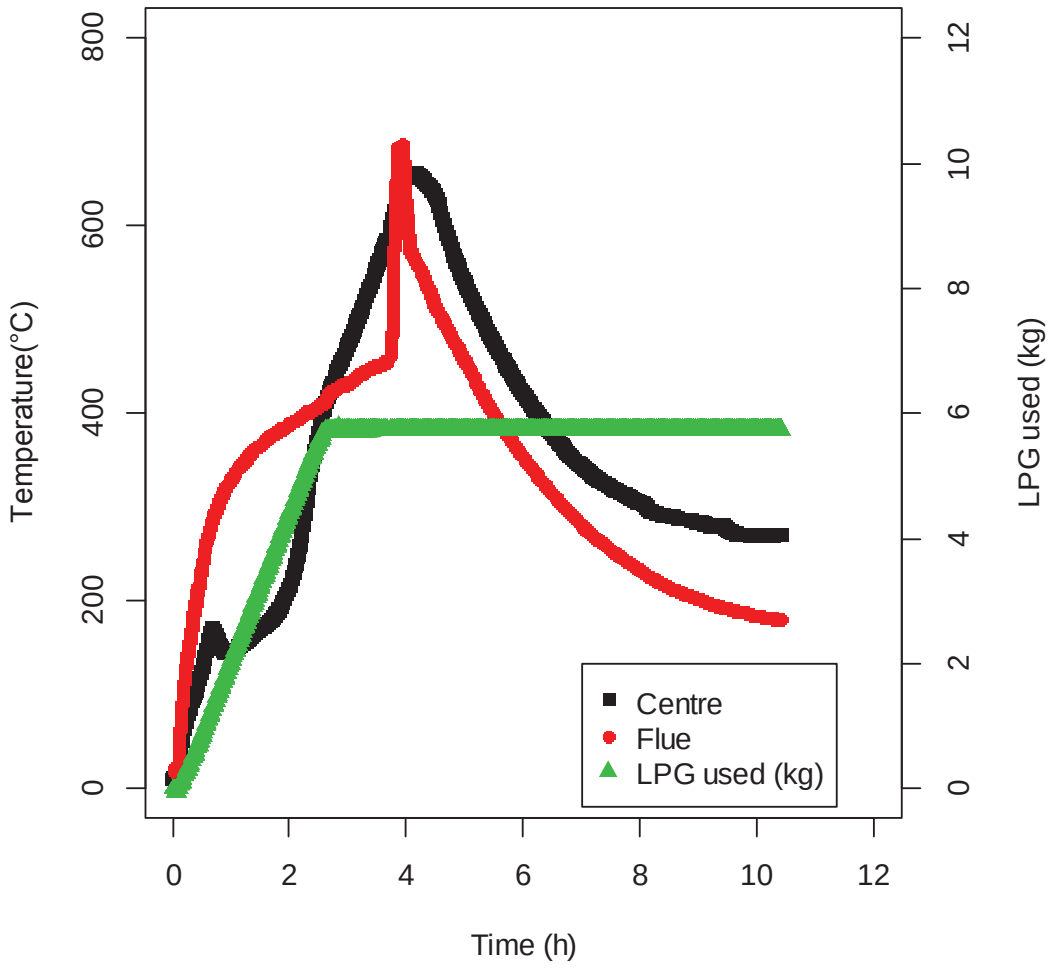

Figure 10.10: Temperature profile for Run 6

Run 6 exhibited the same temperature profiles as earlier runs using the air dried wood however the internal temperature did not decrease below 200 °C after 21 hours. The data logger stopped working after 10.40 hours, but was reset after 21 hours to see the centre temperature was still at 245 °C. This indicated the inner lid did not seal properly which was confirmed upon removal of the lid as it was clear that the insulation rope had moved before initial closing. This meant the pyrolysis gases did not flow downward and out of the inner core into the combustion chamber as designed; instead they flowed upward and out through the gap between the drum and the ill-fitting lid. This draft up the centre of the reactor meant oxygen was able to fuel some charcoal embers around the base of the central perforated core, which kept the reactor temperature high. The embers were put out approximately 24 hours later to try to preserve the yield. At this point, the yield was 17 % indicating the oxygen ingress did have a significant effect on the yield. These repeating problems with the lid were identified by trial 3 and so a new lid was designed, but it was not ready before the other trials were completed. The new design is a countersunk lid which is countersunk enough so that any warping of the lid will not result in a gap developing between the lid and the inner drum.

When such a gap develops, the updraft will draw air up through the reactor core. This is opposite to the intended operation of the unit; where the pyrolysis gases that evolve inside the reactor core move along the pressure gradient down and out through the perforated core and into the combustion chamber.

Due to oxygen ingress, it was decided not to take the eight samples from the different locations but to instead take one representative sample to determine the properties of the batch. Table 10.11 and Table 10.12 summarises the proximate analysis and elemental analysis results respectively. The duplicates show good consistency. A high fixed carbon content was obtained, and the H/C ratios were similar to the other high temperature (700 °C) runs.

Table 10.11: Proximate analysis results for Run 6

Sample	Moisture (wt %)	Volatile Matter (wt %)	Fixed Carbon (wt %)
Run6.001	2.04	6.30	93.34
Run6.002	2.00	6.36	93.27
Average	2.02	6.33	93.31
σ	0.03	0.04	0.04
CV	1.54	0.70	0.05

Note: σ = Standard deviation, CV = Coefficient of variation

Table 10.12: Elemental analysis results for Run 6

Sample	Nitrogen (wt %)	Carbon (wt %)	Hydrogen (wt %)	Sulphur (wt %)	Oxygen (wt %)	H/C (mol%)
Run6.001	0.39	91.97	1.168	0.00	6.11	0.15
Run6.002	0.41	91.62	1.146	0.00	6.46	0.15
Average	0.40	91.80	1.16	0.00	6.29	0.15
σ	0.02	0.25	0.02	0.00	0.25	0.00
CV	3.91	0.27	1.34	0.00	1.00	1.07

Note: σ = Standard deviation, CV = Coefficient of variation

10.7 Operation Summary

From the above six trials, the following conclusions can be drawn:

1. Water was predominately evaporated when the centre temperature was between 100 - 170 °C. The variation is most likely due to an uneven heating profile.
2. Peak temperatures ranged from 646 - 703 °C excluding Run 4. This small variation is possibly due to the initial mass of wood loaded into the reactor which ranged from 34 - 51 kg on a dry basis. The peak is also self-determining for this feedstock, *Pinus*

radiata. As pyrolysis proceeds the exothermic reactions heat the system while consuming the fuel for further reactions. Eventually no more fuel is available and the system begins to cool.

3. Peak gas production occurred when the centre temperature was between approximately 400 - 700 °C. During this period the flare went out. This was an issue for ensuring emissions were kept to a minimum and it is hoped the addition of air dump valves will address this problem.
4. The reactor took approximately 16 hours to cool below 150 °C when there was minimal oxygen ingress as evidenced in Runs 3 and 5. This indicates a 24 hour cycle from the time the reactor is loaded, the start button pushed to unloading it the next day is sufficient to carry out a batch production once a day.
5. Higher peak temperatures resulted in biochar with a higher fixed carbon content. The fixed carbon content is an indicator of char quality. The results indicated the char produced from peak temperatures of 600 - 700 °C is of good quality.
6. The main issue with the operation was ensuring the inner lid was sufficiently sealed. The lid has been redesigned to be countersunk to minimise the opportunity for warping to open a gap between the lid and the inner drum and so allow short circuiting of the gases out of the lid.
7. For air dried wood, with a moisture content of <20 % it is recommended that the main burner set point is 340 °C and the pilot burner set point 400 °C. For wet wood, with a moisture content of >20 %, a higher heat input is required to evaporate the larger quantities of water. Therefore, it is recommended that the pilot burner and main burner be set to 500 °C and 580 °C respectively.

11.0 DISCUSSION OF PILOT RESULTS AND COMPARISON TO LAB RESULTS

The objective of this project was to design a batch pyrolyser to produce biochar and characterise the resulting product. Characterisation was done first at a lab scale, which provided a calibration reference between pyrolysis conditions and char quality. At the pilot scale, the six trials were each sampled at a range of sampling points and analysed for char properties, as seen in Figure 6.2 previously. In this section, the six trials are compared to each other for the performance indicators of yield, composition, carbon footprint, and energy efficiency. The six trials are also compared to the reference characterisation work obtained in lab tests. The sections below address these comparisons.

11.1 Yield

The biochar yield was determined by weighing the biochar once the internal temperature had cooled to 100 °C. At this temperature, it could be assumed the charcoal would be dry. For the runs that were still over 100 °C, the charcoal was cooled with water. In these cases, the hotter temperature was caused by the ill-fitting lid of the internal reactor drum allowing an updraft of air through the drum which kept some embers alive and so preventing the system from cooling completely. For the wetted charcoal, the total mass was recorded and a sample was taken and dried to calculate the total yield on a dry basis.

Table 11.1: Summary of the biochar yields obtained from the six runs

Run #	Wood	HTT (°C)	Mass of wet wood (kg)	Initial wood MC (wt %) (db)	Initial mass wood (kg) (db)	Mass char (kg)	Char MC (wt %) (db)	Final mass charcoal (db)	Yield (wt %) (db)
1	Dry	646	42.9	24.0	34.6	2.2	0.0	2.2	6.5
2	Dry	654	45.2	21.2	37.3	15.8	160.2	6.1	16.2
3	Dry	678	61.6	21.9	50.6	15.0	0.0	15.0	29.7
4	Wet	452	91.1	94.7	46.8	24.1	144.1	9.9	21.1
5	Wet	703	75.5	60.4	47.1	13.6	0.0	13.6	28.8
6	Dry	658	57.1	20.1	47.5	23.8	193.7	8.1	17.0

Note. HTT = highest treatment temperature; MC = moisture content; db = dry basis.

Table 11.1 shows a range of yields. Runs 3 and 5 were considered successful pyrolysis runs as the char was well pyrolysed and both of these runs cooled to approximately 110 °C after 16 hours indicating no combustion was occurring inside the reactor. Run 3 used air dried wood and Run 5 used wet wood with a dry basis moisture content of 22 % and 60 %

respectively. They produced similar high yields of 29.7 % for Run 3 and 28.8 % for Run 5 indicating moisture content did not affect the yield. These yields are comparable to the lab scale results for the largest particle size. The small particle size had a 10 % lower yield. This may have been due to less fracturing occurring in the smaller particles, therefore fewer volatiles released so fewer interactions with the char occur. This means less secondary char formed, which results in lower yields.

The fixed carbon yield is an important parameter because it provides information about the quality of the char. The char yield alone (m_{char}/m_{wood}) does not provide information on the extent of pyrolysis and could provide false high yields if not used in conjunction with the fixed carbon yield. Therefore the fixed carbon yield is a better measure for determining the efficiency of the process in terms of converting biomass into carbon.

The fixed-carbon content of a charcoal approximates the fraction of carbon that is effective as a metallurgical reductant as well as approximating the amount of pure carbon that can be obtained by further thermal treatment of the charcoal (Wang et al, 2011). Equation (11.1) shows how the fixed carbon yield was calculated and Table 11.2 shows the fixed carbon yield on a dry basis. The percentage of ash in the biomass was 0.36 wt % and the fraction of carbon in the biomass was 0.48 wt %, both values on a dry basis. Fixed carbon yields of 44 wt % and 43 wt % for Runs 3 and 5 respectively indicates the charcoal is well pyrolysed and has a high proportion of stable carbon, making it suitable char for soil.

$$Fixed\ Carbon\ Yield = \frac{m_{char} * \%\ FC_{char}}{m_{biomass}(1 - \%\ Ash_{biomass})} * 100 \qquad (11.1)$$

Where m_{char} is dry mass of char (kg), $m_{biomass}$ is the dry mass of biomass (kg), $\%\ FC_{char}$ is the fixed carbon percentage obtained from proximate analysis, and $\%\ Ash_{biomass}$ is the percentage ash relative to the mass of dry biomass.

Table 11.2: Summary of the fixed carbon yield results for all runs

Run	Char FC (wt %)	Mass biomass (kg) (db)	Mass char (kg) (db)	FC Yield (wt %)
1	92.48	34.58	2.24	9.42
2	94.43	37.32	6.05	24.09
3	94.98	50.55	15.04	44.42
4	67.38	46.77	9.86	22.33
5	95.25	47.09	13.59	43.21
6	93.31	47.54	8.09	24.96

Note: The percentage of ash in the biomass was 0.364 wt % on a dry basis. FC = fixed carbon content of the char on a dry basis. db = dry basis.

11.2 Biochar composition

Proximate analysis was used to determine the percentage of fixed carbon, volatile matter and moisture content present in the char samples. Elemental analysis was used to determine the percentage of total carbon, nitrogen, hydrogen and sulphur present in the char. Table 11.3 provides a summary of the char composition. The results displayed are the average ± standard deviation. All results are reported on a dry basis.

Table 11.3: Char composition summary for the experiments (Dry basis)

Run	MC (wt %)	HTT (°C)	Volatile Matter (wt %)	Fixed Carbon (wt %)	Total Carbon (wt %)	Hydrogen (wt %)	Nitrogen (wt %)	n
1	24.0	646	7.2 ± 0.1	92.5 ± 0.1	91.6 ± 0.1	1.3 ± 0.0	0.4 ± 0.0	2
2	21.2	654	5.2 ± 1.4	94.4 ± 1.4	90.4 ± 0.7	1.1 ± 0.4	0.4 ± 0.1	4
3	21.9	678	4.7 ± 1.3	95.0 ± 1.3	90.4 ± 0.7	1.4 ± 0.3	0.4 ± 0.1	8
4	94.7	452	32.2 ± 5.3	69.3 ± 7.2	76.8 ± 3.5	2.7 ± 0.3	0.3 ± 0.0	8
5	60.4	703	4.4 ± 1.2	95.3 ± 1.2	95.3 ± 3.3	1.3 ± 0.2	0.5 ± 0.1	8
6	20.1	658	6.3 ± 0.0	93.3 ± 0.0	91.8 ± 0.2	1.2 ± 0.0	0.4 ± 0.0	2

Note: n = number of samples, MC = Initial wood moisture content on a dry basis, HTT = High treatment temperature or peak temperature, n = the number of samples

The charcoal composition of the runs with similar peak temperatures were consistent indicating moisture did not affect the char composition. It is well known that peak temperature affects the char composition and properties (Baldock & Smernik, 2002; Gaskin, et al., 2008) which is evidenced by the difference in peak temperatures between Run 4 and the other runs. As the pyrolysis temperature increases, devolatilisation reactions occur resulting in the loss of volatile organic compounds. This directly corresponds to the increase in the fixed carbon content.

Figure 11.2 provides a comparison of the molar H/C versus O/C ratios for the pilot scale results to the lab scale results. It can be seen that the pilot H/C ratio results are lower than that obtained from the lab scale pyrolyser. Investigation into the individual elements showed the carbon and oxygen values were similar between the pilot and lab scale pyrolysers and the hydrogen values were lower in the pilot scale pyrolyser. Specifically, at 700 °C, the hydrogen results were approximately 2.0 mol % and between 0.8 – 1.8 mol % for the lab scale and pilot scale results respectively. This difference could be associated with the longer residence time in in the pilot scale pyrolyser and therefore more bonds are broken, resulting in lower overall hydrogen values.

There was a large variation in the hydrogen values within the batch of the pilot scale pyrolyser. Figure 11.3 shows a plot of the effect of the different sample locations on the hydrogen content. Statistical analysis confirmed the sample location had a highly significant effect on the hydrogen content ($p<0.01$).

It can be seen that the bottom samples have lower hydrogen values compared to the top values which is expected as the bottom is where the reactor is heated from. As previously suggested, the prolonged high temperature may break more bonds, resulting in lower hydrogen values.

The top sampling points appear to be less affected by the heating applied, whereas the bottom samples show a lot of variation. The samples on the left side of the reactor have lower hydrogen values than the right, indicating the right side of the reactor was hotter. This is consistent with the positioning of the burners, with the 23 kW burner being on the left. This provides interesting information on the heating profile for a batch reactor designed in this way. It emphasises the heating profile could be improved if the burners were installed in a tangential direction, which would evenly distribute the heat by creating a swirl effect in the combustion section.

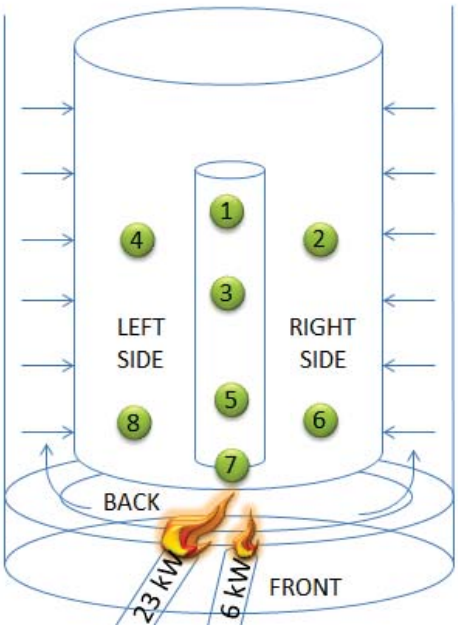

Figure 11.1: Burner location in relation to the sampling points

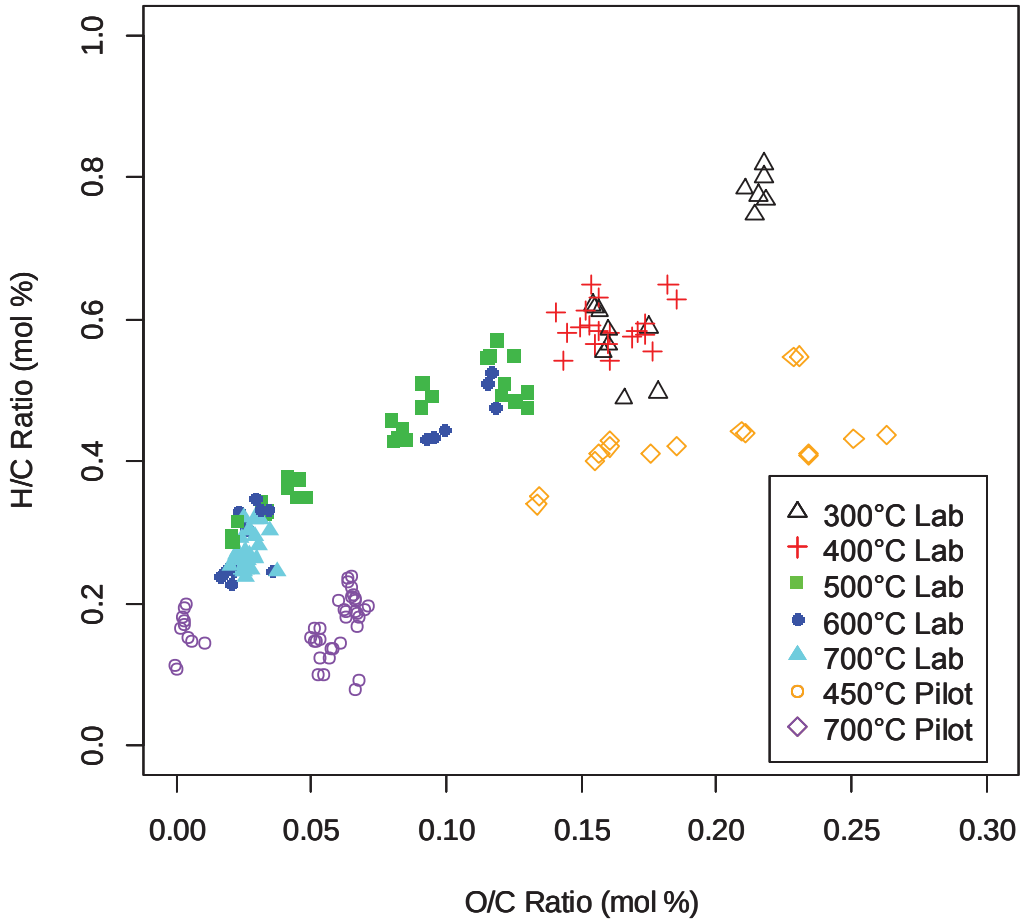

Figure 11.2: Comparison of H/C and O/C ratios between the lab and pilot scale reactors

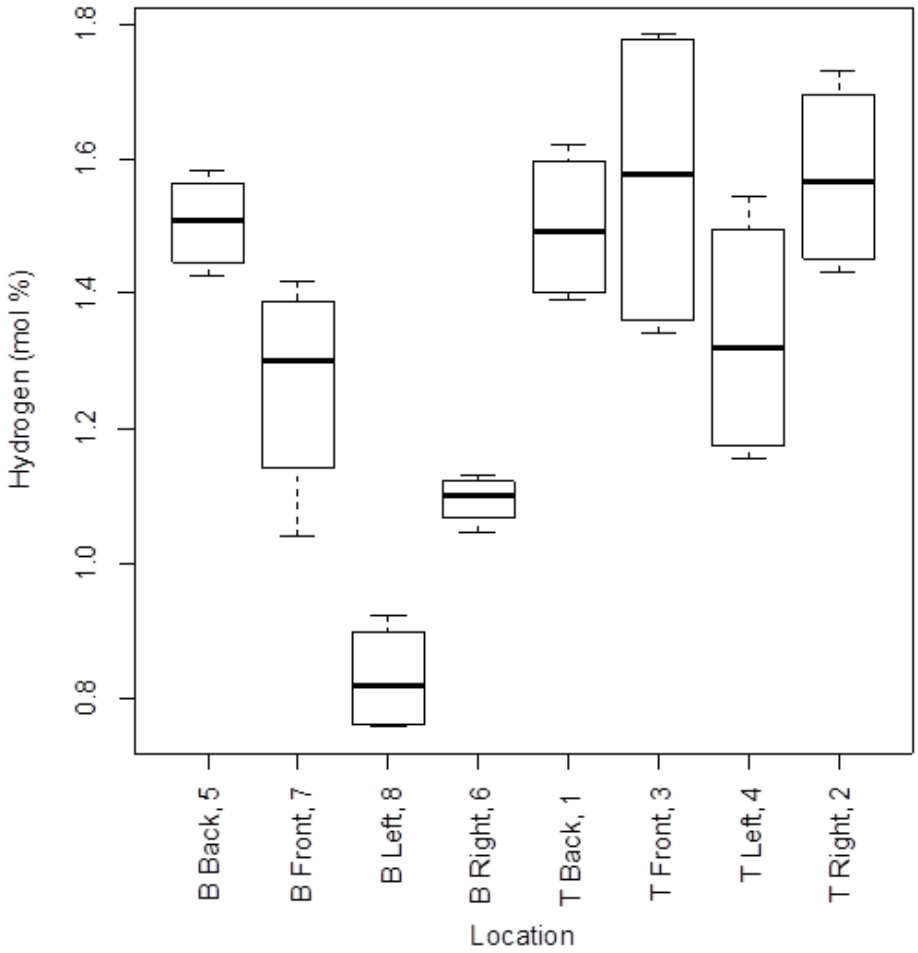

Figure 11.3: The effect of sample position on the hydrogen content of the char in the pilot scale reactor. *Note:* B = Bottom, T = Top. The number refers to the location in which the sample was collected. Front refers to the front side of the reactor which is on the same side as the burners.

11.3 Carbon Footprint

Biochar is considered to be a carbon negative process as it has the potential to sequester carbon in the soil and reduce the atmospheric carbon dioxide. As part of the estimate of carbon footprint, equations (11.2) and (11.3) provide an estimate for the net carbon conversion and the net fixed carbon conversion of biomass to biochar respectively.

The net carbon conversion is defined by the organic carbon in the char minus the fossil fuel inputs divided by the organic carbon in the feedstock. The net fixed carbon conversion defines the stable fraction of carbon.

$$Net\ Carbon\ Conversion = \frac{mass\ of\ C\ in\ Char - mass\ of\ C\ in\ LPG - mass\ of\ C\ in\ ash}{mass\ of\ C\ in\ Biomass - mass\ of\ C\ in\ ash} * 100 \quad (11.2)$$

$$Net\ Fixed\ Carbon\ Conversion = \frac{mass\ of\ FC\ in\ Char - mass\ of\ C\ in\ LPG - mass\ of\ C\ in\ ash}{mass\ of\ C\ in\ Biomass - mass\ of\ C\ in\ ash} * 100 \quad (11.3)$$

Table 11.4 summarises the net carbon and net fixed carbon conversion of the process. It can be seen that the net carbon conversion and the net fixed carbon conversions are significantly impacted by the moisture content of the wood and therefore the amount of LPG required for heat up. The more moisture in the wood, the more energy is required for evaporation. Comparing the best runs, Run 3 (21.9 % MC) and Run 5 (60.4% MC) the NCCs were 10.8 % and 31.9 % respectively, indicating the profound effect of moisture. Run 5 uses more LPG than Run 4 because the set point controlling the LPG for Run 5 was higher as it was established from Run 4 that a higher set point was required to ensure complete pyrolysis. These results show in order for this process to be sustainable it is imperative to use dry wood. The net carbon conversion is expressed as a carbon footprint (kg CO2e/t biomass) by the following calculation, where carbon footprint refers to the global warming commitment of the biomass to char conversion process.

$$Carbon\ Footprint = \frac{\%NCC}{100} * \frac{\frac{M_{CO_2}}{M_C}}{m_{biomass\ dry}} [=] \frac{kgCO_2e}{t\ dry\ biomass} \quad (11.4)$$

Where M_{CO_2} and M_C are the molecular weights of carbon dioxide and carbon respectively and $m_{biomass\ dry}$ is the dry weight of biomass.

Table 11.4: Carbon footprint of the process

Run	MC (wt %)	Mass LPG (kg)	TC (wt %)	Char FC (wt %)	Mass biomass (kg) (db)	Mass char (kg) (db)	Mass C in Biochar	NCC (%)	NFCC (%)	CF (%)
1	24.04	4.55	91.64	92.48	34.58	2.24	2.05	-11.30	-5.38	-1.20
2	21.15	6.25	90.42	94.43	37.32	6.05	5.47	0.56	0.94	0.06
3	21.94	6.1	90.38	94.98	50.55	15.04	13.59	31.86	17.91	2.49
4	94.71	10.35	76.79	67.38	46.77	9.86	7.57	-5.22	-4.70	-0.44
5	60.38	12.1	95.28	95.25	47.09	13.59	12.94	10.77	5.58	0.90
6	20.13	5.8	91.80	93.31	47.54	8.09	7.42	10.97	5.39	0.85

Note: MC = moisture content, TC = total carbon, FC = fixed carbon, NCC = net carbon conversion, NFCC = net fixed carbon conversion, CF = carbon footprint.

In reality, the carbon footprint should consider the emissions of products of incomplete combustion (PICs) and particulate from the flue stack, which are deducted from the numerator of equations (11.2) and (11.3). These have not been considered here even though the flare habitually went out and a smoke plume rose from the top of the stack. The flare problem was due to poor flare design. During one run, the forced draft air lines were removed to the two combustion burners when they were turned off. This created a path of least resistance from the blower and so the flare, which was also supplied by the burner, received less air, meaning that it was easily snuffed out. Therefore the air lines were not removed for the remaining runs. It is recommended that the flare be redesigned.

11.4 Energy Efficiency

In the following section, various definitions of energy efficiency will be discussed with the aim to benchmark the reactor. The objective was to produce biochar that can sequester carbon in a sustainable way.

$$Efficiency\ of\ production = \frac{mass\ of\ C\ in\ Biochar}{mass\ of\ C\ in\ LPG}[=]\frac{kg}{kg} \tag{11.5}$$

$$Fossil\ fuel\ process\ energy\ per\ tonne\ of\ char\ produced = \frac{Fossil\ heat}{Tonne\ biochar\ produced}[=]\frac{MJ}{t} \tag{11.6}$$

The conversion can be expressed purely in terms of energy.

$$Fossil\ heat\ expended\ to\ produce\ a\ MJ\ of\ stored\ energy\ in\ char = \frac{Fossil\ heat}{Energy\ stored\ in\ char}[=]\frac{MJ}{MJ} \quad (11.7)$$

Instead of relating the fossil energy consumption to the biochar product, it can be related to the biomass feedstock,

$$Fossil\ heat\ expended\ per\ MJ\ of\ energy\ in\ biomass = \frac{Fossil\ heat}{Energy\ in\ Biomass}[=]\frac{MJ}{MJ} \quad (11.8)$$

The conversion efficiency of energy from the biomass into stored energy in the char is

$$Conversion\ efficiency\ of\ stored\ energy = \frac{Energy\ stored\ in\ Char}{Energy\ in\ Biomass}[=]\frac{MJ}{MJ} \quad (11.9)$$

Table 11.5 summarises the input values that were used in the calculations of equations (11.5) - (11.9). The mass of carbon in the LPG is calculated on the basis that LPG is a 60:40 ratio of propane to butane.

Table 11.5: Summary of input values for energy efficiency determination

Run	Mass char (kg) (db)	Energy in char (MJ)	Mass of LPG (kg)	Fossil Heat (MJ)	Mass Wood (kg) (db)	Energy in wood (MJ)
1	2.24	67	4.55	210.67	34.58	674
2	6.05	182	6.25	289.38	37.32	727
3	15.04	451	6.10	282.43	50.55	985
4	9.86	296	10.35	479.21	46.77	911
5	13.59	408	12.10	560.23	47.09	918
6	8.09	243	5.80	268.54	47.54	927

Note: Additional input values used in the calculations were 1) The calorific value of char = 30 MJ/kg (Mok, et al., 1992), 2) The heating value for LPG = 46.3 MJ/kg (Snow, 2002) and 3) The calorific value of wood = 19.49 MJ/kg (Mansilla, et al., 1991). db = dry basis.

The optimum run achieved during the 6 pilot scale runs was Run 3. It can be seen from Table 11.6 that the process efficiency, that is, the mass of carbon in the biochar divided by the mass of carbon in the LPG was the highest in Run 3. This means that for every kilogram

of carbon in LPG used, 2.6 kilograms of carbon is produced at 700 °C. Comparing to the lab scale experiments, on average, for every kilogram of carbon in LPG used, 0.25 kilograms of carbon is produced at 700 °C. It is expected that this value is significantly lower than that of the pilot scale reactor. This is because the pilot scale reactor utilised some of the energy it produced and also had a much greater quantity of biomass and the exothermic reactions were able to continue the heating of the process without additional LPG.

The results in Table 11.6 show Run 3 was the best run in terms of having the lowest amount of fossil fuel energy expended per tonne of biochar produced. This was due to two contributing factors. Firstly, the energy in the char is dependent on the yield obtained and Run 3 had the highest yield. Secondly, the fossil heat is dependent on the amount of LPG used. Runs 4 and 5 used the most LPG because Run 4 had a soak period to determine the optimum residence time, and Run 5 had a higher set point in comparison to the other Runs so the LPG was required for a longer duration. Run 3 had no additional soak time and used a similar amount of LPG to Runs 2 and 6.

The fossil fuel heat expended per the energy stored in the biochar, calculated using Equation (11.7), is the largest in Run 1. This is because Run 1 had the lowest yield obtained as a result of combustion occurring from oxygen ingress. Runs 3 and 5 had the highest yields but Run 5 used significantly more LPG than Run 3, 12.1 kg and 6.3 kg respectively. The percentages are overall high because LPG has a much higher calorific value than charcoal.

Equation (11.8) shows the calculation for the amount of fossil fuel heat expended over the energy stored in the biomass. Run 5 was different from the other runs in that the set points used were higher (500 °C for the main burner and 580 °C for the pilot burner) to ensure the system reached its exothermic potential. Therefore, more fuel was used to obtaining the higher set point. It is difficult to directly compare the other runs although they had the same set points (340 °C for the main burner and 400 °C for the pilot burner). This was because Runs 2 and 4 had an additional soak time where the temperature was maintained above 600 °C, near the maximum temperature for a short period of time, and hence these runs used more LPG. The energy stored in the wood was lower in Runs 1 and 2 in comparison to the other runs because the reactor was only half filled with wood chips, and this explains why Runs 1 and 2 have a higher ratio of fossil fuel expended to energy stored in the biomass than in Runs 3 and 6. Overall, Run 3 was the best run.

The conversion efficiency of energy from biomass to char is highest in Runs 3 and 5. This conversion is independent of moisture content as the results are on a dry basis. This conversion efficiency is directly related to the yields obtained, and has a linear dependence. This means the higher the yield the higher the conversion efficiency of energy from biomass to biochar.

Table 11.6: Summary of calculated efficiencies

Run	kg of carbon in biochar per kg of carbon in LPG	Fossil fuel energy expended per tonne biochar produced (MJ/t char)	MJ fossil fuel expended / MJ energy in biochar (%)	MJ fossil fuel expended / MJ energy in biomass (%)	Conversion efficiency of energy from biomass to char (%)
1	0.53	0.09	313.49	31.26	9.97
2	1.04	0.05	159.32	39.79	24.97
3	2.63	0.02	62.62	28.67	45.79
4	0.86	0.05	162.03	52.57	32.45
5	1.26	0.04	137.46	61.04	44.40
6	1.51	0.03	110.70	28.98	26.18

The overall energy efficiency of a process is generally considered to be the theoretical energy divided by the external energy used in the conversion of feedstock into product. If this were a continuous process, the main energy cost would be during start up, but subsequently the process would be self-sustaining because the energy available from evolution of flammable vapours (both condensable and non-condensable) is sufficient to dry the wood and raise its temperature to the pyrolysis range. Unless the wood is particularly wet (or too wet), there is an excess of energy. Therefore, the energy efficiency is a meaningless concept because no external energy is needed for the biomass to char conversion. However, this system is a batch process (for the reason discussed in Section 3.2); here, start-up heat is required before the process reaches pyrolysis conditions. Therefore, an overall energy efficiency is calculable as the heat required to raise the biomass to a temperature where pyrolysis starts divided by the external heat supplied to this point by the LPG. However, to ensure combustion of the evolved gases and flaring of the products of incomplete combustion, further LPG is used and so the divisor should take these additional energies into account. While not regarded as a significant number to this work, Runs 3 and 5 can be compared using the specific heat data for wood and char from Rath et al. (2003) and the heats of reaction citied in Fantozzi et al. (2007b). For Run 3, which contains 50.55 kg of dry biomass with 21.94 % moisture (db), to evaporate the water content of the wood chip requires ~27.2 MJ, to sensibly heat the wood to 300°C requires ~22.5 MJ and the endothermic part of the reaction requires ~46.5 MJ, giving a total of 96.2 MJ. In practise, the biomass is held in a drum and it is logical to include the sensible heat needed to raise the metal temperature of the drum and annulus which, for this system, is ~22.8 MJ. Run 3 used 238.9 MJ of LPG energy so the overall energy efficiency becomes ~50 %. For Run 5 which has 47.09 kg woodchips (db) with 60.38 % moisture (db), the heat of evaporation rises to 74.8 MJ, the sensible heating of the woodchips is ~21.0 MJ, the endothermic part of the reaction is ~43.3 MJ and the sensible heating of the metal is the

same ~22.8 MJ. Run 5 used 405.9 MJ of LPG energy and so the overall energy efficiency is ~40 %. Thus, these calculations show that considerably more energy is input to the process than required for heating. Some of this goes to heat the draft air which goes up the flue and other heat is lost from the surfaces of the combustion chamber and vessel. The fact that the overall energy efficiency is poorer for the wetter woodchips is likely to be related to the extra time required to dry them which means more draft air is heated and more surface heat loss occurs.

11.5 Residence Time

For the air dried wood and wet wood, the residence time was determined as the time the reactor was above 600 °C. Run 4 did not have enough heat input supplied and therefore its residence time was determined by the time the centre temperature was above 400 °C. The average temperatures are shown in Table 11.7. The charcoal was sampled in 8 different locations as shown previously in Figure 6.2.

Run 5 had the lowest residence time of the runs that were characterised. Run 5 reached a maximum temperature of 703 °C before it began to cool and was held for a period of approximately 20 minutes at 610 °C. It can be seen from the fixed carbon results that there was very little variation throughout the batch. This indicates the hold period is not necessary and that the natural pyrolysis cycle is enough to ensure the batch is evenly pyrolysed.

Table 11.7: Residence time

Run	Residence Time (h)	Average temperature (°C)	Peak Temperature (°C)	Fixed Carbon (wt %)
1	0.63	629	646	N/A
2	1.48	622	654	94.4 ± 1.4
3	1.18	646	678	95.0 ± 1.3
4	1.98	419	452	69.3 ± 7.2
5	0.90	652	703	95.3 ± 1.2
6	0.63	639	658	N/A

Note: The average temperature is defined by the average temperature at which the centre temperature was above 600 °C for all runs expect Run 4, which was the average temperature above 400 °C.

11.6 Heating Rate

The heating rate was determined between the reactor core temperatures of 240-340 °C. This range was chosen both the 23 kW and 6 kW burners were going and supplying heat to the process. For the air-dried wood the 23 kW burner turned off when the centre temperature reached 340 °C after which point, the heating rate slightly decreased.

Table 11.8 shows the variation in heating rates between the runs. The higher moisture content woodchips had lower heating rates. This demonstrates that the core temperature is not indicative of the bed temperature because, if it were, all moisture would have evaporated by 240 °C and all runs would be similarly dry. This result indicates that the bed heating is uneven and that pockets of moisture remain even through this temperature range.

Table 11.8: Heating rate

Run	Mass of wood (kg) (db)	Wood MC (wt %) (db)	Heating Rate (°C/min)
1	34.58	24.04	3.94
2	37.32	21.15	3.70
3	50.55	21.94	7.66
4	46.77	94.71	1.96
5	47.09	60.38	3.03
6	47.54	20.13	6.67

Note: db = dry basis. MC = moisture content

12.0 **CONCLUSION**

A batch pyrolyser was designed and constructed for biochar manufacture. The operation is simple and requires minimal operator input making it suitable for the intended target user, a hobby farmer that has limited time available.

This reactor is portable and can be moved to different locations with a forklift. The capacity is 0.43 m^3 which equates to 100 -150 kg of wood chips, depending on the moisture content of the biomass. A gear box was installed to rotate the vertical reactor into a horizontal position to minimise the time required for loading and unloading.

Experiments conducted on a lab-scale drum pyrolyser showed that the properties of biochar are most significantly affected by peak temperature and particle size. The effect of peak temperature is well documented (Antal Jr & Grønli, 2003); however the effect of particle size is not. The results showed that there is a higher percentage of volatile matter in smaller samples, with the medium and large samples correspondingly lower. The reason is that volatiles have less distance to travel before escaping small particles which reduces their intraparticle residence time and so reduces the opportunity for secondary cracking. These results directly correspond to the fixed carbon yield being higher for the larger samples. Moisture content and grain direction had minimal effect on the biochar properties but moisture did affect the energy efficiency of the process. These results provided a basis for the pilot scale experimental trials. The design of the pilot reactor followed the principle observed with particle size that, in order to get maximum residence time of the vapour and tar in the reactor, the reactor was designed with a perforated core so that the vapours have a tortuous path of travel. In this way, the higher yields seen in larger particles are also likely to translate into higher yields in a fixed bed. In addition, this design also means that heat and mass transfer occur in the same direction from the outer wall to the perforated core, which will minimise the heat up time, but also promote volatilisation-condensation cycling of the tar vapours as they move across the bed. This will have a refluxing effect which increases residence time.

The initial pilot scale trial run revealed that the peak temperature was largely self-determining, because there is a balance between the exothermic reactions which continue increasing the temperature of the reactor, while consuming the convertible biomass. This means the system temperature reaches approximately 700 °C after which it begins to cool. This temperature rise occurred despite switching off the combustion burners which ignite the pyrolysis vapours (to heat the system) once the reactor core had reached 400 °C. At 700 °C a high quality char was produced with greater than 90 % fixed carbon and less than 5 % volatile matter, the balance being ash indicating a high fraction of stable carbon. Because the system was well insulated, it remained above 600 °C for more than 1 hour, which was sufficient to ensure the batch was evenly pyrolysed, ascertained by sample measurement at

8 locations in the reactor. This meant an additional soak time was not required. Moisture had a significant impact on the energy efficiency of the process. Due to the uneven heating of the bed being exacerbated with very wet feed charges, the control set points need to be elevated beyond 340 °C for the main burner and 400 °C for the pilot burner (which ignites the pyrolysis vapours) to ensure that the bed gets into the exothermic self-sustaining pyrolysis regime.

Only two of the six pilot trials were rated a success, Run 3 using dry woodchips and Run 5 using wet woodchips. This was because oxygen ingress was a recurring problem due to an inadequately sealed reactor lid. This has been redesigned. When the seal worked, the yield was not affected by the initial wood moisture content with yields of 29.7 wt % and 28.8 wt % being obtained from wood with an initial moisture content of 21 % and 60 % respectively.

Yields of between 20 - 30 wt % were obtained at the peak temperature mark of 700 °C for the lab scale characterisations. On the pilot scale, the upper end of the yield range was achieved with the good runs. It is believed the variation in yield content for the lab scale analysis is due to the variation in particle size, although statistical analysis of the results suggested otherwise.

The carbon footprint of the successful dry run, Run 3 was 19.2 % in comparison to 3.3 % for the successful wet wood run, Run 5. This indicates moisture has a significant effect on the carbon footprint.

The energy efficiency of the pilot scale process is significantly better than the lab scale experimental work. This was expected because some of the energy produced was recycled and the mass of biomass used was significantly higher. This meant that after the set point of 400 °C was reached, and both burners were turned off, the exothermic reactions continued heating the process up to a maximum temperature of 700 °C, with no additional LPG required. The optimum pilot scale run was Run 3. Run 3 had the highest conversion efficiency of energy from biomass to char, with a value of 45.8 %.

The pyrolyser fulfils the aims of the project. Good quality charcoal was produced and high yields were obtained. Recommendations and further work are discussed in the next section.

13.0 **RECOMMENDATIONS**

1. The current system uses a basic ON/OFF feedback controller which changes the state based on the output from the two thermocouples. This was intended to be a short term approach to establish the best operating window for the pyrolyser. However, now that these are established, a programmable logic controller (PLC) will enable the system to be fully automated. A PLC has the advantage of multiple input/output arrangements and has the benefit of not being affected by electrical noise. A PLC would have more flexibility and would enable greater control over the blower which supplies tertiary air to the process.

2. During monitoring, it was noticed the temperature profile across the reactor was not even, with cooler temperatures on the same side of the reactor as the burner ports in the combustion chamber. This was due to the burners both facing directly across the reactor. The problem could be mitigated by installing the burners in a tangential direction, which would evenly distribute the heat by creating a swirl effect in the combustion section.

3. The system works by natural draft; that is, the hot rising gases and combustion products draw secondary air into the base of the combustion chamber. However, in fact, across the pyrolysis range, some smoke and vapours were escaping out of the secondary air holes. The reason is that the primary air supplied to the gas burners is forced draft. This is a safety measure, so that the burners do not go out, but was not taken into account during the design calculations. This forced draft reduces the natural updraft by reducing the pressure gradient. Also, the relatively high velocity of the flame induces turbulence, which may mean some eddies promote smoke release from the secondary air holes. This latter reason was addressed by putting a metal ring in the combustion chamber to reduced turbulence near the holes. This was partially successful. However, the most practical way to address this is to create a better updraft. There are two ways to do this; (i), to increase the flue diameter; or (ii), to get a higher rated blower so more tertiary air could be drawn in through the venturi and hence draw in more secondary air. Both have drawbacks. A larger flue diameter means more secondary air is drawn into the system, which is useful when the pyrolysis vapours need combusting, but a drawback the rest of the time because this air needs heating which uses LPG unnecessarily. Increasing the injection velocity of the tertiary air has the advantage that it is controllable, but the disadvantage that it dilutes and cools the flue gases making the flare less effective, which may make it more difficult to meet emissions limits. (See point 8 below). However, this latter avenue will be pursued as the tertiary air is currently supplied by

a fan, but may in future be supplied by the blower, which is oversized for its burner and flare duties.

4. Due to the high temperatures, the stainless steel inner lid warped and lifted which meant there was not a complete seal, which meant the gases did not exit the drum through the perforated core and into the combustion chamber. Instead, they bypassed upwards and out of the gap between the lid and the drum. This created a draw into the reactor, allowing oxygen to enter. A temporary and reasonably effective fix was to place a high temperature insulation rope around the inner lid to create a seal. At times, the insulation would move when the lid was bayonetted in, resulting in an ineffective seal. The lid is has been redesigned to be countersunk so that warping will not result in the lid lifting above the drum. An alternative is to change to a low expansion material of construction.

5. The flare going out was a reoccurring issue throughout the runs. This was because the flare was poorly designed.

6. A sliding plate was installed over the secondary air holes on the base of the combustion chamber. This plate is not part of the 'Open Source' design, as the design calculations expected the secondary air updraft flow rate to relate to the flue stack temperature and stack diameter and so would not be excessively high. However, to give flexibility for the very first trials (until we were certain that the reactor operated as expected), the sliding plate was installed so that the secondary air flow rate could be modulated. However, the plate became hot and warped making it inoperable. Nevertheless, the reactor did operate as expected and so the sliding plate will be removed.

7. During cool down, it was clear that the natural updraft of secondary air was not only cooling the reactor (as expected) but that a little air was entering the base of the perforated core and so keeping alive some embers of charcoal. This was particularly true when the lid was not secured properly during cool down, and so needs to be revisited with the new countersunk lid. During cool down, for the six trials reported here, this problem was overcome by blocking the secondary air holes with loosely balled aluminium foil. If, after the lid upgrade, air ingress must still be prevented a better system will be needed. The approach will be to redesign the base of the perforated drum to make ingress less likely. This is because the system needs to operate remotely without human intervention between filling and emptying.

8. The pilot-scale design includes an overflow vent (∅125 mm) and can cope with moderate pressure rises. However, for the first trials we installed a pilot light in the

overflow stack in case of an unexpected pressure rise and subsequent escape of flammable gases. The pilot would ignite them before venting up the overflow stack. As the pilot needed air, a hole was cut into the overflow stack and, at the joint between the stack and the combustion chamber, a bursting disc was placed consisting of several sheets of aluminium foil. However, in the six pilot scale runs, excess pressures were not generated and the overflow vent was never required. Therefore, the pilot light can be removed, the hole sealed and the aluminium foil removed.

9. For air dried wood, with a moisture content of < 20 %, the recommended set points are 340 °C for the pilot burner and 400 °C for the main burner. For wet wood, with a moisture content > 20 %, the recommended set points are 500 °C for the pilot burner and 570 °C for the main burner.

10. In future, analysis of the gas composition and flow rates are recommended. This will provide valuable information on the extent of combustion, the carbon footprint of the process the energy efficiency and compliance to emissions limits.

11. Further work is required to model the system. The model was attempted in MATLAB but due to the variation in the dynamics of the reaction rates of the processes, a highly unstable model was created. It is recommended that the model be reformulated in COMSOL which is better able to handle variable dynamics.

14.0 **REFERENCES**

Antal Jr, M. J., Croiset, E., Dai, X., DeAlmeida, C., Mok, W. S. L., Norberg, N., . . . Al Majthoub, M. (1996). High-yield biomass charcoal. *Energy and Fuels, 10*(3), 652-658.

Antal Jr, M. J., & Grønli, M. (2003). The art, science, and technology of charcoal production. *Industrial and Engineering Chemistry Research, 42*(8), 1619-1640.

Antal Jr, M. J., Mochidzuki, K., & Paredes, L. S. (2003). Flash carbonization of biomass. *Industrial and Engineering Chemistry Research, 42*(16), 3690-3699.

Arntzen, C. J. (1994). Wood Properties. In J. E. Winandy (Ed.), *Encyclopedia of Agricultural Science* (Vol. 4, pp. 549-561). Orlando: Academic Press.

ASHRAE Handbook - Fundamentals (SI Edition). (2009). American Society of Heating, Refrigerating and Air-Conditioning Engineers, Inc.

Babu, B. V., & Chaurasia, A. S. (2004). Pyrolysis of biomass: Improved models for simultaneous kinetics and transport of heat, mass and momentum. *Energy Conversion and Management, 45*(9-10), 1297-1327.

Baldock, J. A., & Smernik, R. J. (2002). Chemical composition and bioavailability of thermally altered Pinus resinosa (Red pine) wood. *Organic Geochemistry, 33*(9), 1093-1109.

Bashir, F. (2012). *Fracturing of wood during pyrolysis*. Massey University. Palmerston North.

Bezanson, A. (n.d.). Pyrolysis and Torrefaction of Biomass Retrieved 20/07/2012, from http://poisson.me.dal.ca/site2/courses/mech4840/Pyrolysis%20&%20Torrefaction%20of%20Biomass.pdf

Blackwell, P., Riethmuller, G., & Collins, M. (2009). Biochar Application to Soil. In J. Lehmann & S. Joseph (Eds.), *Biochar for Environmental Management : Science and Technology* (pp. 207-226). London, GBR: Earthscan.

Brewer, C. E., Unger, R., Schmidt-Rohr, K., & Brown, R. C. (2011). Criteria to Select Biochars for Field Studies based on Biochar Chemical Properties. *Bioenergy Research, 4*(4), 312-323.

Bridgwater, A. V. (2003). Renewable fuels and chemicals by thermal processing of biomass. *Chemical Engineering Journal, 91*(2–3), 87-102.

Cai, H. Y., Güell, A. J., Chatzakis, I. N., Lim, J. Y., Dugwell, D. R., & Kandiyoti, R. (1996). Combustion reactivity and morphological change in coal chars: Effect of pyrolysis temperature, heating rate and pressure. *Fuel, 75*(1), 15-24.

Calvelo Pereira, R., Kaal, J., Camps Arbestain, M., Pardo Lorenzo, R., Aitkenhead, W., Hedley, M., . . . Maciá-Agulló, J. A. (2011). Contribution to characterisation of biochar to estimate the labile fraction of carbon. *Organic Geochemistry, 42*(11), 1331-1342.

Carangelo, R. M., Solomon, P. R., & Gerson, D. J. (1987). Application of TG-FT-i.r. to study hydrocarbon structure and kinetics. *Fuel, 66*(7), 960-967.

Cetin, E., Moghtaderi, B., Gupta, R., & Wall, T. F. (2004). Influence of pyrolysis conditions on the structure and gasification reactivity of biomass chars. *Fuel, 83*(16), 2139-2150.

Chun, Y., Sheng, G., Chiou, G. T., & Xing, B. (2004). Compositions and sorptive properties of crop residue-derived chars. *Environmental Science and Technology, 38*(17), 4649-4655.

Dall'Ora, M., Jensen, P. A., & Jensen, A. D. (2008). Suspension combustion of wood: Influence of pyrolysis conditions on char yield, morphology, and reactivity. *Energy and Fuels, 22*(5), 2955-2962.

Dan, S., & Robert, M. (2001). Compost Quality Attributes, Measurements, and Variability. In Stofella & B. A. Kahn (Eds.), *Compost Utilization In Horticultural Cropping Systems* (pp. 95-120). Boca Raton: CRC Press.

De Jong, W., Di Nola, G., Venneker, B. C. H., Spliethoff, H., & Wójtowicz, M. A. (2007). TG-FTIR pyrolysis of coal and secondary biomass fuels: Determination of pyrolysis kinetic parameters for main species and NOx precursors. *Fuel, 86*(15), 2367-2376.

De Jong, W., Pirone, A., & Wójtowicz, M. A. (2003). Pyrolysis of Miscanthus Giganteus and wood pellets: TG-FTIR analysis and reaction kinetics. *Fuel, 82*(9), 1139-1147.

Demirbaş, A., & Arin, G. (2002). An overview of biomass pyrolysis. *Energy Sources, 24*(5), 471-482.

Di Blasi, C. (2008). Modeling chemical and physical processes of wood and biomass pyrolysis. *Progress in Energy and Combustion Science, 34*(1), 47-90.

Di Blasi, C., Branca, C., Santoro, A., & Hernandez, E. G. (2001). Pyrolytic behavior and products of some wood varieties. *Combustion and Flame, 124*(1-2), 165-177.

Elyounssi, K., Blin, J., & Halim, M. (2010). High-yield charcoal production by two-step pyrolysis. *Journal of Analytical and Applied Pyrolysis, 87*(1), 138-143.

Fantozzi, F., Colantoni, S., Bartocci, P., & Desideri, U. (2007a). Rotary kiln slow pyrolysis for syngas and char production from biomass and waste - Part I: Working envelope of the reactor. *Journal of Engineering for Gas Turbines and Power, 129*(4), 901-907.

Fantozzi, F., Colantoni, S., Bartocci, P., & Desideri, U. (2007b). Rotary kiln slow pyrolysis for syngas and char production from biomass and waste - Part II: Introducing product yields in the energy balance. *Journal of Engineering for Gas Turbines and Power, 129*(4), 908-913.

Fuwape, J. A. (1996). Effects of carbonisation temperature on charcoal from some tropical trees. *Bioresource Technology, 57*(1), 91-94.

Garcia-Perez, M., Lewis, T., & Kruger, C. E. (2011). Methods for Producing Biochar and Advanced Biofuels in Washington State Part 1: Literature Review of Pyrolysis Reactors.

Gaskin, J. W., Steiner, C., Harris, K., Das, K. C., & Bibens, B. (2008). Effect of low-temperature pyrolysis conditions on biochar for agricultural use. *Transactions of the ASABE, 51*(6), 2061-2069.

Glaser, B., Dreyer, A., Bock, M., Fiedler, S., Mehring, M., & Heitmann, T. (2005). Source apportionment of organic pollutants of a highway-traffic-influenced urban area in Bayreuth (Germany) using biomarker and stable carbon isotope signatures. *Environmental Science and Technology, 39*(11), 3911-3917.

Glaser, B., Haumaier, L., Guggenberger, G., & Zech, W. (2001). The 'Terra Preta' phenomenon: A model for sustainable agriculture in the humid tropics. *Naturwissenschaften, 88*(1), 37-41.

Green, D. W., & Perry, R. H. (2008). *Perry's Chemical Engineers' Handbook, Eighth Edition* (8 ed.): McGraw-Hill: New York.

Guo, J., & Lua, A. C. (1998). Characterization of chars pyrolyzed from oil palm stones for the preparation of activated carbons. *Journal of Analytical and Applied Pyrolysis, 46*(2), 113-125.

Hayward, M. (2011). Biochar Formulation and Application to Soil Opportunities: NZ Context. Palmerston North, New Zealand.

Hoekstra, E., Westerhof, R. J. M., Brilman, W., Van Swaaij, W. P., Kersten, S. R. A., Hogendoorn, K. J. A., & Windt, M. (2012). Heterogeneous and homogeneous reactions of pyrolysis vapors from pine wood. *AIChE Journal, 58*(9), 2830-2842.

Imam, T., & Capareda, S. (2012). Characterization of bio-oil, syn-gas and bio-char from switchgrass pyrolysis at various temperatures. *Journal of Analytical and Applied Pyrolysis, 93*(0), 170-177. doi: 10.1016/j.jaap.2011.11.010

International Biochar Initiative. (2012). Standardized Product Definition and Product Testing Guidelines for Biochar that is used in Soil: International Biochar Initiative.

Jamil, K., & Li, C. Z. (2006). Volatilisation and Catalytic Effects of AAEM Species on Reactivity of Char from Pyrolysis and Gasification of Victorian Brown Coal. *Journal of Energy & Environment, 5*, 31-43.

Jeffery, S., Verheijen, F. G. A., van der Velde, M., & Bastos, A. C. (2011). A quantitative review of the effects of biochar application to soils on crop productivity using meta-analysis. *Agriculture, Ecosystems and Environment, 144*(1), 175-187.

Kang, W., Kang, C. W., Chung, W. Y., Eom, C. D., & Yeo, H. (2008). The effect of openings on combined bound water and water vapor diffusion in wood. *Journal of Wood Science, 54*(5), 343-348.

Keller, K., McInerney, D., & Bradford, D. F. (2008). Carbon dioxide sequestration: how much and when? *Climatic Change, 88*(3-4), 267-291.

Kockar, Ö. M., Onay, Ö., Putun, A. E., & Putun, E. (2000). Fixed-Bed Pyrolysis of Hazelnut Shell: A Study on Mass Transfer Limitations on Product Yields and Characterization of the Pyrolysis Oil. *Energy Sources, 22*(10), 913-924.

Koufopanos, C. A., Papayannakos, N., Maschio, G., & Lucchesi, A. (1991). Modeling of the Pyrolysis of Biomass Particles - Studies on Kinetics, Thermal and Heat Transfer Effects. *Canadian Journal of Chemical Engineering, 69*(4), 907-915.

Krull, E., J.A. , Baldock, J. S., & Smernik, R. (2009). Characteristics of biochar: Organo-chemical properties. In J. Lehmann & S. Joseph (Eds.), *Biochar for environmental management: Science and technology* (pp. 53–66). London: Earthscan.

Laird, D. A., Rogovska, N. P., Garcia-Perez, M., Collins, H. P., Streubel, J. D., & Smith, M. R. (2011). Pyrolysis and Biochar – Opportunities for Distributed Production and Soil Quality Enhancement. In R. Braun, D. L. Karlen & D. Johnson (Eds.), *Sustainable Alternative Fuel Feedstock Opportunities, Challenges and Roadmaps for Six U.S. Regions* (pp. 257-282): SWCS.

Lee, J. W., Kidder, M., Evans, B. R., Paik, S., Buchanan Iii, A. C., Garten, C. T., & Brown, R. C. (2010). Characterization of biochars produced from cornstovers for soil amendment. *Environmental Science and Technology, 44*(20), 7970-7974.

Lehmann, J., Czimczik, C., Laird, D., & Sohi, S. (2009). Stability of Biochar in the Soil. In J. Lehmann & S. Joseph (Eds.), *Biochar for Environmental Management : Science and Technology* (pp. 183-206). London, GBR: Earthscan.

Lehmann, J., & Joseph, S. (2009). Biochar for Environmental Management: An Introduction. In J. Lehmann & S. Joseph (Eds.), *Biochar for Environmental Management: Science and Technology* (pp. 1-12). London, GBR: Earthscan.

Lehmann, J., Lilienfein, J., Rebel, K., Lima, S. D., & Wilcke, W. (2004). Subsoil retention of organic and inorganic nitrogen in a Brazilian savanna Oxisol. *Soil Use and Management, 20*(2), 163-172.

Lehmann, J., & Rondon, M. (2006). Bio-Char Soil Management on Highly Weathered Soils in the Humid Tropics. In N. Uphoff (Ed.), *Biological Approaches to Sustainable Soil Systems* (pp. 517-530): CRC Press.

Major, J. (2010). Guidelines on Practical Aspects of Biochar Application to Field Soil in Various Soil Management Systems.

Mansilla, H., Garcia, R., Tapia, J., Durán, H., & Urzúa, S. (1991). Chemical characterization of Chilean hardwoods. *Wood Science and Technology, 25*(2), 145-149.

Mason, D. M., & Gandhi, K. (1980). Formulas for Calculating the Heating Value of Coal and Coal Char: Development, Test and Uses. *ACS Division of Fuel Chemistry, Preprints, 25*(3), 235-245.

McKendry, P. (2002). Energy production from biomass (part 1): overview of biomass. *Bioresource Technology, 83*(1), 37-46.

Miller, R. S., & Bellan, J. (1997). A Generalised Biomass Pyrolysis Model Based on Superimposed Cellulose, Hemicellulose and Lignin Kinetics. *Combustion Science and Technology, 126*, 97-137.

Mohan, D., Pittman Jr, C. U., & Steele, P. H. (2006). Pyrolysis of wood/biomass for bio-oil: A critical review. *Energy and Fuels, 20*(3), 848-889.

Mok, W. S. L., Antal Jr, M. J., Szabo, P., Varhegyi, G., & Zelei, B. (1992). Formation of charcoal from biomass in a sealed reactor. *Industrial and Engineering Chemistry Research, 31*(4), 1162-1166.

Mok, W. S. L., & Antal, M. J. (1983). Effects of Pressure on Biomass Pyrolysis. 2. Heats of Reaction of Cellulose Pyrolysis. *Thermochimica Acta, 68*(2-3), 165-186.

Murneek, A. E. (1929). Hemicellulose as a storage carbohydrate in woody plants, with special reference to the apple. *Plant Physiology, 4*(2), 251-264.

Neves, D., Thunman, H., Matos, A., Tarelho, L., & Gómez-Barea, A. (2011). Characterization and prediction of biomass pyrolysis products. *Progress in Energy and Combustion Science, 37*(5), 611-630.

Novak. (2009). Characterisation of Designer Biochar Produced at Different Temperatures and their Effects on a Loamy Sand *Annals of Environmental Science, 3*, 195-206.

Oasmaa, A., Peacocke, C., Gust, S., Meier, D., & McLellan, R. (2005). Norms and standards for pyrolysis liquids. End-user requirements and specifications. *Energy and Fuels, 19*(5), 2155-2163.

Onay, O. (2007). Influence of pyrolysis temperature and heating rate on the production of bio-oil and char from safflower seed by pyrolysis, using a well-swept fixed-bed reactor. *Fuel Processing Technology, 88*(5), 523-531.

Petty, J. A., & Preston, R. D. (1969). The Dimensions and Number of Pit Membrane Pores in Conifer Wood. *Proceedings of the Royal Society of London. Series B, Biological Sciences, 172*(1027), 137-151.

Preston, C. M., & Schmidt, M. W. I. (2006). Black (pyrogenic) carbon: A synthesis of current knowledge and uncertainties with special consideration of boreal regions. *Biogeosciences, 3*(4), 397-420.

R Development Core Team. (2012). R Foundation for Statistical Computing. Vienna, Austria.

Ragland, K. W., Aerts, D. J., & Baker, A. J. (1991). Properties of wood for combustion analysis. *Bioresource Technology, 37*(2), 161-168. doi: 10.1016/0960-8524(91)90205-x

Rath, J., Wolfinger, M. G., Steiner, G., Krammer, G., Barontini, F., & Cozzani, V. (2003). Heat of wood pyrolysis. *Fuel, 82*(1), 81-91.

Roberts, A. F. (1971). Problems associated with the theoretical analysis of the burning of wood. *Symposium (International) on Combustion, 13*(1), 893-903.

Robertson, J. B., & Van Soest, P. J. (1981). *The detergent system of analysis and its application to human food*. New York: Marcel Dekker.

Sánchez, M. E., Lindao, E., Margaleff, D., Martínez, O., & Morán, A. (2009). Pyrolysis of agricultural residues from rape and sunflowers: Production and characterization of bio-fuels and biochar soil management. *Journal of Analytical and Applied Pyrolysis, 85*(1–2), 142-144.

Schimmelpfennig, S., & Glaser, B. (2012). One Step Forward toward Characterization: Some Important Material Properties to Distinguish Biochars. *J. Environ. Qual., 41*(4), 1001-1013. doi: 10.2134/jeq2011.0146

Shafizadeh, F., & Chin, P. P. S. (1976). Thermal Deterioration of Wood. *Abstracts of Papers of the American Chemical Society, 172*(SEP3), 37-37.

Shimazu, F., & Sterling, C. (1966). Effect of Wet and Dry Heat on Structure of Cellulose. *Journal of Food Science, 31*(4), 548-551.

Singh, B., Singh, B. P., & Cowie, A. L. (2010). Characterisation and evaluation of biochars for their application as a soil amendment. *Australian Journal of Soil Research, 48*(6-7), 516-525.

Sinnott, R. K. (1999). *Coulson and Richardson's Chemical Engineering Volume 6 - Chemical Engineering Design (3rd Edition)* (Vol. 6): Butterworth Heinemann.

Sinnott, R. K. (2005). *Coulson and Richardson's Chemical Engineering Volume 6 - Chemical Engineering Design (4th Edition)* (4 ed. Vol. 6): Elsevier.

Snow, D. A. (2002). Plant Engineer's Reference Book (2nd Edition). In R. H. Shipman (Ed.), *Liquefied Petroleum Gas*: Elsevier.

Spokas, K. A. (2010). Review of the stability of biochar in soils: Predictability of O:C molar ratios. *Carbon Management, 1*(2), 289-303.

van Krevelen, D. W. (1950). Graphical-statistical method for the study of structure and reaction processes of coal. *Fuel, 29*, 269-284.

Wang, T., Camps-Arbestain, M., & Hedley, M. (2013). Predicting C aromaticity of biochars based on their elemental composition. *Organic Geochemistry, 62*, 1-6.

Waters, D., Zwieten, L., Singh, B. P., Downie, A., Cowie, A. L., & Lehmann, J. (2011). Biochar in Soil for Climate Change Mitigation and Adaptation: Soil Health and Climate Change. In B. P. Singh, A. L. Cowie & K. Y. Chan (Eds.), (Vol. 29, pp. 345-368): Springer Berlin Heidelberg.

Yonebayashi, K., & Hattori, T. (1988). CHEMICAL AND BIOLOGICAL STUDIES ON ENVIRONMENTAL HUMIC ACIDS : I. Composition of Elemental and Functional Groups of Humic Acids. *Soil science and plant nutrition, 34*(4), 571-584.

APPENDIX A
NOMENCLATURE

Nomenclature		
Variables	Definitions	Units
ADF	Acid detergent fibre	-
A_T	Total Area of the reactor	m^2
A_{flue}	Cross sectional area of the flue	m^2
A_{char}	Pre-exponential factor for char	s^{-1}
A_{gas}	Pre-exponential factor for gas	s^{-1}
A_{tar}	Pre-exponential factor for tar	s^{-1}
A_{RHS}	Surface Area of the reactor RHS	m^2
A_{LHS}	Surface Area of the reactor LHS	m^2
CEC	Cation exchange capacity	-
CO	Carbon monoxide	-
CO_2	Carbon dioxide	-
$C_{p\ biomass}$	Specific heat capacity of biomass	J kg^{-1} K^{-1}
$C_{p\ w}$	Specific heat capacity of water	J kg^{-1} K^{-1}
$C_{p\ wood}$	Specific heat capacity of wood	J kg^{-1} K^{-1}
$C_{p\ char}$	Specific heat capacity of char	J kg^{-1} K^{-1}
$C_{p\ w}$	Specific heat capacity of water	J kg^{-1} K^{-1}
$C_{p\ gas}$	Specific heat capacity of gas	J kg^{-1} K^{-1}
$C_{p\ tar}$	Specific heat capacity of tar	J kg^{-1} K^{-1}
CV	Coefficient of variation	%
db	Dry basis	wt %
d_{flue}	Diameter of the stack	m
DVC	Depolymersiation, vaporisation and cross-linking	-
E_w	Activation energy for water	J mol^{-1}
E_{gas}	Activation energy for gas	J mol^{-1}
E_{tar}	Activation energy for tar	J mol^{-1}
E_{char}	Activation energy for char	J mol^{-1}
f	Fanning friction factor of the pipe	-
g	Gravity	m s^{-2}
$h_{fg\ w}$	Latent heat of vaporisation/condensation of water	J kg^{-1}
$h_{fg\ tar}$	Latent heat of tar	J kg^{-1}
h_f	Head loss due to friction	Pa
h_r	Heat of reaction for primary reactions Fantozzi	J kg^{-1}
h_c	Convective heat transfer coefficient	W m^{-2} K^{-1}
h_i	Inner reactor height	m

h_c	Inner core height	m
H_2O	Water	-
HCV	Higher calorific value	MJ kg^{-1}
J	Number of nodes	-
k	Restriction factors	Velocity heads
k_{gas}	Equilibrium constant for gas	s^{-1}
k_{tar}	Equilibrium constant for tar	s^{-1}
k_{char}	Equilibrium constant for char	s^{-1}
L	Height of the reactor	m
L_s	Stack height	m
LCV	Lower calorific value	MJ kg^{-1}
$\dot{m}_{propane}$	Propane mass flow rate	kg s^{-1}
$\dot{m}_{air}$	Air mass flow rate	kg s^{-1}
$\dot{m}_{gas}$	Mass flow rate of gas	kg s^{-1}
$\dot{m}_{tar}$	Mass flow rate of tar	kg s^{-1}
$\dot{m}_{LPG}$	LPG mass flow rate	kg s^{-1}
$m_{B,i}$	Initial mass of the biomass	kg
$m_{w,i}$	Initial mass of water	kg
$\dot{m}_{w\,vap}$	Mass flow rate of water vapour	kg s^{-1}
MC	Initial moisture content of the wood	-
M_{oxygen}	Molar mass of oxygen	g mol^{-1}
$M_{propane}$	Molar mass of propane	g mol^{-1}
NDF	Neutral detergent fibre	-
n_{oxygen}	Moles of oxygen	mol
$n_{propane}$	Moles of propane	mol
p'	Atmospheric pressure	N m^{-2} 10^{-2}
PAH	Polycyclic aromatic hydrocarbon	-
P_d	The draft	mm H_2O
PDE	Partial differential equation	
P_1	Pressure	Pa
P_2	Pressure	Pa
q_x	Heat transfer rate	
r_i	Inner radius of the reactor	m
r_c	Inner core radius	m
R_o	Outer radius of the reactor	m
Re	Reynolds number	-
R	Universal gas constant	J mol^{-1} K^{-1}

t	Time	s
T_i	Absolute average temperature of the flue gas in the stack	K
T_a	Ambient temperature	K
$T_{1°+2°}$	Average flue gas temperature	K
TG-FTIR	Thermogravimetric-fourier transform infra-red	
u	Air velocity	
V_T	Total volume of the reactor	m^3
$\dot{V}$	Volumetric flow rate	L s^{-1}
V_w	Volume of wood	m^3
Greek Letters		
α_{int}	Absorptivity of the wood	-
α_w	Absorptivity of the wood	-
ε	Stephen Boltzman Constant	W m^{-2} K^{-4}
ε_{wall}	Emissivity of the wall	-
ε_{wood}	Emissivity of the wood	-
Δr	Distance between the nodes	m
Δh_{gas}	Enthalpy change for gas	kJ kg^{-1}
Δh_{tar}	Enthalpy change for tar	kJ kg^{-1}
$\Delta h_c°$	Heat of combustion of propane	kJ kg^{-1}
ΔP_f	Frictional pressure losses	Pa
ΔP_B	Change of pressure due to buoyancy	Pa
θ_a	Ambient temperature	°C
θ_i	Initial wood temperature	°C
$\lambda_{mixture}$	Thermal conductivity of the first slice	W m^{-1} K^{-1}
λ_{wood}	Thermal conductivity of the wood	W m^{-1} K^{-1}
μ	Viscosity	kg s^{-1} m^{-1}
ρ_{wood}	Density of wood	kg m^{-3}
ρ_{water}	Density of water	kg m^{-3}
ρ_d	Density of dry pine wood chips	kg m^{-3}
ρ_{wood}	Density of wood chips at 50% MC	kg m^{-3}
$\rho_{1°+2°}$	Average density of primary and secondary air	kg m^{-3}
ρ_a	Density of ambient air	kg m^{-3}
ρ_w	Density of water	kg m^{-3}

APPENDIX B

DESIGN

CALCULATIONS

B.1 Introduction

Calculations to predict heat losses, pressure differentials and flows are fundamental to a pyrolyser design. These calculations enable us to predict performance and to establish whether the design meets current performance recommendations. These recommendations are being developed by the International Biochar Initiative and involve producing sustainable biochar that can help reduce the impacts of global warming (International Biochar Initiative, 2012).

The significant components of interest for the design calculations were the reactor volume, stack design, air requirements and heat losses (via radiation, convection and conduction) from the reactor.

The inner reactor volume was determined by the batch size that would be appropriate for a hobby farmer with a moderate amount of waste, between 100 - 200 kg of wood (predominantly branches) which would be put through a chipper prior to pyrolysis.

The reactor is heated by a mixture of primary air and LPG, based on stoichiometry and the assumption that 20 % excess air is required for complete combustion. The reactor is designed so that when pyrolysis gases evolve, they ignite with the flame source and provide a somewhat self-heating process. However, a secondary air supply is required to ensure complete combustion of the pyrolysis gases. A natural draft has been designed to achieve this through secondary air holes in the bottom of the reactor, which are open to the atmosphere. This also aims to minimise the chance of a pressure build up in the system. The stack height is critical to establish the draw pressure differential, after which the gas temperature and the stack diameter determines the air intake flow rate. However, the secondary air flow induced by natural draft may not be enough to ensure complete combustion so a tertiary air system using a venturi was designed at the top of the flue to draw in additional air if required. Additionally, this may be useful during start up to assist the natural draft. As the dynamics of pyrolysis gas production are uncertain, due to the uncertain influence of heat and mass transfer limitations, it is possible that more pyrolysis gas evolves than the capability of the draft and tertiary air to supply enough air to combust this gas. For this reason, a continuously operating flare is positioned at the top of the stack. However, if combustion of the pyrolysis gas causes the combustion chamber and annular regions of the pyrolyser to get too hot, then the tertiary air will be turned off and all pyrolysis gases that are not combusted by the secondary air (drawn in by the natural draft) will be combusted in the flare. These operational safety issues are dealt with in the control strategy (see x).

Heat is used mainly in three ways; to heat the draft air, the vessel and the wood. Air should not be heated up unnecessarily, because this affects the energy efficiency of the process. This is achieved by using an 80 mm flue of 2.5 m in height. The height achieves the draft, the 80 mm diameter controls the flow rate, thus the flow rate of secondary air is limited at low temperatures below the pyrolysis range. During pyrolysis the high combustion gas temperature creates a good draw of secondary air, then above the pyrolysis range as the combustible gas flow decreases, the secondary air draw should ease slightly.

Heat can be lost from the reactor via radiation from the surfaces and through secondary air holes as well as by convection and conduction. Insulation thicknesses were calculated for various surface temperatures. Although a surface temperature of 50 - 60 °C was desired for safety reasons (people touching the reactor), a surface temperature of 100 °C was decided to ensure the overall reactor size was not too large.

B.2 Reactor Volume

The reactor was designed for a hobby farmer with a small amount of waste, around 100 - 200 kg. To reduce heat and mass transfer limitations it was decided the waste material will be put through a chipper. Two densities were used in the volume estimation, the bulk density of dry pine wood chips and the bulk density of wood chips with a moisture content of 50 %.

Table 14.1 Reactor Volume

Symbol	Description	Value	Units
h_i	Inner reactor height	1	m
r_i	Inner reactor radius	0.75	m
h_c	Inner core height	0.9	m
r_c	Inner core radius	0.1	m
ρ_d	Bulk density of dry pine wood chips	181	kg m^{-3}
ρ_w	Bulk density of wood chips at 50% MC	354	kg m^{-3}
V_w	Volume of wood chips	0.43	m^3

$$Volume\ of\ a\ cylinder, V = \pi r^2 h \quad \text{(B.1)}$$

The maximum volume of area for the wood chips is determined by the difference between the reactor volume and the volume of the inner core giving,

$$Volume\ of\ wood, V_w = (\pi {r_i}^2 h_i - \pi {r_c}^2 h_c)$$

$$V_w = \left(\pi(0.375)^2(1) - \pi(0.05)^2(0.9)\right) = 0.43 m^3$$

$$mass_{Dry\ Wood} = V * \rho_d = 0.43 * 181 = 75\ kg \quad \text{(B.2)}$$

$$mass_{Wet\ Wood} = V * \rho_w = 0.43 * 384 = 146\ kg \quad \text{(B.3)}$$

B.3 Excess Air Required to Combust LPG

The calculations below assume that LPG is 100 % propane. LPG is sold in variety of propane / butane mixes with butane having a slightly lower calorific value than propane.

Table 14.2: Summary of system inputs for excess air requirements

Symbol	Description	Value	Units
n_{oxygen}	Moles of oxygen	5	mol
M_{oxygen}	Molar mass of oxygen	32	g mol^{-1}
$n_{propane}$	Moles of propane	1	mol
$M_{propane}$	Molar mass of propane	44.1	g mol^{-1}
λ_{O2}	Excess oxygen	1.2	-
$\dot{V}$	LPG flow rate	0.036	L min^{-1}

Combustion of propane occurs in the presence of oxygen in the following stoichiometric ratios to produce carbon dioxide and water.

$$C_3H_8 + 5O_2 \rightarrow 3CO_2 + 4H_2O \qquad \Delta hc^\circ = 49.9\ kJ/g \quad \text{(B.4)}$$

The mass of oxygen needed to combust with 1 mole of propane is determined by number of moles of oxygen multiplied by its molar mass.

$$m = nM \quad \text{(B.5)}$$

$$m_{oxygen} = 5\ * 32[=]\ mol\ *\ \frac{g}{mol}$$

$$m_{oxygen} = 160\ g$$

The mass of one mole of propane is also determined by the same equation

$$m = nM \tag{B.6}$$

$$m_{propane} = 1 * 44.1\ [=]\ mol * \frac{g}{mol}$$

$$m_{propane} = 44.1\ g$$

The LPG flow rate comes from either a 6 kW burner or a 23 kW burner. The following calculations are based on the 23 kW burner. A rough estimate for the LPG flow rate can be determined by dividing the heat input by the calorific value. The calorific value of propane is 46350 kJ kg^{-1} (*ASHRAE Handbook - Fundamentals (SI Edition)*, 2009).

$$\dot{m}_{LPG} = \frac{Heat\ Input}{Calorific\ Value} = \frac{23000}{46350} = 0.0005\ [=]\ \frac{\frac{kJ}{s}}{\frac{kJ}{kg}}\ [=]\ \frac{kg}{s} \tag{B.7}$$

The oxygen flow rate required was based on the assumption of 20 % excess oxygen is required for complete combustion. Also, noting that air is composed of approximately 21 % oxygen.

$$\dot{m}_{air} = \dot{m}_{LPG}\frac{n_{propane}}{M_{propane}} * n_{O2} * M_{O2} * \frac{Excess\ air}{\%\ oxygen\ in\ air}\ [=]\ \frac{kg}{s}\frac{mol}{\frac{kg}{mol}} * mol * \frac{kg}{mol}\ [=]\frac{kg}{s} \tag{B.8}$$

$$\dot{m}_{air} = 0.0005 * \frac{1}{44.1} * 5 * 32 * \frac{1.2}{0.21}\ [=]\ 0.01\frac{kg}{s} \tag{B.9}$$

The mass flow rate was converted to a volumetric air flow rate using the molar volume of air at standard temperature and pressure, 22.4 L mol^{-1}

$$\dot{V}_{air} = \frac{\dot{Q}_{air}}{M_{air}} * \frac{L}{mol}\ [=]\frac{\frac{kg}{s}}{\frac{kg}{mol}}\frac{L}{mol}\ [=]\frac{L}{s} \tag{B.10}$$

B.4 Stack Design for a Natural Draft

The stack height was calculated based on a draft pressure differential of 2 mm H_2O. This equates to 20 Pa. Equation A.11 determines the stack height required to achieve the desired pressure draw. The derivations of this equation from Coulson and Richardson (Sinnott, 1999) are shown below

$$L_s = \frac{P_d}{0.35(p')\left(\frac{1}{T_a} - \frac{1}{T_{1°+2°}}\right)} \quad \text{(B.11)}$$

Where L_s is the stack height (m), p' is atmospheric pressure (millibar or N/m^2*10^{-2}), T_a is ambient temperature (K), $T_{1°+2°}$ is the average flue gas temperature (K) and P_d is the draft (mm H_2O).

This equation above is derived from the gas buoyancy

$$\Delta P_B = L_s(\rho_{1°+2°} - \rho_a)g[=]m\frac{kg}{m^3}\frac{m}{s^2}[=]Pa \quad \text{(B.12)}$$

Where ΔP_B is the change of pressure due to buoyancy (Pa), $\rho_{1°+2°}$ is the average density of primary and secondary air (kg/m^3) and ρ_{amb} is the density of ambient air (kg/m^3).

Expressing the above equation to predict the water suction head in the form of a height differential (Δh) with the units mmH_2O. Δh is the same as P_d in equation 10 above.

$$\Delta h = \frac{1000}{\rho_w g}L_s(\rho_{1°+2°} - \rho_{amb})g[=]\frac{mm}{m}\frac{m^3}{kg}\frac{s^2}{m}m\left(\frac{kg}{m^3}\right)\frac{m}{s^2}[=]mm\ H_2O \quad \text{(B.13)}$$

Where ρ_w is the density of water (kg/m^3) and g is gravity (m/s^2)

This simplifies to

$$\Delta h = L_s(\rho_{1°+2°} - \rho_a)[=]\frac{mm}{m}\frac{m^3}{kg}\frac{s^2}{m}m\left(\frac{kg}{m^3}\right)\frac{m}{s^2}[=]mm\ H_2O \quad \text{(B.14)}$$

Gas density relates to the ideal gas equation by

$$\rho_{gas} = \frac{M_{air}}{1000}\frac{P}{RT}[=]\frac{g}{mol}\frac{kg}{g}\frac{J}{m^3}\frac{mol}{J}\frac{1}{K}[=]\frac{kg}{m^3} \quad \text{(B.15)}$$

With flue gas density molecular weight equal to that of air at 28.9 g/mol and R = 8.3144J/mol/K, the ratio of M/R = 3.5 to two significant figures and the pressure P = atmospheric pressure. This simplifies the density term to

$$\rho_{gas} = \frac{3.5}{1000}\frac{P}{T} \quad \text{(B.16)}$$

Substituting ρ_{gas} into equation A.13 yields

$$\Delta h = \frac{3.5}{1000}L_s\left(\frac{P_{1°+2°}}{T_{1°+2°}} - \frac{P_a}{T_a}\right)[=]mm\ H_2O \quad \text{(B.17)}$$

As the pressure differential is small and the temperature variations are large, the equation can be simplified to

$$\Delta h = \frac{3.5}{1000}L_s P_a\left(\frac{1}{T_{1°+2°}} - \frac{1}{T_a}\right)[=]mm\ H_2O \quad \text{(B.18)}$$

Converting pressure units from Pa to mbar, 1 millibar = 100 Pa and then simplifying yields

$$\Delta h = 0.35L_s P_a\left(\frac{1}{T_{1°+2°}} - \frac{1}{T_a}\right)[=]mm\ H_2O \quad \text{(B.19)}$$

Δh is equivalent to P_d and P_a is equal to p'. Rearranging for L_s, it can be seen that the two equations (Eq. A.18 and Eq. A.10) are identical, with the exception of the bracketed terms, which are round the other way. This is a convention issue. The equation from Coulson and Richardson on page 774 (Sinnott, 1999) predicts draw as a positive number, which means a negative pressure gradient as used in Eq. A.10.

B.5 Number of 2° Air Holes and Diameter

The natural draft draws air up through the holes in the base of the combustion chamber. A radiation shield is placed above each hole to minimise heat loss from the holes. The total hole area required is calculated based on ensuring the resistance to flow is minimal outside the stack. Therefore, a simple rule of thumb is applied that the flow area ratios increase by 1.5 for each change in channel.

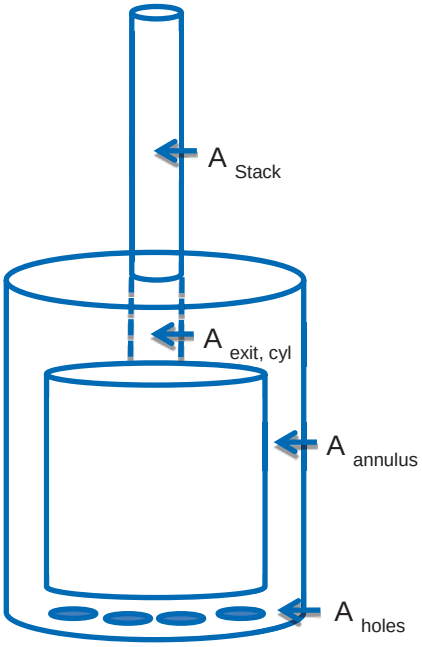

$A_{exit\ cyl} > 1.5\ A_{stack}$

$A_{annulus} > (1.5)^2\ A_{stack}$

$A_{holes} > (1.5)^3\ A_{stack}$

Based on the rule of thumb, the total hole area is 1.5 times greater than the area of the annulus and 1.5 cubed greater than the stack area.

$$A_{holes} = 1.5^3 A_{stack} = 0.017\ m^2 \quad \text{(B.20)}$$

A hole diameter was selected and the area of one hole was calculated

$$A_{hole} = \pi \frac{0.05^2}{4} = 0.00196\ m^2 \quad \text{(B.21)}$$

The total number of holes required was calculated by dividing the total hole area by the area of one hole, producing a total of 9 holes required.

In order for the radiation shield to be installed, it requires some form of mounting. Therefore, it was decided to have a pipe that protrudes through the base where the radiation shield can be placed on

top of. It was decided to have four slots around the pipe to draw the secondary air in. Multiplying by 1.5 to minimise the resistance, the area required for one hole

$$A_{required} = 1.5A_{hole} = 0.00295\ m^2 \quad \text{(B.22)}$$

The area required per slot is therefore a quarter of the area of one hole.

$$A_{required} = \frac{1}{4} * 0.00295 = 0.00065 m^2 \quad \text{(B.23)}$$

$$0.00065 = \frac{\pi}{8} * (0.015)^2 * 0.03L$$

Therefore, rearranging for L, the height (L) of the pipe is 0.019 m. Allowing for water to drain, 3mm of length was added so the hole sits just proud of the bottom of the slot, so the new height (L) becomes 0.022 m. A total of 9 holes are required, each containing four slots for the secondary air to enter.

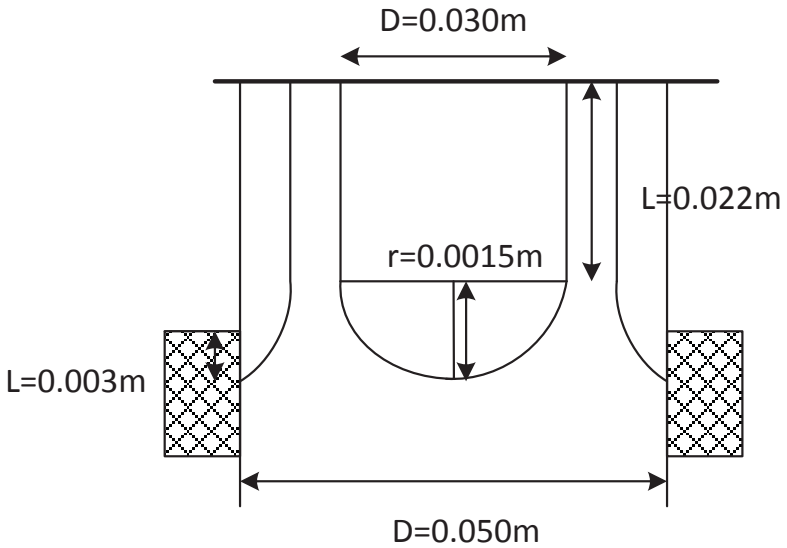

B.6 Determining Flow with no Frictional Pressure Losses

Flow is related to pressure losses due to friction. Flow through a pipe can be determined using Bernoulli's Equation for compressible flows, however, for this calculation, the pressure losses due to friction have been ignored to provide a quick rough estimation for the gas flow in the stack. Later, the pressure losses due to friction will be accounted for.

$$P_1 + \frac{1}{2}\rho {v_1}^2 + \rho g h_1 = P_2 + \frac{1}{2}\rho {v_2}^2 + \rho g h_2 + \Delta P_f \quad \text{(B.24)}$$

The assumptions are no frictional pressure losses, the potential energy of the air does not change over the height of the stack therefore, $h_1=h_2$ and the area of the stack is constant, $A_1=A_2$, therefore $u_1=u_2=u$.

Taking account of the above assumptions, Bernoulli's equation reduces to

$$(P_2 - P_1) = \frac{1}{2}\rho u^2 \quad \text{(B.25)}$$

The equation can then be rearranged and solved for velocity and then converted to a volumetric flow.

$$u = \sqrt{\frac{P_2 - P_1}{0.5\rho}} \quad \text{(B.26)}$$

B.7 Determining Flow with Frictional Pressure Losses

Frictional pressure losses can contribute to a significant energy loss in the system. These losses are due to the shear stress between the stack walls and the gas. The Reynolds number provides an indication for the type of flow in a pipe; laminar or turbulent. Fannings friction factor incorporates the Reynolds number and is used for situations where the flow is turbulent. The Fanning friction factor is used to determine the frictional loss in the head of the pipe. Other frictional losses that must be taken into account are as a result of restrictions in the pipe such as entrance and exit losses.

1. Determine the Reynolds Number

$$Re = \left(\frac{Du\rho}{\mu}\right) \quad \text{(B.27)}$$

2. Determine Fanning's Friction Factor

$$\frac{1}{\sqrt{f}} = -4log_{10}\left(\frac{\varepsilon}{D} + \left(\frac{7}{Re}\right)^{0.9}\right) \quad \text{(B.28)}$$

ε=0 for smooth pipes

$$f = \left(\frac{1}{-4log_{10}\left(\left(\frac{7}{Re}\right)^{0.9}\right)}\right)^2 \quad \text{(B.29)}$$

3. Determine the velocity with frictional pressure losses

Frictional Pressure Losses using Bernoulli's Equation

$$P_1 + \frac{1}{2}\rho {v_1}^2 + \rho g h_1 = P_2 + \frac{1}{2}\rho {v_2}^2 + \rho g h_2 + \Delta P_f \quad \text{(B.30)}$$

Assumptions:

1. The potential energy of the air does not change over the height of the stack therefore, $h_1=h_2$
2. The area of the pipe is constant, $A_1=A_2$, therefore $u_1=u_2=u$
3. The gas is incompressible

Taking account of the above assumptions, Bernoulli's equation reduces to

$$P_T = (P_2 - P_1) = \frac{1}{2}\rho u^2 + \Delta P_f \quad \text{(B.31)}$$

Frictional pressure loss using Fanning's friction factor for turbulent flow

$$-\Delta P_f = \left(\rho g h_f\right) \tag{B.32}$$

Where the head loss due to friction is given by the Darcy-Weisbach equation

$$h_f = 4f\frac{Lu^2}{D2g} \tag{B.33}$$

Where f is the Fanning friction factor of the pipe, L is the length of the stack (m), D is the diameter of the stack and u is the gas velocity in the stack (m s^{-1}).

Substituting in the head loss due to friction and writing the equation in terms of pressure loss gives

$$\Delta P_f = 2f\frac{L}{D}\rho u^2 \tag{B.34}$$

Substituting in ΔP_f yields and rearranging for total pressure losses

$$\Delta P_T = \frac{1}{2}\rho u^2 + \left(4f\frac{L}{D}\right)\frac{\rho u^2}{2} \tag{B.35}$$

Simplifying the above equation yields

$$\Delta P_T = \left(1 + 4f\frac{L}{D}\right)\frac{\rho u^2}{2} \tag{B.36}$$

Adding in entrance and exit losses to the flue the pressure drop can be written

$$\Delta P_T = \left(1 + 4f\frac{L}{D} + \sum k\right)\frac{\rho u^2}{2} \tag{B.37}$$

Where k refers to the sum of the restriction factors (velocity heads). The restriction factors comprise of exit losses (1 velocity head), entrance losses (0.5 velocity head) creating a total loss of 1.5 velocity heads (Sinnott, 2005).

Rearranging for velocity gives

$$u = \sqrt{\left(\frac{P_T}{\rho\left(1 + 2f\frac{L}{D} + \sum k\right)}\right)} \qquad \text{(B.38)}$$

Example calculation for air velocity including frictional losses

This example is based on a temperature of 100 °C and a flue diameter of 0.08m. Assume an initial velocity for the calculation.

$$Re = \left(\frac{Du\rho}{\mu}\right) = \left(\frac{Du}{\nu}\right) = \left(\frac{0.08 * 2.28}{0.0000231}\right) = 6834$$

Where ν = μ/ρ, kinematic viscosity ($m^2\ s^{-1}$)

$$f = \left(\frac{1}{-4log_{10}\left(\left(\frac{7}{Re}\right)^{0.9}\right)}\right)^2 = \left(\frac{1}{-4log_{10}\left(\left(\frac{7}{6834}\right)^{0.9}\right)}\right)^2 = 0.008$$

Enable the circular reference function on excel to calculate the actual velocity. If an error occurs then the initial velocity assumption needs to be changed to a more suitable value.

$$u = \sqrt{\left(\frac{P_T}{\rho\left(1 + 2f\frac{L}{D} + \sum k\right)}\right)} = \sqrt{\left(\frac{20}{0.943\left(1 + 2 * 0.008\frac{2.5}{0.08} + 1.5\right)}\right)} = 2.4\ m/s$$

Calculating the frictional pressure loss

$$-\Delta P_f = 4f\frac{lV^2}{d2}\rho = 4 * 0.008\frac{2.5 * 2.4^2}{0.08 * 2}0.943 = 3.3\ Pa$$

The above calculation for pressure loss due to friction shows that the pressure losses do impact on the secondary air flow rate. The table below summarises the effect of increasing temperature on air flow rate and pressure losses.

Table 14.3: The effect of flue temperature on the secondary air flow rate

θ_{flue} (°C)	ρ_{dryair} (kg/m^3)	Secondary Air Intake (L s^{-1})	ΔP_f (Pa)
0	1.290	11.44	0.0
100	0.943	13.27	3.3
200	0.740	14.87	3.5
300	0.610	16.28	3.7
400	0.520	17.53	3.9
500	0.455	18.65	4.0
600	0.400	19.71	4.2
700	0.360	20.76	4.3

Table 14.3 shows that as the flue temperature increases, the secondary air flow rate increases. In terms of heat loss this means more heat is required to heat the air with higher flow rates.

B.8 Heat Required to Warm 2° Air

Energy is required to heat up the air entering at the base of the combustion chamber. The stoichiometric ratio enables the amount of oxygen required to combust the propane. Subsequently, the secondary air flow rate can be determined by the difference between the updraft flow and the flow from the primary air with the propane.

1. Determine the stoichiometric ratios for the combustion of propane; refer to equation (B.4).

2. Determine the flow rate of pyrolysis gases and secondary air

Firstly, calculate the mass flow rate of propane

$$\dot{m}_{propane} = \frac{Heat\ Input}{Calorific\ Value\ Propane}[=]\frac{\frac{kJ}{s}}{\frac{kJ}{kg}}[=]\frac{kg}{s} \qquad \text{(B.39)}$$

Convert to molar flow rate

$$\dot{V}_{M\ Propane} = \frac{Q_{propane}}{M_{Propane}} = \frac{\frac{kg}{s}}{\frac{g}{mol}} * 1000\frac{g}{kg} = \frac{mol}{s} \quad \text{(B.40)}$$

Calculate the mass flow rate of air assuming 20 % excess oxygen is required for complete combustion

$$\dot{m}_{air} = \dot{V}_{M,propane} * \frac{n_{oxygen}M_{oxygen}}{1000} * \frac{\lambda}{0.208}[=]\frac{mol}{s}mol\frac{g}{mol}\frac{kg}{1000g}\frac{1}{mol}[=]\frac{kg}{s} \quad \text{(B.41)}$$

Converting to molar flow rate

$$\dot{V}_{M\ Air} = \frac{\dot{m}_{air}}{M_{air}} = \frac{\frac{kg}{s}}{\frac{g}{mol}} * 1000\frac{g}{kg} = \frac{mol}{s} \quad \text{(B.42)}$$

Determine the molar flow rate of gas production using the stoichiometric ratio. For every mole of propane combusted, 7 moles of gas ($3CO_2$ and $4H_2O$) are produced

$$\dot{V}_{M\ Gas\ Produced} = \dot{V}_{M\ Propane} * 7 = \frac{mol}{s} \quad \text{(B.43)}$$

Calculating total molar flow rate of gases and air

$$\dot{V}_{M\ Total} = \left(7 + 1 + \frac{5}{0.208} + \frac{1}{0.208}\right)\dot{V}_{M\ Propane} = \frac{mol}{s} \quad \text{(B.44)}$$

Converting to volumetric flow rate using the molar volume of an ideal gas at 1 atmosphere of pressure, 22.4 L mol^{-1}

$$\dot{V}_{Total} = \dot{V}_{M\ Total} * \dot{V}_{M\ Air} = \frac{mol}{s} * \frac{22.4L}{mol} = \frac{L}{s} \quad \text{(B.45)}$$

The flow rate of the secondary air can be calculated by subtracting the updraft flow from the flow rate of the combustion gases and air.

$$\dot{V}_{2^\circ air} = \dot{V}_{air} - \dot{V}_{Total} \quad \text{(B.46)}$$

3. Calculate the energy required to heat up the secondary. The energy required is a function of temperature.

$$\frac{\dot{V}_{air}}{V_{M\ air}} M_{air} * C_{p\ air} * (T_2 - T_a)[=] \frac{\frac{L}{s}}{\frac{L}{mol}} * \frac{kg}{mol} * \frac{J}{kgK} * K[=]W \quad \text{(B.47)}$$

B.9 Tertiary Air Requirements

Tertiary air may be required to assist with creating the draft during start up and also to provide additional air when pyrolysis gases are being generated. In order to calculate the tertiary air requirements, the primary air velocity (entering with the burner) and the secondary air velocity (entering through the open holes in the base of the combustion chamber) must be determined. Then mass and energy balances are applied over two points (the top of the flue where the tertiary air enters, and the base of the flue) to determine the tertiary air required.

1. Calculate the primary air velocity which enters with the burner

As mass is conserved, the flue gas flow originating from the primary air and LPG will be the sum of these two flows (kg s^{-1}). Firstly, the mass flow rate of the propane was determined by the heat input, either 6 kW heat input (6 kJ s^{-1}) or 23 kW heat input (23 kJ s^{-1}) divided by the calorific value of propane (42300 kJ kg^{-1}).

$$\dot{m} = \frac{Heat\ Input}{Calorific\ Value} \quad \text{(B.48)}$$

Assuming 20% excess oxygen is required to ensure complete combustion, the velocity can be calculated by

$$u = \frac{\dot{m}}{A_{flue}\rho} \quad \text{(B.49)}$$

2. Calculate the secondary air flow rate

The secondary air enters through the holes in the bottom of the combustion zone. These holes mean the combustion zone is open to the atmosphere. A buoyancy force, F_B, arises due to the density differences between the mixture gas in the stack and the ambient surrounding air. For a column of hot gases of height, L_s (stack height), the buoyancy force is the volume x density difference x gravitational acceleration (m^3 x kg m^{-3} x m s^{-2} = N). Given that it is the 1° + 2° air that rises over most of the pyrolyser and stack height (the tertiary air only enters near the top), the buoyancy force is given by

$$F_B = AL_s(\rho_{1°+2°} - \rho_{amb})g \tag{B.50}$$

Force is related to pressure by $F_B = A\Delta P_B$ and so

$$\Delta P_B = L_s(\rho_{1°+2°} - \rho_{amb})g \tag{B.51}$$

Both the impulse force and the buoyancy force act upwards in the same direction and so are additive. Therefore the total driving force is $\Delta P = \Delta P_I + \Delta P_B$ and the total driving pressure is

$$\Delta P = \Delta P_I + \Delta P_B = \frac{\dot{m}_{mix}u_{mix} - \left((\dot{m}_{1°} + \dot{m}_{2°})u_{1°+2°} + \dot{m}_{3°}u_{3°}\right)}{A} + L_s(\rho_{1°+2} - \rho_{amb})g \tag{B.52}$$

Energy is conserved in this system, meaning that the sum of the stored energy (via pressure), kinetic energy (via velocity), potential energy (via height as affect by gravity) and heat energy (due to friction) is conserved between the inputs and outputs of the system. The energy may convert between these forms. The word balance below describes the energy balance over the system.

$$\Delta pressure\ energy + \Delta kinetic\ energy + \Delta potential\ energy + \Delta heat = 0 \tag{B.53}$$

Frictional losses are proportional to the velocity squared and conventionally losses are expressed in terms of kinetic energy density. For gases, the change in potential energy is usually ignored; therefore the above word balance is converted and simplified to the following equation

$$\Delta P + \frac{1}{2}\rho u^2(1 + \xi_{1°+2°}) = 0 \tag{B.54}$$

This balance needs to be applied over two points in the system. Point (a) is defined as the tertiary air inlet, which is located at the top of the stack. Point (b) is defined at the base of the stack, and is imagined to be outside the system, i.e., $u_b = 0$. (This imagines the scenario of the combustion gases entering the stack from a hot cavernous chamber where the velocity is essentially zero, which is clearly untrue, but is reasonably accurate with respect to losses because few are attributable). If negligible temperature loss is assumed over the stack height, the densities are essentially the same and the velocity differences relate only to the change in flow area of the stack, $A_a u_a = A_b u_{1°+2°}$, because at a the flow is in an annular region around the tertiary air inlet. Keeping with the above definition of velocity, $u_a = (A_b/A_a)\, u_{1°+2°}$, the energy balance becomes

$$\Delta P = P_a - P_b = \frac{1}{2}\rho_{1°+2°}{u^2}_{1°+2°}\left(\frac{A_b}{A_a}\right)^2 + \sum \xi_{1°+2°}\left(\frac{1}{2}\rho_{1°+2°}{u^2}_{1°+2°}\right) \qquad \text{(B.55)}$$

The system can now be solved by equating the right hand sides of equations A.58 and A.55. In the simple case where no tertiary air is used, the equation becomes

$$\Delta P = L_s(\rho_{1°+2°} - \rho_{amb})g - \frac{1}{2}\rho_{1°+2°}{u^2}_{1°+2°}\left(\left(\frac{A_{stack}}{A_{3°\,Inlet}}\right)^2 + \sum \xi_{1°+2°}\right) \qquad \text{(B.56)}$$

Where

- ρ_{amb} = Average flue gas density (kg m^{-3})
- ΔP = The draft (mm H_2O)
- L_s = Stack height (m)
- $\rho_{1°+2°°}$ = Average flue gas density (kg m^{-3})
- $u_{1°+2°}$= Average flue gas velocity (m s^{-1})
- A_{stack}=Area of the flue
- $A_{3°\,Inlet}$=Area of the tertiary air inlet
- $\xi_{1°+2°}$=Total losses

Rearranging for velocity

$$u = \sqrt{\frac{L_s(\rho_{1°+2°} - \rho_{amb})g}{0.5 * \rho_{1°+2°} * \left(\left(\frac{A_{stack}}{A_{3°\,Inlet}}\right)^2 + \sum \xi_{1°+2°}\right)}} \qquad \text{(B.57)}$$

3. Calculate the tertiary air flow rate required when there is no natural draft

The tertiary air (3°) is injected through a venturi near the top of the stack supplied by an externally mounted centrifugal fan.

This calculation represents the situation where the process is either starting up or shutting down and the natural draft has not yet been established, so $\dot{m}_{2^\circ} = 0 \; and \; u_{2^\circ} = 0.$ The ambient temperature and the internal temperature are equal and hence there is no natural draft so the draft equation in the RHS of the equation goes to 0.

The full equation for the total driving pressure, ΔP, is the pressure difference induced by the impulse force caused by momentum transfer plus the pressure difference due to the buoyancy force as stated earlier in equation A.55

$$-\Delta P = -\frac{\dot{m}_{mix}u_{mix} - \left((\dot{m}_{1^\circ} + \dot{m}_{2^\circ})u_{1^\circ+2^\circ} + \dot{m}_{3^\circ}u_{3^\circ}\right)}{A_{flue}} - L_s(\rho_{1^\circ+2^\circ} - \rho_{amb})g \qquad \text{(B.58)}$$

$\dot{m}_{mix}$ is the sum of the mass flow rates from the primary, secondary and tertiary air. The mixture velocity, u_{mix}, is the sum of the mass flow rates divided by the density of the mixture gas

$$\dot{m}_{mix} = \dot{m}_{1^\circ} + \dot{m}_{2^\circ} + \dot{m}_{3^\circ} \qquad \text{(B.59)}$$

$$u_{mix} = \frac{\dot{m}_{1^\circ} + \dot{m}_{2^\circ} + \dot{m}_{3^\circ}}{\rho_{mix}} \qquad \text{(B.60)}$$

Substituting in $\dot{m}_{mix} \; and \; u_{mix}$ and setting $\dot{m}_{2^\circ} = 0 \; and \; u_{2^\circ} = 0$ yields

$$-\Delta P = -\frac{(\dot{m}_{1^\circ} + \dot{m}_{3^\circ})\left(\frac{\dot{m}_{1^\circ} + \dot{m}_{3^\circ}}{\rho_{mix}}\right) + \left((\dot{m}_{1^\circ})u_{1^\circ} + \dot{m}_{3^\circ}u_{3^\circ}\right)}{A_{flue}} \qquad \text{(B.61)}$$

Substituting in the tertiary air mass flow rate so there is only one unknown variable gives

$$\dot{m}_{3^\circ} = A_{3^\circ}u_{3^\circ}\rho_{3^\circ} \qquad \text{(B.62)}$$

The equation can now be solved for the tertiary air velocity

$$-\Delta P = -\frac{(\dot{m}_{1^\circ} + A_{3^\circ}u_{3^\circ}\rho_{3^\circ})\left(\frac{\dot{m}_{1^\circ} + A_{3^\circ}u_{3^\circ}\rho_{3^\circ}}{\rho_{mix}}\right) + \left((\dot{m}_{1^\circ})u_{1^\circ} + A_{3^\circ}u_{3^\circ}\rho_{3^\circ}u_{3^\circ}\right)}{A_{flue}} \quad \text{(B.63)}$$

Calculate the pressure head to check it is a reasonable value

$$h = \frac{P}{\rho_{water}g} * \frac{m}{1000\ mm}\ [=]\ \frac{\frac{kg}{ms^2}}{\frac{kg}{m^3} * \frac{m}{s^2}} * \frac{m}{1000\ mm} = mm\ H_20 \quad \text{(B.64)}$$

4. Use literature to estimate water vapour and gas flow rates

Fantozzi et al. (2007) reports that the peak production of gas and tar volatiles is 0.057 kg/s or 57 g/s.

5. Estimate the secondary air required to combust the pyrolysis gases

$$\dot{m}_{2^\circ\ air} = \dot{m}_{pyrogas} * \frac{20\%\ excess\ air}{21\%\ oxyen\ in\ air} \quad \text{(B.65)}$$

6. Estimate the total primary gases, evolved gases and the secondary air required to be drawn upward either by natural draft or by natural draft plus induced tertiary air

$$\Delta P = -\frac{1}{2}\rho u^2\left(1 + \sum losses\right) \quad \text{(B.66)}$$

7. Determine the volumetric fan flow rate required

$$Q_{fan} = u_{3^\circ}A_{3^\circ}\rho_{air}\ [=]\ \frac{m}{s} * m^2 * \frac{kg}{m^3} * \frac{L}{kg} = \frac{L}{s} \quad \text{(B.67)}$$

B.10 Radiation Heat Losses from the Reactor Surfaces

Radiation can be a major form of heat loss. In our system, radiation losses can occur from the reactor surfaces (lid, base and sides) or through the secondary air holes at the base of the combustion chamber.

Calculate the radiation heat transfer coefficient assuming the surface of the unit assuming the surface of the unit is at 100 °C. In order to reduce the insulation thickness and overall reactor size, a surface 100 °C was selected.

$$h_{rad} = \sigma\varepsilon\left({T_{surf}}^2 + {T_{surr}}^2\right)\left(T_{surf} + T_{surr}\right) \quad \text{(B.68)}$$

$$\varphi_{rad} = h_{rad} A_{surf}\left(T_{surf} - T_{surr}\right)$$

Example calculation for the radiation heat transfer coefficient for a surface temperature of 50 °C.

$$h_{rad} = 5.67 * 10^{-8} * 0.23 * (323.15^2 + 283.15^2) + (323.15 + 283.15)$$
$$= 1.46 \ \frac{W}{m^2 K}$$

Table 14.4: Radiation heat losses from the reactor sides

T_{surf} (°C)	h_{rad} (W/m^{2}K)	Q_{rad} (W)
50	1.46	191.14
100	1.88	553.32
150	2.39	1094.37
200	3.00	1865.29

The heat losses due to radiation become more significant as the surface temperature of the reactor increases. It is therefore critical that the system is insulated to minimise the surface losses.

B.11 Radiation Heat Losses through the 2° Air Holes

The 2° air is drawn in through open holes in the base of the combustion chamber and then flows out of the flue by natural system draft. The heat is supplied in the combustion section and hence the holes in the base create an area for heat losses to occur. The following assumptions have been made to calculate the heat losses through the 2° air holes:

i. The 6 kW and 23 kW of heat from the burner is all emitted as radiant energy
ii. The amount received by the hole area is proportional to the view area of the flame
iii. Conservatively that the flame only sees the bottom of the unit, not the radiation plate underneath the internal chamber

The total hole area was determined in section A.5. The total base area was determined so the radiant energy leaving through the holes could be calculated.

$$Q_{rad} = \frac{Total\ Hole\ Area}{Total\ Base\ Area} * Heat\ Input \quad \text{(B.69)}$$

$$Q_{rad} = \frac{0.017}{0.500} * 23 = 0.78kW$$

The radiant energy through the holes indicates it is important to install radiation shields above the holes to minimise the heat loss.

B.12 Convection Heat Losses

Convection heat losses can occur from the top of the reactor, the side of the reactor, the base of the combustion chamber and the walls of the combustion chamber.

Losses due to convection can be determined by a variety of methods. The first method uses literature values for natural convection of air. Method 2 uses a standardised method for a vertical surface. Method 3 is another standardised method which employs the nusselt number and method 4 takes into account the effect of wind.

These methods are all calculated for heat losses from the top of the reactor with an area of 0.789 m^2, a surface temperature of 50 °C, an ambient temperature of 10 °C and a radiation coefficient of 1.46 W m^{-2} K^{-1}.

Method 1

1. Determine a suitable natural heat transfer coefficient from literature

A typical natural convection heat transfer coefficient range is reported to be 2-25 W m^{-2} K^{-1} (ASHRAE, 2009). A conservative value was chosen for method 1 with h_c=25 W m^{-2} K^{-1}

Determine the overall heat transfer coefficient

$$U = h_{rad} + h_c = 1.46 + 25 = 26.46\ W/(m^2K) \quad \text{(B.70)}$$

2. Calculate the heat loss

$$\varphi = UA\left(T_{surface} - T_{ambient}\right) \quad \text{(B.71)}$$

Example calculation for convection heat losses from the side of the cylindrical reactor

From literature the maximum value for the convective heat transfer for natural convection was chosen

$$h_c = 25\frac{W}{m^2K}$$

The area was determined by

$$A = \pi\frac{d^2{}_{insulated\ reactor}}{4} = \pi\frac{1.004^2}{4} = 0.789\ m^2 \quad \text{(B.72)}$$

Heat loss due to convection

$$\varphi = UA\left(T_{surf} - T_a\right) = 26.46 * 0.789 * (323.15 - 283.15) = 0.83\ kW \quad \text{(B.73)}$$

Method 2

Calculate the convective heat transfer coefficient using a standardised method (*ASHRAE Handbook - Fundamentals (SI Edition)*, 2009). This method employs a simplified calculation for a vertical surface and is dependent on the Rayleighs number.

$$Ra = \frac{g\beta\left(T_{surf} - T_{surr}\right)L^3}{\nu\alpha} \quad \text{(B.74)}$$

Where g is gravity ($m\ s^{-2}$), β is the inverse of temperature (K^{-1}), T_{surf} is the surface temperature (K), L is the reactor height (m), ν is the kinematic viscosity ($m^2\ s^{-1}$), and α is equal to $\lambda/(\rho C_p)$.

Example calculation for $T_{surface}$=50 °C

$$Ra = \frac{g\beta\left(T_{surf} - T_a\right)L^3}{\nu\alpha} = \frac{9.81 * 0.00309(323.15 - 283.15)1.3^3}{0.0000178 * 0.00003} = 5.29E + 09$$

$$h_c = 1.26(323.15 - 283.15)^{1/3} = 4.3\ W/(m^2K)$$

$$U = h_{rad} + h_c = 1.46 + 4.3 = 5.76\ W/(m^2K)$$

$$\varphi = UA\left(T_{surf} - T_a\right) = 5.76 * 0.789 * (323.15 - 283.15) = 0.18\ kW$$

Method 3

1. Calculate the convective heat transfer coefficient using a standardised method (Welty, 1978) where the heat transfer coefficient, h_c, is a function of the Nusselt number, Nu. k is the thermal conductivity and L_T is the length of the reactor plus the base

$$h_c = \frac{Nu * k}{L_T} \quad \text{(B.75)}$$

Where the Nusselt number is approximated for a vertical wall

$$Nu = 0.021(GrPr)^{0.4}\ for\ GrPr > 10^9$$

Example

$$Gr_L = \frac{gL^3\left(T_{surf} - T_{surr}\right)/(T_{surr})}{\nu^2} = \frac{9.81 * 1.3^3(323.15 - 283.15)/(283.15)}{0.0000178^2}$$
$$= 9.6E + 09$$

Where the Prandtl number is

$$Pr = 0.703$$

$$GrPr = 0.703 * 9.6E + 09 = 6.8E + 09$$

Calculating the Nusselt number

$$Nu = 0.021(6.8E + 09)^{0.4} = 180$$

Determine the heat transfer coefficient using the Nusselt number from above

$$h_c = \frac{Nu * k}{h} = \frac{180 * 0.028}{1.3} = 3.87\ W/(m^2K)$$

Calculate the overall heat transfer coefficient

$$U = h_{rad} + h_c = 1.5 + 3.9 = 5.4\ kW$$

Calculate the heat loss

$$\varphi = UA\left(T_{surf} - T_a\right) = 5.4 * 0.789 * (323.15 - 283.15) = 0.17\ kW$$

Method 4 Heat transfer due to wind

Calculate heat transfer calculation, where h is not dependent on the Re number

$$h = \frac{(3.76 - 0.00497 * T_a)V^{0.8}}{D^{0.2}} \qquad \text{(B.76)}$$

Where T_a is the ambient temperature (°C), V is the wind velocity (m s^{-1}), D is the diameter of lagged pyrolyser (m).

Example

A velocity of 9 m s^{-1} or 32 km h^{-1} was chosen as an estimate to calculate the heat transfer coefficient. The velocity was based on an estimate of windy day in Palmerston North. The diameter of the lagged pyrolyser was 0.91 m.

$$h_1 = \frac{(3.76 - 0.00497 * 20)9^{0.8}}{0.91^{0.2}} = 21.6 \frac{W}{m^2 K}$$

$$U = h_{rad} + h_c = 1.5 + 21.6 = 23.1\ W/(m^2 K)$$

$$\varphi = UA\left(T_{surf} - T_a\right) = 23.1 * 0.789 * (323.15 - 283.15) = 0.72\ kW$$

Summary of methods

Method 1 $\varphi = 0.83$ kW

Method 2 $\varphi = 0.18$ kW

Method 3 $\varphi = 0.17$ kW

Method 4 $\varphi = 0.72$ kW

Method 4 was the preferred method because it was the most conservative of the three calculated values and takes into account wind as a factor. It tells is that 25 W m^{-2} K^{-1} is a good design heat transfer coefficient on a windy day at 32 km h^{-1}.

B.13 Conduction Heat Losses through the Base of the Combustion Chamber

The base of the combustion chamber is lined with a fire resistant brick. For this calculation, it is assumed that it has the properties of diatomaceous brick.

1. Determine the area of the base of the combustion chamber

$$A = \frac{\pi d^2}{4} \quad \text{(B.77)}$$

Where d is the inner diameter of the outer annulus (m)

2. Determine the heat loss through the base of the combustion chamber

$$\varphi = \frac{kA}{L}\left(T_{Chamber} - T_{Surface}\right) \quad \text{(B.78)}$$

Where k is the thermal conductivity of diatomaceous earth brick (W m^{-1} K^{-1}), A is the base area of the combustion chamber (m^2) and L is the thickness of the insulated material (m)

Example for conduction from the base of the combustion chamber

$$A = \frac{\pi d^2}{4} = \frac{\pi 0.85^2}{4} = 0.57 m^2 \quad \text{(B.79)}$$

$$\varphi = \frac{kA}{L}\left(T_{Chamber} - T_{Surface}\right) = \frac{0.065 * 0.57}{0.05}(700 - 50) = 0.48\ kW \quad \text{(B.80)}$$

B.14 Conduction Heat Losses through the Insulated Lid of the Reactor

1. Determine the area of the lid of the combustion chamber

$$A = \frac{\pi d^2}{4} \quad \text{(B.81)}$$

Where d = inner diameter of the outer annulus

2. Determine the heat loss through the lid of the reactor

$$\varphi = \frac{kA}{L}\left(T_{Chamber} - T_{Surface}\right) \quad \text{(B.82)}$$

Example for conduction through the lid of the reactor

$$A = \frac{\pi d^2}{4} = \frac{\pi 0.85^2}{4} = 0.57 m^2$$

$$\varphi = \frac{kA}{L}\left(T_{Chamber} - T_{Surface}\right) = \frac{0.065 * 0.650}{0.05}(700 - 50) = 0.47\ kW$$

B.15 Conduction Heat Losses through the Insulated Sides of the Reactor and the Combustion Chamber

1. Calculate heat loss through the wall of a cylinder

$$\varphi = 2k\pi L \frac{\left(T_{Chamber} - T_{Surface}\right)}{\ln\left(\frac{r_2}{r_1}\right)} \quad \text{(B.83)}$$

Where k is the thermal conductivity of superwool PLUS (W m^{-1} K^{-1}), L is the height of the reactor wall (m), r_2 is the radius of the outer reactor with insulation (m) and r_1 is the radius of the outer reactor with no insulation (m).

Example Calculation for heat loss through the cylindrical wall of the main chamber

The equation below assumes a lagging thickness of 0.05 m and a surface temperature of 50 °C

$$\varphi = 2k\pi L \frac{\left(T_{Chamber} - T_{Surface}\right)}{\ln\left(\frac{r_2}{r_1}\right)} = 2 * 0.055 * \pi * 1.04 * \frac{700 - 50}{\ln\left(\frac{0.555}{0.455}\right)} = 0.65\ kW$$

Table 14.5: Summary of conduction heat losses from the reactor for a lagging thickness of 0.1m

T_{surf} (°C)	Sides (kW)	Top (kW)	Side of combustion chamber (kW)	Base of combustion chamber (kW)	Total Heat Loss (kW)
50	1.05	0.18	0.30	0.42	1.95
100	1.0	0.17	0.28	0.39	1.80
150	0.9	0.15	0.26	0.36	1.65
200	0.7	0.14	0.23	0.32	1.42

In summary, the heat loss by conduction is limited, not by convection. The heat loss is greater from the sides of the reactor due to the larger surface area.

A lagging thickness of 0.1 m was required to reduce the heat losses from the reactor.

B.16 Explosion Vent

As discussed in section 5.2.11, during the pyrolysis process, an aerosol and soot cloud may form. The high surface area of such a cloud may absorb all the available oxygen and snuff out combustion resulting in a build-up of fuel.

Even though the natural draft is drawing this cloud upward and away from the combustion zone, if the rate of cloud formation is high, then there will be an accumulation of combustible energy. This is unlikely to occur because a number of ignition sources are present.

Below are the design calculations for an explosion vent.

Table 14.6: Summary of system inputs for explosion vent design

Symbol	Description	Range	Value	Units
V	Volume of the vessel		0.435	m^3
L/D	Length to diameter ratio of the vessel	0-3	1.333	m
$P_{red,max}$	Max reduced explosion overpressure	0.1<2	1	bar
P_{max}	Max explosion overpressure	7-10	10	bar
A_{vent}	Vent area, without vent duct			m^2
K_{max}	Explosion constant of the fuel	10-300	300	bar m s^{-1}
P_{stat}	Static activation overpressure of rupture disk	<=0.1	0.09	bar
K_{st}	Deflagration index for activated carbon		44	bar m s^{-1}
L_D	Length of vent duct			m
$P'_{red,max}$	Max explosion overpressure with vent duct			bar

The maximum reduced explosion over pressure without a vent duct is estimated between 0.1-2 bar. A value of 1 bar was estimated for subsequent calculations. The vent area can be sized according to the values found in the summary table.

This equation is valid for a **flammable gas-air mixture** with the following conditions as stated in Green and Perry (2008):

- Vessel volumes 0.1 $m^3 \leq V \leq$ 1000 m^3
- Vessel length to diameter ratio of 1 $\leq L/D \leq$ 5
- Static activation overpressure of rupture disk 0.1 bar ≤ P_{stat} ≤ 0.1 bar
- Maximum reduced explosion overpressure 0.1 bar ≤ $P_{red,max}$ ≤ 2 bar
- $P_{red,max} \geq P_{stat}$ + 0.05 bar
- Maximum explosion constant 50 bar m $s^{-1} \leq K_{max} \leq$ 550 bar m s^{-1}
- Gas-air mixtures ignited at zero turbulence
- Venting efficiency EF=1
- For equipment located outside

$$A_{vent} = \left[(0.1265 log K_{max} - 0.0567) {P_{Red\ max}}^{-0.5817} + 0.1754 {P_{Red\ max}}^{-0.5722} (P_{stat} - 0.1)\right] V^{2/3} + \frac{\left[AK_{max}\left(\frac{L}{D} - 2\right)^2\right]}{750} \quad \text{(B.84)}$$

$$\begin{aligned} A_{vent} &= [(0.1265 \log(400) - 0.0567)(1)^{-0.5817} \\ &\quad + 0.1754(1)^{-0.5722}(0.09 - 0.1)]V^{2/3} + \frac{[A(400)(1.33 - 2)^2]}{750} \\ &= 0.17\ m^2 \end{aligned} \quad \text{(B.85)}$$

If the reactor is to be located inside, vent ducts should be used which will increase the pressure development in the equipment during venting.

B.17 Exothermic Runaway

An exothermic runaway can potentially occur if the heat from the gases produced is greater than the heat loss.

1. Determine the secondary air flow rate

The secondary air velocity was determined using bernoullis equation which included frictional pressure losses, as discussed in section A.8. Subtracting the primary air velocity and the LPG velocity yielded the maximum amount of secondary air available to combust the pyrolysis gases. The induced draft is a function of the temperature of the rising gases.

2. Convert the secondary air flow rate to oxygen flow rate

Air is composed of 21% in volume of oxygen, therefore

$$Q_{air} * 0.21 = Q_{oxygen}$$

Converting to the molar flow rate

$$Q_{oxygen} * V_{m\ oxygen} [=] \frac{L}{s} * \frac{mol}{L} [=] \frac{mol}{s}$$

Table 14.7: Oxygen flow rate as a function of temperature for the 6 kW and 23 kW burners

T	Q oxygen (mol s^{-1})	Q oxygen (mol s^{-1})
°C	6 KW	23 KW
100	0.1017	0.0373
200	0.1167	0.0524
300	0.1299	0.0655
400	0.1416	0.0773
500	0.1521	0.0877
600	0.1629	0.0985
700	0.1719	0.1076

Determine the amount of pyrolysis gases that can be combusted with the oxygen available based on the stoichiometric ratio. The composition of pyrolysis gases and tar is shown in tables 12.2 and 12.3 respectively. Using Fantozzi et. al (2007), the ratio of tar to gas at peak production is approximately 2.5:1 with a total flow calculated for this system of 0.073 kg s^{-1}.

Table 14.8: Pyrolysis Gas Composition

Components	Formula	Volume %	Moles of O_2 required per mole of substance	L s^{-1}
Carbon dioxide	CO_2	36.5	0.5	2.87
Ethylene	C_2H_4	0.4	3	0.19
Ethane	C_2H_6	1.2	3.5	0.66
Propylene	C_3H_6	0.3	4.5	0.21
Propane	C_3H_8	0.2	5	0.16
Hydrogen	H_2	11.7	0.5	0.92
Methane	CH_4	19.8	2	6.22
Carbon monoxide	CO	29.9	0.5	2.35

Table 14.9: Tar Composition

Components	Formula	Wt %	Moles of O_2 required per mole of substance	L/s
Water	H_20	0.4	0.5	13.19
Acetic acid	$C_2H_4O_2$	0.3	2	11.87
Formic acid	CH_2O_2	0.1	0.5	1.29
Phenol	C_6H_5OH	0.2	7	17.68

Minimum oxygen requirements is based on the combustion of each component which is then summed. The combustion of carbon monoxide and ethane for example is below

$$2CO + O_2 \rightarrow 2CO_2 \quad \text{(B.86)}$$

$$2C_2H_6 + 7O_2 \rightarrow 4CO_2 + 6H_2O \quad \text{(B.87)}$$

Using the mole fractions of each component, the full equation is

$$\frac{1}{2}(CO + H_2) + 2CH_4 + 3C_2H_4 + 3.5C_2H_4 + 3.5C_2H_6 + 4.5C_3H_6 + 5C_3H_8 \quad \text{(B.88)}$$

Determine the total mass flow of the pyrolysis gases and tar for each component based on the peak flows estimated by Fantozzi et al., 2007.

$$\frac{kg}{s} = mass\ \% * \frac{Q_{pyro}}{Q_{total}} * Q_{total} \quad \text{(B.89)}$$

Converting to moles of component in total flow

$$\frac{mol}{s} = \frac{\frac{kg}{s} * \frac{1000g}{kg}}{\frac{g}{mol}}$$

Using the moles of oxygen gas required per mole of substance to convert the above to moles of oxygen required per second

$$moles\ of\ oxygen\ gas\ required\ per\ second$$
$$= moles\ of\ component\ in\ total\ flow$$
$$* moles\ of\ oxygen\ gas\ required\ per\ mole\ of\ substance$$

Converting to volumetric flow rate using the molar volume of air, 22.4 L/mol at standard temperature and pressure

$$\frac{mol}{s} * \frac{L}{mol} = \frac{L}{s}$$

The total heat losses have been calculated earlier and are summaried in the table below.

Heat Loss from 6KW burner (kW)	Heat Loss from the 23 kW burner (kW)	Heat Loss from 6KW burner (kg/s)	Heat Loss from the 23 kW burner (kg/s)
5.63	6.21	0.00012	0.00013
11.89	12.47	0.00026	0.00027

B.18 Thermal Expansion

Thermal expansion is an important consideration when dealing with high temperatures. Stainless steel and mild steel are both used in the pyrolysis reactor design. As the metal heats up, a change in volume occurs, which is known as thermal expansion. Table x below shows the expansion coefficient for the two types of metal.

Table 14.10: Expansion coefficients for mild steel and stainless steel

Steel Type	Expansion coefficient x 10^{-6}
Mild Steel	13
Steel Stainless Austenitic (304)	17.3

The maximum temperature was assumed to be 600 °C for the subsequent calculations using Equation B.90 below.

$$Thermal\ expansion = Length * expansion\ coefficient * temperature \quad \text{(B.90)}$$

Table 14.11: Summary of expansion from different reactor components

Measurement	Value (mm)	Expansion SS304 (mm)
Lid Diameter	750	7.79
Reactor Height	1000	10.38
Height of Lip on inner lid	30	0.31
Circumference of inner reactor	2356	24.46

The results from Table 14.11 show the most significant expansion occurs from the inner reactor wall (circumference). However, this has the largest amount of stainless steel. The lid can expand up to 7.8 mm in the horizontal direction and up to 10.4 mm in the vertical direction. This movement, or warping at higher temperatures potentially creates gaps for gases to escape out of the lid.

APPENDIX C
EXPERIMENTAL RAW DATA

Table 14.12: Experimental Results

Run #	Tset (°C)	Stock size	Dry / Wet	Grain / A.Grain	No. of Samples	Tmax (°C)	Run time (min)	Average holding temperature (°C)	Holding time (min)
1	300	Small	Dry	Grain	6	356.3	41.5	–	–
2	300	Medium	Dry	Grain	3	415.5	41.9	–	–
13	300	Large	Dry	Grain	1	392.8	19.6	388.2	2.1
16	300	Large	Dry	Grain	1	402.3	40.9	393.1	20.7
25	300	Large	Dry	Grain	1	483.9	102.5	–	–
35[1]	300	Medium	Wet	Grain	3	280.3[2]	157.7[2]	–	–
1	300	Small	Dry	A. Grain	6	356.3	41.5	–	–
4	300	Medium	Dry	A. Grain	3	382.5	35	–	–
37	300	Medium	Dry	A. Grain	3	325.1	71.7	304	23.6
10	300	Large	Dry	A. Grain	1	410.8	57.1	–	–
38	300	Large	Dry	A. Grain	1	350.2	76.5	304.5	58.6
17	300	Large	Dry	A. Grain	1	413.5	33.5	377.4	19.9
36	300	Large	Wet	A. Grain	1	420	130	–	–
24	300	Large	Wet	A. Grain	1	423.5	84.5	396	61
5	500	Small	Dry	Grain	6	552.1	24.1	533.8	5.5
14	500	Medium	Dry	Grain	3	522.8	22.6	517.8	5.3
29	500	Large	Dry	Grain	1	556.2	48.2	523.5	26.4
27	500	Large	Dry	Grain	1	606.4	42.3	–	–
18	500	Small	Wet	Grain	6	439.5	71.7	409.4	54.9
21	500	Medium	Wet	Grain	3	519.7	62.7	510.9	30.2
31	500	Large	Wet	Grain	1	601	100.4	516.9	69.2
23	500	Large	Wet	Grain	1	527.8	77.5	504.5	43.1
5	500	Small	Dry	A. Grain	6	552.1	24.1	533.8	5.5
15	500	Medium	Dry	A. Grain	3	553.8	21.1	–	–
30	600	Medium	Dry	A. Grain	3	634.7	38.2	–	–
26	500	Large	Dry	A. Grain	1	540.7	39.1	502.4	11.8
28	500	Large	Dry	A. Grain	1	578.6	45.9	528.2	25.3
18	500	Small	Wet	A. Grain	6	439.5	71.7	409.4	54.9
20	500	Medium	Wet	A. Grain	3	513.8	31.7	507.7	3
32	500	Medium	Wet	A. Grain	3	579.6	65.8	521.3	32.5
22	500	Large	Wet	A. Grain	1	533.8	37.2	–	–

3	700	Small	Dry	Grain	6	719.8	41.1	699.6	12.8
6	700	Medium	Dry	Grain	3	709	39.7	699.9	7.1
12	700	Large	Dry	Grain	1	709.9	34.7	697.1	5.7
9	700	Large	Dry	Grain	1	722.5	46.9	–	–
3	700	Small	Dry	A. Grain	6	719.8	41.1	699.6	12.8
11	700	Medium	Dry	A. Grain	3	713.4	51	697.3	11.6
7	700	Large	Dry	A. Grain	1	409	31	–	22.5
8	700	Large	Dry	A. Grain	1	714	37	–	–
19G	700	Small	Wet	Grain	6	611.2	24.2	–	–
33G	700	Small	Wet	Grain	6	738	47	707.07	16
34	600	Large	Wet	Grain	1	693.1	109.7	655.4	57.1
19AG	700	Small	Wet	A. Grain	6	611.2	24.2	–	–
33AG	700	Small	Wet	A. Grain	6	738	47	707.07	16

The highlighted yellow cells mean the wood was not pyrolysed well so analysis was not conducted on these runs.

The highlighted grey cells is when the data logger stopped working so this data was analysed but not all mass and energy balances could be completed with the missing data.

Table 14.13: Elemental Analysis Results

Sample	Weight (mg)	Nitrogen (wt%)	Total Carbon (wt%)	Hydrogen (wt%)	Sulphur (wt%)	Ash (wt%)	Total Oxygen (wt%)	HHV (kJ/kg)
1G	48.96	0.22	71.75	4.59	0.00	0.76	22.68	26732
1G	47.94	0.11	71.72	4.78	0.00	0.76	22.62	27001
1G	50.98	0.16	71.61	4.88	0.00	0.76	22.59	27110
2	52.55	0.27	76.81	3.46	0.00	1.02	18.44	27608
2	54.94	0.22	77.16	3.63	0.00	1.02	17.98	28034
2	53.83	0.13	76.72	3.71	0.00	1.02	18.42	27927
16	56.28	0.22	75.10	4.06	0.00	0.66	19.96	27597
16	49.80	0.21	74.96	3.92	0.00	0.66	20.25	27298
1AG	51.95	0.20	72.46	4.73	0.00	–	22.61	27177
1AG	50.93	0.16	72.40	4.51	0.17	–	22.94	26787
1AG	52.42	0.09	72.22	4.66	0.00	–	23.03	26924
4	28.62	0.24	76.63	3.12	0.00	0.91	19.10	26951
4	50.49	0.22	75.58	3.13	0.00	0.91	20.16	26424
4	51.56	0.13	75.50	3.70	0.00	0.91	19.76	27267
37	55.10	0.18	77.25	3.57	0.00	0.91	18.10	27961
37	47.23	0.14	77.24	3.97	0.05	0.91	17.69	28589
37	51.53	0.15	77.28	3.99	3.41	0.91	17.68	28640
17	46.57	0.29	77.10	3.75	0.00	0.80	18.06	28176
17	53.30	0.13	77.12	4.17	0.00	0.80	17.77	28823
17	50.93	0.17	76.92	4.04	4.09	0.80	18.06	28519
38	28.10	0.21	76.83	3.61	0.00	0.94	18.41	27819
38	53.55	0.17	76.74	3.74	0.00	0.94	18.41	27980
38	53.29	0.21	76.85	3.92	0.00	0.94	18.07	28328
10	45.41	0.16	77.52	3.80	0.00	0.97	17.56	28469
10	48.74	0.15	77.20	3.80	0.00	0.97	17.88	28310
10	49.01	0.15	77.21	3.94	0.00	0.97	17.73	28538
5G	23.25	0.25	84.63	3.02	0.00	1.21	10.88	30957
5G	48.95	0.32	84.11	3.12	0.00	1.21	11.24	30852
5G	55.98	0.25	84.18	3.02	0.04	1.21	11.30	30734
14	27.26	0.20	79.40	3.14	0.00	1.14	16.12	28432
14	52.92	0.28	79.65	3.21	0.00	1.14	15.71	28696
14	51.14	0.15	79.29	3.29	0.00	1.14	16.13	28602
29	53.54	0.45	88.92	2.76	0.00	1.29	6.57	32802
29	28.98	0.32	89.32	2.70	0.08	1.29	6.29	32899
29	45.68	0.21	89.34	2.82	0.00	1.29	6.34	33061

27	55.60	0.24	91.85	2.32	0.37	1.08	4.52	33529
27	50.25	0.21	91.99	2.54	0.00	1.08	4.19	33939
27	56.72	0.33	91.70	2.34	0.00	1.08	4.56	33500
5AG	27.10	0.27	84.08	3.04	0.00	1.15	11.46	30691
5AG	47.35	0.22	84.35	3.22	0.00	1.15	11.06	31109
5AG	50.17	0.32	84.21	3.04	0.00	1.15	11.28	30777
15	50.87	0.31	80.41	3.30	0.00	1.05	14.93	29213
15	51.19	0.15	80.32	3.41	0.00	1.05	15.07	29309
15	49.10	0.21	80.66	3.67	0.00	1.05	14.41	29910
30	47.76	0.37	90.56	1.85	0.00	1.28	5.93	32194
30	22.22	0.48	92.29	1.76	0.00	1.28	4.19	32953
30	52.87	0.35	92.21	1.90	0.00	1.28	4.26	33105
28	28.68	0.24	90.91	2.47	0.00	1.02	5.36	33272
28	55.68	0.30	90.92	2.61	0.00	1.02	5.15	33517
28	54.93	0.29	90.76	2.50	0.00	1.02	5.43	33250
26	48.90	0.40	88.54	2.58	0.00	1.10	7.38	32272
26	23.68	0.38	88.93	2.59	0.00	1.10	6.99	32494
26	52.22	0.25	88.82	2.77	0.00	1.10	7.05	32694
3G	27.74	0.41	91.50	1.81	0.00	1.61	4.67	32670
3G	56.45	0.34	91.57	1.87	0.00	1.61	4.61	32796
3G	56.24	0.32	91.50	1.89	0.00	1.61	4.68	32781
6	54.84	0.51	91.07	2.04	0.00	–	6.38	32543
6	52.81	0.21	91.10	2.01	0.00	–	6.68	32458
6	50.05	0.26	90.89	2.23	0.00	–	6.62	32714
9	22.48	0.28	91.62	1.90	0.00	1.14	5.06	32764
9	49.61	0.27	92.02	2.10	0.00	1.14	4.47	33291
9	55.07	0.22	92.06	1.99	0.00	1.14	4.59	33121
12	55.37	0.38	91.61	1.97	0.00	1.39	4.66	32933
12	28.88	0.42	91.93	1.91	0.12	1.39	4.35	33013
12	47.98	0.35	91.99	2.07	0.00	1.39	4.21	33280
3AG	29.53	0.32	92.02	1.90	0.00	1.27	4.49	33011
3AG	46.29	0.40	91.72	2.00	0.00	1.27	4.61	33029
3AG	53.77	0.35	91.63	1.87	0.00	1.27	4.88	32769
11	23.84	0.33	91.53	2.23	0.00	1.23	4.68	33272
11	45.98	0.32	91.22	2.44	0.00	1.23	4.79	33437
11	51.20	0.29	91.14	2.31	0.00	1.23	5.03	33186
8	27.13	0.27	90.67	2.29	0.00	1.14	5.64	32889
8	49.90	0.35	91.12	2.43	0.00	1.14	4.97	33356

8	49.42	0.23	91.00	2.41	0.00	1.14	5.23	33248
36	45.39	0.29	78.22	3.53	0.02	0.91	17.03	28428
36	52.15	0.12	78.00	3.77	0.00	0.91	17.20	28653
36	54.44	0.12	78.20	3.98	0.00	0.91	16.80	29083
18G	24.14	0.22	76.51	3.60	0.00	0.96	18.70	27655
18G	47.19	0.20	75.24	3.48	0.03	0.96	20.09	26810
18G	55.23	0.14	75.38	3.63	0.00	0.96	19.88	27108
21	27.98	0.19	83.01	3.40	0.00	1.04	12.36	30679
21	48.35	0.27	83.40	3.31	0.00	1.04	11.98	30752
21	48.44	0.15	83.26	3.54	0.00	1.04	12.00	31025
23	52.99	0.13	78.75	3.59	0.00	0.90	16.62	28763
23	49.11	0.22	79.44	3.63	0.00	0.90	15.81	29185
23	50.28	0.15	79.13	3.76	0.00	0.90	16.06	29227
31	47.26	0.35	90.41	2.50	0.00	1.13	5.62	33100
31	52.38	0.22	90.83	2.52	0.00	1.13	5.30	33326
31	54.05	0.21	90.99	2.64	0.00	1.13	5.04	33592
34	28.86	0.40	93.32	1.85	0.00	1.19	3.24	33597
34	56.68	0.29	93.09	1.90	0.00	1.19	3.53	33540
34	48.66	0.25	92.96	1.95	0.00	1.19	3.65	33533
18AG	28.80	0.21	76.68	3.67	0.00	1.09	18.35	27868
18AG	55.62	0.13	76.28	3.77	0.00	1.09	18.73	27810
18AG	49.42	0.15	76.40	3.71	0.00	1.09	18.65	27772
32	24.26	0.38	91.93	2.20	0.00	1.46	4.03	33478
32	50.44	0.16	92.11	2.26	0.00	1.46	4.00	33628
32	50.96	0.18	91.86	2.42	0.00	1.46	4.08	33750
19G	22.02	0.32	83.30	3.09	0.00	1.14	12.16	30374
19G	49.41	0.30	83.76	3.03	0.00	1.14	11.78	30510
19G	45.14	0.33	83.98	3.03	0.00	1.14	11.53	30630
33G	23.68	0.40	90.65	1.85	0.00	1.30	5.80	32241
33G	49.97	0.28	91.23	2.15	0.00	1.30	5.04	32988
33G	51.81	0.33	91.71	1.99	0.00	1.30	4.66	33002
33AG	22.00	0.34	92.24	1.96	0.00	1.51	3.95	33252
33AG	51.37	0.35	91.48	2.06	0.00	1.51	4.59	33031
33AG	49.99	0.21	91.73	2.09	0.00	1.51	4.46	33184
19AG	22.95	0.21	81.37	3.22	0.00	–	15.20	29378
19AG	51.93	0.22	81.42	3.45	0.00	–	14.90	29775
19AG	49.78	0.15	81.25	3.56	0.00	–	15.05	29832

The highlighted boxes show values that are outliers.

Table 14.14: Proximate Analysis Results on a Dry Basis

Sample	Moisture wt%	Volatile Matter wt%	Fixed Carbon wt%	ROI Ash wt%	Proximate Ash wt%
Run1G	1.968	40.260	58.935	0.805	4.09
Run1G	1.781	40.295	58.921	0.785	1.78
Run2G	2.195	30.136	68.832	1.032	0.38
Run2G	1.917	28.636	70.316	1.048	2.22
Run16	1.869	33.292	66.040	0.669	0.00
Run16	1.620	33.114	66.207	0.679	1.47
Run1AG	1.452	39.159	60.338	0.503	0.92
Run1AG	1.313	39.069	60.426	0.505	1.62
Run4	2.249	30.116	68.961	0.923	0.43
Run4	2.191	30.205	68.860	0.935	1.78
Run37	1.676	28.721	70.362	0.917	0.34
Run37	2.014	28.916	70.148	0.936	2.06
Run17	1.795	29.653	69.538	0.810	0.32
Run17	2.204	29.744	69.466	0.789	0.00
Run38	1.964	31.316	67.711	0.974	2.23
Run38	2.117	29.138	69.923	0.939	0.00
Run10	1.741	28.302	70.703	0.996	2.22
Run10	2.559	28.734	70.284	0.983	0.06
Run5	1.684	20.641	78.075	1.284	5.23
Run5	2.113	18.303	80.431	1.266	3.38
Run14	1.965	25.134	73.701	1.165	1.13
Run14	2.899	25.299	73.540	1.162	0.00
Run29	1.359	10.993	87.666	1.341	3.52
Run29	1.644	11.217	87.459	1.323	1.93
Run27	1.563	8.008	90.869	1.123	3.93
Run27	1.294	8.127	90.793	1.080	0.22
Run5AG	2.190	18.399	80.423	1.178	1.48
Run5AG	2.021	18.469	80.362	1.169	0.80
Run15	2.228	23.415	75.461	1.124	5.50
Run15	2.074	23.630	75.269	1.101	3.67
Run30	1.835	6.674	92.028	1.298	0.61
Run30	1.490	6.886	91.848	1.266	2.63
Run28	1.391	9.120	89.866	1.014	0.00
Run28	1.404	9.478	89.451	1.071	4.62
Run26	1.682	11.711	87.186	1.102	0.00

Run26	1.764	12.117	86.758	1.124	1.27
Run3G	1.655	7.077	91.304	1.619	0.57
Run3G	1.466	6.665	91.707	1.629	1.38
Run6	1.862	7.774	91.678	0.548	1.66
Run6	1.690	8.170	91.284	0.546	1.66
Run9	1.734	7.411	91.417	1.172	2.15
Run9	1.736	7.230	91.592	1.179	2.67
Run12	1.650	6.714	91.886	1.400	0.82
Run12	1.384	6.755	91.823	1.422	2.63
Run3AG	1.729	7.166	91.573	1.262	0.00
Run3AG	1.804	7.583	91.114	1.303	2.22
Run11	1.841	8.616	90.089	1.294	4.53
Run11	1.830	8.595	90.125	1.280	3.44
Run8	1.671	8.675	90.203	1.122	0.00
Run8	1.205	9.925	88.924	1.151	1.08
Run36	1.944	28.056	71.008	0.936	2.12
Run36	2.371	28.412	70.680	0.908	0.00
Run18G	2.439	30.727	68.318	0.956	0.00
Run18G	2.378	30.877	68.155	0.968	0.00
Run21	1.532	19.895	79.013	1.093	4.24
Run21	2.210	20.624	78.301	1.074	1.91
Run31	1.484	8.701	90.178	1.122	0.00
Run31	1.565	9.305	89.576	1.120	0.00
Run34	1.271	5.883	92.901	1.215	2.05
Run34	1.368	5.879	92.884	1.237	3.76
Run18AG	2.064	29.030	69.837	1.132	2.96
Run18AG	2.384	29.301	69.584	1.115	1.10
Run32	1.129	7.278	91.229	1.494	2.40
Run32	1.159	7.510	91.001	1.489	2.06
Run19G	1.748	18.246	80.617	1.137	0.00
Run19G	6.477	19.464	79.321	1.215	1.79
Run33G	1.693	7.905	90.750	1.345	2.81
Run33G	1.992	12.493	86.164	1.342	2.33
Run33AG	6.827	8.689	89.644	1.667	4.97
Run33AG	2.302	8.695	89.813	1.492	0.00
Run19AG	1.977	21.074	78.389	0.537	3.02
Run19AG	2.208	21.414	78.043	0.543	4.24
Run23	3.733	26.549	72.536	0.915	0.00

Run23	3.430	26.356	72.705	0.939	1.47

The ash values in the table are the average of the results obtained from the residue on ignition test replicates and are not from the proximate analysis. Although the biochar samples were treated in the same way, i.e. ground into a powder, oven dried and stored over a desiccator until used, the ash values provide an estimate of the ash content of biochar formed under the same conditions and therefore the average ash value from the ignition test replicates was used. This was then converted to a dry basis based on the moisture results obtained from proximate analysis.

APPENDIX D

DESIGN

DRAWINGS

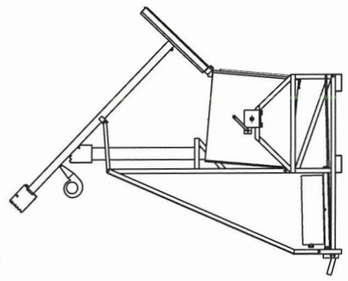

Operation: Loading:

1. Pull Explosion vent out at the base and pin in place.
2. Undo Lid Latch.
3. Release Foot Lever, Lower End of Rail
4. Release Spring Latch on the Rail.
5. Pull Burner clear of the Pyrolyser.
6. Rotate Drum Using the Crank Handle.
7. Fill Drum with Wood Chips
8. Rotate Drum back to the Operation Position (Vertical).
9. Push Burner back under Drum
10. Raise and lock rail back into place.
11. Re Latch the Lid.
12. Put the explosion vent back in place and secure with the pin.
13. Start Pyrolyser.

Follow the same Procedure to unload Drum once pyrolysis is complete.

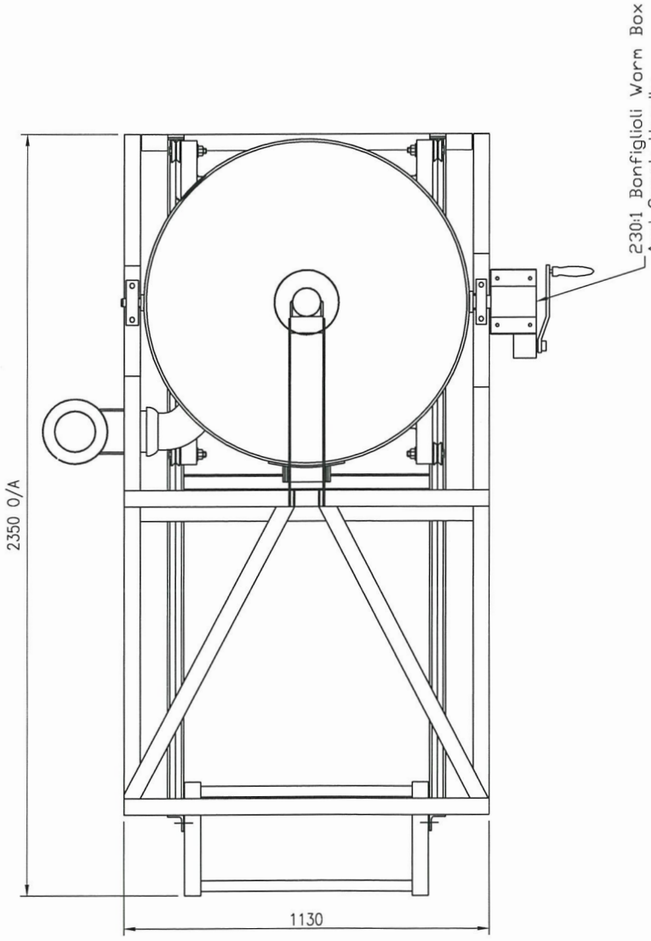

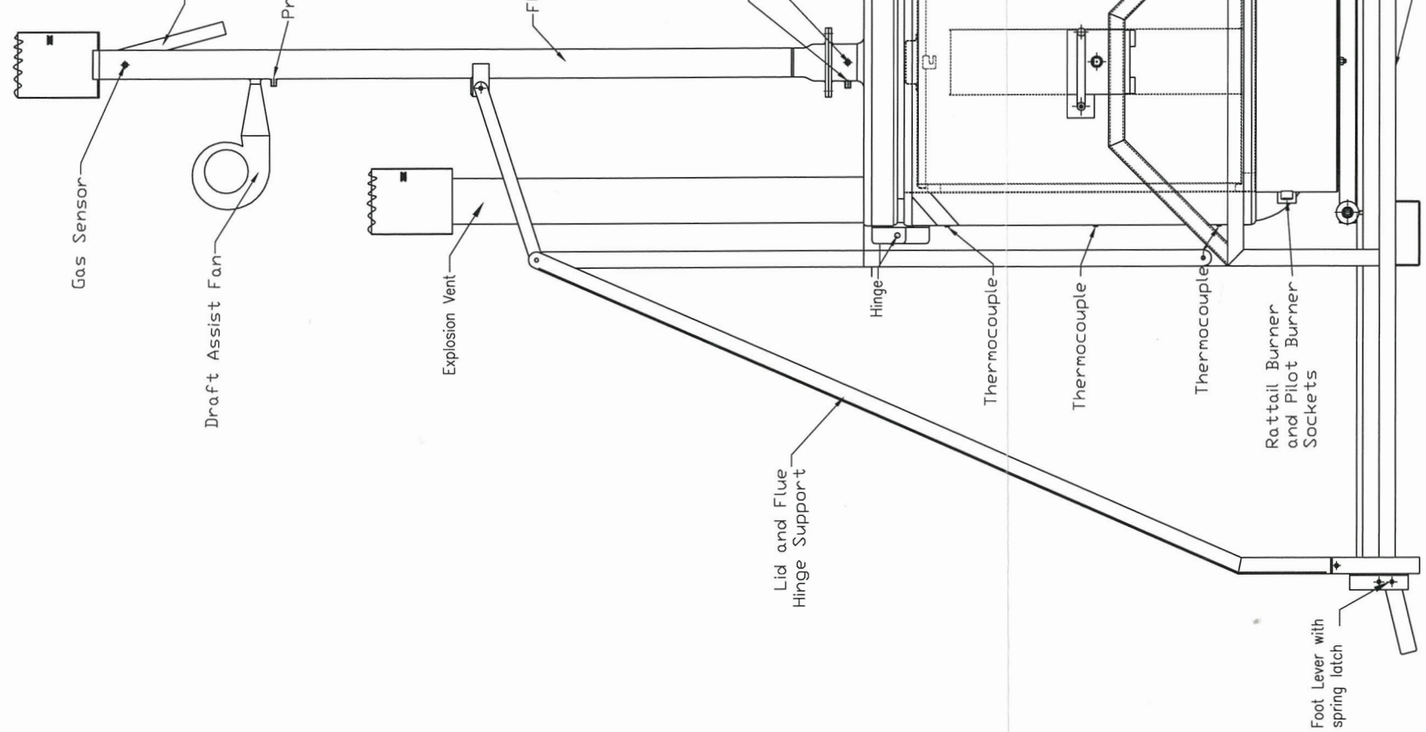

MASSEY UNIVERSITY
TE KUNENGA KI PŪREHUROA
UNIVERSITY OF NEW ZEALAND

DEVELOPED BY MASSEY UNIVERSITY,
DRAWINGS & ENGINEERING BY JJ NIVEN ENGINGEERING LIMITED,
GAS SYSTEMS & CONTROL BY MORRINSVILLE PLUMBING & GAS LIMITED.

DRAWN	R Thompson
DATE	19-06-2013
SCALE (A3)	NTS

J.J. NIVEN ENGINEERING LTD.
36-50 ARMSTRONG STREET, PO BOX 5121
PALMERSTON NORTH, NEW ZEALAND
PH 06 357 4039 FAX 06 358 3498

Open Source Batch Pyrolyser Developed By Massey University General Arangement

DRG No.	37644 00
REV.	_
CAD Ref:	37644

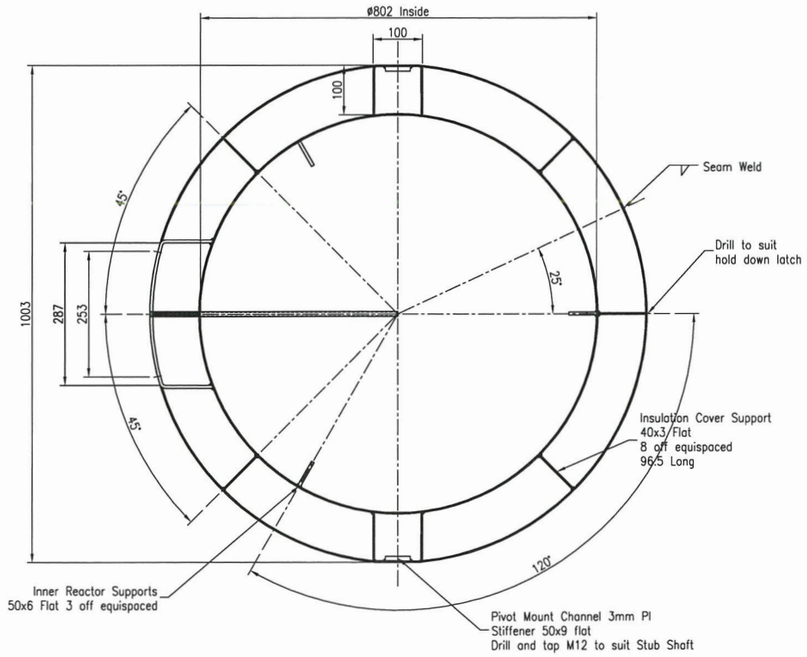

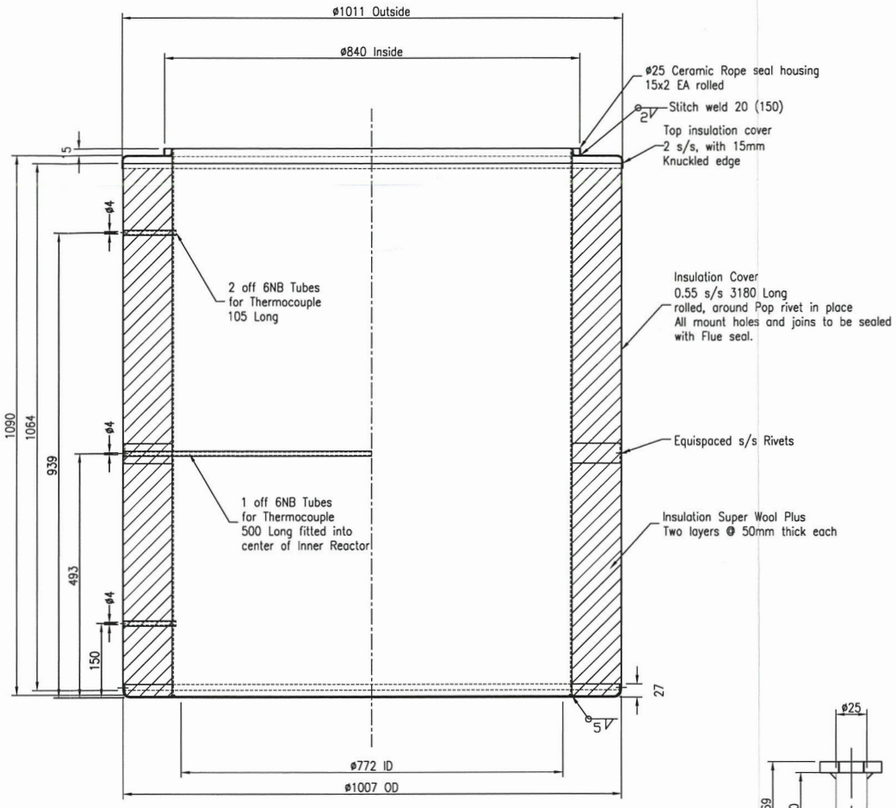

Outer Reactor Insulation Details
All material 304 s/s UDS

Inner Reactor
Support Lug
3 off regd 50x6 flat

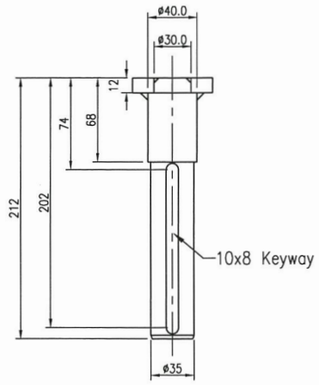

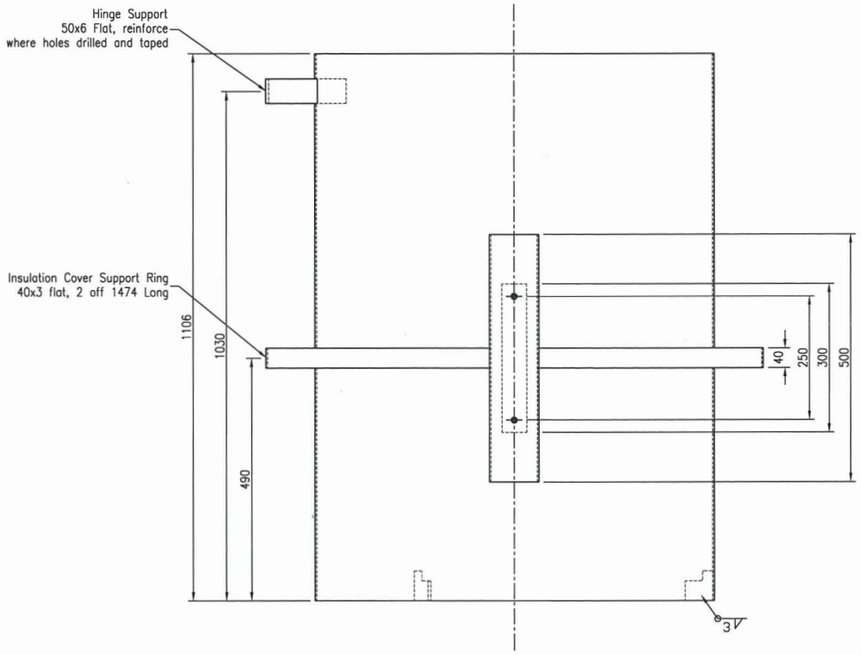

Outer Reactor
Fabrication Details
All material 304 s/s

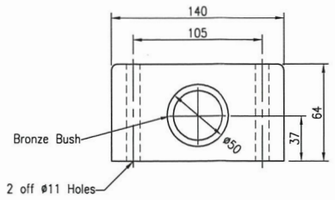

Drive side Bearing Block
1 off Required
32mm PL Profiled

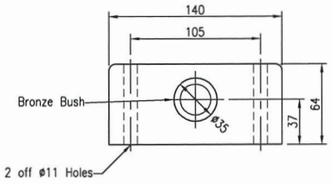

Bearing Block
1 off Required
32mm PL Profiled

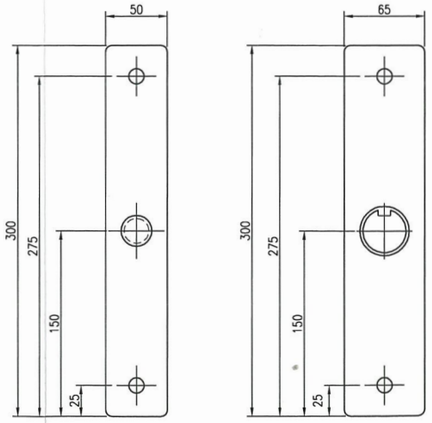

Stub Shaft Details
ø25 AISI 1020
304 s/s Flat

MASSEY UNIVERSITY
TE KUNENGA KI PŪREHUROA
UNIVERSITY OF NEW ZEALAND

DEVELOPED BY MASSEY UNIVERSITY,
DRAWINGS & ENGINEERING BY JJ NIVEN ENGINGEERING LIMITED,
GAS SYSTEMS & CONTROL BY MORRINSVILLE PLUMBING & GAS LIMITED.

DRAWN R Thompson
DATE 19-06-2013
SCALE (A3)
NTS

J.J. NIVEN ENGINEERING LTD.
36-50 ARMSTRONG STREET, PO BOX 5121
PALMERSTON NORTH, NEW ZEALAND
PH 06 357 4039 FAX 06 358 3498

MASSEY UNIVERSITY
Carbon Generating Pyrolyser
Outer Reactor and Insulation Detail

DRG No. 37644 01
REV. –
CAD Ref: 37644

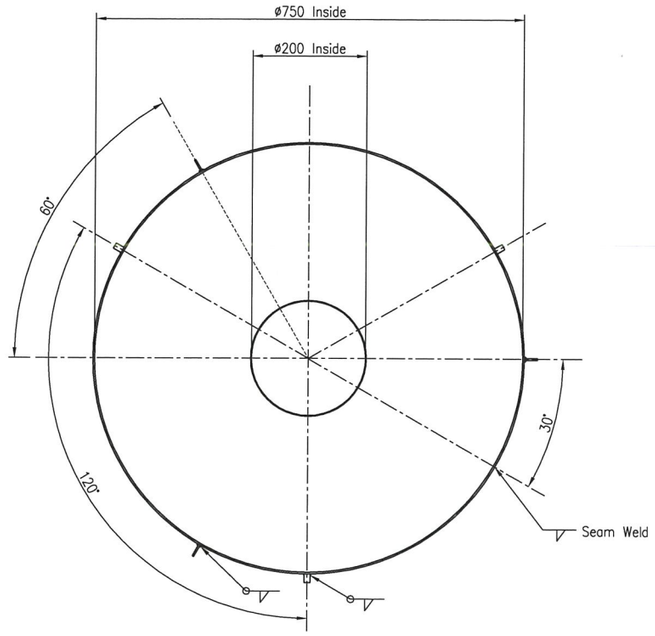

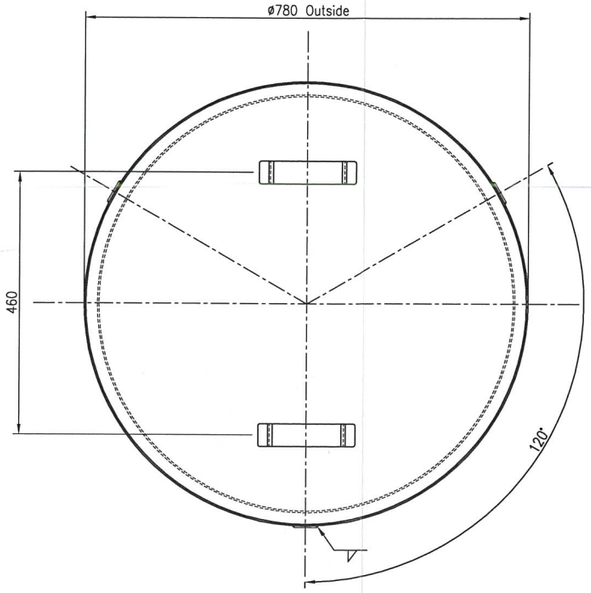

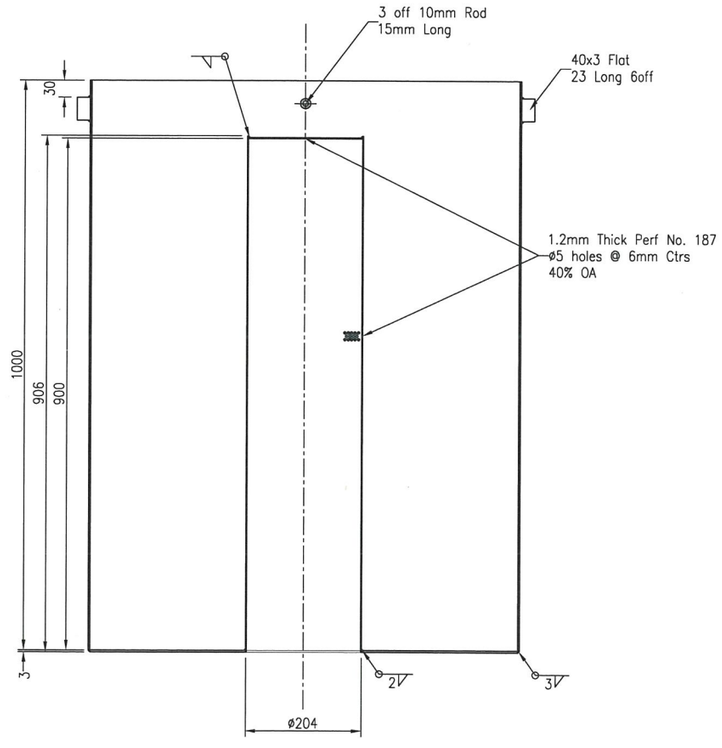

Inner Reactor
1 off Required
All Material 3mm 304 S/S UOS

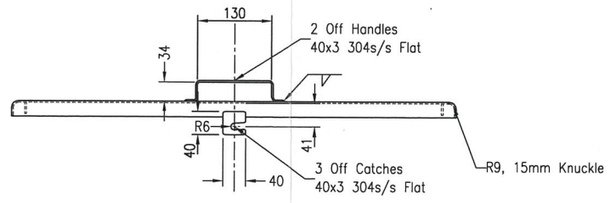

Inner Reactor Lid
1 off Required
All material 3mm 304 S/S UOS

MASSEY UNIVERSITY
TE KUNENGA KI PŪREHUROA
UNIVERSITY OF NEW ZEALAND

DEVELOPED BY MASSEY UNIVERSITY,
DRAWINGS & ENGINEERING BY JJ NIVEN ENGINGEERING LIMITED,
GAS SYSTEMS & CONTROL BY MORRINSVILLE PLUMBING & GAS LIMITED.

DRAWN	R Thompson
DATE	19-06-2013
SCALE (A3)	NTS

J.J. NIVEN ENGINEERING LTD.
36-50 ARMSTRONG STREET, PO BOX 5121
PALMERSTON NORTH, NEW ZEALAND
PH 06 357 4039 FAX 06 358 3498

MASSEY UNIVERSITY
Carbon Generating Pyrolyser
Inner Reactor and Lid

DRG No.	37644 02
REV.	_
CAD Ref:	37644

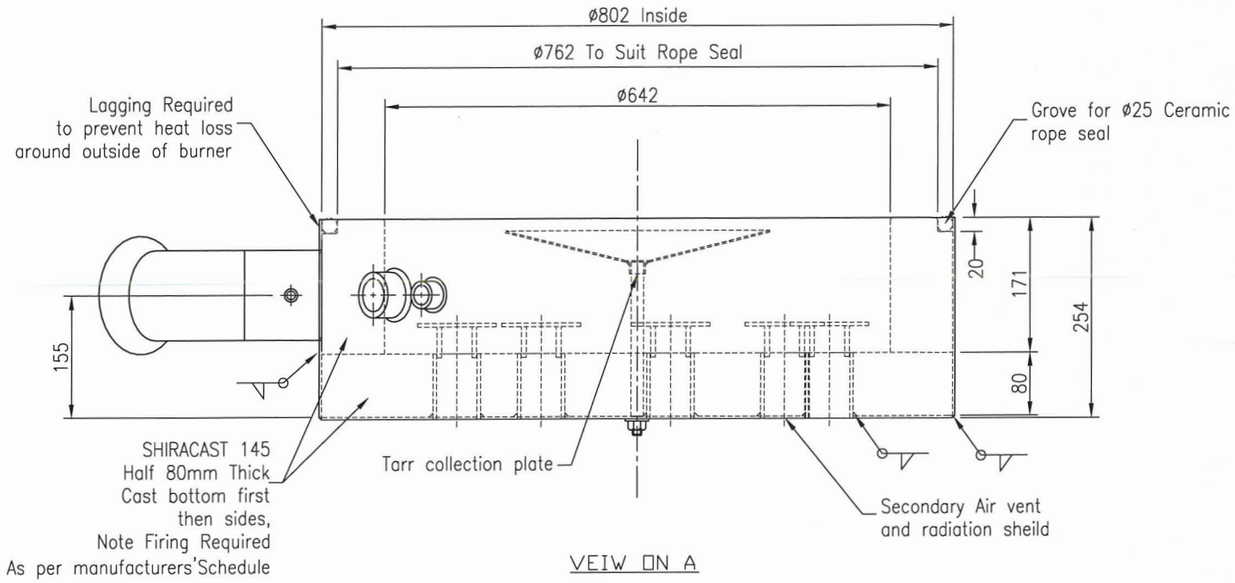

VEIW ON A

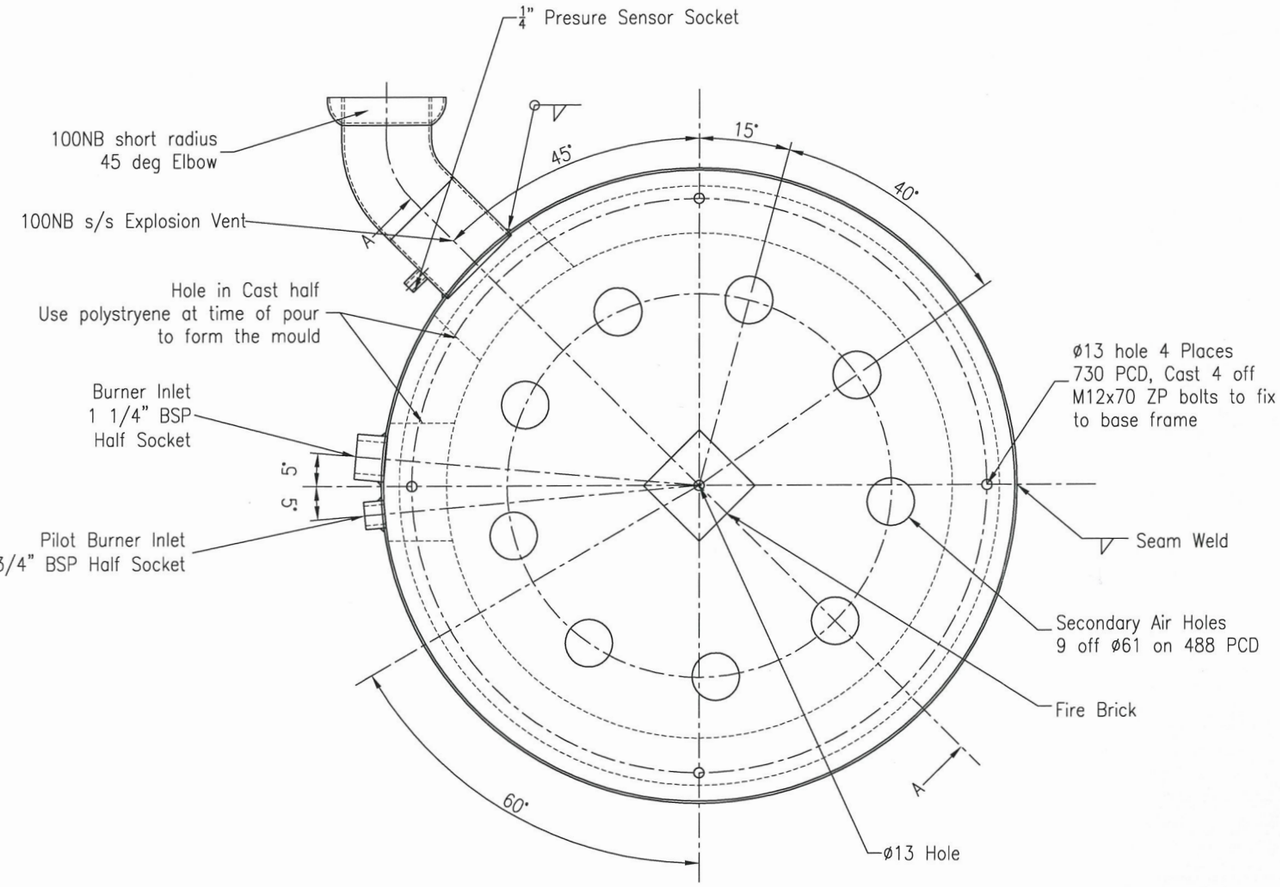

Base Outer Shell
1 off Required
All material 3mm 304 S/S UOS

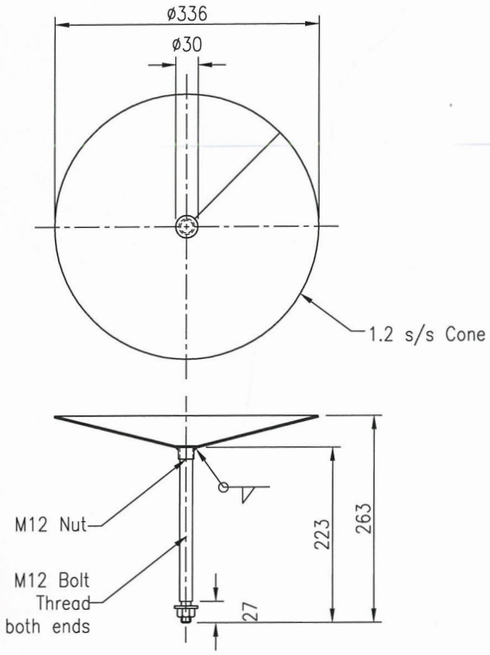

Tarr Collection Platel
1 off Required, Cast into base
All material 304 S/S UOS

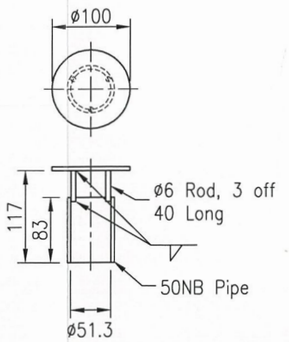

Secondary Air Vents
9 off Require
304 s/s

MASSEY UNIVERSITY
TE KUNENGA KI PŪREHUROA
UNIVERSITY OF NEW ZEALAND

DEVELOPED BY MASSEY UNIVERSITY,
DRAWINGS & ENGINEERING BY JJ NIVEN ENGINGEERING LIMITED,
GAS SYSTEMS & CONTROL BY MORRINSVILLE PLUMBING & GAS LIMITED.

DRAWN R Thompson
DATE 19-06-2013
SCALE (A3)
NTS

J.J. NIVEN ENGINEERING LTD.
36-50 ARMSTRONG STREET, PO BOX 5121
PALMERSTON NORTH, NEW ZEALAND
PH 06 357 4039 FAX 06 358 3498

MASSEY UNIVERSITY
Carbon Generating Pyrolyser
Burner Details

DRG No. 37644 03
REV. _
CAD Ref: 37644

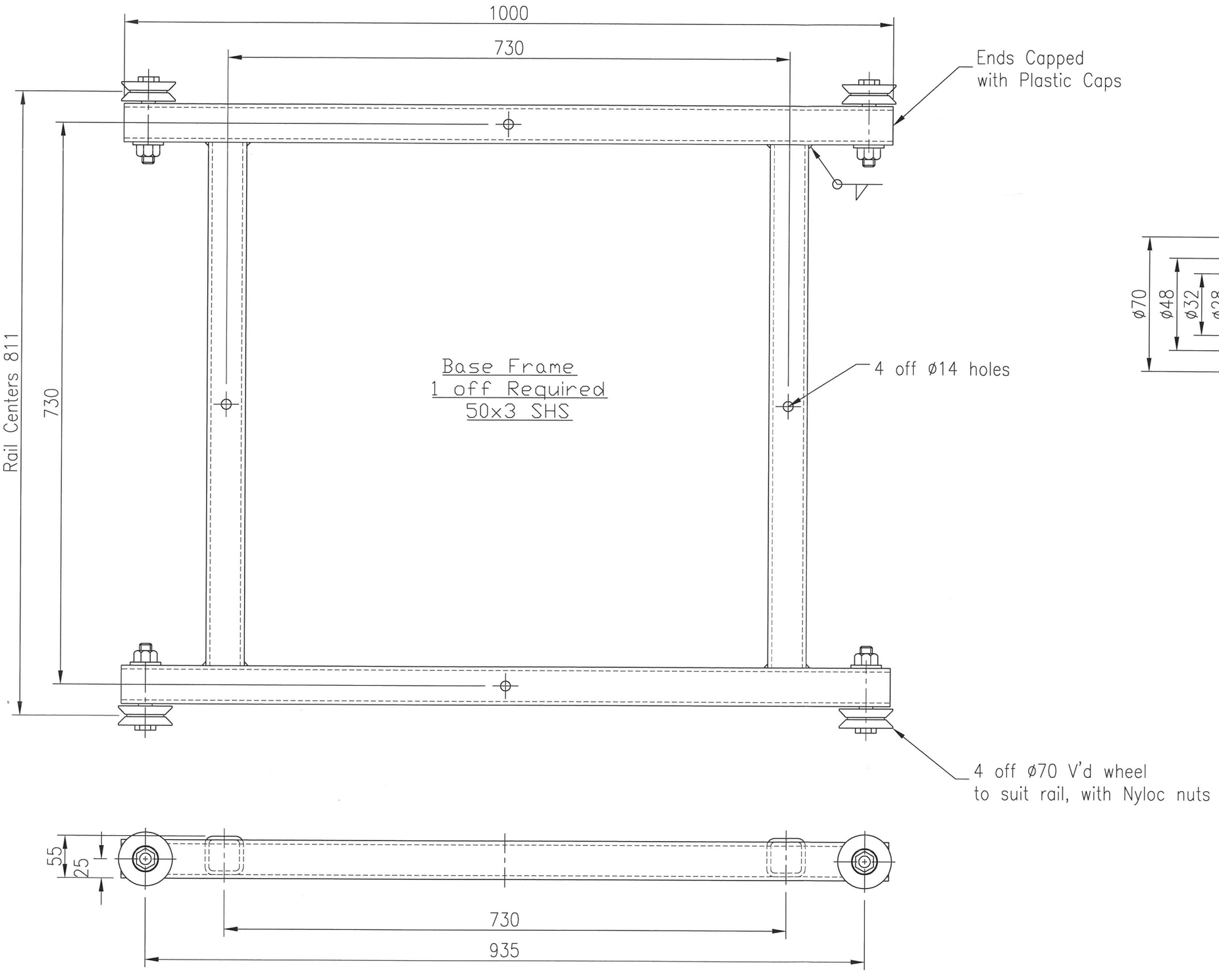

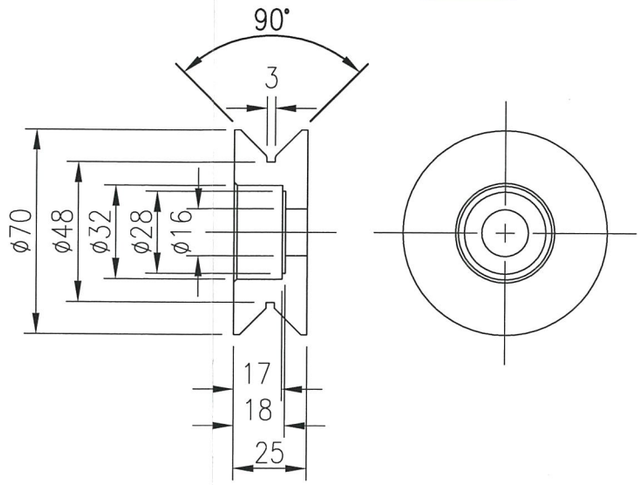

V Wheel
4 off Required
AISI 1040
To Suit 16002 Bearing

MASSEY UNIVERSITY
TE KUNENGA KI PŪREHUROA
UNIVERSITY OF NEW ZEALAND

DEVELOPED BY MASSEY UNIVERSITY,
DRAWINGS & ENGINEERING BY JJ NIVEN ENGINGEERING LIMITED,
GAS SYSTEMS & CONTROL BY MORRINSVILLE PLUMBING & GAS LIMITED.

DRAWN R Thompson
DATE 19-06-2013
SCALE (A3)
NTS

J.J. NIVEN ENGINEERING LTD.
36-50 ARMSTRONG STREET, PO BOX 5121
PALMERSTON NORTH, NEW ZEALAND
PH 06 357 4039 FAX 06 358 3498

MASSEY UNIVERSITY
Carbon Generating Pyrolyser
Burner Base Frame/Wheel Detail

DRG No. 37644 04
REV. _
CAD Ref: 37644

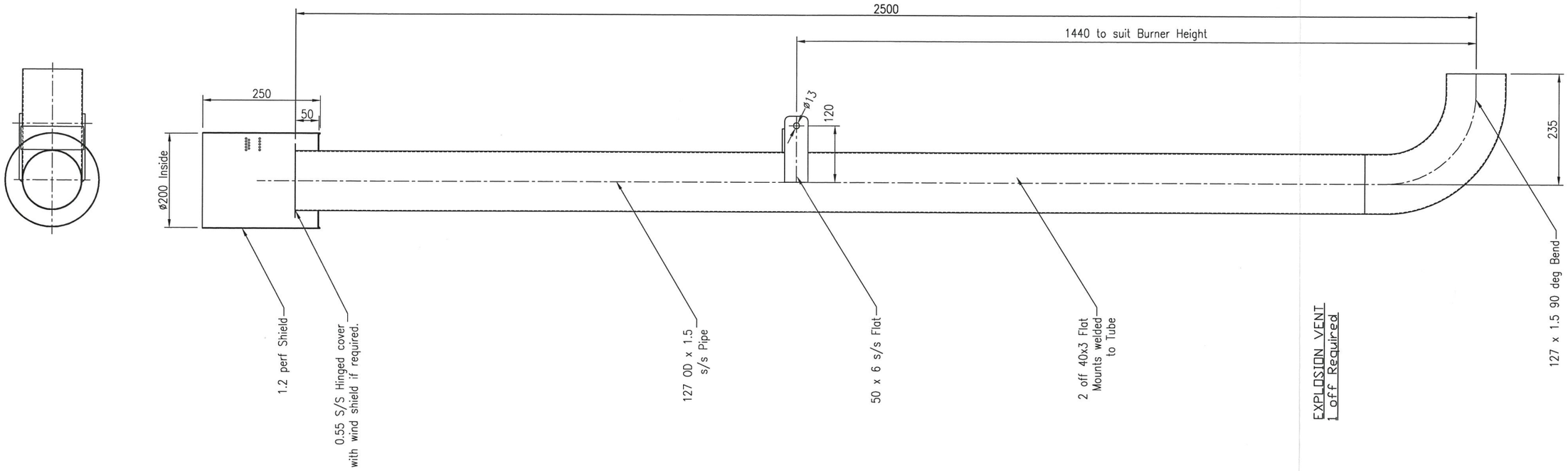

MASSEY UNIVERSITY
TE KUNENGA KI PŪREHUROA
UNIVERSITY OF NEW ZEALAND

DEVELOPED BY MASSEY UNIVERSITY,
DRAWINGS & ENGINEERING BY JJ NIVEN ENGINGEERING LIMITED,
GAS SYSTEMS & CONTROL BY MORRINSVILLE PLUMBING & GAS LIMITED.

DRAWN R Thompson
DATE 25-01-2013
SCALE (A3)
NTS

J.J. NIVEN ENGINEERING LTD.
36-50 ARMSTRONG STREET, PO BOX 5121
PALMERSTON NORTH, NEW ZEALAND
PH 06 357 4039 FAX 06 358 3498

MASSEY UNIVERSITY
Carbon Generating Pyrolyser
Explosion Vent

DRG No. 37644 05
REV. _
CAD Ref: 37644

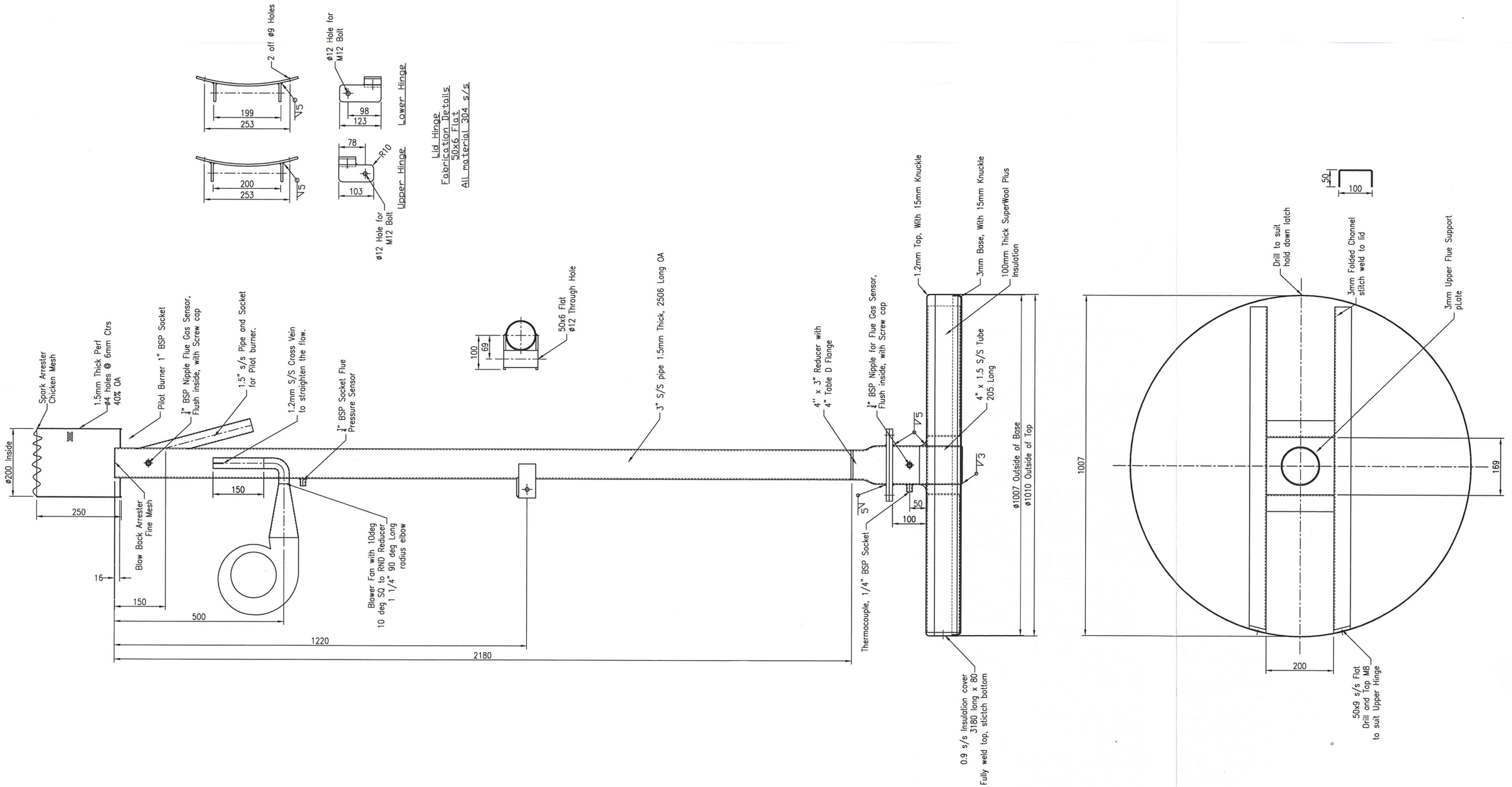

MASSEY UNIVERSITY
TE KUNENGA KI PŪREHUROA
UNIVERSITY OF NEW ZEALAND

DEVELOPED BY MASSEY UNIVERSITY,
DRAWINGS & ENGINEERING BY JJ NIVEN ENGINGEERING LIMITED,
GAS SYSTEMS & CONTROL BY MORRINSVILLE PLUMBING & GAS LIMITED.

DRAWN	R Thompson
DATE	19-06-2013
SCALE (A3)	NTS

J.J. NIVEN ENGINEERING LTD.
36-50 ARMSTRONG STREET, PO BOX 5121
PALMERSTON NORTH, NEW ZEALAND
PH 06 357 4039 FAX 06 358 3498

MASSEY UNIVERSITY
Carbon Generating Pyrolyser
Flu, Lid and Hinge Details

DRG No.	37644 06
REV.	_
CAD Ref:	37644

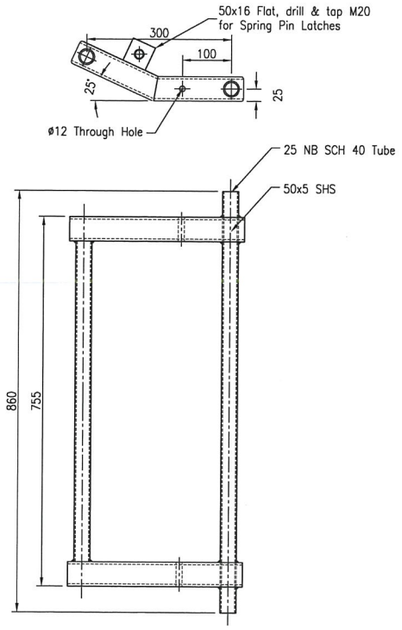

FOOT LEVER
1 off Required
With Sping Pin Latches

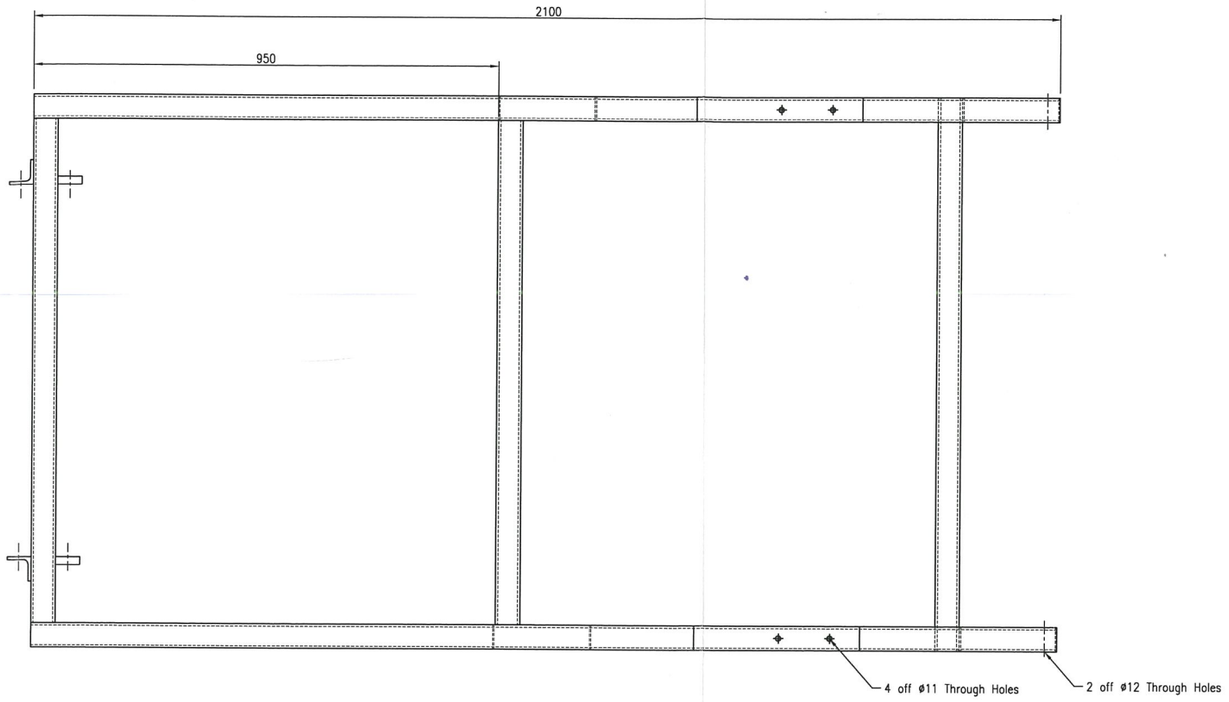

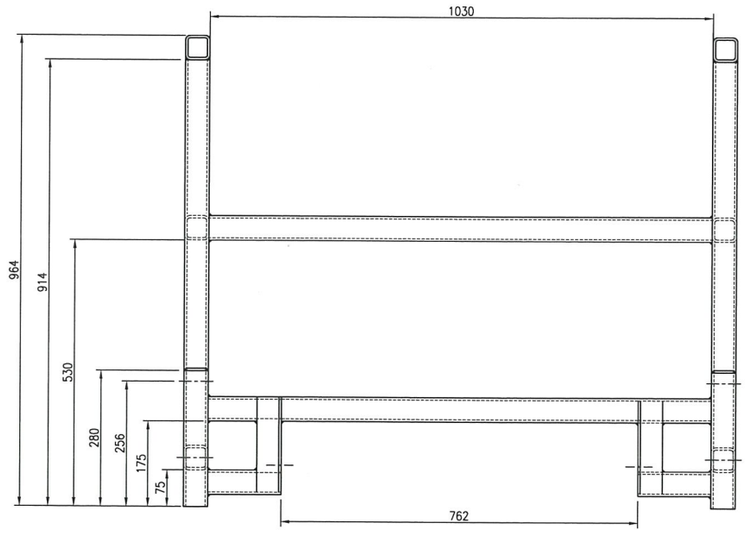

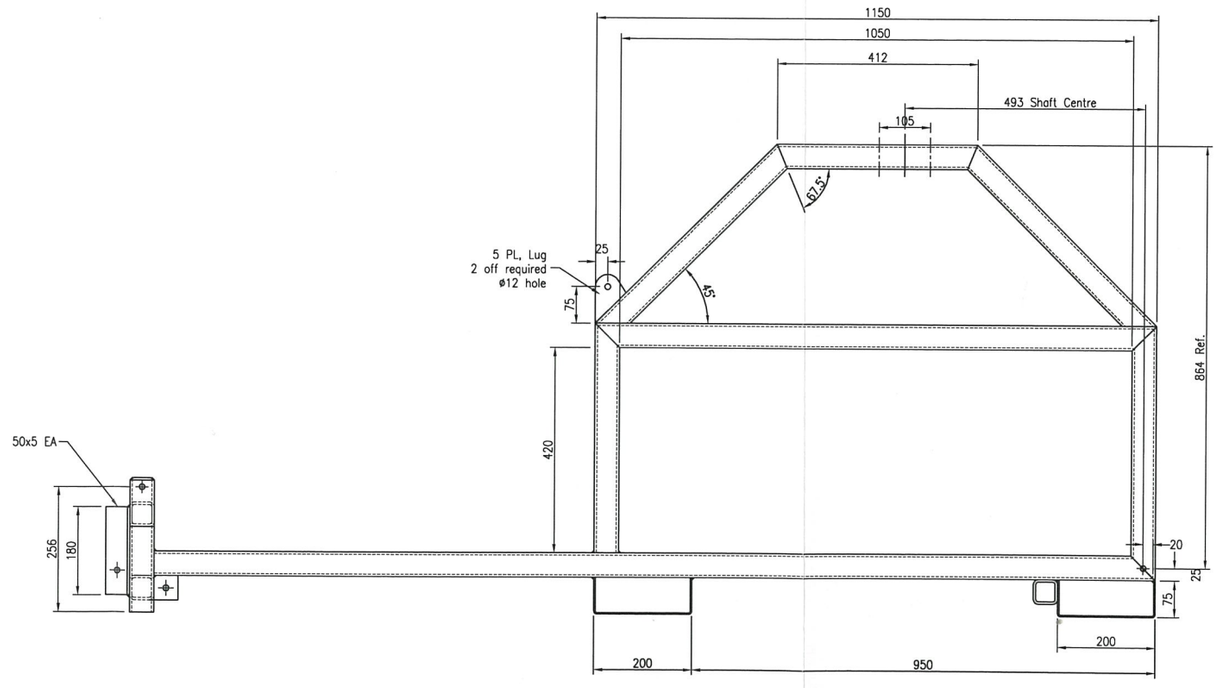

SUPPORT FRAME
1 off Required
50x5 SHS

MASSEY UNIVERSITY
TE KUNENGA KI PŪREHUROA
UNIVERSITY OF NEW ZEALAND

DEVELOPED BY MASSEY UNIVERSITY,
DRAWINGS & ENGINEERING BY JJ NIVEN ENGINGEERING LIMITED,
GAS SYSTEMS & CONTROL BY MORRINSVILLE PLUMBING & GAS LIMITED.

DRAWN R Thompson
DATE 25-01-2013
SCALE (A3)
NTS

J.J. NIVEN ENGINEERING LTD.
36-50 ARMSTRONG STREET, PO BOX 5121
PALMERSTON NORTH, NEW ZEALAND
PH 06 357 4039 FAX 06 358 3498

MASSEY UNIVERSITY
Carbon Generating Pyrolyser
Support Frame & Foot Lever

DRG No. 37644 07
REV. _
CAD Ref: 37644

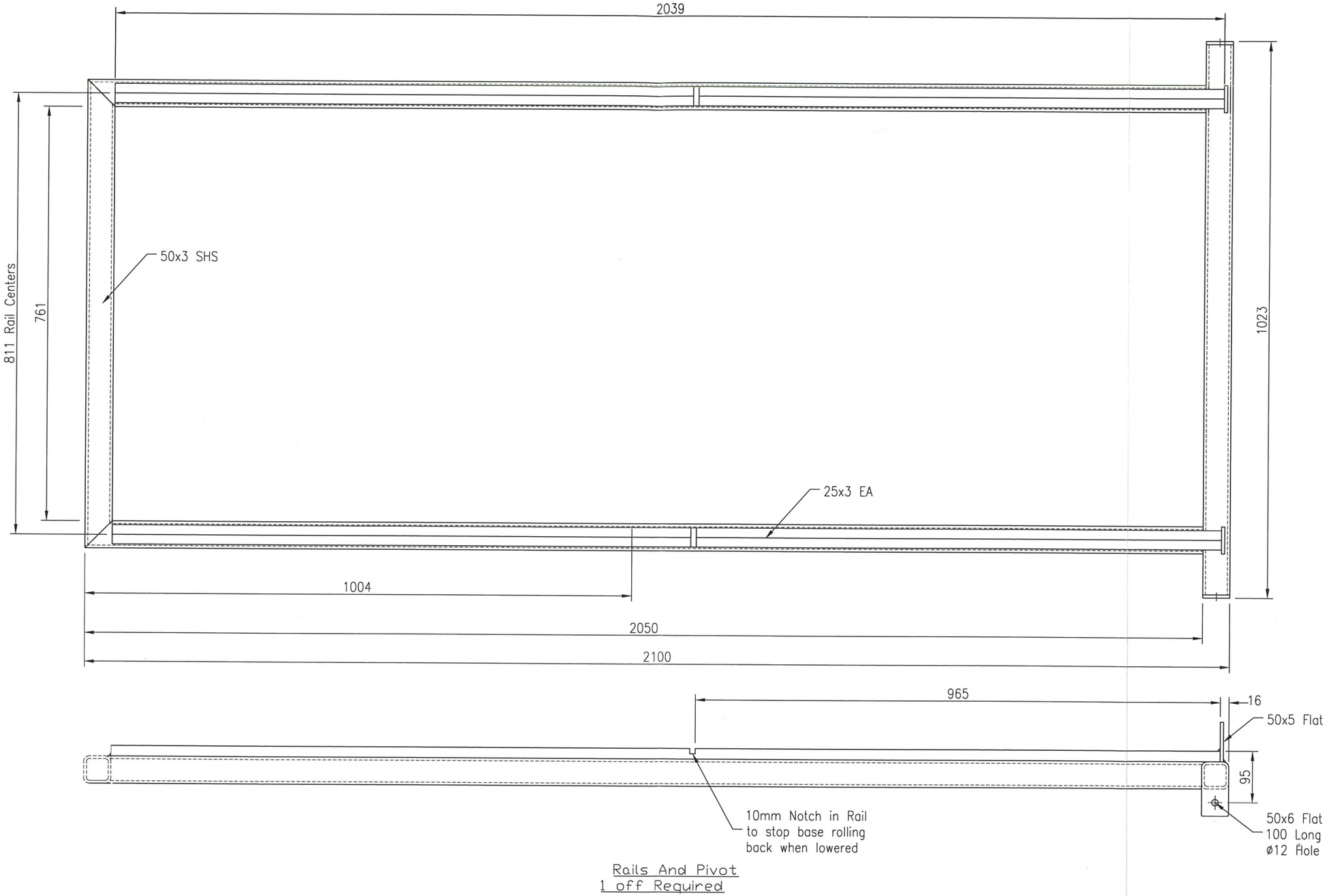

Rails And Pivot
1 off Required

MASSEY UNIVERSITY
TE KUNENGA KI PŪREHUROA
UNIVERSITY OF NEW ZEALAND

DEVELOPED BY MASSEY UNIVERSITY,
DRAWINGS & ENGINEERING BY JJ NIVEN ENGINGEERING LIMITED,
GAS SYSTEMS & CONTROL BY MORRINSVILLE PLUMBING & GAS LIMITED.

DRAWN	R Thompson
DATE	19-06-2013
SCALE (A3)	NTS

J.J. NIVEN ENGINEERING LTD.
36-50 ARMSTRONG STREET, PO BOX 5121
PALMERSTON NORTH, NEW ZEALAND
PH 06 357 4039 FAX 06 358 3498

MASSEY UNIVERSITY
Carbon Generating Pyrolyser
Rails

DRG No.	37644 08
REV.	_
CAD Ref:	37644

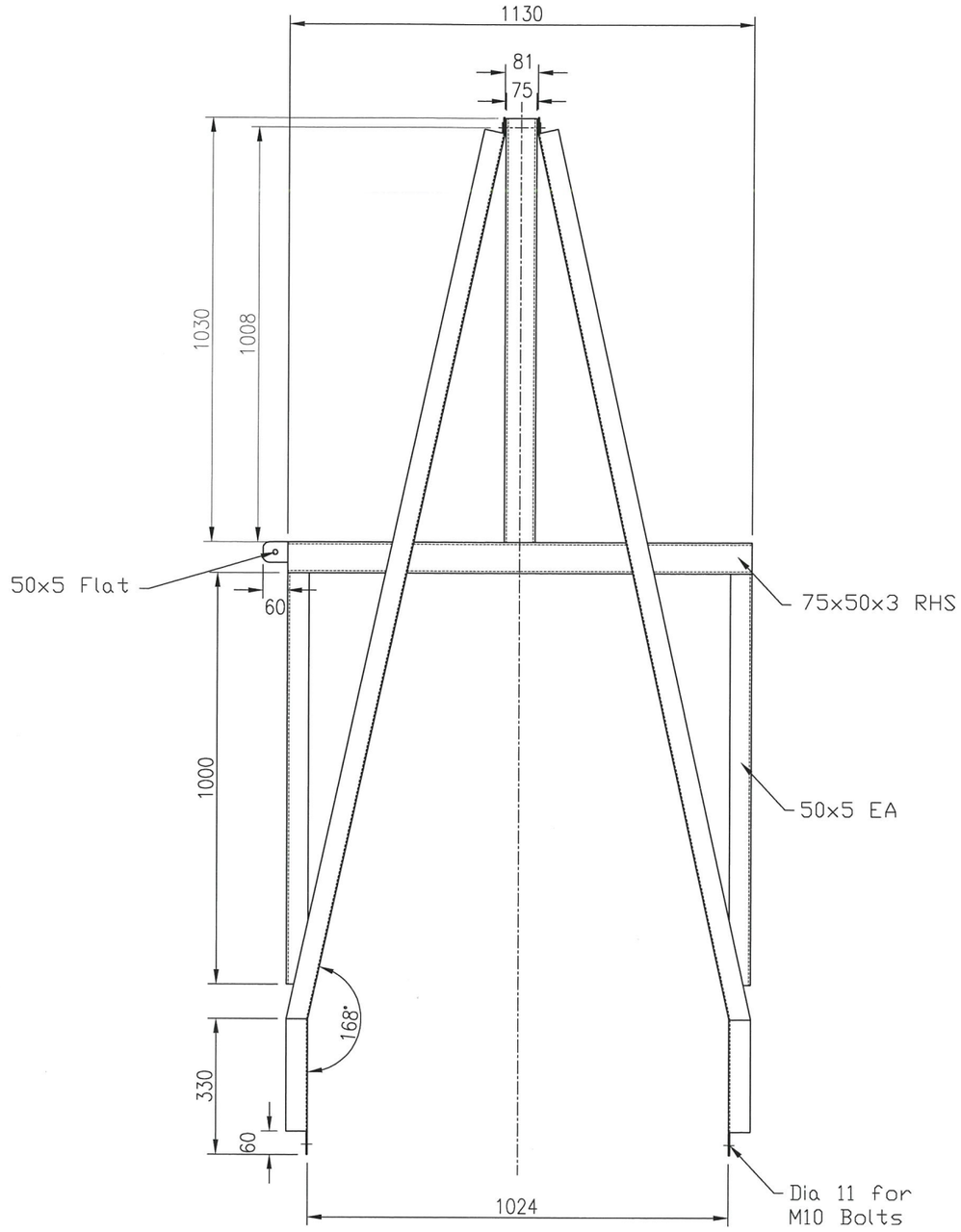

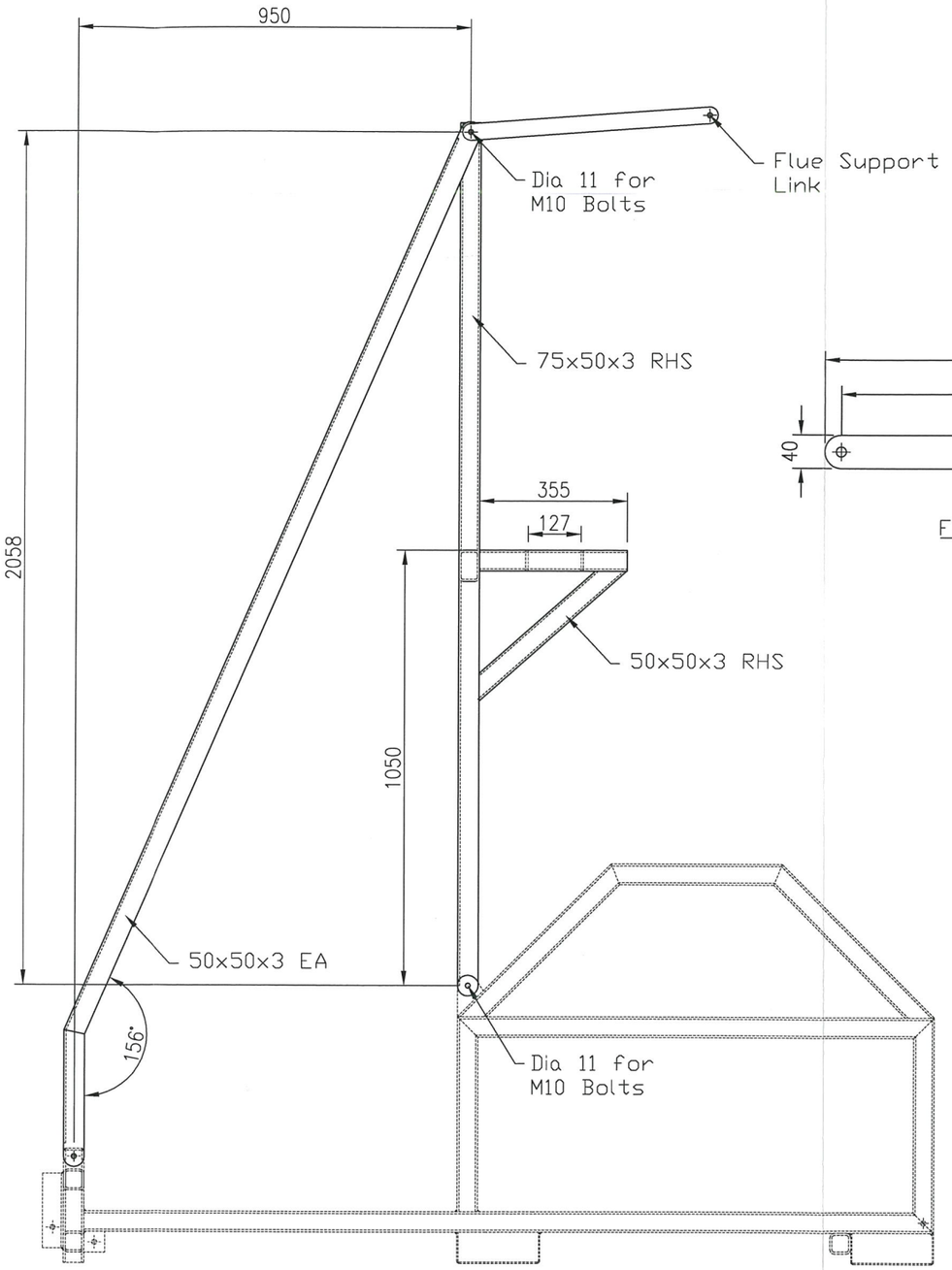

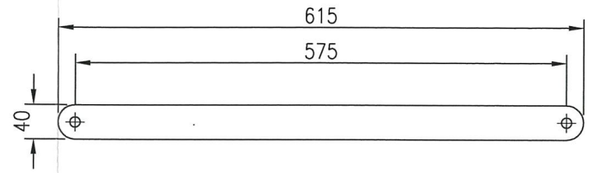

Flue Support Linkage
2 off Required
40x4 Flat

Flue SUPPORT
FRAME ASSEMBLY

MASSEY UNIVERSITY
TE KUNENGA KI PŪREHUROA
UNIVERSITY OF NEW ZEALAND

DEVELOPED BY MASSEY UNIVERSITY,
DRAWINGS & ENGINEERING BY JJ NIVEN ENGINGEERING LIMITED,
GAS SYSTEMS & CONTROL BY MORRINSVILLE PLUMBING & GAS LIMITED.

DRAWN R Thompson
DATE 19-06-2013
SCALE (A3)
NTS

J.J. NIVEN ENGINEERING LTD.
36-50 ARMSTRONG STREET, PO BOX 5121
PALMERSTON NORTH, NEW ZEALAND
PH 06 357 4039 FAX 06 358 3498

MASSEY UNIVERSITY
Carbon Generating Pyrolyser
Flue Support Frame Assembly

DRG No. 37644 09
REV. _
CAD Ref: 37644

APPENDIX E

OPERATING CHECKLIST

Checklist for loading and unloading

Task	Description	Check
1	Remove the pin and pull the overflow vent from the combustion unit	
2	Put some weight on the foot lever. Release lock pins, lift up the foot lever and the combustion unit will drop	
3	Release the lock pin on the combustion unit and slide the unit back	
4	Release the latches on the reactor lid	
5	Turn the lever anticlockwise, the reactor should tilt towards the ground	
6	Place the rope back on the handle	
7	Rotate inner lid and remove	
8	Load wood chips	
9	Place the inner lid back on	
10	Rotate the unit back into vertical alignment by turning the lever clockwise	
11	Slide in the combustion unit, it will lock in place, if not, the reactor may not be vertical	
12	Put the overflow vent back in	

Checklist for the Control

Task	Description	Check
1	Push SET twice and AL1 should appear	
2	Use the left arrow to adjust AL1 to the set point recommended for either air dried wood or wet wood. When the set point is reached the MAIN BURNER will go OFF	
3	Push set to go to the main screen	
4	Push the left arrow to change the set point temperature on the main screen	
5	The value on the main screen controls the PILOT BURNER. When the specified set point in reached the pilot burner will turn OFF	

Operation checklist

Task	Description	Check
1	Place reactor in folded position to move outside, check loading procedure	
2	Connect gas line	
3	Place LPG bottles on weigh scales	
4	Open gas bottle, checking the service light is not red, red indicated empty or gas off	
5	Load reactor, check loading procedure	
6	Connect gas bottle to overflow vent	
7	Plug in the main blower to a power socket	
8	Plug in the blower in the flare to the TRANSFORMER and NOT into a power socket	
9	Place thermocouples in position; T002 is the centre temp and T004 is the flue temp	
10	Turn on the blower and adjust the set points	
11	Turn the computer on, open pyrolyser data logging	
12	Click the run button. The thermocouples and LPG bottle should give an output	
13	When ready to go push the data logging button	

APPENDIX F

MATLAB CODE

Matlab Code for internal nodes

```
function dY=CondEvapRxnConv(t,Y)

global J dr Ta L  Ti Ro Ri sigma emisswall absorpint Agas Atar Achar Egas
Etar Echar R MC hr hfgwater hfgform hfgacet hfgphen Vtotal hlatent mmetal
Cpmetal Cpb Cpchar Cpwater Cpwatergas Cpgas Cptar kmixture0 kmixture1
kmixture2 Cpaaliq Cpaagas Cppheliq Cpphegas Cpforliq Cpforgas hc density
absorpwood emisswood hfgwatercond hvwater

T=Y(1:J+1);
mb=Y(J+2:2*(J+1));
mgas=Y(2*(J+1)+1:3*(J+1));
mtar=Y(3*(J+1)+1:4*(J+1));
mchar=Y(4*(J+1)+1:5*(J+1));
mwater=Y(5*(J+1)+1:6*(J+1));

dT=zeros(J+1,1);
dmb=zeros(J+1,1);
dmgas=zeros(J+1,1);
dmtar=zeros(J+1,1);
dmchar=zeros(J+1,1);
dmwater=zeros(J+1,1);

%case 2 internal nodes j=2 to J
% Equations
for j=2:J

%Area
Arhs=2*pi*(Ri+(j-1.5)*dr)*L;
Alhs=2*pi*(Ri+(j-0.5)*dr)*L;

%Equilibrium Constants
k1gas=Agas*exp(-Egas/(R*(T(j)+273.15)));
k2tar=Atar*exp(-Etar/(R*(T(j)+273.15)));
k3char=Achar*exp(-Echar/(R*(T(j)+273.15)));

%Enthalpy of Gas and Tar
hgas=Cpgas*(T(j)-Ti);
htar=0.4*(Cpwater*(100-Ti)+hfgwater+Cpwatergas*(T(j)-
100))+0.3*(Cpaaliq*(118-Ti)+hfgacet+Cpaagas*(T(j)-118))+0.2*(Cppheliq*(182-
Ti)+hfgphen+Cpphegas*(T(j)-182))+0.1*(Cpforliq*(101-
Ti)+hfgform+Cpforgas*(T(j)-101));

%Switches
d=0;
m=0;
f=0;
g=0;
h=0;
k=0;

%Wet wood
if T(j)<=100
    m=1;            %Conduction <100 °C  (k=wood+water+air)
end

%Evaporation
if mwater(j)>0 && T(j)>=100
```

```
   d=1;              %Evaporation at 100 °C
else
    d=0;             %Mass flow rate of water = 0
end

%Conduction
if T(j)>100 && T(j)<200
   f=1;              %Conduction between 100-200 °C
end

%Decomposition Reactions
if T(j)>=200
    g=1;             %Conduction >200 °C
    h=1;             %Convection of gas and tar
    k=1;             %Energy produced from the reactions
end

Qcond0=(kmixture0*Alhs*(T(j+1)-T(j))-kmixture0*Arhs*(T(j)-T(j-1)))/dr;
%m) Conduction <100 °C
Qcond1=(kmixture1*Alhs*(T(j+1)-T(j))-kmixture1*Arhs*(T(j)-T(j-1)))/dr;
%f) Conduction between 100-200 °C
Qcond2=(kmixture2*Alhs*(T(j+1)-T(j))-kmixture2*Arhs*(T(j)-T(j-1)))/dr;
%g) Conduction >200 °C

Qgasconv=-k1gas*mgas(j)*hgas(j);
%h) Energy produced from the reaction of gas >200 °C Units: J/s
Qtarconv=-k2tar*mtar(j)*htar(j);
%h) Energy produced from the reaction of tar >200 °C

QoutH20evap=-(m*Qcond0+f*Qcond1)/(1-Cpwater*T(j)/hfgwater);
%d) Evaporation of water at 100 °C
Qsens1=-(Cpb*(-
(k1gas+k2tar+k3char)*mb(j))*h+Cpwater*QoutH20evap/hfgwater*d+h*Cpchar*k3cha
r*mb(j))*T(j);

Qrxn=-(k1gas+k2tar+k3char)*mb(j)*hr;

dmb(j)=-(k1gas+k2tar+k3char)*mb(j)*k;
dmgas(j)=(k1gas*mb(j)*k);
dmtar(j)=(k2tar*mb(j)*k);
dmchar(j)=(k3char*mb(j)*k);
dmwater(j)=QoutH20evap/hfgwater*d;
dT(j)=(Qsens1+d*QoutH20evap+m*Qcond0+f*Qcond1+g*Qcond2+h*Qgasconv+h*Qtarcon
v+Qrxn*k)/(mb(j)*Cpb+mchar(j)*Cpchar+mwater(j)*Cpwater);
end

dY=[dT; dmb; dmgas; dmtar; dmchar; dmwater];
```